Groundwater Dynamics in Hardrock-dominated Headwaters Regions of Paschimi Nayar River, Mid-Himalaya through Assessment of Stream flow, Spring flow and Borehole Data

A Thesis

Submitted in Partial Fulfilment of the Requirements for

the Award of the Degree of

DOCTOR OF PHILOSOPHY

By

Soukhin Tarafdar

Department of Civil Engineering
Indian Institute of Technology Guwahati
Guwahati – 781039, Assam, India
June 2023

Dedicated to my Parents and my Wife and Daughter

&

Mighty Himalaya

Declaration

I hereby certify that the work presented in this thesis entitled '**Groundwater Dynamics in Hardrock-dominated Headwaters Regions of Paschimi Nayar River, Mid-Himalaya through Assessment of Stream flow, Spring flow and Borehole Data**' is entirely my own account of research performed under the guidance of Professor Subashisa Dutta. Any part of this work has not earlier been submitted for the award of any degree, diploma, associate-ship, fellowship or its equivalent to any University or Institution.

Date: 15/06/2023

Soukhin Tarafdar

(Soukhin Tarafdar)
Registration No. 166104022
Department of Civil Engineering
Indian Institute of Technology- Guwahati
Guwahati – 781039, India

Department of Civil Engineering
Indian Institute of Technology Guwahati
Guwahati – 781039, Assam, India

Certificate

It is certified that the work presented in the thesis entitled '**Groundwater Dynamics in Hardrock-dominated Headwaters Regions of Paschimi Nayar River, Mid-Himalaya through assessment of stream flow, spring flow and Borehole Data**' submitted by Mr. Soukhin Tarafdar, a student in the Civil Engineering Department, Indian Institute of Technology Guwahati, India for the award of the degree of Doctor of Philosophy has been carried out under my supervision. This work has not been submitted previously elsewhere for the award of any other degree or diploma.

Date: 15/06/2023

(Subashisa Dutta)
Professor
Department of Civil Engineering
Indian Institute of Technology Guwahati
Guwahati – 781039, India

Acknowledgement

I take this opportunity to express my gratitude and deepest regard to my supervisor, Professor Subashisa Dutta, Department of Civil Engineering, IIT Guwahati, India, for his relentless guidance, constant support and full cooperation throughout this journey of learning. I owe my deepest gratitude to doctoral committee members Prof. Ujjwal K Saha, Department of Mechanical Engineering, Prof. Suresh A. Kartha and Prof. Sreeja P., Department of Civil Engineering for their productive suggestions and advice towards my research findings.

I wish to express my sincere gratitude to Director, GBPNIHE for providing all the research facilities to carry out research work. The financial support received from the South Asian Water Initiative (SAWI), Space Application Centre–ISRO, and National Mission on Himalayan Studies (NMHS), Forest& Climate Change (MoEF & CC), New Delhi Nodal and Serving hub with G.B. Pant National Institute of Himalayan Environment & Sustainable Development(GBPNIHESD), Almora, Uttarakhand for providing the funding and research facilities during this research work is gratefully acknowledged.

The research scholars Dhruv Pandey, Vipin Kumar, Prateek Dev and Abhineet Kumar had extended their help throughout the endeavour. The students from IIT Guwahati Anjaneyulu, Sameer Singh, Suman Padhe, Chandan Pradhan and Ketan have always extended their help and support in many matters including the registration process at IIT Guwahati. The field assistant Harender Rawat, Harikrishan and Dhiraj is acknowledged for the meticulous data collection and upkeep of instruments in the experimental microwatersheds.

I would like to thank my parents, Smt. Shova Rani Tarafdar (Late) and Shri. S.K.Tarafdar (father) and my sister (Sanchita Tarafdar) for all their love and encouragement. Lastly, I thank my wife (Arpita) and my child (Anshika) for having the patience to let her husband complete this long journey of learning and pray to the almighty for good health.

Soukhin Tarafdar
May 4, 2023

Abstract

Mountain as a mosaic of steep headwaters has great hydrological significance. Small basin research has contributed significantly to the process-based understanding of the internal functioning of the catchments. In this study, two microwatersheds of area < 10km^{2}and a small hydrological response unit (HRU) (< 0.4km^2) nested within one of the experimental microwatershed are being investigated through hydrological instrumentation in terms of rain gauges, water level recorders at the outlet for continuous stream gauging as well groundwater level measurements in shallow and deep fractured bedrock aquifers in the smallest HRU to better understand the hydrological functioning in the headwater regions of Paschimi Nayar Basins. The precipitation variability of Indian Summer Monsoon during the 2009 to 2018 period showed inter-annual variability with drought, intermittent multiple deficient rainfall periods and normal monsoon rainfall years. Analysis of long-term records of springflow through flow duration curve indicates a significant reduction in lowflows as well as high flow periods. Recession curve analysis using single non-linear and two exponential linear reservoir models for the recession period indicates an overall non-linearity in storage-discharge relationship. A parallel offset was observed between years in the yearly-prolonged post-monsoon recession curve in $-dQ/dt$ versus Q plot indicating the control of antecedent storage over rate of outflow. Shallow piezometer (< 4 m) and deep borewell (< 80 m) monitored over two monsoon periods indicate a rapid response to any rainfall amount exceeding 5mm. The episodic recharge and water level fluctuation method indicate a monsoonal recharge of 4% to 24% for a low specific yield value (1 to 5%). The study also highlights that the effectiveness of recharge is controlled by the rainfall intensity. A near 2.08 to 2.4mm/hr rainfall intensity generates maximum recharge in the terrain dominated by metasedimentary rock. The aquifer transmissivity and storativity were estimated using homogeneous confined and dual-porosity aquifer model applying falling-head and rising-head slug test methods suitable for low yielding bedrock aquifers for five shallow piezometer located within the HRU. The landuse change analysis highlights that for eight years in the two selected microwatersheds the area under the pine forest has increased by (+) 38 to 40 % whereas, the agricultural land has reduced by (-) 95 to 109%. The unsaturated near-surface soil hydraulic conductivity (K_h) showed significant alteration in the Pine-dominated fallow land as compared to the agricultural landuse whereas saturated hydraulic conductivity (K_{fs}) measurements up to 30 cm depth do not show marked difference due to the ‘memory effect’ of past landuse.

Nomenclature

Notations

A	Test statistic for Anderson-Darling test	λ	Interporosity flow, dimension index
α	Dimensionless storage parameter	ω	Ratio of specific storage of fractures over a specific storage of both fracture and matrix
β	Trend magnitude(Sen slope)	ϕ	Total porosity
C	Shape factor	ϕ_m	Matrix flux potential
D	Drainage	Q_t	Discharge at time t
Df	Degrees of freedom	R	Recharge
δi	Rainfall variability index	R_b	Test statistic for Buishand range test
E	Modeling error	S	Sorpivity
$\in_s$	Storage sensitivity	S_k	Rescaled adjusted partial sum (Buishand range test)
$H(t)$	Head at time t	S^2	Estimator of common variance
K	Recession constant	S_r	Specific retention
k'	Matrix Hydraulic Conductivity	Ss'	Matrix storage
K_{fs}	Hydraulic conductivity	S_y	Specific yield

T_c	Critical time	T	Transmissivity
T_j	Test statistic for SQ-MK test	$u(t)$	Sequential values of statistic
t	t-test statistics (Independent-test)	W	The W statistic/ Shapiro-Wilk normality test
t_k	Cramer's test statistics	Z	MK trend
τ	Recession timescale (in days)	Z_{mk}	Standardized test statistics

Abbreviations

APHRODITE	Asian Precipitation –Highly Resolved Observational Data Integration Towards Evaluation
EMR	Episodic Master Recession method
EPM	Equivalent Porous Medium
ET	Evapo-Transpiration
GCM	Global Climate Model
GLEAMS	Global Land Evaporation Amsterdam Model
GP	Guelph permeameter
IHR	Indian Himalayan Region
IMD	Indian Meteorological Department
IML-CZO	Managed Landscapes – Critical Zone Observatory
ISMR	Indian Summer Monsoon Rainfall

ISSS	International Society of Soil Science
LPA	Long period average rainfall
LULC	Land Use and Land Cover
MDI	Mini disk Infiltrometer
MRC	Master Recession Curve
NRSC	National Remote Sensing Center
PTFs	Pedo-Transfer Functions
RPR	Recharge to precipitation ratio
SPEI	Standardized Precipitation Evapotranspiration Index
SPI	Standardized Precipitation Index
TRMM	Tropical rainfall measurement mission
USDA	USDA and ISSS
USGS	U.S. Geological Survey
UTM	Universal Transverse Mercator
WFD	Water Framework Directives
WIO	Western Indian Ocean
WTF	Water table fluctuation method

List of Figures

List of Tables

List of Photographs

CHAPTER 1

Introduction

1.1 General

The biggest river basin in India i.e., the Ganga Basin extends from the mighty Himalaya in the north to the deltaic plains in the south. In recent years, the River Ganga has become a hotspot of many activities ranging from clean Ganga mission to unregulated upper reaches of the river (Aviral Ganga), and most importantly the holistic assessment of the ecological needs of the holy River. A significant contribution to the available vast water resources, both in the form of surface and groundwater in the Ganga basin of 8,61,452 km^2 area, may have its source in the western and central Mountain regions of the Himalaya. It is well known that the seasonal major influx of water comes when the high-relief mountain forces the moisture-laden monsoonal clouds to precipitate due to orographic enhancement. Mountains do act as 'water towers' for not only the population living within the mountain basins but also for the rapidly growing downstream population and ecosystem.

However, in the past four to five decades, the western Himalayan Mountains are witnessing unprecedented changes both in terms of social as well environmental changes making the existing ecosystems as well as mountain communities more vulnerable. The headwaters of River Ganga in the most populace the Middle-Himalaya are constrained by data gaps and very limited research on the understanding processes that regulate the flow in springs and streams as well as the long-term variability in rainfall. The study area of this research proposal is located in the headwaters of the ecologically sensitive Nayar River. The Nayar basin lies between latitudes 29°45'N to 30°15'N and between longitudes 78°40'E to 78°60'E in the western Himalaya. The ecologically sensitive spring-fed Nayar River is

located in the mid-Himalayan region of Garhwal Himalaya, formed by the confluence of two rivers, Paschimi Nayar River and Purbi Nayar River. The total basin area under Nayar River is 1760 km^2, of which Purbi Nayar Basin covers an area of 1010 km^2. The rivers originated from the Dudhatoli ranges of the Garhwal region in the Pauri district. The elevation ranges between 557m to 3076m.

1.2 Problem statement and motivation of work

The availability of groundwater outflowing as springs, seeps, and streams originating from hardrock fracture networks in diverse hydrogeological setups mostly ensures the water resources sustainability for rural and urban communities in the rugged mountainous terrain of the Indian Himalaya. Nonetheless, summer season water scarcity is getting aggravated in the remote rural settlements falling in the middle Himalaya under the changing climate variables such as precipitation, evapotranspiration, and the resultant flow from springs and streams making the life and the ecosystem more susceptible. Additionally, the anthropogenic drivers, for example, the outmigration of the workforce causing the conversion of agricultural land to fallow and increase in the pine forest area, and secondly, the expansion of rural road network impacting the hydrological connectivity altering the hydrology at the catchment scale and understandably, at large basin scale also.

As a parallel remedial measure, hundreds of microwatershed are brought under the state-level integrated watershed management plans to strengthen the water resources sustainability. However, the sloping landscape of the mountainous Himalaya largely underlain by hardrock under variable soil thickness, rock type, and topography, remains poorly characterized and quantified in terms of its role as a storage of fresh water. Very limited knowledge exists about the understanding of inherent characteristics of the heterogeneous catchments in headwaters and how the ongoing modifications in the rainfall characteristics, land use trends, and the associated soil hydrological properties are going to impact the hydrology of the catchments nested with the large basin. Most importantly little is

known about the groundwater recharge component during the main monsoon months of the Indian summer monsoon which sustains the life of all the smaller water resources such as springs and low-order streams essential for rural water supply, irrigated and rain-fed subsistent agriculture system. Hydrological instrumentation in terms of gauging the springflow, and streamflow and setting up the rain gauge in rugged topography holds the key, although maintaining the monitoring stations is challenging under the changing climate and unplanned anthropogenic activities.

The motivation for the Ph.D. work is to address some of the scientific challenges in the rain-dominated middle mountains on developing an understanding of hillslope shallow and deeper hardrock groundwater aquifers sustaining the springs and streams, groundwater recharge processes and its quantification, rainfall-recharge ratio and threshold in metasedimentaries, recession characteristics, storage discharge relationship of a linear or non-linear water-bearing geological formation and its storativity and transmissivity. The trends and patterns of land use change as well as the long-term monsoon and winter rainfall and the associated drought vulnerability in recent time remains poorly reported and hence covered for the study area. Additionally, the landuse-soil interrelationship remains an important research question that needs to be deciphered in the middle Himalaya, especially for the most dynamic landsue category under fast transformation i.e., pine-dominated permanent fallow and agricultural land which may or may not impact the near-surface and sub-soil physical and hydraulic characteristics of soil formation.

The central aim of the Ph.D. thesis is to provide valuable information to policy planners for the most appropriate adaptive land policy for wise natural resource management, drought mitigation, and supporting water management decisions.

1.3 Research Objectives

Springs and Streams in Indian Himalayan Region (IHR) have acted as reliable sources of fresh water for centuries. Although a very large population is dependent on smaller water resources, little attention has been paid to investigating the surface and subsurface soil characteristics, understanding of recharge processes, and shallow groundwater aquifer systems that sustain the perennial springs and streams. The research objectives of this research proposal are the following:

- To carry out trend analysis of long-term rainfall data and drought analysis.
- To perform recession curve analysis of spring and stream hydrographs.
- To carry out drilling and establishment of shallow piezometer in hardrock to determine aquifer characteristics through slug testing.
- Estimation of groundwater recharge using borehole water level data and spring hydrograph using water table fluctuation approach in micro catchment scale.
- To carry out mapping of landuse/landcover using high-resolution satellite data and assessment of landuse change at microwatershed and regional scale.
- To characterize soil hydraulic properties in the two dynamic landuse classes (Pine-dominated fallow and agricultural land) and infer the dominant hydrological pathways.

1.4 Organization of the Thesis

The Ph.D. thesis primarily focuses on understanding some of the aspects related to water and its management which is becoming central to water and livelihood security through assessment of long-term trends in rain, patterns of drought, storage-

outflow relationship using recession analysis, aquifer hydraulic property estimation, quantification of groundwater recharge, assessment of landuse change and associated alteration of soil hydraulic characteristics and possible changes in surface and subsurface pathways from the mountainous headwaters systems in Garhwal Himalaya and is divided into 9 main chapters.

The thesis has been organized keeping in mind the overall sequence that is followed in any of the well-thought-out catchment based investigations which begins with the delineation of microwatershed or catchment reflecting the regional scenario of long-term transformation that the larger basin might be witnessing as a consequence of changes in biophysical and socio-economic drivers including the climate change impacts. **Chapter 1** primarily gives a general introduction to the large basin and the importance of mountain headwaters as a source region for water resources and the objectives which have not been widely explored due to remoteness and may be financial limitations. **Chapter 2** reiterates briefly the relevance of each identified objective in the global as well as Indian Himalayan context through a literature review and portrays the identified two small catchments in the western Nayar river basin with details of hydrological instrumentations essential for monitoring and analysis of catchment response of the changing inputs. **Chapter 3** covers a very concise review of the literature of past rainfall studies on the Indian Summer Monsoon(ISM), as well as reported trends in annual, ISM, and winter rainfall in western Himalaya. The methodological approach of statistical trend analysis using the two gridded rainfall data is being discussed and elaborates analysis of drought and the recent trend of rainfall in the study area falling in the middle Himalaya. **Chapter 4** consists of a review of widely investigated recession curve analysis which currently is bringing new insights into the inner processes causing the recession in different climatic regions. The storage-discharge relation was established through analysis of spring hydrograph by applying two exponential and power law model for prolonged post-monsoon recession periods observed in a wet and dry climate.

Chapter 5 deals with the most challenging aspect of establishing a series of shallow borewells or piezometer through drilling using an imported coring machine in the sloping, remote catchment for understanding the shallow groundwater characteristic through a series of slug tests. **Chapter 6** covers the aspect of groundwater recharge estimation from the headwater catchment which is completely unexplored in any of the past studies. The instrumented shallow piezometer/borewell, as well as deep borewell assessed through the water level fluctuation method quantifies the monsoonal recharge in the hardrock-dominated shallow and deeper aquifer systems in a headwater catchment. In **Chapter 7** the relevance of landuse and the impact of landuse change on the hydrology of the catchments at small and large scales are reviewed. The assessment of present and past landuse use was carried out using high-resolution satellite data, toposheet, and old revenue maps as well as change over an eight-year period is presented at local microwatershed scale as well as regional watershed scale. **Chapter 8** deals with the review of literature on aspects of alteration of soil hydraulic characteristics change due to the landuse change. Near-surface unsaturated and saturated hydraulic conductivity properties under the two landuse categories are being investigated and analysis of the dominant hydrological path under the rapid landuse change is assessed using measurements obtained from Mini disk infiltrometer and Guelph permeameter. In the concluding chapter i.e. in **Chapter 9**, the key findings and some future scopes are highlighted.

CHAPTER 2

The Headwaters of Nayar River Basin

2.1 Introduction

Rain-dominated middle mountains could store groundwater in hillslopes often for month's together supporting life through feeding the smaller water resources like headwater streams, springs, and seeps. The headwaters is the uppermost part of the mountainous basin and elements of headwaters include hillslopes; zero-order basin; first and second -order streams (Gomi et al. 2002). Forested headwater streams because of their abundance in number, length, shallower depth, and high surface area, plays an inordinate role in 1) nutrient cycling (Bormann and Likens, 1967) 2) flood regulation 3) maintaining instream biodiversity as well as downstream river species richness (Meyer et al. 2007) and 4) water quality and quantity (Alexander et al. 2007).

Growing footprints of seasonal water scarcity in the Mid-Himalayan basins are primarily dependent on changing seasonal rainfall flux of Indian Summer Monsoon (ISM), which is getting affected over past four to five decades. A significant reduction in rainfall during the Indian Summer Monsoon(ISM) over the past century (1901-2012) is reported from the Ganga-Brahmaputra basins and the foothill regions of Himalaya (Roxy et. al. 2015) resulting out of weakening in land-sea thermal contrast under warming environment. Basistha et al. 2009 also reported a declining trend of monsoonal rainfall between 1965-1980 periods from the most populated mountain region of lesser Himalaya in Uttarakhand. Observation from the Hilly region of Uttarakhand throughout the last half-a-decade (1951-2008) from the IMD gridded database shows an increase in high-intensity rainfall over India whereas a significant decrease in moderate- intensity rainfall (11.01-72.5 mm/day) as well as low-intensity short spell rainfall event. A substantial reduction in the contribution of low- intensity short duration, as well as low-intensity long duration to total seasonal rainfall was reported for Uttarakhand (Dash et al. 2011). These characteristic changes in duration and intensity of rainfall patterns would lead to alteration in diffuse and preferential

recharge processes, which may threaten the immediate shallow groundwater sustaining the spring flow and low-order streams.

There is growing recent evidence based on regional climate modelling studies (Halder et al. 2016; Quesada et al. 2017) that land-use land-cover change could be one of the drivers impacting the Indian summer monsoon. Although, these land-use land-cover change drivers are large-scale forest to agriculture or pasture land conversion. In the past (in the mid-1900's or so), a reverse transformation of conversion of agricultural land to fallow land, reforestation and gradual forest regeneration in permanent fallow and pasture land is reported from the middle mountain region of Uttarakhand, India (Tarafdar et al. 2019) as well as in Nepal (Ghimire et al. 2013; Paudel et al., 2016).

The shallow groundwater sustains flow in smaller water resources not only during the lean-flow period but also during the surplus months. Recent studies on runoff generation from headwater regions have shown a significant contribution of bedrock groundwater (Salve et al. 2012 and the reference cited therein), which gives due emphasis on hydrogeological control (Tangue and Grant, 2004; Onda et al. 2006; Gabrielli et al. 2012). The dynamic nature of groundwater in hard rocks is reported by many drilling intensive studies (Haria and Shand, 2004; 2006, Bank et al. 2009; Salve et al. 2012; Gabrielli et al. 2012) in sustaining the stream flow governed by highly heterogeneous fracture-dominated flow paths.

The knowledge of the storage-outflow relationship of groundwater aquifers that sustains the small water resources (springs, seeps, and low-order streams) is critical as it provides information on storage characteristics as well as baseflow recession rates. (e.g. Brutsaert and Nieber1977; Wittenberg, 1999; Shaw and Riha, 2012; Biswal et al. 2014; Bart and Hope, 2014; Chen and Krajewski, 2015). As against the lumped recession curve approach (Brutsaert and Nieber 1977; Kirchner, 2009), event-scale recession analysis holds promising information for understanding seasonal variation in evapotranspiration (Shaw and Riha, 2012) and the role of antecedent storage in making the catchment a 'non-unique' dynamic system (Bart and Hope, 2014; Patnaik et al. 2015).

Scientific investigation in terms of aquifer properties, assessment of recharge and stream-aquifer interactions are very limited in the headwaters region of western

Himalaya, dominated by metasedimentary and gneissic hardrock aquifers. Recent research findings on groundwater recharge indicate a positive (Zhang et al. 2016; Tashie et al. 2015) as well as negative impact (Tashie et al. 2015) of high- intensity rainfall. A better understanding of the role of shallow and deeper groundwater aquifers is required under the reported altered rainfall regimes in Uttarakhand. New advancement in analyzing time series of water-level as well as rainfall data provides an opportunity for the assessment of episodic groundwater recharge in terrains dominated by preferential flows like the western Himalaya (Healy and Cook, 2002; Crosbie et al. 2005; Nimmo et al. 2015).

2.2 Study area and details of instrumentation

The study area is a part of Paschimi Nayar sub-basin having the highest elevation of 2143 m to the lowest elevation of 1240 m. The two selected experimental watersheds are located between latitudes 30° 02' N and 30° 06' N and between longitudes 78° 45'E and 78°50'E (Figure 2.1 through 2.3, and Table 2.1). The district head quarter, the town of Pauri is located approximately 20km north of Paidul (the outlet of the second experimental watershed) and 12 km north of Dugar Gad microwatershed. The drainage pattern of the study area is dendritic with central streams are perennial and joined by several ephemeral streams of lower order originating from the steep hillslopes. The two selected watersheds, namely Dugar Gad and upper Paidul micro-watershed of 3.2 km^2 and 8 km^2 are elongated basin having a narrow central valley and significant hillslope area. Interestingly, water demand for meeting the basic human need comes either from springs, seeps and hand pumps whereas the agricultural water demand is met through the utilization of stream discharge through the gul system (small distributaries canal connected to streams). The major Landuse/Land cover classes for the watersheds in the study area is classified as forest area including village forest, terraced agriculture land, Fallow land, wasteland, and settlements. The study area falls under humid temperate climatic conditions; with average annual rainfall for the district is 1582 mm (Indian Meteorological Department). More than seventy-five percent of the annual rainfall falls between June to September (Monsoon period). The slope of the watershed falls broadly under three categories. The higher slopes fall under very steep sloping category (>35% slope)

occupies the higher ridge slopes, the intermediate slopes just above the agricultural land falling under the class of moderately steep to steep sloping category (15-35%) and the valley portions of the microwatershed falls under the 10-15% category. Geologically the study area falls in the Lesser Himalaya, which ranges between 1500-to-2500 m high and is represented by Pauri Phyllite and Khirsu Quartzite rock types which are members of the Maithana Formation in the Dudatoli Group. The soil type in the study area ranges between shallow to medium range, with loamy skeletal soil at the side slopes and summits. In the two-selected experimental watersheds, daily spring discharge is measured through volumetric method (Photograph 2.3) whereas the stream discharge is either gauged through 90^{o} V-notch or cutthroat flume (Photograph 2.1) and rectangular weir (Photograph 2.2). The ninety-degree V-notch gauged the streamflow from Bhimlitalli micro-catchment having an area of 0.4 km^2. The right angle V-notch can measure a total head of 45 cm, was measured manually at daily time-step for a period of three years (2010-2012) and was instrumented with water level recorder and barologger in the year 2017. The Bhimlitalli micro-catchment is a part of Dugar Gad micro-watershed. At the outlet of the Dugar Gad micro-watershed, a gauging station with cutthroat flume was established in the year 2017 and instrumented with water level recorder and barologger. A rectangular weir at the outlet of the upper Paidul micro-watershed (Photograph 2.2) is also supported with water level recorder and a barologger. The rainfall data was collected using ordinary rain gauge and with rainfall tipping bucket event logger.

Table 2.1: Details of experimental micro-watershed selected for hydrological investigation.

	Area(Sq.km)	Geology	Relief ratio	Elevation (m) (*Min,Max*)	Broad Landuse
Dugargad micro-watershed	3.2	Quartzite/ Phyllite	0.18	1400,1920	Rainfed agriculture, Pine forest, Fallow land, Settlement
Bhimlitalimicro-catchment	0.41	Quartzite/ Phyllite	0.23	1460,1680	Permanent Fallow, Pine forest,rainfed agriculture land, settlement
Upper Paidulmicro-watershed	8.0	Quartzite/ Phyllite	0.13	1300,1940	Rainfed agriculture, Irrigated land, Village forest, Fallow land, Settlement

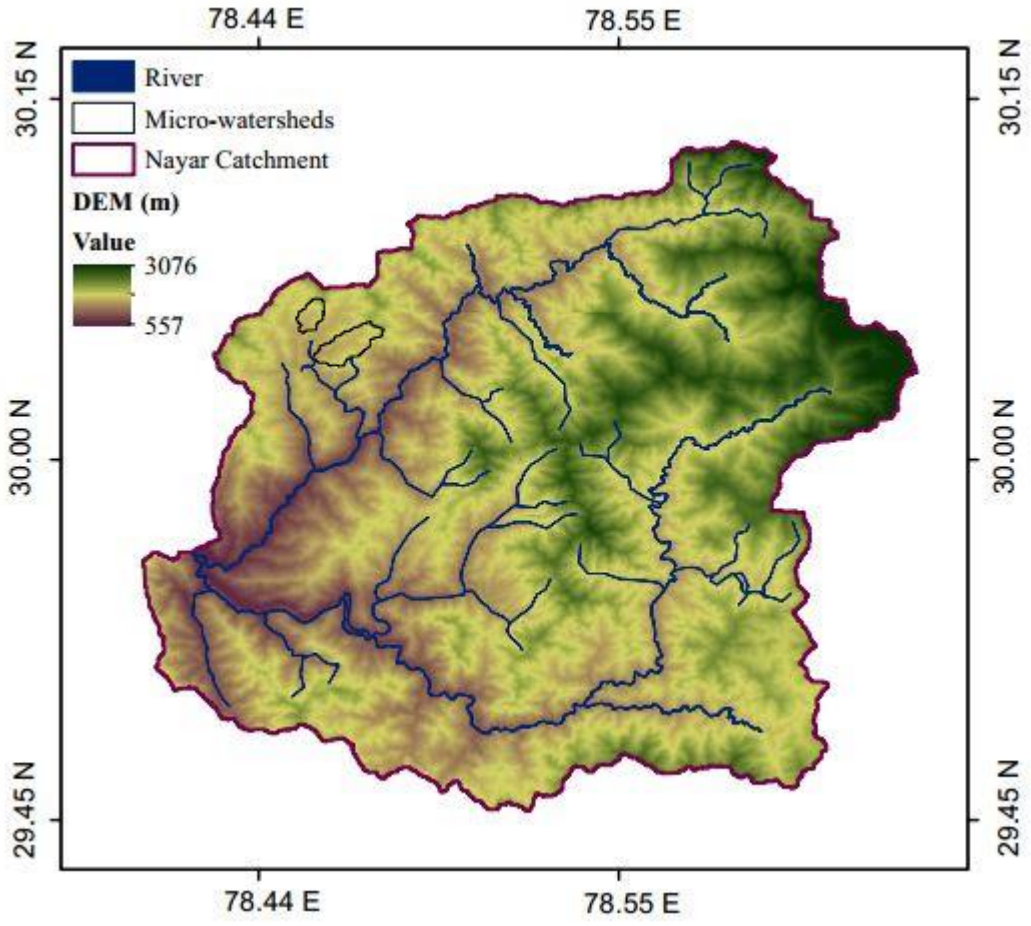

Figure 2.1: Nayar River basin with location of two selected experimental micro watersheds in headwater region.

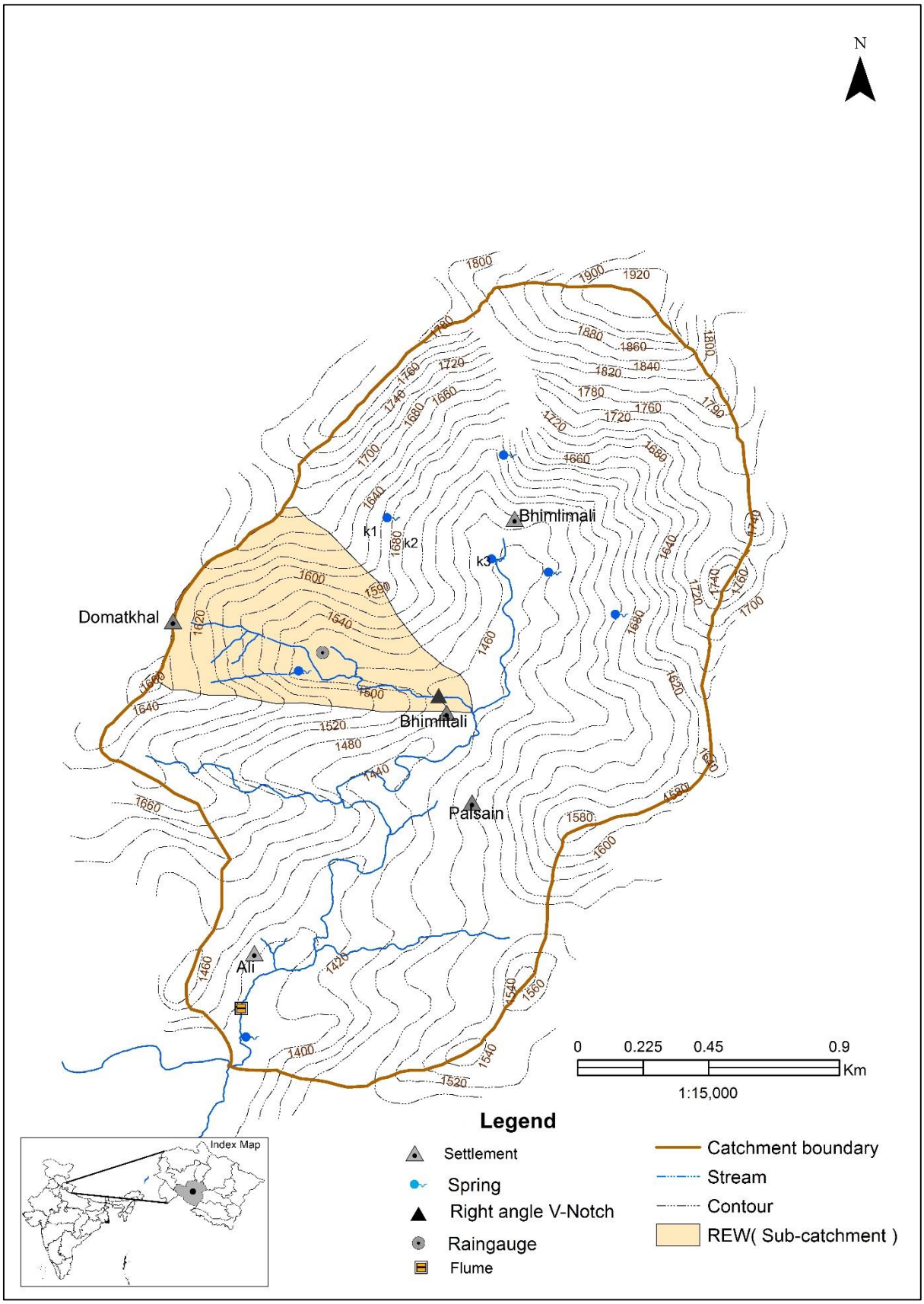

Figure 2.2: Study area map of the Dugar Gad micro-watershed and nested Bhimlitalli micro-catchment (Hydrological Response Unit, HRU) showing the locations of rain gauge, stream gauging sites, as well as the springs.

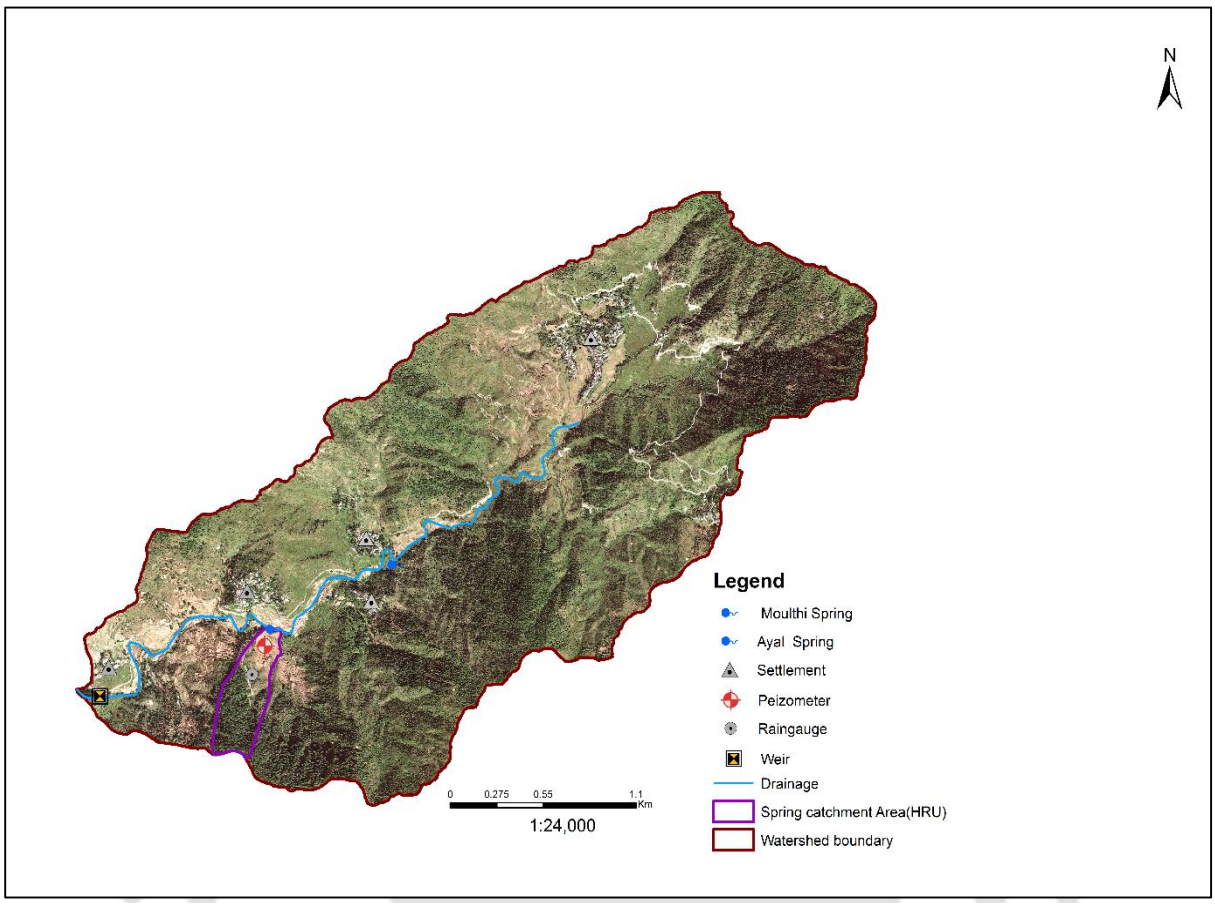

Figure 2.3: Study area map of the upper Paidul micro-watershed showing the locations of rain gauges, stream gauging site at the outlet, as well as the springs and probable catchment boundary of Ayal spring.

Photograph 2.1: Right angle V-notch (a) at the outlet of Bhimlitali catchment and cutthroat flume (b) at the outlet of the Dugar Gad headwater catchment.

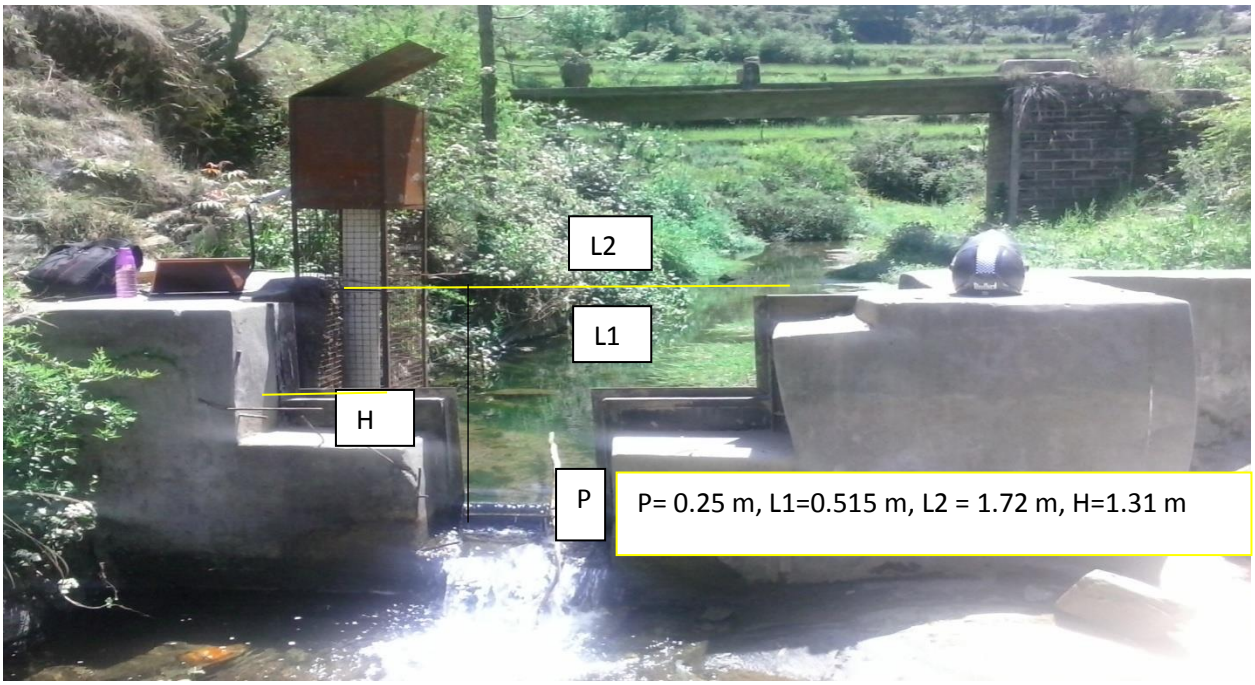

Photograph 2.2: Picture of stream flow gauging station at the outlet of the experimental upper Paidul watershed at Paidul with water level recorder.

Photograph 2.3: Springs near Ayal village monitored daily through volumetric assessment.

2.3 Recent rainfall patterns in the study area

The year 2009 was reported to be a moderate drought year wherein the country received the lowest monsoon rainfall in the recent decade whereas the state of Uttarakhand received 29% less rainfall than long period average (LPA) rainfall. The study area received only 590 mm (48%) less than the normal monsoon rainfall for the district. The year 2010 was a wet year wherein the study area received surplus rainfall of 1500 mm. The year 2011 recorded normal rainfall during the monsoon period (1020 mm) but June and August were months of high rainfall whereas the month of July and September recorded deficient rainfall. The year 2012 records only 740 mm of delayed monsoonal rainfall and a very low annual rainfall year (i.e. 800 mm). The month of June, July and September recorded significant deficient rainfall for the 2012 monsoon period. The year 2013 recorded 910 mm of monsoon rainfall. The year 2014 again records 678 mm of delayed monsoon rainfall with below-normal rainfall in June, August and September months whereas July records only 389 mm of rainfall.

The year 2015 recorded 733mm of rainfall with 243mm of rainfall between 15 June to 30June with two major high rainfall events of rainfall (66,88 mm). Deficient rainfall in July (278 mm), Aug (194 mm), and September (38.6 mm) months was recorded. The year 2016 was again a wet year with total monsoon rainfall of 1105 mm, and July being the wettest month (556 mm). The year 2017 recorded 948mm of monsoonal rainfall (Figure 2.5) with deficient rainfall in August and September months. The year 2018 (Figure 2.6) is also a deficient monsoon rainfall year (770 mm) with deficient rainfall in all the monsoonal months except September (213 mm) with high rainfall events. The monsoonal rainfall variability index (Figure 2.4 and Table 2.2) for the period of 2009 to 2018 shows that a series of drought periods intercepted by normal or wet years. The recent year of 2019 was also a drought year with less than 400 mm of rainfall during the monsoon period (15 June to 20 September) and 140 mm of rainfall in late September to the first week of October. The main monsoon months of July and August records deficient rainfall (Figure 2.4).

Table 2.2: Monsoon rainfall amount over a period of ten years (2009-2018) from the study area.

Monsoon	Rainfall amount(cm)
2009	59
2010	150
2011	100
2012	74
2013	91
2014	68
2015	73
2016	111
2017	95
2018	77

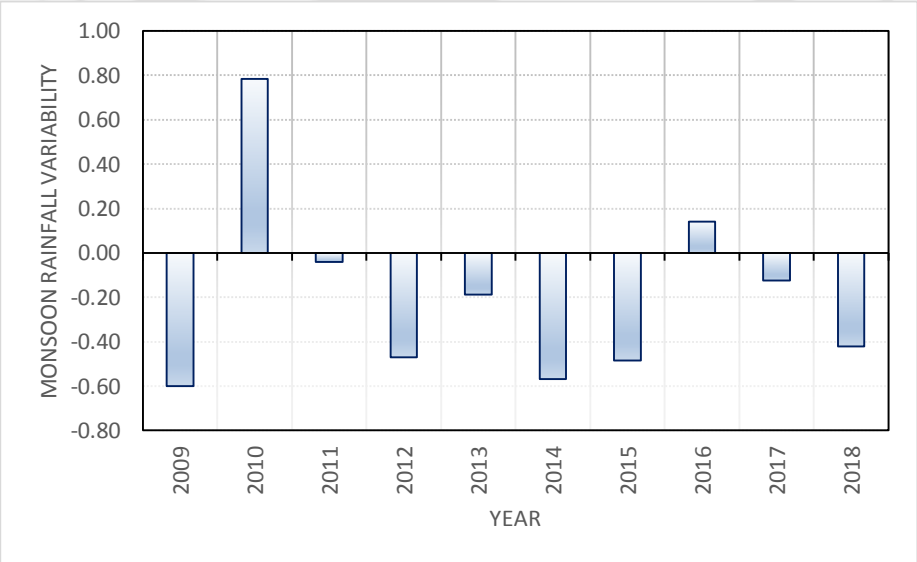

Figure 2.4: Monsoon rainfall variability index over a period of ten years indicating a series of drought years (2009,2011,2012,2013,2014,2017and 2018) intercept by wet or normal monsoonal years (2010 and 2016)

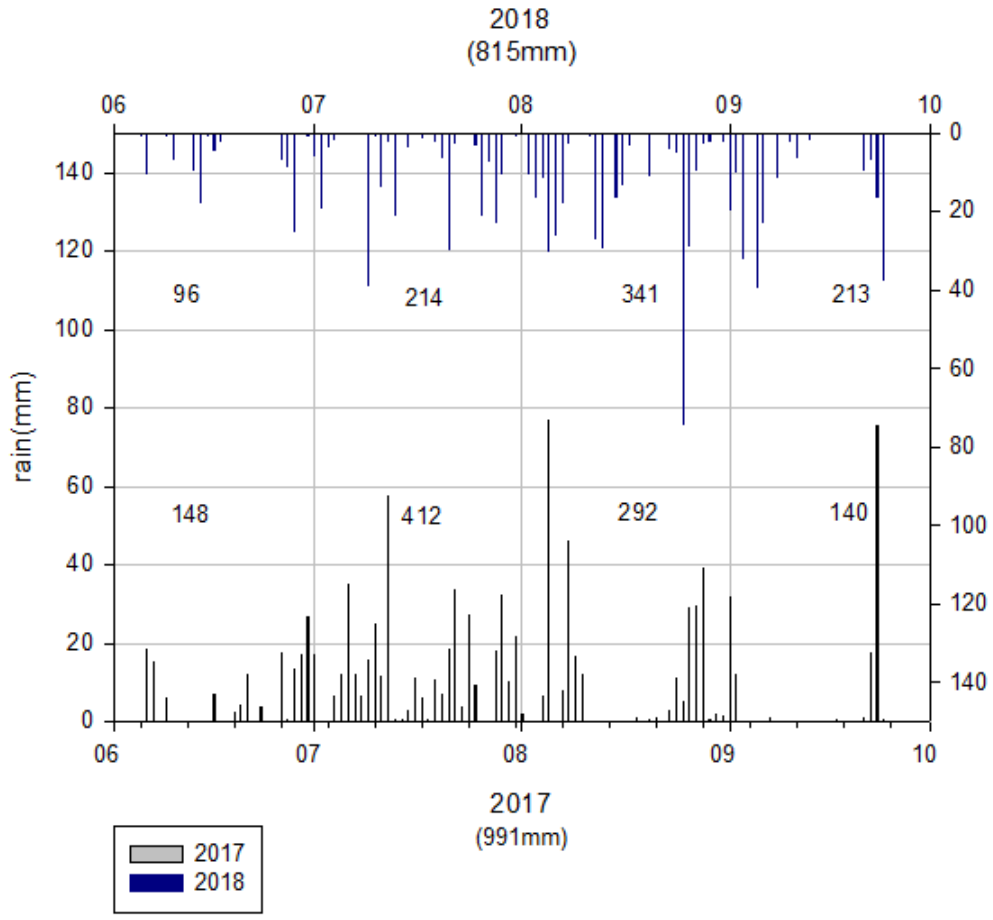

Figure 2.5: Monsoon rainfall characteristics highlighting large intra-monthly variability recorded from rainfall event logger installed at Dugar Gad micro watershed for the year 2017 and 2018.

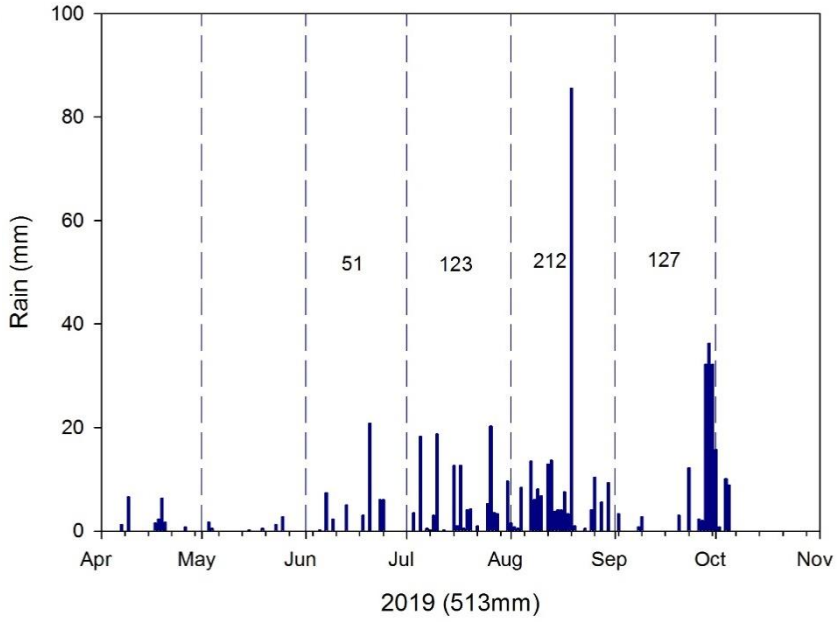

Figure 2.6: Monsoon rainfall pattern for 2019. Another deficient monsoon period with less than 400mm of rainfall recorded between 15June to 20 September 2019.

2.4 Conclusion

Research in headwater catchments is generally short-term in nature limited to two to three years of observations with expectations of quick success stories. But on the contrary, seemingly simple-looking catchments are very complex and need long-term research to bring new insight that would lead to the development of an understanding of catchment processes which may further result in better management policies. Furthermore, alterations in the precipitation patterns and future drought severity are expected to increase under the projected climate change impacts making future water management even more challenging. Two experimental micro watersheds and two spring catchments nested within the micro watersheds are gauged through hydrological instrumentation for measurement of rainfall, spring and stream outflow as well as groundwater water level fluctuation measurements. The relief ratio of the micro watersheds ranges between 0.13 – 0.18 whereas the observed relief ratio for the two spring catchments is high ranging between 0.23-0.4. Monsoon rainfall records over the recent decade highlight multi-year deficient rainfall years.

CHAPTER 3

Rainfall Time Series and Drought Analysis

3.1 Introduction

Precipitation is not only an important meteorological parameter but also acts as an important agent in shaping the landform in the mountain range caused by erosional processes. It is also a driver for hydrological processes and gets transformed into the vital surface and subsurface freshwater resources, which is vital not only for the remotely located vulnerable civilization and ecosystem but for the billions of inhabitants of downstream regions. However, the understanding of its space and time variability is still poorly constrained due to the sparse density of rain gauges as well as limited stations at higher elevations in the Indian Himalayan Region (IHR). Setting up of rain gauge monitoring network and regular upkeep of rain gauges in the rugged topography of the Indian Himalaya is challenging and at times financially constrained. Nonetheless, under the present context of changing climate and associated threats on mountain water security, more distributed observation with better representation of variable topography in the monitoring network is essential to gain an understanding of underlying processes at a local to regional scale and should be in line with the world densest, and highly reliable *in-situ* measurement systems from European Alps mountain range (Frei and Schar, 1998; Roe, 2005).

The spatial distribution of rainfall is dependent on the elevation but other physiographic features such as slope, terrain orientation to wind direction, among many other factors regulates its distribution in rugged topography. Hence making an accurate assessment is difficult unless gauged appropriately under variable physiographic disposition. Understanding long-term annual and seasonal precipitation variability is essential for a

range of planning purposes which include primarily water resource management, agriculture and forestry. Another pertinent issue associated with point measurement of rainfall using conventional rain gauge and tipping-bucket rain gauge (TBRG) measurement device is the errors caused by wind- induced losses resulting in an undercatch, wetting and evaporation of gauge wall and collecting funnel surface (Sieck et al. 2007; Upton and Rahimi, 2003). Blockage, underestimation of extreme rain rate due to failure to measure high rain rates and deposition of fine sediments in the pair of adjacent buckets of TBRG's are some problems associated with the use of TBRG's and requires proper site selection, regular monitoring and maintenance (Upton and Rahimi, 2003).

Hence, many satellites-based rain measurements corrected with limited field observations in the complex mountain of the Indian Himalaya could be an important alternative. The satellite-based rainfall data such as TRMM (Tropical rainfall measurement mission) revealed a fivefold difference in the observed precipitation between major valleys and their adjacent ridges (Anders et al. 2006) at a 10 km resolution, unique night-time peak of rainfall over the Himalaya caused by meridional circulation (Bhatt and Nakamura, 2005) and many other insight on orographic control of monsoon dominated rainfall (Barros et al. 2004) as well as hydrological water budget with a reported major difference in snowmelt, monsoon rainfall contribution along the basins located along the east-west arc of Himalaya (Bookhagen and Burbank, 2010).

Increasing evidence of weakening of Indian Summer Monsoon rainfall(ISMR), particularly after the 1960's caused a decline in monsoon rainfall as well as a higher occurrence of drought observed over the Indian sub-continent (Krishnan, 2013; Preethi et al. 2019). The decades from 1956 to 2016 are showing clear evidence of negative trends in SPI with an increase in the percentage of area under drought using the results obtained from IMD high resolution (0.25° longitude × 0.25° latitude) long period rainfall dataset throughout 1901–2016. Further, two of the CMIP 5 climate models, well-suited for monsoon variability simulation, indicate more propensities of droughts in near and mid-future terms over the 2010-2069 period (Preethi et al. 2019). The analysis using SPEI calculated using rainfall and temperature of IMD gridded (1° × 1°) data for the period

1901-2010 highlights a rise in the intensity (decrease in SPEI value since 1951) and area of moderate drought which was mainly attributed to the significant increasing trend of mean temperature from mid-1970's (Kumar et al. 2013). Additionally, it is anticipated that the projected mean surface temperature may rise above 4.4^{o} by the end of the 21st century under the extreme scenario of greenhouse gas emission (Yaduvanshi et al. 2021). Warmer temperature will likely cause more frequent drought and increase in the incidence of extreme events in the twenty-first century. Cook et al. 2014 highlighted that assessment of the threat to the regional water resources arising out of multi-year drought will additionally require a critical understanding of the rise of evaporative demand and its trend caused by the increase in temperature with an increasing focus on precipitation decline and change in its characteristics.

3.2 Literature Review

Precipitation is a critical component of climate, as well as water balance and long-term change in its pattern or alteration in its frequency, which may have a positive or adverse effect in the region. Therefore, identifying trends in climatic variable such as rainfall, temperature, snowfall, evapotranspiration, etc., have received more focused attention over the past many decades.

Understandably, the long-standing history of interest in the assessment of the Indian Summer Monsoon(ISM) arises due to its immense importance to the largely agrarian economy of India and to address the concern arising out of deficient monsoon rainfall from the mid-sixties (Parthasarathy and Dhar, 1976; Parthasarathy and Mooley, 1978). The results from the statistical analysis of 105 years (1866-1970) do not find a significant change in mean rainfall between the two subseries, ranging between 1866 and 1917(first half) and the second half (1918-70). However, the hilly area (mountainous regions) due to the insufficient number of rain gauges were excluded in the past countrywide assessment of variability of ISM (June to September) based on 306 rain gage stations for a period of 108 years (1871-1978) over the country (Parthasarathy, 1984). Further, a new all-India monthly rainfall data series was developed for the twentieth century (1901-2003) based on 1476 rain gage stations of 36 meteorological subdivisions of the country which includes the hilly regions (Guhathakurta and Rajeevan, 2008). A thirty-year

periodicity (multi-decadal period) of deficient (drought) and surplus (flood) is marked in the century-long dataset. The ISM for the country as a whole lacks a significant trend but an observed decrease in rainfall in both annual as well as monsoon rainfall is apparent in the analysis for the state of Uttarakhand in 100 years. An important study for the state of Uttarakhand (Basistha et al. 2009) highlights a declining trend (26 out of 30 stations showing a decrease) over 79 years for the entire state of Uttarakhand with a change magnitude (as a percentage of mean) around -13.7% with the probable year of sudden shift around 1964. Alarmingly, a significant negative percentage of change is observed in five stations falling within the Pauri district (Bironkhal, Kotdware, Lansdowne, Pauri, and Srinagar) in both monsoon and annual series. Observation from the Hilly region of Uttarakhand throughout the last half a decade (1951-2008) highlights a substantial reduction in the contribution of low-intensity short duration, as well as the low-intensity long duration to total seasonal rainfall, was reported for Uttarakhand (Dash et al. 2011). A recent report (Guhathakurtha et al. 2020) based on the analysis of recent years (1989-2018) highlights that the district Pauri is having a significant decrease in rainy days, an increase in dry days, a significant decrease in SW monsoon rainfall as well as annual rainfall based on the analysis of 30 years of daily rainfall data.

As compared to the bountiful rainfall during the summer monsoon, winter precipitation contributes both in terms of rain and snowfall and holds equal importance for Rabi crops; horticulture crops, snow and glacier-fed streams, forested ecosystems of higher Himalaya, and the downstream regions. Important studies on winter rainfall distribution, climatology, and long-term trends (Yadav et al. 2012; Meher et al. 2018) report a statistically significant declining trend in winter rainfall over the western Himalaya. The contribution of winter precipitation accounts for almost 10 to 15% of annual rainfall for the western Himalaya. The long-term study for a period from 1902-2005 using 14 rain gauges over Uttarakhand reported declining rainfall over 104 years but with cyclical increase (decrease) over almost thirty years' period. The four stations (Bironkhal, Lansdowne, Kotdwar, Srinagar) located in the Pauri Garhwal district reported declining trends (-19.4 to -75.1 mm/104 years) of winter rainfall (Meher et al. 2018). An increase in winter temperature (Bhutiyani et al. 2007), as well as a decrease in the frequency of western disturbance (Kumar et al. 2015), are some of the reasons attributed to a

statistically significant decline in winter precipitation.

In the early 21st century, a series of interesting studies have emerged identifying the root cause of such a large-scale observation of widespread drying trends in monsoon rainfall amount as well as its characteristics. The ongoing escalation of the hydrological cycle due to global warming with an enhancement of the rate of evaporation and precipitation is being slowed down with the rising contribution of anthropogenic aerosol (mainly from Asia and other regions with heavy aerosol loading) with its competing effects causing reduced evaporation and subsequent decrease in rainfall (Ramanathan et al. 2005). The coupled atmospheric-ocean Global Climate Model(GCM) with all forcing ensemble, natural as well as anthropogenic (greenhouse gases, ozone, aerosol and landuse) captures well the observed drying trend over central India and attributed to aerosol which induced differential cooling, reducing the land-ocean surface temperature contrast and leading to weakening of monsoon circulation (Bollasina et al. 2011; Chung and Ramanathan, 2006). The study by Roxy et al. (2015) pointed to the role of the Indian Ocean warming over the past half a century in weakening the monsoon. The relatively subdued warming of the Indian subcontinent possibly caused by anthropogenic aerosols as compared to anomalous warming of the Western Indian Ocean (WIO) warming, could have played a key role in reducing the land-sea thermal contrast. The weakened land-sea thermal contrast slowed down the summer monsoon Hadley circulation, reducing the rainfall over the monsoon-dominated South Asian countries. Nonetheless, Jin and Wang (2017) revival observation of summer monsoon could be premature (Roxy, 2017) even though the authors present all the supporting evidence of monsoon revival due to the strengthening of land-ocean contrast since 2002 due to very strong warming (ranging from 0.1 to 1^{o}C per decade) of the entire Indian continent. Indeed, a very short period of observation of only over a decade (2002-2012) cannot conclusive indicate a sharp transition into the long-term revival of summer monsoon given some of the factors responsible for persistent drying remains unaltered.

3.3 Data used and study area

The Rugged Mountain of the Indian Himalayas is a region of complex relief and remains insufficiently gauged for various important hydrometeorological parameters. The low-

density conventional rain gauge network datasets represent the valley region or regions of easy access and suffer from a limited representation of ridge-top. Spatially interpolated gridded datasets generated from quality controlled station rainfall data such as IMD daily gridded rainfall data set over India (Pai et al. 2014) and Asian Precipitation-Highly Resolved Observational Data Integration Towards Evaluation of the Water Resources (APHRODITE) (Yatagai et al. 2012) provides an opportunity to evaluate the historical as well as recent space–time variability of the distribution of precipitation over the complex topography of Garhwal Himalaya. The applicability of gridded satellite-based rainfall estimates in the data scares region of Himalaya is demonstrated by several workers (Bookhagen et al. 2006; Khandelwal et al. 2015). The high spatial resolution gridded rainfall data at a spatial resolution 0.25° × 0.25° - IMD4 was created out of the highest density of rain gauge stations of 6955 with varying availability of periods representing high orographic regions more realistically. A similar product, Aphrodite daily precipitation data covering the whole of Asia for 57 years (1951-2007) and with improved accuracy for orographic precipitation is also recommended as a reliable database. Like precipitation, evapotranspiration is one of the dominant components of water balance but remains under-studied in mountainous regions. Remote sensing-based derived ET products provide some estimates but could suffer from high uncertainties (Miralles et al. 2016). The terrestrial evaporation estimate in the present study is derived from the Global Land Evaporation Amsterdam Model (GLEAM) which is based on a set of algorithms that separately estimate the different components of terrestrial evaporation (i.e. 'evapotranspiration') based on satellite observations of transpiration (*Et*), interception loss (*Ei*), bare-soil evaporation (*Eb*), snow sublimation (*Es*) and open-water evaporation (*Ew*) (Miralles et al. 2016; Martens et al. 2017). GLEAM v3.5b: a global dataset spanning an approximately 18-year period (2003–2020) of 0.25° × 0.25° resolution is used for the estimation of standard precipitation evapotranspiration index (SPEI) for assessment of drought vulnerability in the middle Himalaya watershed. *In-situ* rainfall measurements through ordinary rain gauge and tipping-bucket rain gauge were analysed for 2009-2019 in the two microwatersheds (Dugar Gad and upper Paidul) nested within the Irgad watershed (Figure 3.1).

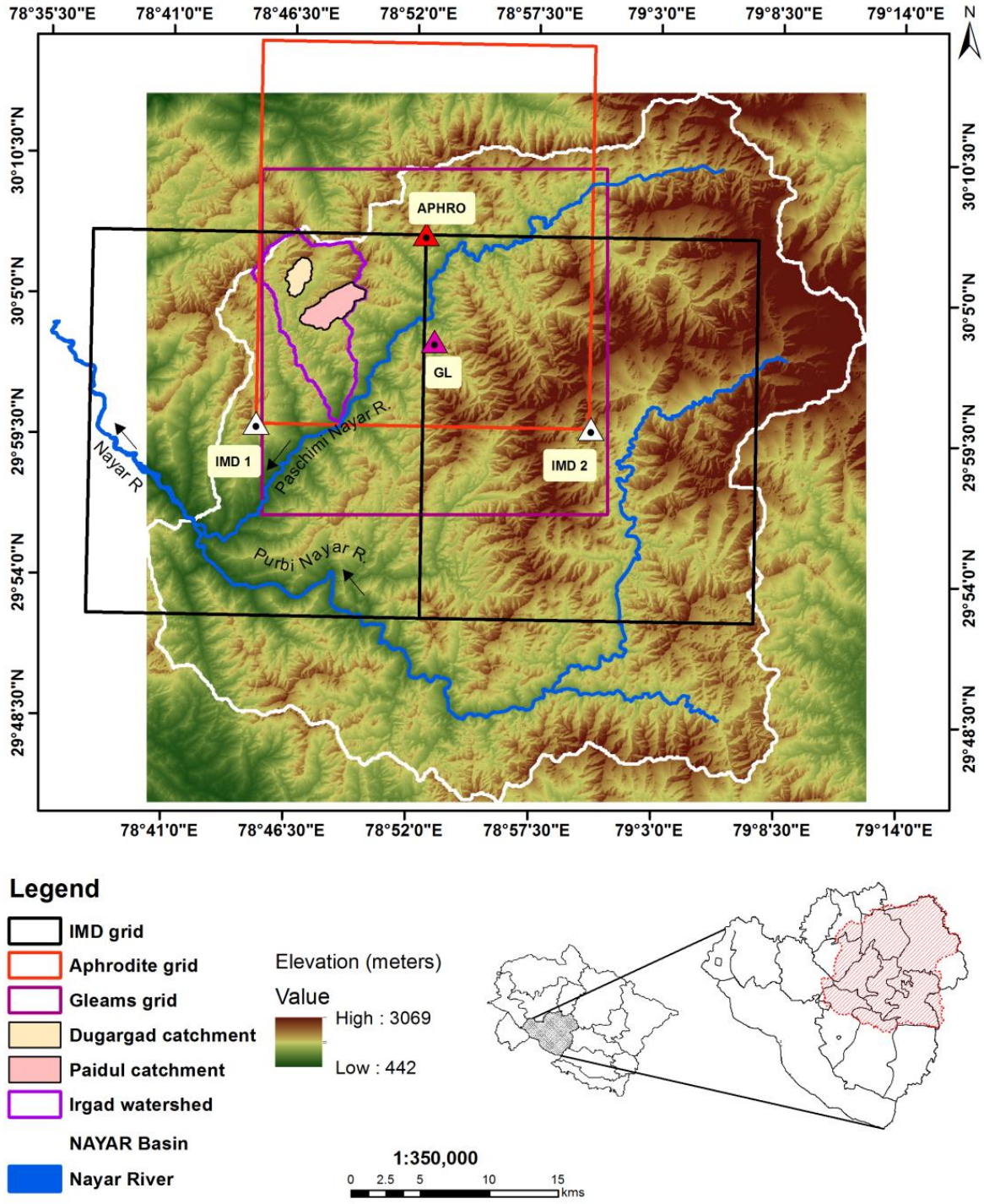

Figure 3.1: The study area map showing the location of two micro watersheds (Dugar Gad &upper Paidul) within the Irgad watershed which falls in the Nayar River basin of Middle Himalaya. The two rainfall IMD (0.25° × 0.25°) grids, one rainfall Aphrodite grid (0.25° × 0.25°) and Gleams grid for PET data set are shown in the topography map of entire Nayar basin. The Index map shows the regions of Pauri district covered by the Nayar River Basin.

3.4 Methodology

The new high spatial resolution (0.25° × 0.25°) long period daily gridded rainfall data set over India was procured from India Meteorological Department (IMD), Pune for assessment of historical long-term changes in the study area in Irgad watershed. The annual, seasonal and monthly rainfall time series for 1901-2018 using IMD4 gridded data set in two adjoining grids as well as one Aphrodite data grid (1951-2007) falling in the study area were analyzed for detecting trends by applying the statistical test like Man-Kendall trend test, Sen slope, Sequential Mann-Kendall test, Pettitt test, Buishand Rang test and Innovative trend analysis. The detailed theory of monotonic trend estimation can be found in Buishand, 1982; Kendall, 1975; Mann, 1945; Pettitt, 1979; Sen, 1968; Şen, 2012; Sneyers, 1990 and in an excellent review of trend detection technique by Sonali and Kumar, 2013. The theory of above-mentioned range of statistical tests is briefly explained in the subsequent section also. The time series data were checked for normality, and serial correlation (Hirsch and Slack, 1984). The normality of timeseries data were checked graphically by plotting the data in a Q-Q plot (Quantile-Quantile plot) as well as a histogram plot of rainfall data. The serial correlation or the autocorrelation of annual, seasonal and monthly timeseries data was evaluated for a lag of 1 day. Stationarity of the timeseries data was accessed by dividing the entire times series data into two subseries. The first subseries range over a period of 1901-1960 for a sixty-year time frame and the second subseries ranges from 1961 to 2018 for a fifty-eight year's time frame. Student's t-test for parametric data and Wilcoxon-Mann-Whitney Rank sum test for non-parametric data were applied to test the statistical properties of the two subseries and to accept or reject the null hypothesis that the mean or the median of each subseries is statistically equal (Figure 3.2). The rainfall variability index which is a measure of standardized rainfall departure from the mean was estimated for the monsoon period to categorize the time series rainfall data into years of wet, dry and normal periods (Machiwal and Jha, 2012). Cramer's test (WMO 1966) statistics were estimated for comparison of means of sub-series with the overall mean during the monsoon period for the entire rainfall time series data to assess the statistically significant decadal change. Two widely used estimates of drought vulnerability i.e. SPI (McKee et al. 1993) and SPEI (Vicente Serrano et al. 2010) were used in the present study. The SPI and SPEI

were estimated for 6 months and 12 months to assess the seasonal and multi-year drought (Kumar et al. 2013). The potential evapotranspiration data was downloaded from the website (www.gleam.eu) for a period of sixteen year period for the estimation of a standardized precipitation evapotranspiration index. The gridded data was processed through Grads and ArcGIS software for conversion of NetCDF data to tabular data. The trend analysis was performed through R software (R Core Team 2016).

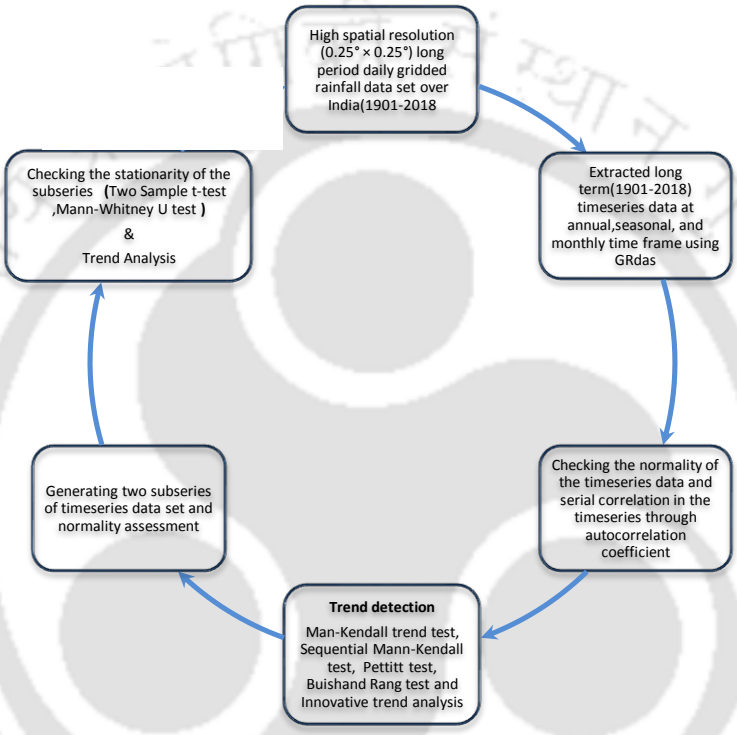

Figure.3.2: Methodology used for trend analysis of rainfall data (1901-2018).

3.5 Trend detection methods

3.5.1 Pettitt's test

This test, formulated by Pettitt (1979) is widely used to detect a single change-point in hydrological series or climate series with c $_{1\le k\le n}$ data. This is a non-parametric test, which is useful for evaluating the occurrence of abrupt changes in climatic records (Sneyers,1990). This test is more sensitive to breaks in the middle of the time series.

The non-parametric statistic is defined as:

$$K = \max \left| U_k \right| \tag{3.1}$$

The first step is to compute Uk statistic using the following formula

$$U_k = 2\sum_{i=0}^{n} \mathrm{m_i} - \mathrm{k(n+1)}, \tag{3.2}$$

where m_i is the rank of the ith observation when the values $x_1, x_2, \ldots, x_n$ in the series are arranged in ascending order and k takes values from 1,2, . . ., n.

When U_k attains maximum value of K in a series, then a change point will occur in the series. The critical value is obtained by:

$$K_\sigma = [-1n\sigma(n^3 + n^2)/6]^{1/2}, \tag{3.3}$$

Where K_σ is the maximum of absolute sums($|U_k|$), n is number of observations and α is level of significance which determines the critical value.

3.5.2 Sequential Mann–Kendall test (SQ-MK test)

The approximate year of the beginning of a significant trend can be determined from the SQ-MK test proposed by Sneyers,1990. The SQ-MK test sets up two series, a progressive one u(t) and a backward one u'(t). The series is rearranged based on the ranks of the original series. Prograde and retrograde series plots are generated as per Sneyers,1990. The point where prograde and retrograde series intersect will approximately indicate the possible point of change.

Herein, u(t) is the same as the z values that are found from the first to last data point. This test considers the relative values of all terms in the time series ($x_1, x_2, \ldots, x_n$). The following steps are applied:

The magnitudes of x_j annual mean time series (j = 1 . . . n) are compared with x_k, (k = 1. .

. j−1). At each comparison, the number of cases $x_j > x_k$ is counted and denoted by n_j.

The test statistic t is then given by equation:

$$T_j = \sum_{1}^{j} n_j \tag{3.4}$$

The mean and variance of the statistic are:

$$e(t) = \frac{n(n-1)}{4} \tag{3.5}$$

and

$$\text{var } t_j = \frac{j(j-1)(2j+5)}{72} \tag{3.6}$$

The sequential values of statistic u are then calculated as:

$$u(t) = \frac{t_j - e_{(t)}}{\sqrt{\text{var}(t_j)}} \tag{3.7}$$

The values retrograde series of u'(t) are computed backward, starting from the end of series. The beginning year of a trend could be located effectively with the sequential version of the Mann–Kendall test. The crossing of prograde and retrograde series of the curves showing the forward (u) and back-ward (u') represents the approximate time when a trend may have started.

3.5.3 Buishand Range Test for Change-Point Detection

The assumption related to the Buishand test is that the x comes from a normal distribution with average μ and a known variance σ^2. Assuming a change in the mean at time k and let x denote a normal random variate, then the following model with a single shift (change-point) can be given:

$$x_i = \begin{cases} \mu + \epsilon_i , & i = 1, \dots, m \\ \mu + \Delta + \epsilon_i & i = m+1, \dots, n \end{cases} \quad (3.8)$$

with$\epsilon \approx$ N (0, σ). The null hypothesis Δ = 0 is tested against the alternative Δ ≠ 0. In the Buishand range test (Buishand, 1982), the rescaled adjusted partial sums are calculated as

$$S_k = \sum_{t=1}^{k} (\mathrm{x_i} - x) \qquad (1 \le i \le n) \quad (3.9)$$

The test statistic is calculated as:

$$Rb = \frac{\max \mathrm{S_k} - \min \mathrm{S_k}}{\sigma} \quad (3.10)$$

The *p* value is estimated with a Monte Carlo simulation using m replicates.

3.5.4 Checking the normality of the time series data

To apply appropriate trend detection statistical test, it is important to decipher the normality of the time series data using both graphical and statistical methods. The parametric or the non-parametric approach to trend detection can only be deciphered by understanding the distribution of the time series data sets. In the present study Shapiro-Wilk test and Anderson-Darling test for normality in applied both on time series and subseries of data sets of a complete 118 years of daily rainfall derived from the IMD gridded data.

3.5.5 Shapiro-Wilk Test:

S-W test is being widely used statistical test to decide on whether the time series data set comes from a normal distribution.

The W statistic is calculated as follows:

$$W = \frac{\left(\sum_{i=1}^{n} a_i \, x_{(i)}\right)^2}{\sum_{i=1}^{n} (x_i - \bar{x})^2} \quad (3.11)$$

where $x_{(i)}$ ordered sample value and a_i is constant generated from means, variances and covariance of the order statistics of a sample of size ***n*** from a normal distribution. Departures of value of W from 1 indicate deviation from normality and if the significance value of the Shapiro-Wilk test is greater than 0.05, the data is normal.

3.5.6 Anderson-Darling Test

The Anderson-Darling test is another statistical test to check the normality of the population distribution. It is a modification of the Kolmogorov-Smirnov (K-S) which gives more weight to tails. The test statistics (A) is evaluated if the data ($y_1<y_2<y_3\ldots\ldots<y_n$) comes from a cumulative distribution function (CDF) F, is given as defined as:

$$A^2 = - n - S \tag{3.12}$$

where

$$S = \sum_{i=1}^{n} \frac{(2i-1)}{N} \left[\ln F(Y_i) + \ln\left(1 - F(Y_{N+1-i})\right)\right] \tag{3.13}$$

The value of A is computed is compared with the corresponding critical value of the theoretical distribution. The normality is accepted or rejected based on the value of A is greater or less than critical value.

3.5.7 Checking the stationarity of the time series

Stationarity of the hydrological data for two non-overlapping interval representing two subseries of a complete time series data should be investigated before applying trend detection statistical test. Two methods of finding out the stationarity of two subseries could be parametric and non-parametric approach. Independent Student's *t*-test parametric approach as well as Mann-Whitney Rank sum test falling into a non-

parametric method is applied in the present investigation of time series rainfall data set analysis.

3.5.8 Independent-test

The t test statistic value to test whether the means are different can be calculated as follow:

$$t = \frac{m_A - m_B}{\sqrt{\frac{s^2}{m_A} + \frac{s^2}{m_B}}} \tag{3.14}$$

S^2 is an estimator of the common variance of the two samples. It can be calculated as follow

$$S^2 = \frac{\sum(x - m_A)^2 + \sum(x - m_B)^2}{n_A + n_B - 2} \tag{3.15}$$

Once t-test statistic value is determined, you have to read in t-test table the critical value of Student's t distribution corresponding to the significance level alpha. The degrees of freedom (df) used in this test are:

$$Df = n_A + n_B - 2 \tag{3.16}$$

3.5.9 Mann-Whitney Rank Sum Test

The Mann Whitney U test or the Wilcoxon Rank Sum Test, is used to test whether two samples are likely to derive from the same population (i.e., that the two populations have the same shape). Some investigators interpret this test as comparing the medians between the two populations. The test on hypothesis testing presented techniques for testing the equality of median in two independent samples

3.5.10 Mann-Kendall test

Mann Kendall test is a statistical test widely used for analysis of the trend in hydrologic and climatologic time series. The Mann-Kendall test (Mann,1945; Kendall,1975) is a

non-parametric rank-based test. There are two advantages to using this test. First, it is a non-parametric test and does not require the data to be normally distributed. Second, the test has low sensitivity to abrupt breaks due to inhomogeneous time series.

Test statistic S is calculated as

$$S = \sum_{i=1}^{n-1} \sum_{j=i+1}^{n} \text{sgn}(x_j - x_i) \tag{3.17}$$

here, x_i andx_j are the sequential data values, n is the length ofthe data set and

$$\text{sgn}(t) = \begin{cases} 1, & for\, t > 0 \\ 0, & for\, t = 0 \\ -1, & for\, t < 0 \end{cases} \tag{3.18}$$

The value of S indicates the direction of trend. A positive (negative) value indicates rising (falling) trend. Mann-Kendall has documented that when n≥8, the test statistic S is approximately normally distributed with mean and variance as follows:

$$E(S) = 0 \tag{3.19}$$

$$Var(S) = \frac{1}{18}\left(n(n-1)(2n+5) - \sum_{i=1}^{m} t_i(t_i - 1)(2t_i + 5) \right) \tag{3.20}$$

The standardized test statistics Z_{mk} is computed as follows

$$Z_{mk} = \begin{cases} \dfrac{S-1}{\sqrt{Var(S)}}, & for\, S > 0 \\ 0, & for\, S = 0 \\ \dfrac{S+1}{\sqrt{Var(S)}}, & for\, S < 0 \end{cases} \tag{3.21}$$

Positive values of Z indicate increasing trends while negative Z values show-decreasing trends. Testing trends is done at the specific α significance level. When $|Z| > Z_{1-\alpha/2}$, the null hypothesis is rejected and a significant trend exists in the time series. $Z_{1-\alpha/2}$ is obtained from the standard normal distribution table.

The statistic S is closely related to Kendall's τ as given by:

$$\tau = S/D \tag{3.22}$$

$$D = \left[\frac{1}{2}n(n-1) - \frac{1}{2}\sum_{j=1}^{p} tj(tj-1)\right]^{\frac{1}{2}} \left[\frac{1}{2}n(n-1)\right]^{\frac{1}{2}} \tag{3.23}$$

The Mann-Kendall statistical test has been frequently used to quantify the significance of trends in hydro-meteorological time series (Yue et al. 2002). Trend magnitude is estimated using a nonparametric median based slope method proposed by Sen, 1968 and extend by Hirsch et al. 1982 as given below:

$$\beta = median\left[\frac{xi - xj}{i - j}\right] for\ all \quad i < j \tag{3.24}$$

Where, 1<k<j<n. β is median of all possible combinations of pairs for the whole data set.

3.6 Drought Index

3.6.1 Rainfall variability Index

The long-term time series data can be segmented into regimes of 'very dry climate year', 'normal climate year', 'wet climate year', 'very wet climate year' etc., using standardized rainfall departure which is estimated as

$$\delta i = (Pi - \mu)/\sigma \tag{3.25}$$

where δi is the rainfall variability index for a particular year i, Pi annual rainfall for year

i, and mean (μ) and standard deviation (σ) of annual rainfall for the entire period under investigation. The normal rainfall years are having values of δ within ± 0.5 and values > 0.5 to < 1 are classified as wet years whereas values > 1 represents 'very wet year'. Similar logic is followed for classifying the deficient rainfall years into dry and very dry years with values falling in the negative range.

3.6.2 Standard Precipitation Index (SPI) and standardized precipitation evapotranspiration index (SPEI)

Standardized Precipitation Index (SPI) is one of the simplest and temporally flexible index which is widely used for monitoring the onset as well as the progress of the drought event and requires a long-term monthly precipitation dataset for more than 30-year (Mckee et al. 1995). The Palmer Drought Severity Index – PDSI (Palmer, 1965) on the other hand requires additional inputs of temperature as well as local antecedent soil moisture including precipitation data and lacks temporal flexibility (9 and 12 months only). The PDSI is believed to be more appropriate for the assessment of agricultural-related impacts than hydrological impacts. The SPI due to its use of variable time steps (1-month to 36 months or 48 months) can detect short-term water supplies concern such as soil moisture deficit as well as long-term water resources issues such as depleting groundwater aquifer water levels or streamflow. As the time lag in the manifestation of drought or water deficits differs and has different accumulation times for different drought types such as hydrological, environmental, agricultural, and meteorological, etc. SPI has an apparent advantage over other indexes as it is calculated at different time-scale. SPI quantifies the precipitation deficit or surplus at multiple timescales and requires prolonged time series of at least thirty years or more to have statistical confidence in the probability of estimates. The rainfall data is fitted to gamma distribution and further fitted to gamma cumulative probability and is transformed into normal distribution so that the mean and standard deviation becomes equal to 0 and 1 respectively. Normalized precipitation with positive SPI values is indicative of greater than median precipitation, whereas negative values indicate less than median precipitation. The details of the computational method as well as the limitation are discussed in McKee et al. 1993 and McKee et al. 1995. Most importantly, the intrinsic

assumption associated with the Standardized Precipitation Index (SPI) is that the variability in precipitation is much higher as compared to any other factors such as temperature, evapotranspiration, wind speed, and soil water holding capacity and assumed to be static which may be true in some climatic conditions only. The SPEI on the other hand includes the effects of temperature variability as well as precipitation data on drought (Table 3.1). The SPEI calculates the difference between precipitation(P) and reference evapotranspiration (ET_0) giving a measure of climatic water balance and is considered to be a better measure of drought severity (Beguería et al. 2014).

The procedure for the calculation of SPEI is similar to SPI but is adjusted to a log-logistics probability distribution. The climatic regions are witnessing a higher demand for water due to an increase in evapotranspiration under warming conditions; SPEI is a more appropriate tool for the assessment of drought severity (Vicente-Serrano et al. 2010).

The study in Northern China Plain by Wang et al. 2015 compared the applicability of three drought indices (sc-PDSI, SPI, and SPEI) in their respective performance in the evaluation of typical historical droughts. The finding suggests that the drought indices detect drought but portray a different picture of drought severity and its duration. Drought impacts estimation through indices depends on the cumulative time of assessment (three-month or six-month) as well as specific dominant factors like deficiency of rainfall or higher air temperature causing higher evaporation decide the appropriateness of particular indices like SPI or SPEI.

Table 3.1: Drought categorization based on SPI and SPEI values

SPI /SPEI Values	Drought Category
≥ 2	extremely wet
1.5to 1.99	very wet
1 to 1.49	moderately wet
0.99 to -0.99	mild drought
-1.00 to -1.49	moderate drought
-1.50 to -1.99	severe drought
≤ -2.0	extreme drought

3.7. Results and Discussion

3.7.1 Long-term annual and seasonal rainfall variability and drought analysis

Gridded rainfall analysis of two adjoining grids in the study area indicates an average 74% contribution during the SW monsoon (JJAS) months. Gridded rainfall data show almost equal contribution during the Pre-monsoon (MAM) and winter period(DJF) of 10-12% and 2-4% during the post-monsoon (October, November) from the long-term average annual rainfall of 1100-1200 mm rainfall for 1901-2018. The average four months of monsoon rainfall is close to 850 mm, three months of winter rainfall is around 130 mm, whereas the post-monsoon contribution is around 35 mm. No significant change in the percentage of contribution is observed in the monthly subset dataset for 1901-1960 and 1961-2018. All India estimates (Guhathakurta and Rajeevan, 2008) of the seasonal contribution based on area-weighted rainfall of 36 meteorological subdivisions of India show an almost similar proportion of seasonal contribution. The Aphrodite data over the study area also showed similar values of annual and seasonal contribution. The percentage change of the mean following an approach used in Basistha et al. 2009, for annual, and monsoon periods over 118 years by approximating a linear trend and median slope indicate a nominal change (-) 6 to 8 %. But a very significant change magnitude as a percentage of the mean of (-) 40% is recorded for the winter period precipitation record over 118 years.

Precipitation departure from the mean was assessed through the rainfall variability index. The rainfall data of more than a centennial period indicate nearly 39% of normal years, 31 % of wet years and 30% year of dry and very dry years. Interestingly, the second half of the rainfall time series revealed an almost 50% increase in the frequency of dry years and an approximately 20% reduction in the incidence of normal years as compared to the first part of the subseries (1901-1960) of the twentieth century. However, the percentage of incidence of wet years has remained the same. The Aphrodite data showed a 36%

incidence of dry years for years between 1961 and 2007.

The twelve months SPI index for the entire span of 118 years indicates 74% of near-normal occurrence whereas nearly equal percentage of wet and dry month occurrence (Figure 3.3a). However, a significant decrease in the near-normal twelve months SPI index as well as an increase in dry months, marked by a substantial rise of severe and extreme dry months is observed in the second half of the twentieth century and early twenty-first century. The heat map (Figure 3.4) facilitates the visualization of the period of 1902-1960, largely dominated by normal rainfall months and with very infrequent occurrence of deficient rainfall during years i.e. 1903, 1904, 1939, 1940, and 1960. The years beyond the 1960's are more frequented with deficient rainfall i.e. 1968-1969, 1971-1974, 1980-1981, & 2008-2009. Interestingly, IMD-2 grid SPI values showed a very pronounced multi-year drought period over 1996-2003 with extreme drought SPI (≤ -2.0) dryness categories is recorded. This period is represented by normal and mild to moderate drought years in the IMD-1 grid. Pai et al. 2011 estimated the district-wise drought occurrence based on SPI for the 1901–2003 period and found several districts of Uttarakhand showing significant negative trends as well as falling into moderate drought category.

A period from 2003-2018(16 years) of SPEI value shows a more frequent occurrence of mild to moderate drought (SPEI value -0.5 to -1.5) till 2010 and subsequent years of normal rainfall years with mild drought (Figure3.3b). The increasing drought intensity was observed from 1951 to 2010 with more incidence of multi-year drought with an increase in the area impacted by moderate drought using a 1^{o} X 1^{o} gridded IMD dataset of rainfall and air temperature (Kumar et al. 2013). No significant difference can be marked in drought detected by twelve-month SPEI and SPI. No observed difference in the measure of drought severity and almost similar start and end of drought period can be observed in SPEI and SPI graphs for 16 years (Figure 3.3).

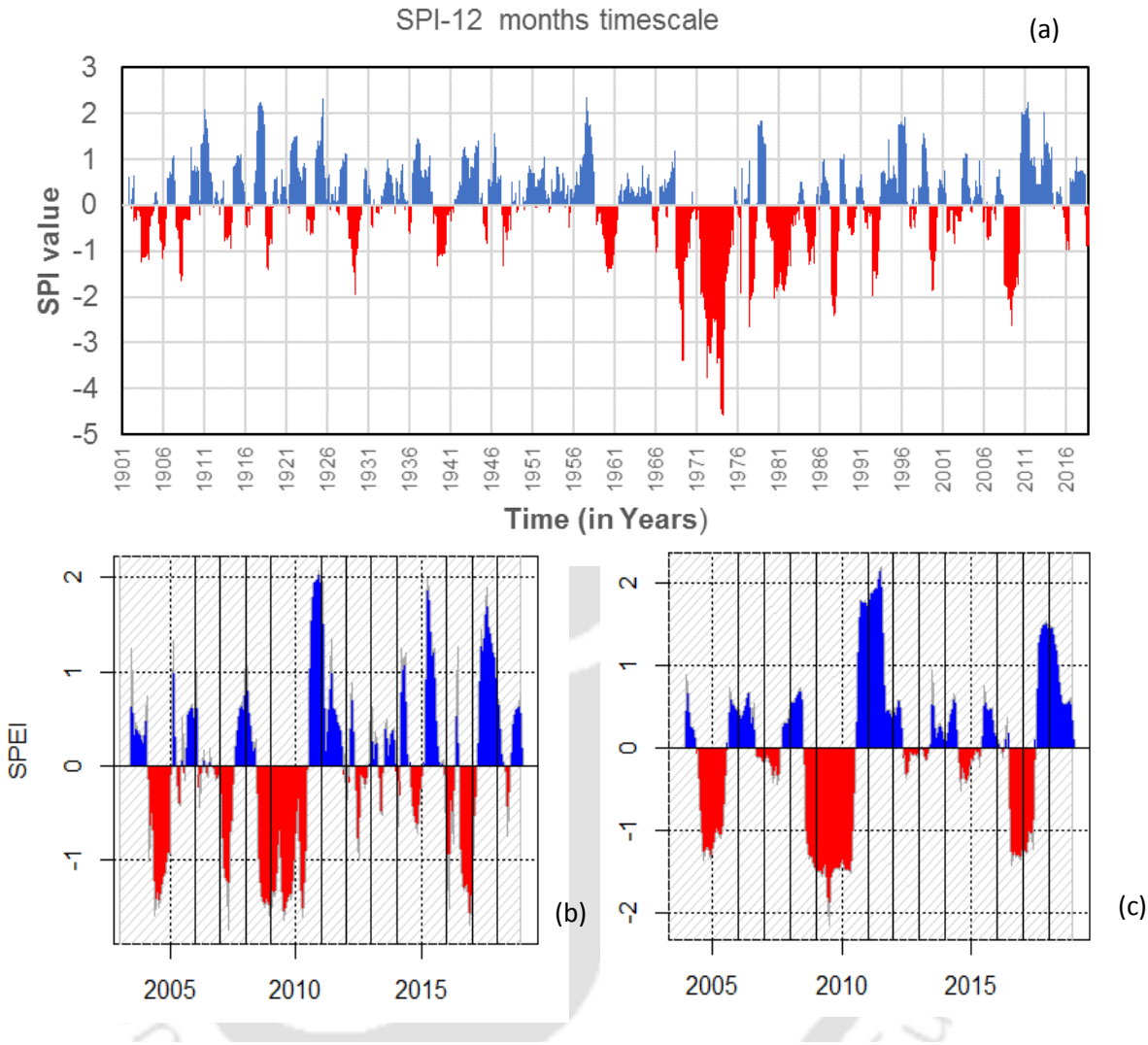

Figure 3.3: The graphical representation(a) of 12 months SPI (standard precipitation Index) for 1902-2018 period using the IMD (0.25° × 0.25°) gridded rainfall time series highlights the rise in frequency of droughts beyond the period of 1960's in the second half of twentieth century. The SPEI for 6(b) and 12(c) months accumulation period for a time series of 2003-2018 also show dominance of moderate drought in the early part of twenty first century.

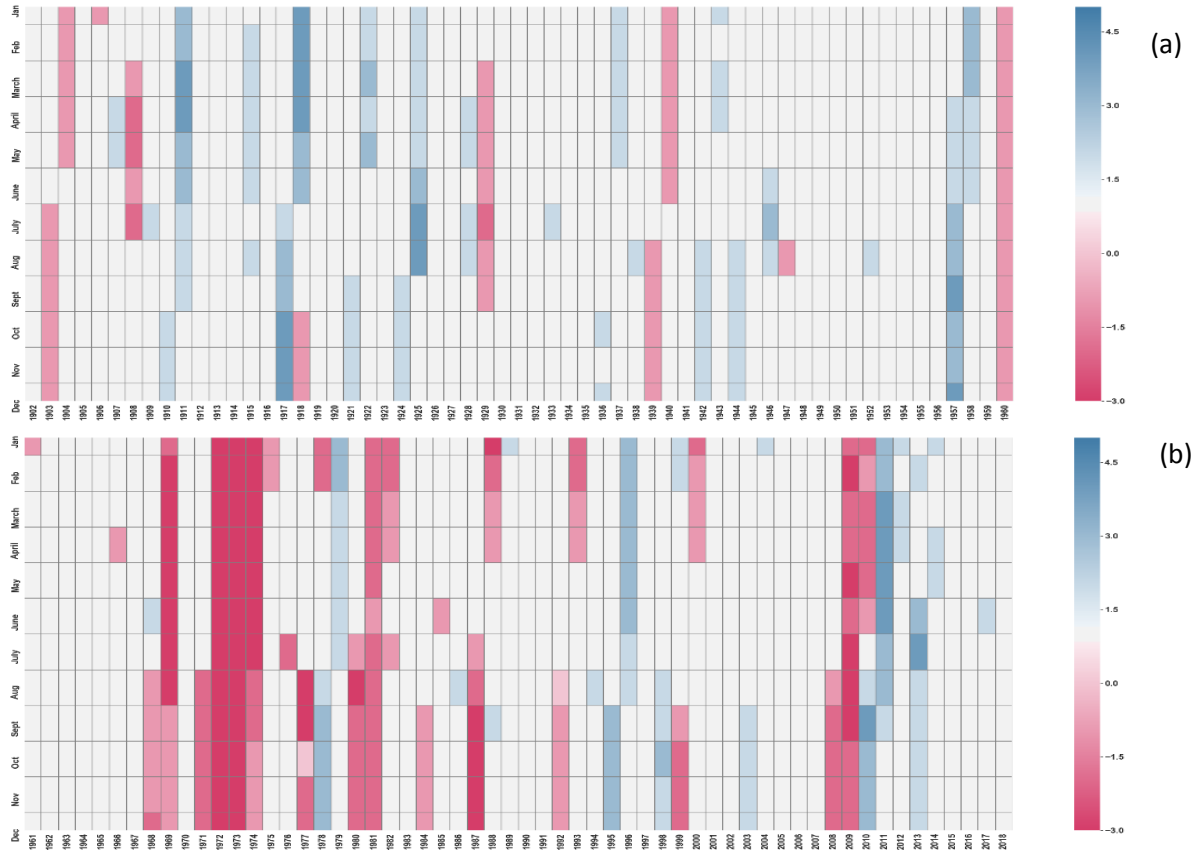

Figure 3.4: Heat map generated using 12-months SPI index data clearly depicts that the first subseries(a) is marked with dominance of normal rainfall years whereas the second time sub-series(b) is dominated by moderate drought years. The shades of red represent the negative SPI values whereas the shades of blue represent the positive SPI numbers.

Cramer's test statistics of decadal averages monsoon period (11 decades and a single eight-year block) (Table 3.2) compared with mean monsoon months(JJAS) of the complete time series highlights the decade of 1971-1980 show a statistically significant decline at 95% confidence level whereas rest of the test statistics are not statistically significant. The highest average mean is 97.27 cm for the eight-year period (2011-2018) and the lowest is 67.34 cm for the decade 1971-1980. Table 3.2 shows that the decades till 1950 are almost dominated by increase whereas the decades beyond 1950's record mostly negative change. The test statistics partly agree with some of the decades of all India estimates of decadal average till 1970 (Parthasarathy and Mooley,1978).

The number of rainy days observed from the IMD gridded data in the study area indicates a median value of 68 days with values as low as 35 days (1973) to as high as 101days

(1917) during the drought and wet years. No significant shift in the average rainy days is observed between the two subsets (1901-1960 & 1961-2018) timeseries data. The observation does not vary much in terms of rainy days in the two grids (IMD 1& IMD 2) falling in the study area. However, the year 1969 only records 14 rainy days (58.2 cm) during the four monsoon months observed in the gridded cell -IMD 2. The winter period (DJF) is marked by the median value of 13 rainy days, with a minimum value of no rainfall (1976) to a maximum value of 28 rainy days (1905). An important study (Meher et al. 2018) using long-term station rainfall data in Uttarakhand highlights a significant decrease in the number of rainy days with an area average mean number of rainy days of around 7 days during winter(DJF) and a decline ~ 4 to 6 days/35 years for a long-term station records during 1902-2005.

Table 3.2: Results of Cramer's test with other statistical parameters for each standard decades in the complete time series of rainfall data set basedon IMD 0.25° × 0.25° gridded database.

Decade(n*)	Mean(cm)	SD(cm)	Cramer's test statistics(t_k)	Diff. of decadal mean from the overall average
1901-1910(10)	81.13	21.52	-0.365	-2.681
1911-1920(10)	87.70	22.95	+0.530	3.885
1921-1930(10)	92.46	25.53	+1.185	8.645
1931-1940(10)	84.95	15.14	+0.155	1.136
1941-1950(10)	92.01	15.70	+1.123	8.197
1951-1960(10)	81.04	17.77	-0.379	-2.779
1961-1970(10)	83.60	19.36	-0.030	-0.219
1971-1980(10)	67.34	36.08	-2.296*	-16.479
1981-1990(10)	73.06	22.14	-1.478	-10.749
1991-2000(10)	85.30	25.78	+0.202	1.485
2001-2010(10)	82.61	33.61	-0.164	-1.204
2011-2018(8)	97.27	20.94	+1.664	13.453

n = number of years and * 5% level of significance with average overall monsoonal mean (1901-2018) is 83.81 cm

The annual, monsoon and winter period graphs (Figure 3.5 a, b and c) clearly show the spread of rainfall around the 10-year moving average curve and the overall average rainfall line over the complete time series of IMD gridded rainfall data. The contrasting period can be segmented into blocks of normal to above-normal rainfall period and time blocks of below-average rain. The time window of above or near average rainfall is the period during which the 10-year moving average hovers around the long-term average and is represented from 1901 to 1965. A sudden downward shift in the moving average curve below the long-term average rainfall line is noticed afterward for a period till the late twentieth century. Subsequently, a near-average annual and monsoonal rainfall is marked in the 10-year moving average curve in the early part of the twenty-first century. It is interesting to note that the 10-year moving average curve remains mostly below the long-term average line during the winter period of 2000-2018. A similar observation is recorded for the Aphrodite gridded rainfall data for the study area region for 1951-2007. The period of transition from above-average rainfall to below-average rainfall has now shifted to the early 1970's and late 1970's in the annual and monsoon rainfall records respectively. Surprisingly, the 10-year moving average rainfall data mostly follows the long-term average winter rainfall (116 mm) with a decline in the early 21st century. Such an observation of the rising frequency of drought is reported from Nepal (Hamal et al. 2020), and especially from the western part of Nepal adjoining Uttarakhand (Wang et al. 2013).

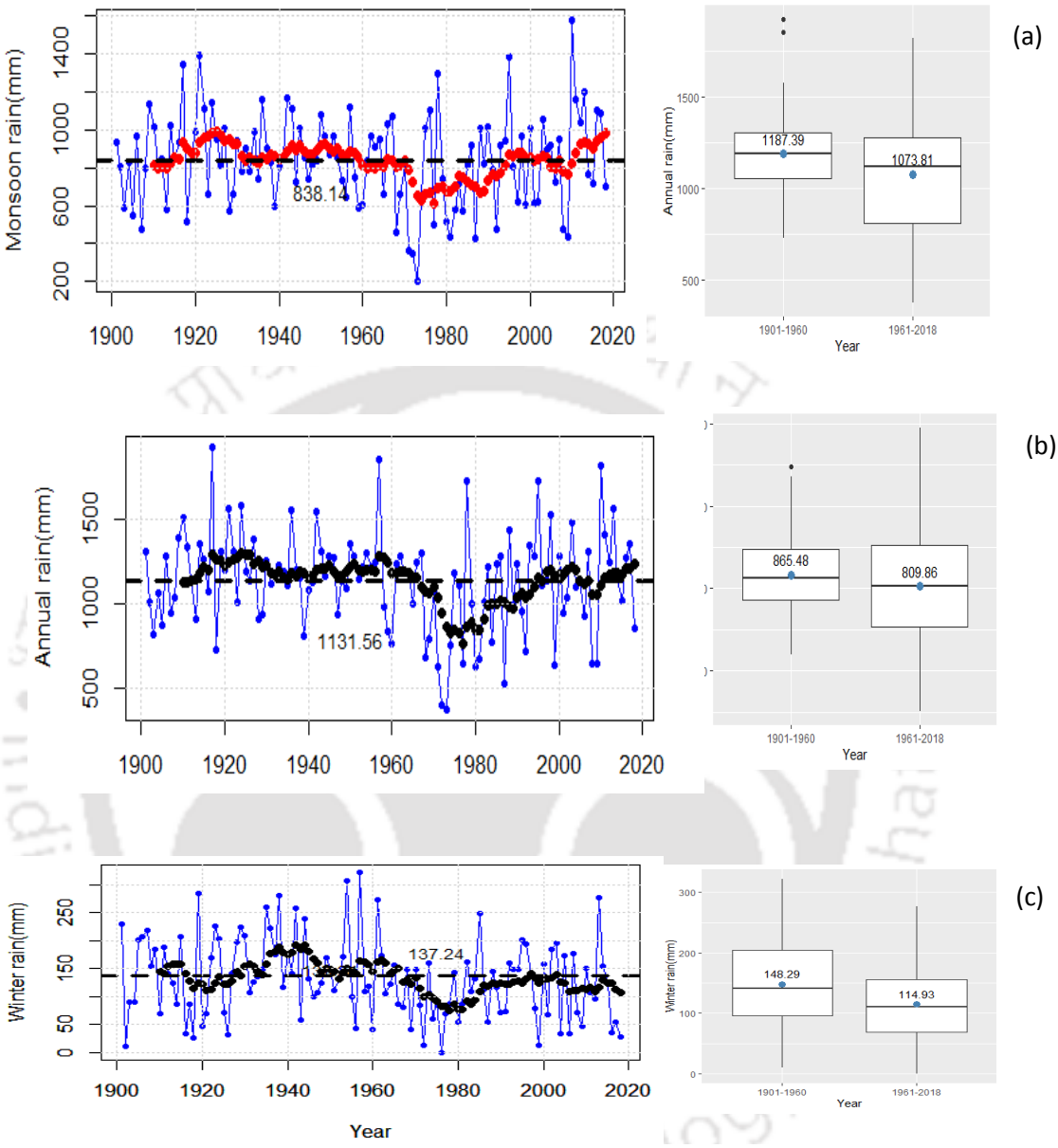

Figure 3.5: The annual (a), monsoon (b) and winter(c) time series plot with ten years moving average curve (dotted line) and complete mean of the time series (dash line) reveal the long-term trends with varying phases of rise and decline with intervening period of normal rainfall with an abrupt decline beyond 1965.The boxplot showing the mean value (figure above the blue dot) and median mark in the two sub-series points towards a decline in the second half of the time series (1961-2018).

3.7.2 Trend analysis of rainfall timeseries

Trend detection in long-term data could be misleading and requires an understanding of the distribution and serial correlation of data series. The graphical assessment of the time series data through Quantile-Quantile and histogram plot visually agrees well with the normal distribution plot during the monsoon and winter season but deviation from the normal distribution in the distribution of time series data in the annual plots. The result of the statistical test for normality using the Shapiro-Wilk and Anderson-Darling statistical test also highlights the same observation, although the S-W test indicates a normal distribution for the annual time series rainfall data as the p-value was found to be greater than 0.05 at 95% confidence interval. The Anderson-Darling statistical test disproves the normality of distribution at a 95% confidence level. The autocorrelation coefficient plots do not indicate serially correlated timeseries data for annual, seasonal and monthly time series except for the post-monsoon period and month of October. The most significant change point was obtained by using the Buishand range test, Pettitt test and Sequential Mann-Kendall test. The results of Pettitt test and Buishand range test point towards a similar break year i.e. 1958 to 1967 for the annual, monsoon and winter data series (Figure 3.6a). However, an early crossover point around the year 1950 is marked in the progressive and backward series in the Sequential Mann-Kendall test for annual and monsoon periods (Figure 3.6b). But the winter series show identical break year results as with the other two statistical tests. The IMD-2 grid data show an identical result of break years during the annual, monsoon and winter timeseries in all three tests i.e. the year of abrupt change is around 1965. These results of break years are in agreement with Basistha et al. 2009 for annual and winter rainfall over Uttarakhand as well as Pettitt test results for the winter period shift year for station rainfall data of Pauri Garhwal (Meher et al., 2018). The widely investigated non-parametric Mann-Kendall trend analysis of annual, seasonal and monthly time series rainfall data points toward a declining trend (negative Z_{mk} and negative Sen's Slope value) in annual, seasonal as well as monthly time series except for the month of pre-monsoon months of March and April as well as post-monsoon months of September and November which are showing a rising trend (Table 3.3). But the statistical results of trend analysis are only significant for January and the

winter period (DJF) (Table 3.3). The IMD-2 grid data almost show similar results of decline in all the annual and seasonal data but positive Z_{mk} values can be observed in March, April, July, August, September and November. The trend is statistically significant during the winter as well as in August month. The statistically significant winter period (DJF) rainfall showed a decline which is as severe as 47-54mm/100 years. The results from the closest station data at Lansdowne indicate a decline of -19.4mm/104 years (Meher et al. 2018). The trend estimates using the Aphrodite data also suggest a decline in the annual and seasonal rainfall except for the pre-monsoon period for the data series period of 56 years (1951-2007). The annual and post-monsoon decline is statistically significant at 0.05 and 0.1 levels of significance. However, Mukherjee et al. 2015 did not find statistically significant trend in the central and western Himalaya with the seasonal average estimate of rainfall from the Aphrodite data.

The Innovative trend analysis also suggests a decline in the second half of the sub-series i.e. between 1961-2018 period in rainfall both in annual and seasonal time slots as the data points are falling below the 1:1 line. The winter period is showing a monotonic decline. The plot of both the annual and monsoon time series reveals non-monotonic decline, no trend and increase at different periods as the data points hover around the line of no trend (1:1 line) (Figure 3.7c).

The two non-overlapping subseries from the complete time series data were further assessed for their stationarity using both parametric and non-parametric tests i.e. independent t-test and Mann-Whitney U test. The annual mean of 1187mm for the period 1901-1960 and a decline in mean annual rainfall is observed (1072mm) between 1961-2018 (Table 3.4). The monsoon period in both subseries shows a nominal decline but the winter period decline in rainfall was statistically significant (Table 3.3).

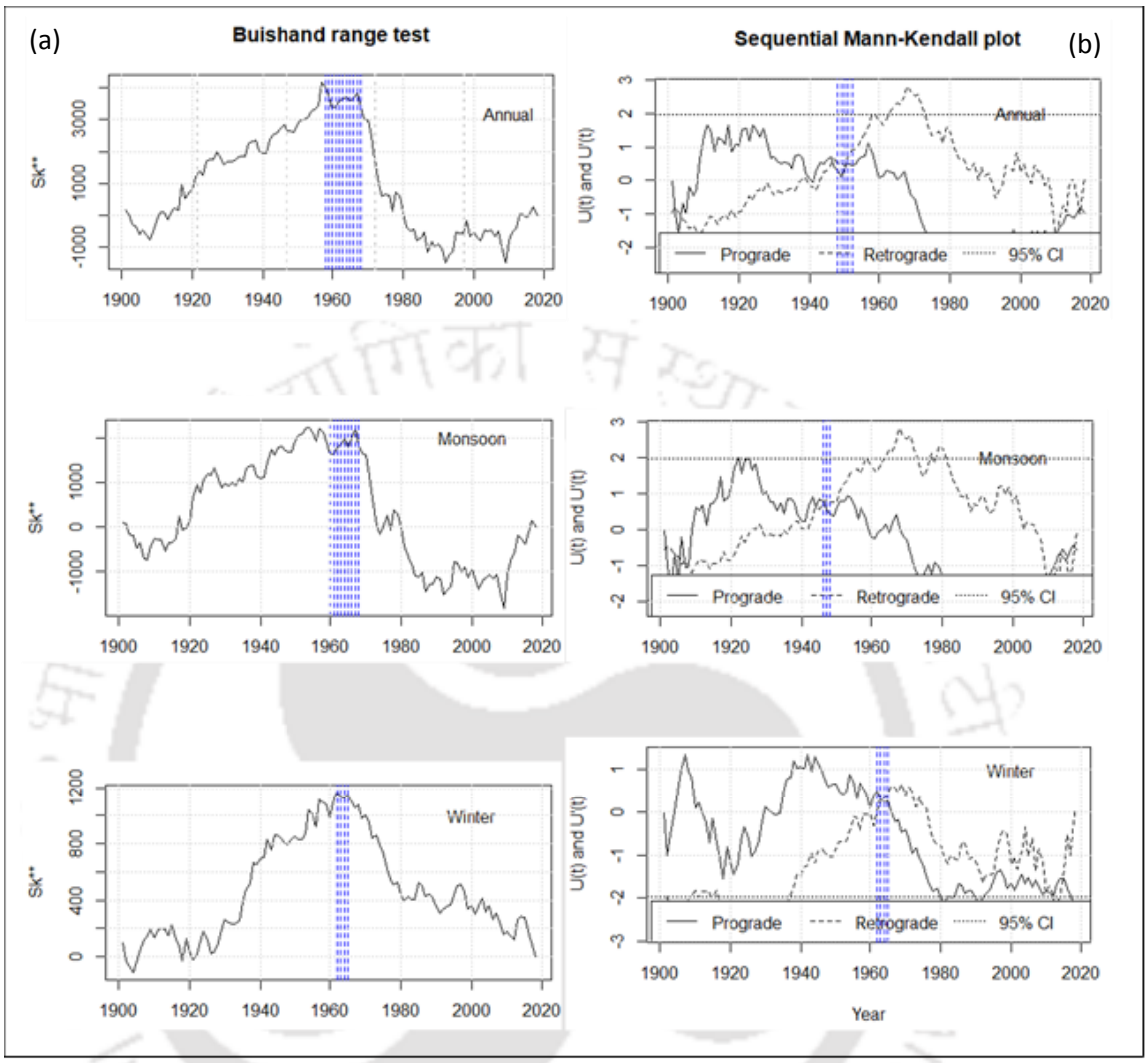

Figure 3.6: Buishand range test (a) and sequential Mann-Kendall test (b) for the annual, monsoon and winter time series data with probable break years' region (highlighted in blue dash line) showing an overall decline in the rainfall during the period 1961-2018.

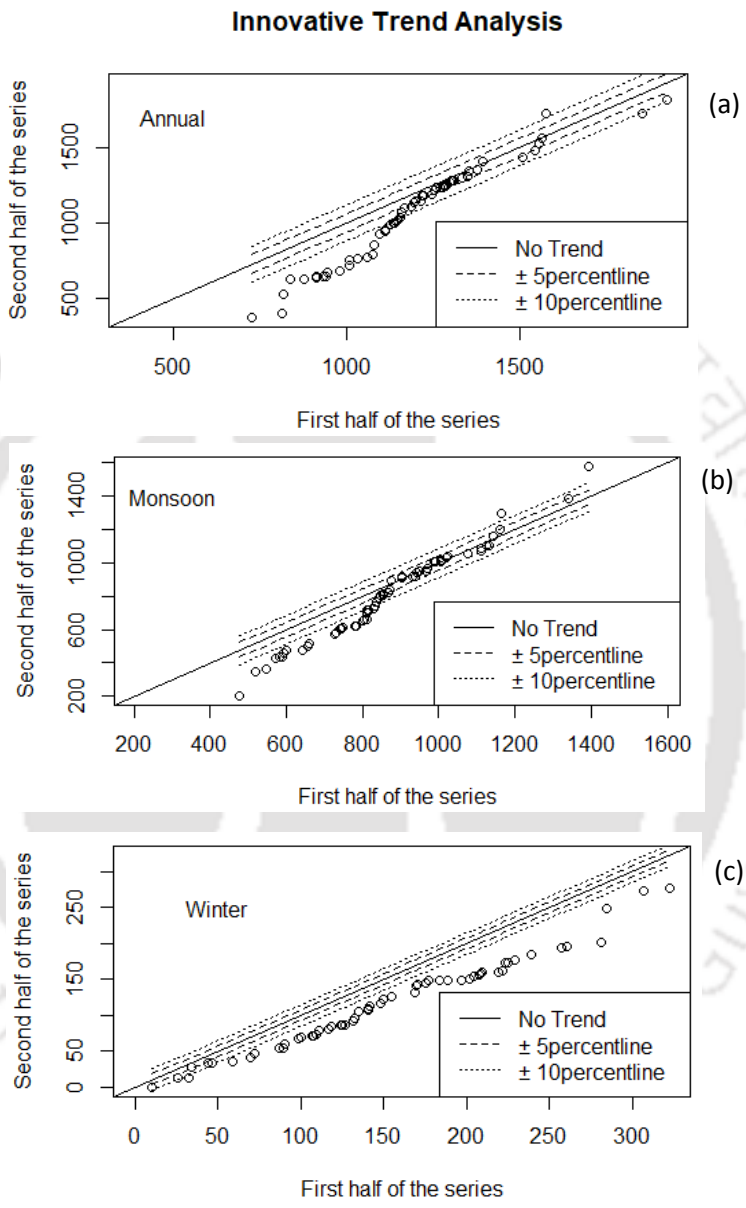

Figure 3.7: Innovative trend analysis results highlighting a decreasing trend in annual (a), monsoon (b) and winter (c) in the second half of the subseries (1961-2018) with respect to 1:1 line.

Table 3.3: The results of Mann-Kendall trend analysis of annual, seasonal and monthly time series precipitation data based on IMD 0.25° × 0.25° gridded database over the study area

IMD high spatial resolution(0.25°×0.25°) daily gridded rainfall data set (1901-2018)									
Time series	Zmk	n	p-value	S	varS	tau	Sen's slope	Lower Sigf.	Upper Sigf.
Jan	-2.0445	118	0.0409	-8.800000e+02	1.848373e+05	-1.275455e-01	-0.2292056	-0.472342307	-0.0064
Feb	-0.3582	118	0.7202	-1.550000e+02	1.848423e+05	-2.246051e-02	-0.03663541	-0.2960192	0.1781
March	0.088386	118	0.9296	3.900000e+0	1 1.848423e+05	5.651355e-03	0.007691249	-0.1712965	0.1875
April	1.2561	118	0.2091	5.410000e+02	1.848017e+05	7.849691e-02	0.07409283	-0.03594498	0.1918
May	-1.0234	118	0.3061	-4.410000e+02	1.848450e+05	-6.389452e-02	-0.09560037	-0.29217179	0.0979
June	-0.0023	118	0.9981	-2.000000e+00	1.848460e+05	-2.897501e-04	-0.001600352	-0.4186935	0.3657
July	-0.74197	118	0.4581	-3.200000e+02	1.848460e+05	-4.636001e-02	-0.2336789	-0.7899723	0.3772
Aug	-0.70941	118	0.4781	-3.060000e+02	1.848460e+05	-4.433176e-02	-0.2308517	-0.8841360	0.4523
Sept	0.16979	118	0.8652	7.400000e+01	1.848460e+05	1.072075e-02	0.04777992	-0.3934448	0.4974
Oct	-0.97174	118	0.3312	-4.180000e+02	1.841500e+05	-6.123581e-02	-0.01352385	-0.08946037	0.0145
Nov	0.16832	118	0.8663	7.100000e+01	1.729550e+05	1.120058e-02	0	0	0
Dec	-1.352	118	0.1764	-5.800000e+02	1.834133e+05	-8.560482e-02	-0.02877339	-0.125209120	0.0014
Annual	-1.035	118	0.3007	-4.460000e+02	1.848460e+05	-6.461427e-02	-0.7715543	-2.296228	0.7176
Monsoon	-0.56055	118	0.5751	-2.420000e+02	1.848460e+05	-3.505976e-02	-0.39438	-1.6214964	0.9677
Winter	-2.2631	118	0.02363	-9.740000e+02	1.848460e+05	-1.411083e-01	-0.4723071	-0.87383752	-0.0657
Post-monsoon	-1.4751	118	0.1402	-6.350000e+02	1.847210e+05	-9.229703e-02	-0.0671086	-0.18224179	0.0123
Pre-Monsoon	-0.32795	118	0.7429	-1.420000e+02	1.848460e+05	-2.057226e-02	-0.04424865	-0.3959199	0.3008

Table 3.4**:** The normality test using Shapiro-Wilk and Anderson-Darling statistical test for precipitation series (1901 – 2018) based on IMD gridded database.

Time series	IMD high spatial resolution(0.25°×0.25°) daily gridded rainfall data set (1901-1960),				IMD high spatial resolution(0.25°×0.25°) daily gridded rainfall data set (1961-2018),						
	MK trend (n=60)		Sen's slope estimate		MK trend (n=58)				Two Sample t-test/ Mann-Whitney U test		
	Z	*p-value*	Sen's slope	*Mean*	*Z*	*p-value*	Sen's slope	*Mean*	*t/W*	*df*	p-value
Annual	0.070157	0.9441	0.115	1187.392	1.4825	0.1382	3.415	1072.121	2.1738 2080	103.57	0.032 0.06762
Monsoon	-0.19772	0.8433	-0.432	865.479	1.4959	0.1347	3.725	811.473	1.2183	103.28	0.2259
Winter	0.082913	0.9339	0.053	148.2941	-0.50311	0.6149	-0.250	114.2508	2.6627	116	0.008854

Table 3.5: The results of stationarity analysis of two subseries of time series data for period of 1901-1960 &1961-2018 using parametric and non-parametric approach as well as results of Mann-Kendall test statistics and Sen's slope

IMD high spatial resolution(0.25°×0.25°) daily gridded rainfall data set (1901-2018)			
Shapiro-Wilk normality test		Anderson-Darling normality test	
W	*p-value*	*A*	*p-value*
0.98151	0.1042	0.93059	0.01764
0.9935	0.8604	0.23172	0.7975
0.97995	0.07502	0.45431	0.2651

3.8 Conclusion

Over the last four to five decades reports of the diminishing supply of water from the springs and streams are emerging from the middle mountains of the Himalayan region. To understand the reasons for such a widespread diminishing flow in local water resources, the trends in the historical changes in the rainfall as well as evaluation of the recent changes through the analysis of quality-assured gridded rainfall data falling in the study area was attempted. The percentage change of the mean highlights a very significant magnitude of change of –40 percent in the winter period whereas the annual and monsoon periods showed a nominal decline of 6 to 8 percent change of mean over 118 years of IMD gridded rainfall data from the study area. Almost fifty percent increase in the frequency of dry years and a 20 percent reduction in the normal years can be observed between 1961-2018 as compared to the subseries of 1901-1960. The results from the rainfall variability index and 12-month SPI also highlight the increasing occurrence of moderate to severe droughts in the periods beyond 1965. SPEI also indicates moderate drought years till 2010 whereas droughts of mild nature are more frequent during the recent decade. The statistical change point test points towards break years from 1958 to 1967 for annual and seasonal rainfall timeseries and matches well with the findings of the other gauge based observation from Uttarakhand. The non-parametric Mann-Kendall trend analysis of annual, monsoon and winter timeseries of rainfall data indicates a declining trend. But the declining trend in the winter period is statistically significant at a 95% confidence interval. The decline in the winter period (DJF) rainfall is as severe as 47-54 mm/100 years which is three times the reported results from the closest station data at Lansdowne which indicate a decline of -19.4mm/104 years using IMD station rain gauge data.

CHAPTER 4

Recession Curve Analysis of Springflow and Streamflow

4.1 Introduction

The gradual decline of spring and stream hydrograph has been investigated for more than a century. Widely investigated decline curve in the past has given rise to significant volumes of literature which gives insight into the fundamental of recession analysis (Werner and Sundquist, 1951; Toebes and Strang, 1964; Hall, 1968; Singh and Stall, 1971; Brutsaert and Nieber, 1977, Tallaksen, 1995; Dewandel et al. 2003) and more recently an advancement in approach is reported in terms of event-scale recession analysis (Shaw and Riha, 2012; Biswal et al. 2014; Bart and Hope, 2014; Chen and Krajewski, 2015; Patnaik et al. 2015; Roques et al. 2017).

The recession characteristics of the spring hydrograph differ from that of a stream hydrograph as it does not get influenced by bank storage or direct precipitation and may have greater potential to provide information relating to aquifer characteristics (Kresic, 1997; Malvicini et al. 2005). In an era when water is becoming a limiting resource, especially in the middle mountains, it will be crucial to decipher the storage-discharge relationship of bedrock-dominated heterogeneous hillslopes and catchments sustaining the spring-and streamflow. In a catchment, aquifer storage could be single or multiple and could behave as a linear or non-linear system at different spatial and temporal scales (Wittenberg and Sivalapalan, 1999; Malvicini, 2005; Clark et al. 2009; Bart and Hope, 2014).

4.2 Literature Review

The observed downturn in summer monsoons as well as failure in winter led to the rising frequency of droughts (Krishnan et al. 2016; Kumar et al. 2013) in the recent time making 'water' a limiting resource, particularly in middle mountains. The understanding of the storage-discharge relationship of the spring-and-stream flow sustained by bedrock-dominated heterogeneous hillslopes and catchments will be crucial. Widely investigated decline curve in the past has given rise to significant volumes of literature which gives insight into the fundamental of recession analysis (Brutsaert and Nieber, 1977; Dewandel et al. 2003; Hall, 1968; Singh and Stall, 1971; Tallaksen, 1995; Toebes and Strang, 1964; Werner and Sundquist, 1951) and more recently an advancement in approach is reported in terms of event-scale recession analysis (Bart and Hope, 2014; Biswal et al. 2014; Chen and Krajewski, 2015; Patnaik et al. 2015; Roques et al. 2017; Shaw and Riha, 2012). The storage-discharge relationship is investigated at various spatial scales ranging from small hillslope units (Clark et al. 2009) to very large drainage basins (Chen and Krajewski, 2015). The finding suggests that the hillslope, as well as the large basin, could be modelled through linear reservoir theory. However, recent work by Biswal et al. 2014 as well as many other workers (e.g. Shaw and Riha, 2012) raises apprehensions about the widely-used single reservoir model (Brutsaert and Lopez, 1998) based on event-based individual recession curve analysis. Although, many initial workers found recession curve analysis using a non-linear equation more appropriate (Wittenberg and Sivapalan, 1999). Clark et al. 2009 used two linear model to investigate the recessionary behaviour at different spatial scales whereas Bart and Hope, 2014 used two nonlinear storages to model the baseflow recession.

More clarity has emerged into the associated ambiguity, firstly arising out of the methodological approach adopted for recession analysis (Stoelzle et al. 2013; Dralle et al. 2017) and understanding of some of the hydrological processes that regulated the recession characteristics at different spatial as well as temporal scale (Tashie et al. 2019; Tashie et al. 2020; Jachens et al. 2020). Stoelzle et al. 2013 assessed the comparability between the results obtained by using different logic of recession extraction and parameter fitting methods to the well-established power-law relationship for the storage-

discharge model from 20-mesoscale catchments in Germany. The study highlights limited comparability between the nine recession analysis methods and almost two orders of variability in results depending on the specific extraction and fitting of the decline curve in an overall lumped recession analysis approach. Subsequently, Dralle et al. 2017 demonstrated through a systematic study using 16 combinations of methodological choices based on the minimum length of recession curve, defining the initiation and end of each event and on the choice of log-transformed power- law fitting or non-linear fitting of stream discharge data from 16 catchments from highly seasonal Mediterranean climate from the USA. The results indicate that the parameters are sensitive to the methodological choices and the suggested ideal combination of procedural options to maximize the fitting and minimize the bias was to select a minimum of four day's length with flow strictly decreasing ($dQ/dt < 0$) and nonlinear least-squares fitting of the event-based individual recession analysis. Recently, Jachens et al. 2020 used a synthetic time series hydrograph with known parameters to investigate the sensitivity of watershed parameters to different methodological approaches (lower envelope, central tendency, binning and individual recession approach for recession events more than 5 days long) for recession analysis and found contrasting results. The point cloud approach does not represent the average watershed properties as it was found to reflect more of antecedent conditions and climate prevalent before the recession event and can only be estimated using individual recession curve analysis. The results point towards a similar finding as reported by Stoelzle et al. 2013 of the variability of parameters with a difference in approaches with the Brutsaert point cloud or the individual recession approach.

Tashie et al. 2019 unravelled the reasons for the failure to find a good correlation (Biswal and Kumar,2014; Shaw and Riha,2012) between the possible driver(s) such as seasonal variability in transpiration (PET), VMC in the unsaturated zone and water table elevation (Groundwater) to the temporal variability of recession characteristics (log(A) and B). The seasonal variability of two power-law recession parameters and their hysteretic relationship is caused by the decoupling of transpiration from the unsaturated zone as the groundwater table falls during the summer season which acts as the only source of streamflow. But during the high water table and high VWC, ET consumes water from the

shallow subsurface and partially causes the decay in streamflow during the growing seasons causing sinusoidal variability of recession characteristics observed from the Coweeta basin in the humid headwater region. Base flow stability and its nonlinearity were reported from 1000 watersheds in the United States at a continental scale. The interesting study highlights concurrent storage primarily controls the stability of streamflow whereas the effect of evapotranspiration on the streamflow recession lags by 2 to 3 months in the majority of the watershed (Tashie et al. 2020). The results indicate that seasonality does not influence the nonlinearity and a significant increase in nonlinearity post-1980 was reported from the majority of watersheds. Assessment of storage and its sensitivity to climate change (Berghuijs et al. 2016) through recession analysis holds much relevance as threats to water security loom large on the remote rural settlements spread in the mountains capes of middle Himalaya which are primarily sustained by low-yielding springs and low-order streams.

4.3 Method

Spring flow data collected at the daily time step was measured volumetrically with a calibrated drum and stopwatch whereas the rainfall observations were made daily using collectors consisting of a 200 cm^2 orifice with a 2-L container. The spring discharge is normalized by the spring catchment area which represents the surface water hydrological divide. The study tested the applicability of two linear reservoir model, power law model as well as single non-linear model to investigate the prolonged post-monsoon decline curve observed in the spring flow representing the groundwater outflow from the hillslope. The two exponential linear reservoir models can be expressed by the relationship,

$$Q(t) = Q(0_1)e^{-\alpha_1 t} + Q(0_2)e^{-\alpha_2 t} \tag{4.1}$$

where Q(t) is the discharge of spring at time t, $Q(0_1)$ and $Q(0_2)$ are the initial discharge at time *t=0* and at the beginning of next exponential decay, t is the time lapse between observation times of Q(0) and Q(t); α is known as recession constant.

The power-law relationship between storage and discharge (Brutsaert and Nieber, 1977) is expressed as

$$dQ/dt = AQ^B \tag{4.2}$$

where constant A and B being critical recession parameters reflecting slope and intercept of bilogarithmic plot which is controlled by the geometric and hydraulic properties of aquifer and the temporal aquifer condition. The single nonlinear reservoir relation (Wittenberg and Sivapalan, 1999) is describe as

$$Q_t = Q_0\left[1-\frac{(1-B)At}{Q_0^{1-B}}\right]^{\frac{1}{1-B}} \tag{4.3}$$

The details of the single non-linear fitting approach can be found in Shaw and Riha, 2012 and Chen and Krajewski, 2015. The modeling error (E) for non-linear fitting approach is expressed as

$$E = \left[\frac{V_{\text{mod}} - V_{obs}}{V_{obs}}\right] * 100\% \tag{4.4}$$

where V_{obs} and V_{mod} represent the volume of modeled and input hydrograph.

The interannual recession analysis was carried out by selecting prolonged recession periods during the post-monsoon period (September, October and November) as well as the up to three months of winter period (December to February) which is mostly precipitation-free and has minimum monthly evapotranspiration. The recession period starting from September up to December and till February in some years was selected for recession analysis and understanding of the linearity or nonlinearity of the system at a catchment scale. The decreasing springflow and decreasing springflow derivative ($dQ/dt < 0$) were selected to assess the interannual variability of recession characteristics of springflow at catchment level. Normalized daily discharge data of spring outflow was plotted in *-dQ/dt* versus Q where *dQ/dt* is calculated as $dQ/dt = Q_i + Q_{i-1}/t_i - t_{i-1}$ and average discharge as $Q = (Q_i + Q_{i-1})/2$. The interannual post-monsoon continuous individual recession event for five years (2012-2015 and 2017) was fitted using two parallel exponential model as well as a single nonlinear model for

approximately more than 100 days of daily discharge observations. This could remove the observational error from the manually measured daily springflow data. The fitted data was plotted in the Brutsaert recession method to have an estimate of exponent (B) and coefficient (A) in a power-law relation. The exponent B which is dimensionless indicates the existence of nonlinearity in the system whereas the exponent A with unit $T^{-1}(L/T)^{1-B}$ indicates rate of recession or recession timescale of decline curve. Note if B=1, the groundwater aquifer sustaining the springflow becomes linear and the reciprocal of intercept (A) referred to as recession timescale (τ) can be represented in days and becomes static parameter with respect to Q. But for a nonlinear system ($B \neq 1$), the recession timescale will vary depending on Q (Kirchner, 2009**)**. Since the intercept of a line is controlled by the slope which is defined by the relationship of the derivative of discharge and Q in log-log space, independent interpretation of either of the two recession parameters becomes meaningless (Tashie et al. 2019**)**. Some of the approaches to overcome this interdependency is to restrain the B to its median value and assess the shift in the intercepts (Bart and Hope, 2014; Biswal and Kumar, 2014), whereas Dralle et al. 2015 suggest methods to decorrelate the two interdependent parameters. The stability of the springflow log (A) and storage sensitivity of springflow was assessed following the approach discussed in Berghuijs et al. 2016 at a local scale for the spring catchment. Similar approach was used to access the recession characteristics of the streamflow data. Matlab toolbox (Arciniega-Esparza et al. 2017) as well as application of exponential time step method (Roques et al. 2017) was used for spring-flow and streamflow recession analysis.

4.4 Results and discussion

4.4.1Baseline data of spring-flow and stream flow

Mandir dhara spring-flow discharge (Figure 4.1) ranges as low as 0.003lps to maximum of 1.85lps with an average discharge of 0.18lps for five years. Flow duration curve over a period of five years (i.e. between 2010 to 2013 and 2015 to 2016) shows that 80-percent duration flow (i.e. flow during the summer months) was minimum(low-flows) during the year 2010,2012 and 2016 (Figure 4.2). This could be because of deficient rainfall during the monsoon period of 2009, 2011 and 2015 (*cf.* Figure 2.4) whereas the 20-percent

duration flow (i.e. flow during high-flow period) was maximum during 2010 and 2016, which were surplus monsoon rainfall years.

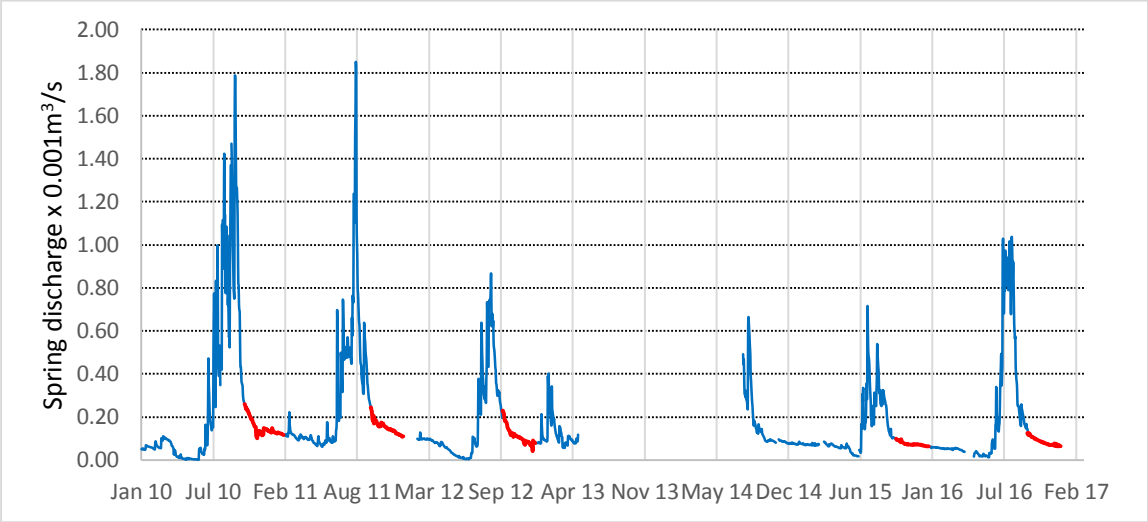

Figure 4.1: The spring flow hydrograph measured over a period of five years showing a decline trend. The post monsoon recession periods are also highlighted for the mandir dhara (spring-flow) which is located within the nested catchment (Bhimlitali micro-catchment).

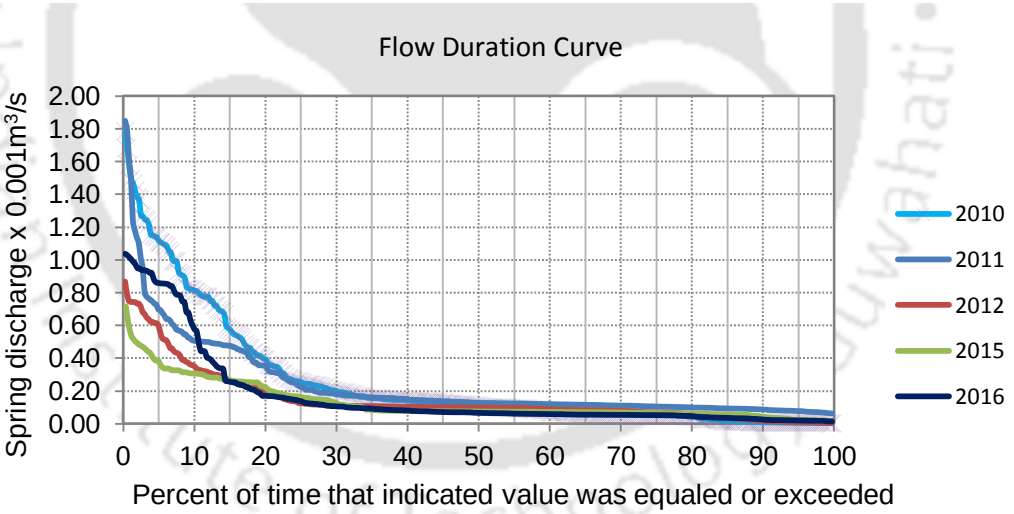

Figure 4.2: Flow duration curves highlights the declining trends in high-flows as well as low-flow periods after 2010 year of surplus monsoon during the monitoring period of five years.

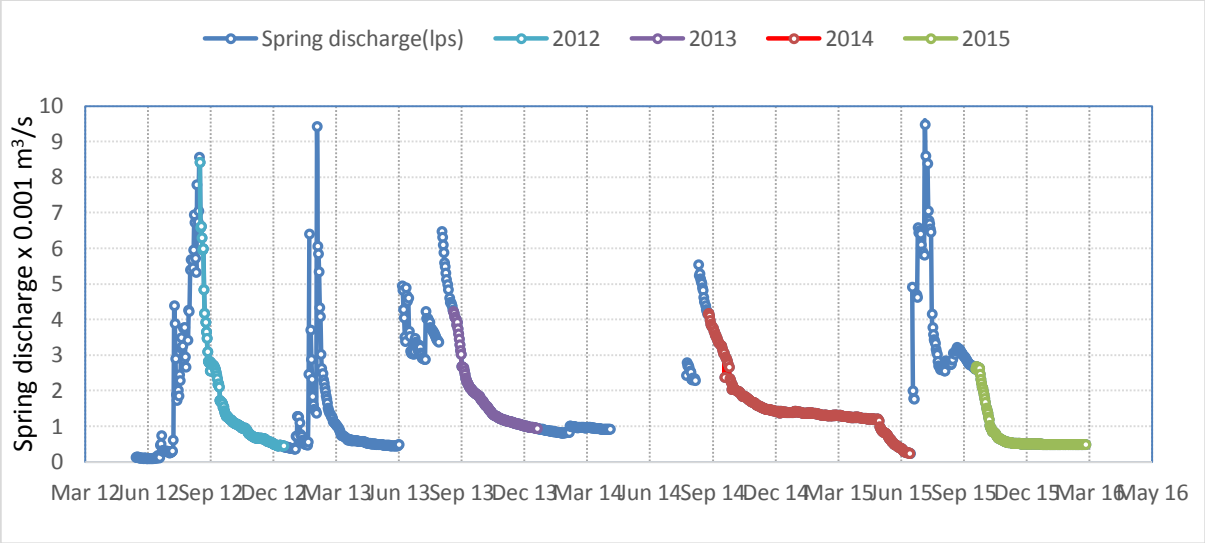

Figure 4.3: The Ayal village spring-flow hydrograph located in upper Paidul micro-watershed measured over a period of four years showing a decline trend in summer period of 2015. The prolonged recession periods are also highlighted in different colors.

Ayal dhara village spring which act as a dependable source of fresh water for Ayal village is having an average flow of 1.67 lps with maximum flow of 9.5lps during monsoon period with 0.078lps of summer low-flow discharge (Figure 4.3). Multiple years of drought period have resulted in decline in winter as well as summer season flows.

The stream hydrograph constructed from the daily water stage records at Bhimlitalli catchment outlet (Figure 4.4) from 90-degree v-notch data collected for 2010-2012 shows a maximum value 136 lps cubic feet second (approximately) to a lowest recorded value of 0.56lps. Recent data collected for 2018 at above location using water level recorder shows a maximum value only 6.5 lps to a lowest recorded value of 0.359 lps with an average value of 1.02 lps for the monsoon period (Figure 4.6). The discharge for the 90° V-notch was calculated using the following equations:

$$Q = 2.52H^{2.47} \tag{4.5}$$

where Q represents discharge in cubic feet per second and H is the head.

Discharge at the outlet of the upper Paidul micro-watershed (Figure 4.5; Figure 2.3 and Photograph 2.2) is recorded at Paidul where the measurement is being taken at 15-minute interval. The discharge is calculated using Ditchrider's head-discharge rating table for

partially contracted rectangular weir up to a head of 60 cm. The rating equation for discharge calculation is

$$Q = 5.4186\,h^{1.4958} \tag{4.6}$$

where h represents the water head at the gauging station. For head above 60cm, a velocity-stage rating curve is generated using velocity measured by universal current meter for the falling head period.

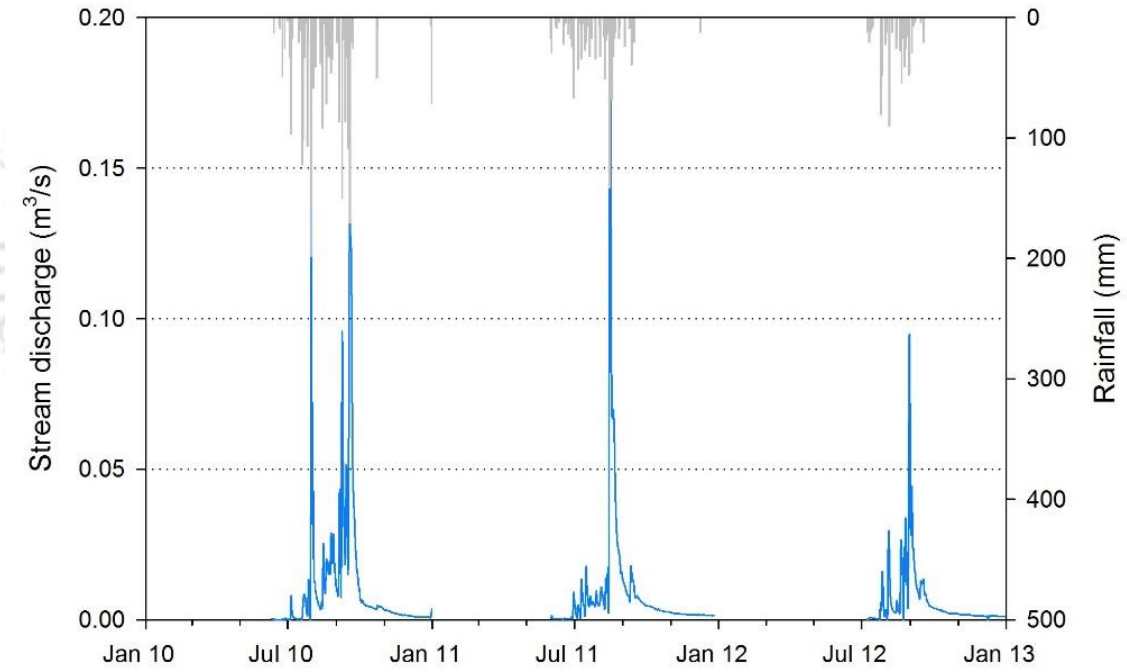

Figure 4.4: Streamflow discharge measured at the Bhimlitali outlet through right angle V-notch.

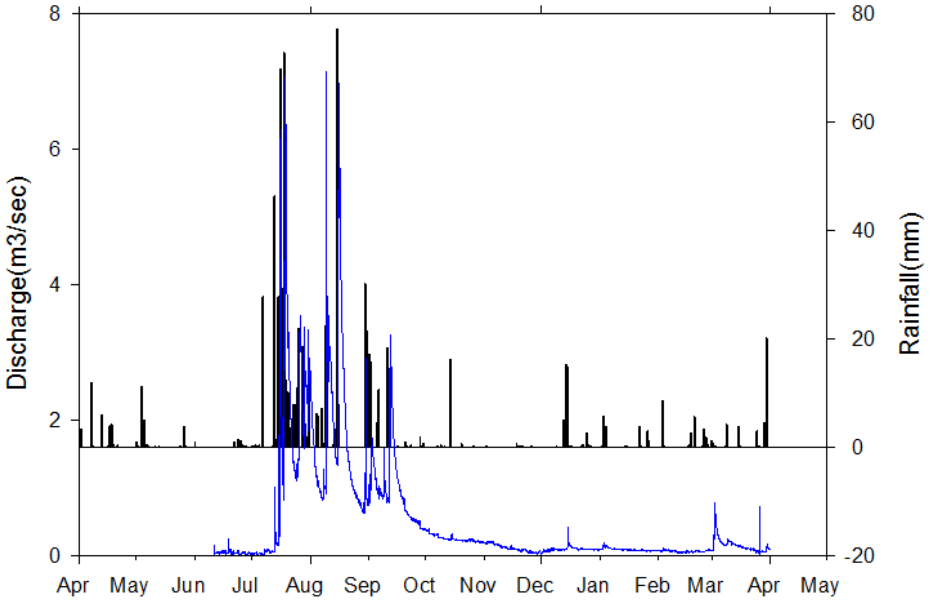

Figure 4.5: Stream discharge measured at the outlet of upper Paidul micro-watershed through water level recorder at 15 minutes logging interval.

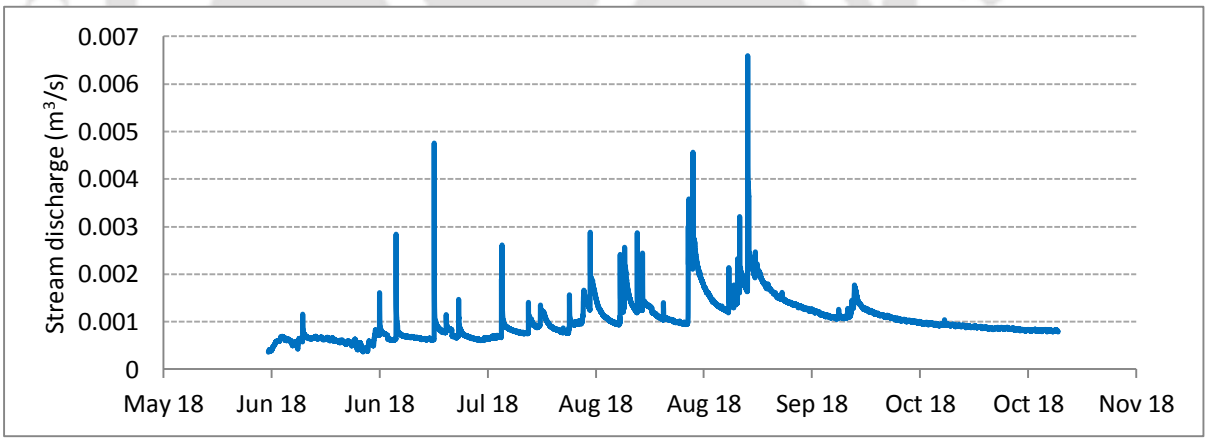

Figure 4.6: Stream discharge measured at the Bhimlitali outlet through right angle V-notch at 15 minutes logging interval.

4.4.2 Recession flow analysis of spring flow and streamflow using matlab toolbox

A matlab toolbox (Arciniega-Esparza et al., 2017) was used for spring-flow and streamflow recession analysis. The initial assessment of the available data was carried through extraction of segments (Figure 4.7a) of hydrograph recession using well-established methods. The master recession curve and linearity of the hillslope through spring-flow or micro watershed through streamflow was assessed graphically by generating Qi verses $Q_{i+1}$for the extracted recession periods (Figure 4.7b and c; Figure 4.8). The initial linearity may be assumed as observed for mandir dhara (spring) as well as the Ayal spring as majority of the data points fall into the 1:1 line for extracted the recession segments. However, the exponents of best-fit regression line indicate a close to linearity value (1.18) for mandir dhara whereas the Ayal spring with limited periods of recession data showed an exponent of 1.86 (Figure 4.9). The streamflow recession period indicates an exponent of 0.87 for Bhimlitali micro-catchment and upper Paidul micro-watershed showed an exponent of 1.53.

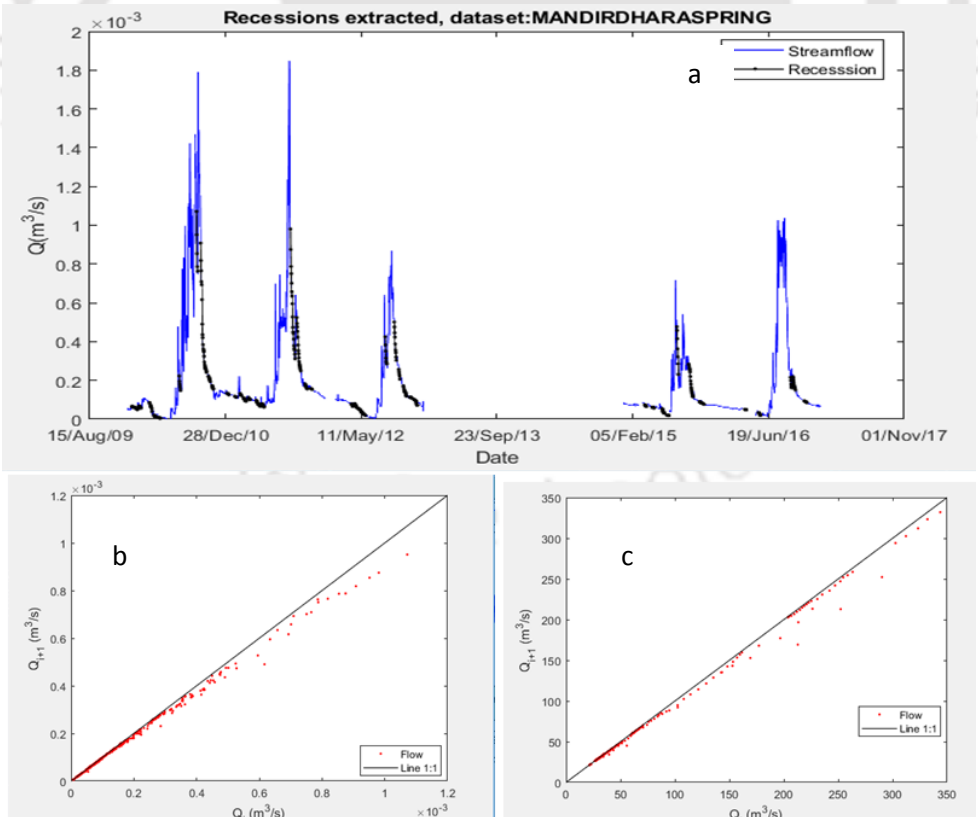

Figure 4.7: Segments of recession period separated (a) using Hydrorecession toolbox and Qi verses Q_{i+1} plot for the extracted recession showing near linearity of mandirdhara spring (b) and Ayal spring(c).

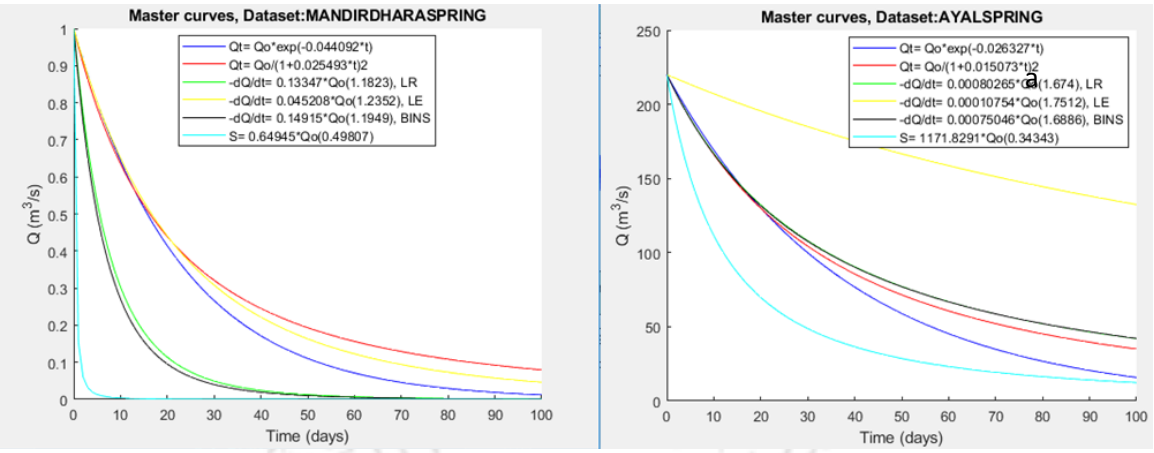

Figure 4.8: Master recession curve (MRC) for two springs generated from the separated recession curve using Maillet exponential equation, Boussinesq and other forms of storage-discharge relationship.

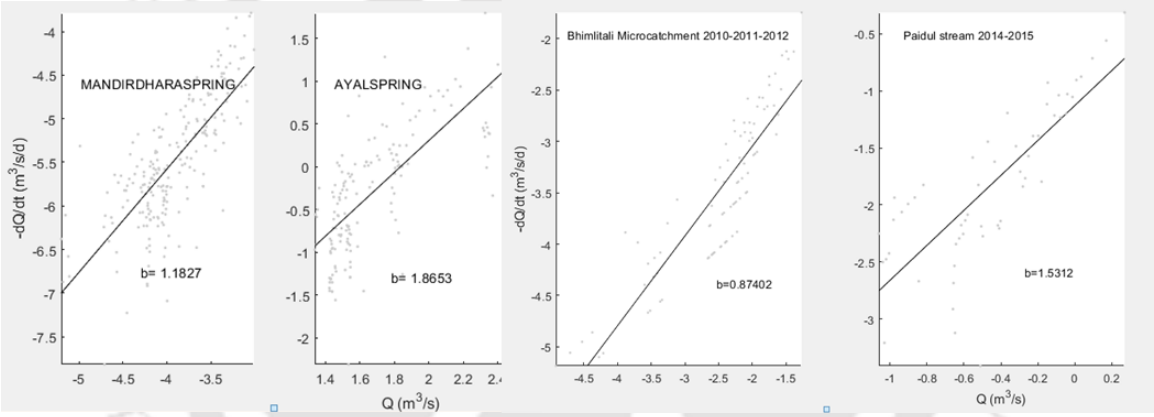

Figure 4.9 -dQ/dt verses Q plot of spring-flow and stream flow with exponents indicating linearity or non-linearity of the observed data at daily time step.

4.4.3 Interannual recession analysis of spring-flow data

The storage-discharge relationship is investigated at various spatial scales ranging from small hillslope unit (Clark et al. 2009) to very large drainage basins (Chen and Krajewski, 2015). Finding suggests that the hillslope as well as large basin could be modeled through linear reservoir theory. Recent work by Biswal et al. (2014) as well as many other workers (e.g. Shaw and Riha, 2012) raise apprehensions of widely used single reservoir model (Brutsaert and Lopez, 1998) based on event based individual recession curve analysis. Although, many initial workers found recession curve analysis using a non-

linear equation more appropriate (Wittenberg and Sivapalanam, 1999). Clark et al. 2009 used two linear model to investigate the recessionary behavior at different spatial scale whereas Bart and Hope, 2014 used two nonlinear storages to model the base flow recession. They demonstrated that antecedent storage could be regulating the base flow recession rate and Shaw and Riha, 2012 attributed the observed parallel lateral shift in the individual recession event in log-log space plot could be caused by the variations in the evapotranspiration. In this study an attempt is made to understand the applicability of two linear reservoir model, power law model as well as single non-linear model (Figure 4.10a and b) to investigate the prolonged post-monsoon decline curve observed in the spring- and streamflow representing the groundwater outflow into the low-order streams and hillslope-fed spring outflow. The daily discharge data of Mandir dhara spring outflow was plotted in -dQ/dt verses Q where dQ/dt is calculated as $dQ/dt = Q_i + Q_{i-1}/t_i - t_{i-1}$ and mean discharge as $Q = Q_i + Q_{i-1}/2$. Since it is difficult to interpret the recession characteristics from the data cloud approach (Figure 4.11a), the entire recession period data was fitted using two parallel exponential fitting method to approximately 75 days of discharge observations. The fitted data was again plotted in Brutsaert recession method to have an estimate of exponent (B) and coefficient (A) in a power law relation. The recession period for 2011 showed a very high slope with an exponent of 8.27 whereas lower best fit line indicates an exponent of 1 (Figure 4.11b). The recession period of 2012 can be segmented into two slopes with upper exponent of 3 and lower slope again can be a linear model with exponent close to 1. The 2015recession period can be fitted to a single best-fit line with an exponent of 7.7 indicating a very higher rate of change. The 2016 recession period upper best fit line showed an exponent of 1.82. The recession period of Ayal spring was separated from September to December month i.e. approximately 120days and similar approach was followed for recession analysis. The two reservoir exponential model fitted data was analyzed following Brutsaert method. The linear regression fit of the all the data cloud for recession period indicates a close to 2.0 exponents with R^2 value of 0.599 (Figure 4.12a and b). The upper segment of recession period for 2012 indicates a slope of 2 whereas the lower segment exponent is 1. The recession period for 2013, 2014 and 2015 showed a slope of 2.0, 1.74 and 1.66

respectively (Figure 4.12 b). The finding highlights that in a two linear reservoir approximation approach, the responses deviate from non-linearity to linearity between reservoirs. Since two parallel reservoirs and a single non-linear reservoir (Figure 4.10) show a very significant r-square value, subsequently, single non-linear reservoir fitted data for Ayal spring was analyses through bi-logarithmic plot and the median value of exponent (B) was found to be 1.89 (2.2599 - 1.7798) and coefficient (A) of 0.07 (0.0548-0.1187). The recession timescale ranges between 8 to 19 days. Brutsaert and lopez, 1998 showed a timescale of 34.4 days for drought flow drainage and Sánchez-Murillo et al. 2015 reported relatively greater values of recession timescale (33.3–66.7 days). Interestingly, a parallel lateral shift is observed in different yearly recession responses for the post monsoon and winter period (Figure 4.13a and b).

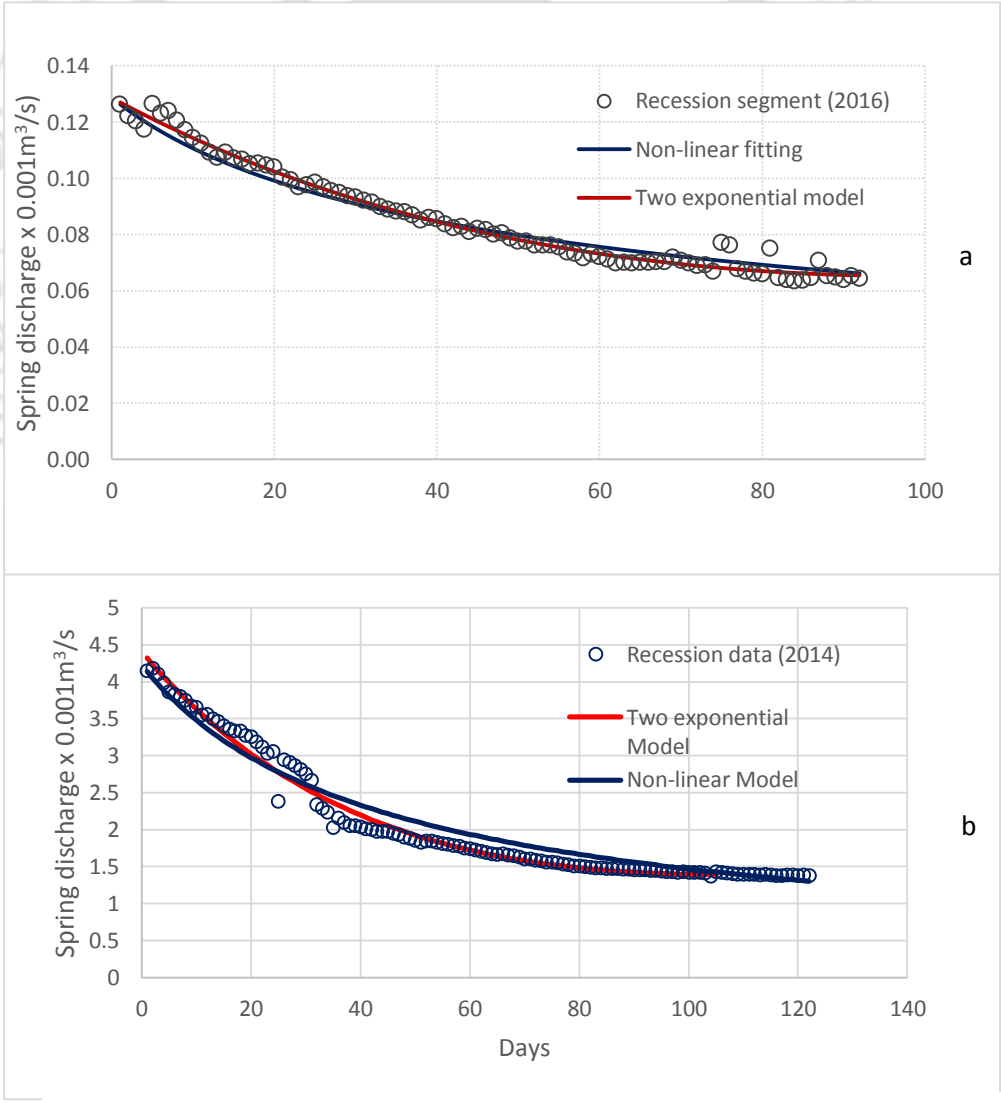

Figure 4.10: Plot of Mandir dhara (a) and Ayal spring (b) with seasonal recession period and exponential fitted (two parallel reservoir) line as well the single reservoir nonlinear fitted line with significant high R-square value in both the models.

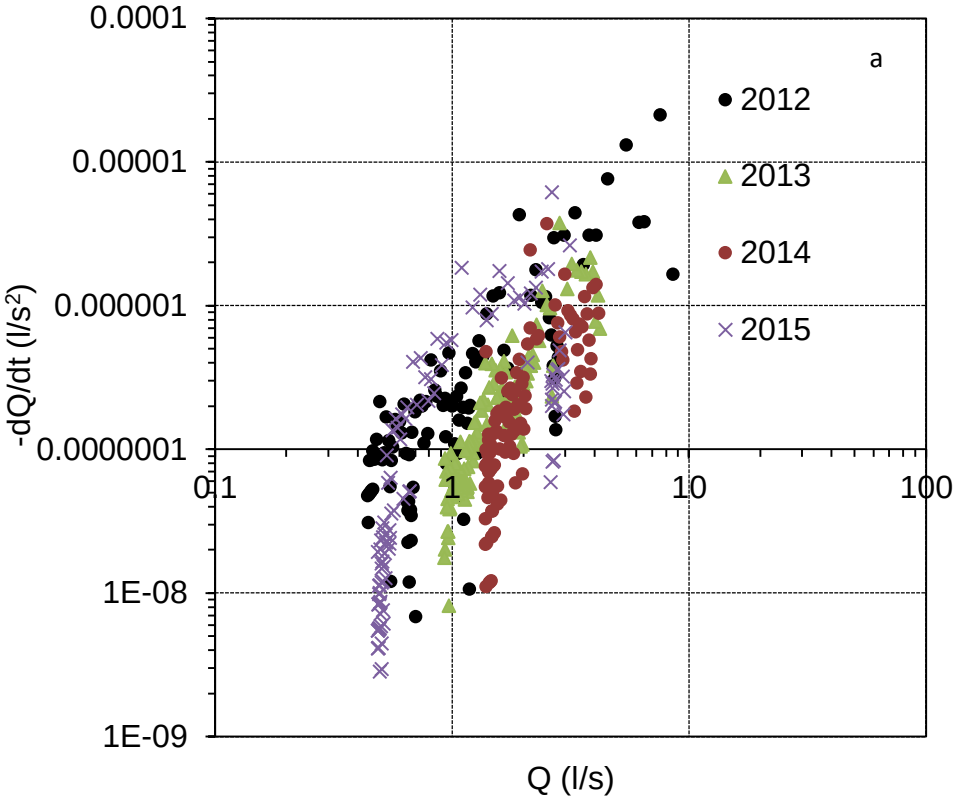

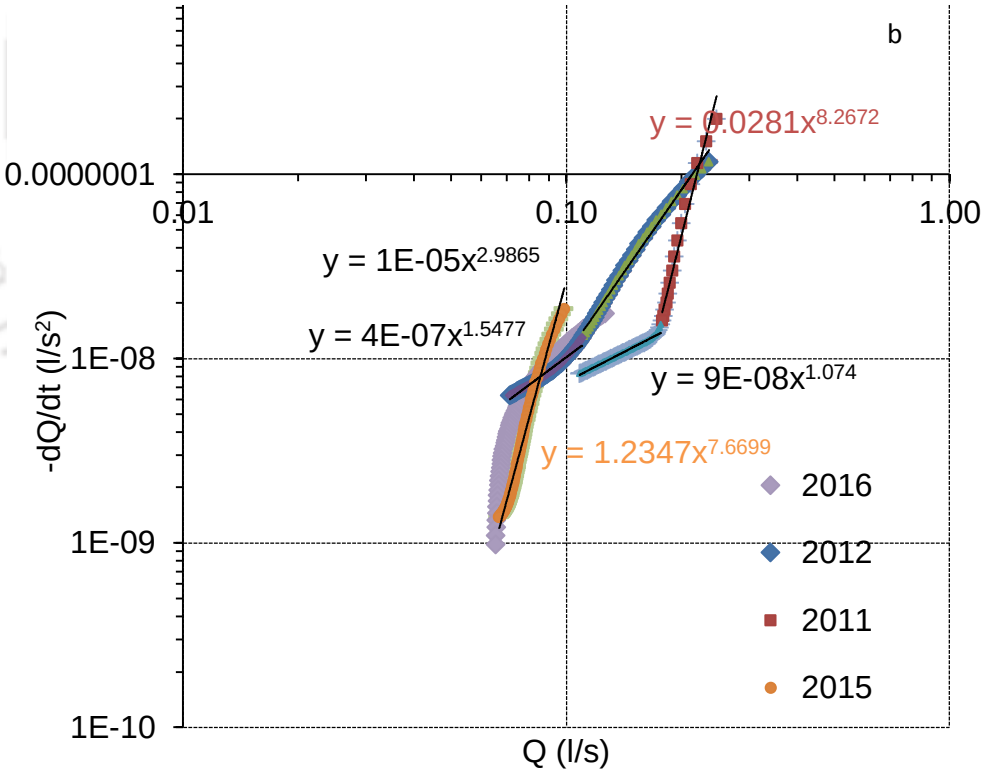

Figure4.11: *-dQ/dt* verses Q_{av}plot of mandirdharaspring-flow with cloud of all data points of recession period(a) and exponential fitted (two parallel reservoir) data points(b) of seasonal recession for four years with linear regressed line in power law form.

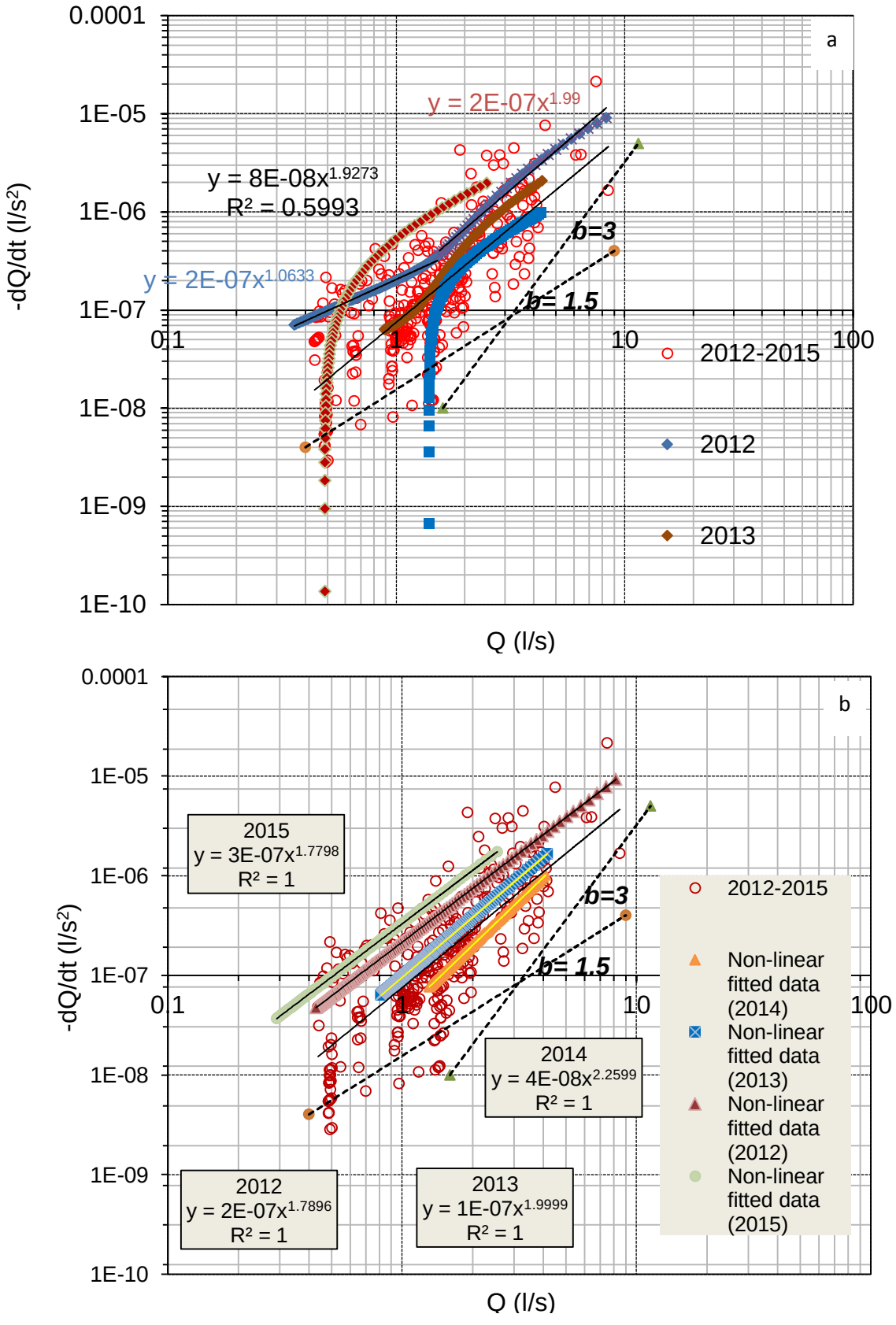

Figure4.12: *-dQ/dt* verses Q_{av} plot of Ayaldhara spring-flow with cloud of all data points in the seasonal recession period (a) and exponential fitted (two parallel reservoir) data points (b) of seasonal recession for four years with linear regressed line in power law form.

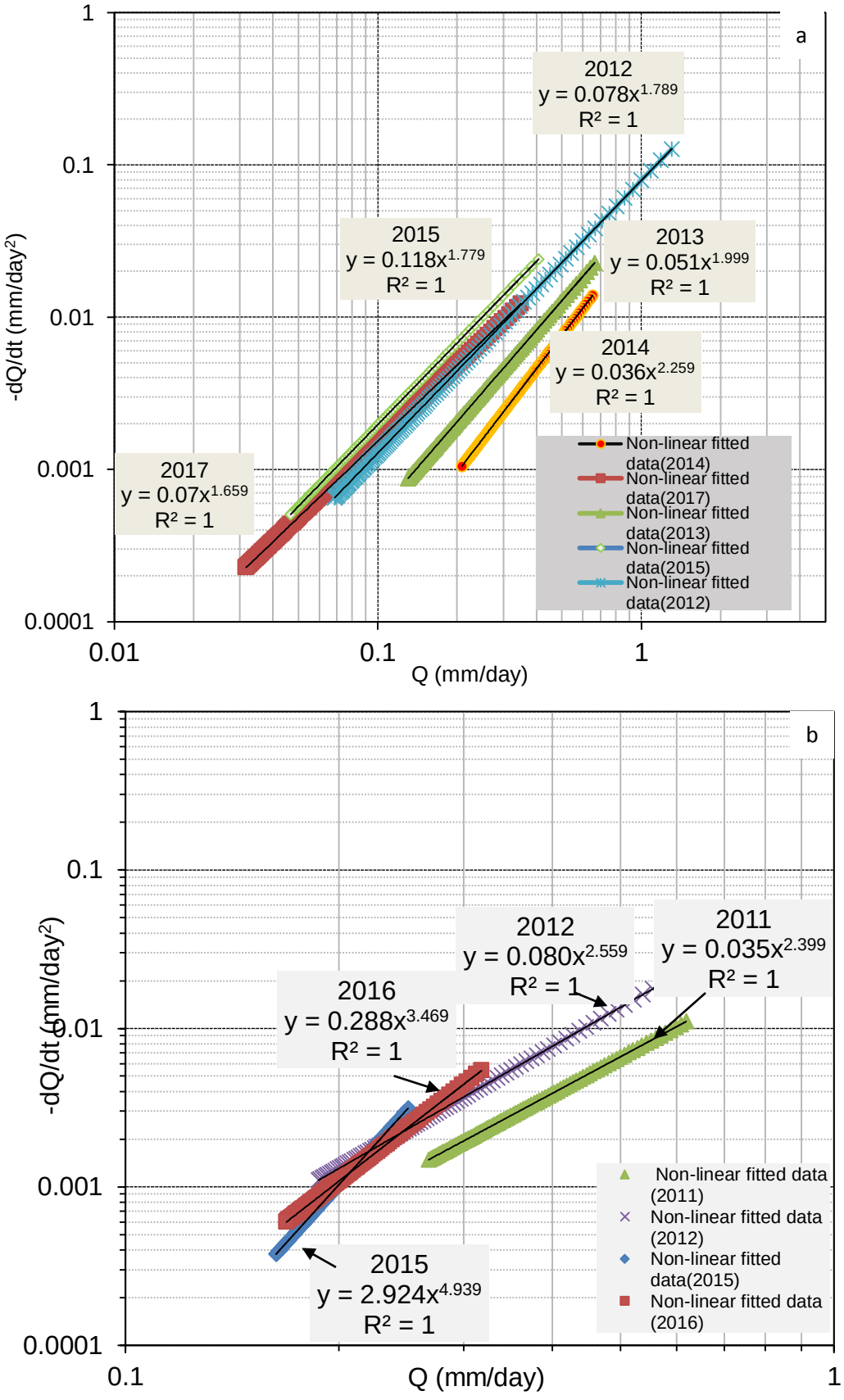

Figure 4.13: *-dQ/dt* verses Q_{av} plot of normalized Ayal spring-flow for recession period of five years (a) and Mandir dhara spring for four years (b) using single non-linear model fitted data for recession segments. The power law best-fit line indicates parallel offset.

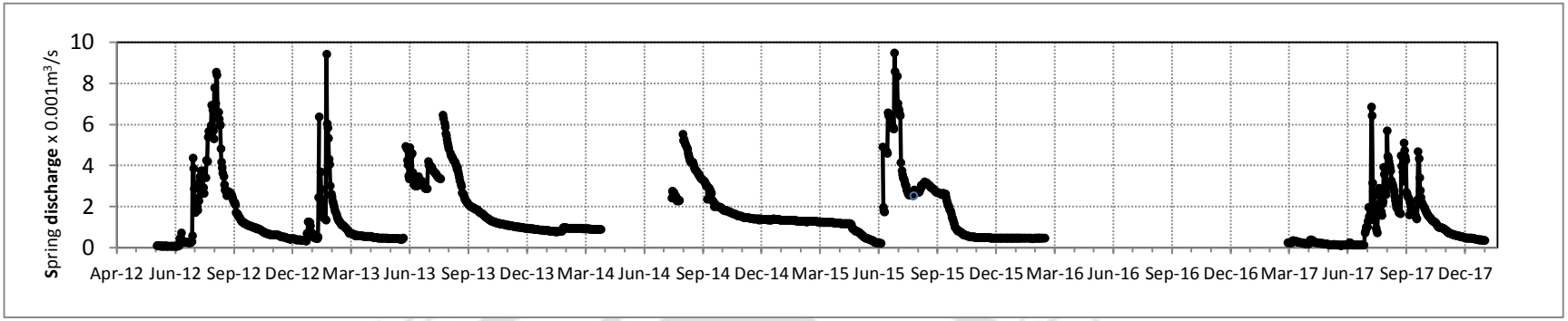

Figure 4.14: The Ayal village spring-flow hydrograph located in Paidul micro-watershed measured over a period of five years showing a decline trend in summer period of 2015.

Table 4.1: Results of three approaches (single non-linear reservoir, power law fitted data as well as two-store exponential model)

Recession period	**No. of Days**	**Single non-Linear model**			**Power law model using Non-linear model fitted recession data**			**Two- store Exponential model**		**storage sensitivity of springflow**	
		A	B	E	A	B	Recession timescale (τ) in days	α_1	α_2	$\epsilon_S(\alpha; \beta; Q)$ Q = 0.03 mm/d	$\epsilon_S(\alpha; \beta; Q)$ Q = 1 mm/d
25 Sept 12 to 24 Jan 13	122	0.079	1.8	0.0019	0.078	1.789	13	-4.7	-0.6028	0.16	0.08
1 Sept13 to 31 Dec 13	122	0.0514	2.01	1.4882	0.051	1.999	20	-2.358	-0.2147	0.05	0.05
1 Sept14 to 31 Dec 14	122	0.0548	2.75	0.0015	0.036	2.259	28	-1.465	-0.1914	0.004	0.05
25 Sept 15 to 31 Dec 15	98	0.1187	1.79	3.0224	0.118	1.779	8	-2.272	0.05845	0.25	0.12
29 Sept 17 to 28 Feb 18	154	0.07	1.67	0.0084	0.07	1.659	14	-1.955	-0.3066	0.22	0.07

The results (Table 4.1) of a single nonlinear model fitted springflow recession data for prolonged post-monsoon and winter period recession characteristics, show B ranges between 1.67 to 2.75 and the median value 1.8 (with standard error of± 0.19). The value A for five-year interannual variability ranges from 0.0548 to 0.1187 with a median value of 0.07/day. The recession timescale ranges between 8 to 19 days with a median value of 14 days. This indicates an overall nonlinearity at the catchment scale (4-54ha) with a very good fit to the nonlinear model and having very low values (≤3%) of modeling errors. Our finding (Table 4.1) also shows a median slope value of close to two which is consistent with the values obtained by individual recession analysis by Biswal and Marani (2010); Biswal and Kumar (2014); Shaw and Riha (2012) from several basins of USA. Log transformed nonlinear model fitted data in a power-law model also indicate similar results with minor difference in the year 2014 in A value of 28days of recession timescale.

Clark et al. (2009) reported nonlinearity for catchments of 10ha and 41ha area but smaller hillslope of 0.1ha could be modelled through linear reservoir as observed from streamflow recession analysis in the nested Panola Mountain Research Watershed (PMRW), USA. However, late-time recession curves for ~ 150days during drought years from basins ranging in drainage area from 66 km^2 to 16854 km^2 in the United States could be represented through linear groundwater reservoir (Chen and Krajewski, 2015**)**. Manifestation of nonlinearity (B≠ 1) in the storage-discharge relationship could be attributed to heterogeneity within a hillslope or among hillslopes, hydraulic of flow in different landscapes (hillslopes, riparian zone, etc.), a large difference in the depletion rate between two storages, bedrock leakage and return flow and past recharge events (Biswal and Kumar, 2014; Brutsaert and Neiber, 1977; Clark et al., 2009; Harman et al., 2009;Wang, 2011).The classical method of streamflow recession analysis, Brutsaert and Neiber (1977) constrain the slope between 3, 1.5 and 1 representing the short and long-time solutions to the outflow which is not strictly baseflow emerging from the idealized groundwater aquifer. Harman et al. (2009) summarized the

published values of exponent (B) from multiple studies with difference in approach and ranges from < 1 to > 3 (e.g. Biswal and Kumar,2014; Chen and Krajewski, 2015; Shaw and Riha, 2012; Tague and Grant, 2004). Very recently Ghosh et al. (2016) reported an early-time recession exponent which is consistent with the above observation but the late-time exponent show higher values (median of 8.7) whereas Tashie et al. (2019) reported a median value of 11. The point which needs to be reiterated while comparing results originating from the difference in methodological approach while estimating exponent of power-law relationship is that the individual recession event will provide higher values as compared to the point cloud approach and vice versa for log(A) (Jachens et al. 2020). Tashie et al. (2019) and Wittenberg and Sivapalan (1999) reported a value of close to 0.5 for B using the nonlinear groundwater reservoir equation for large basins. The value of intercept (A) in a bilogarithmic plot has physical meaning in time units (days) when the reciprocal of intercept (1/A) is evaluated and represents the recession timescale of a recession event. The intercept A is controlled by aquifer hydraulic, geometric properties as well as storage (Tashie et al., 2019; Tashie et al. 2020; Torch et al. 2013**).** The storage half-life estimated using a linear reservoir assumption for eight large and small springs in the Philippines (Malvicini et al. 2005) indicate 11 to 51 days of half-life whereas Brutsaert and lopez, 1998 showed a timescale of 34.4 days for drought flow drainage from Washita Experimental Watershed complex, USA. Sánchez-Murillo et al. (2015) reported relatively greater values of recession timescale (33.3–66.7 days) for watersheds underlain by metamorphic and sedimentary rocks as compared to catchments with dominant basalt rock type with 12.5–20.0 days' recession timescale from the United States. An insightful discussion on basin drainage timescale can be found in Brutsaert (2008). These reported results are following the cloud point approach and in all these studies drainage timescale was assumed to be relatively static characteristic of a basin. However, Bart and Hope, (2014); Tashie et al. (2019); Wittenberg and Sivapalan (1999) showed the seasonal and sinusoidal annual variability in A with a faster timescale during the winter months (relatively higher A) and lower timescale for summer months

controlled by storage and evapotranspiration. The late-time recession timescale of 34 days using linear reservoir storage was reported from medium to large Iowa Cedar River basins, USA during drought **(**Chen and Krajewski, 2015). Interestingly, for a prolonged recession period for approximately more than 100 days for five years after the major annual event of monsoonal recharge to the groundwater storage sustaining the springflow, a year-to-year lateral shift is observed (Figure 4.14). The precipitation-free recession period of the non-linear fitted recession data plotted in bilogarithmic plot showed a more than two orders of interannual variability in A values over the five years. The apparent near-parallel horizontal shift in the plot (Figure 4.14) with faster recession characteristics in the post-monsoon recession period of 2012, a slower storage depletion in the year 2014 and the results from other years falling in between the bounds can be relatable with the variable monsoon yearly influx as potential evapotranspiration observed from GLEAMS data is fairly invariant. Bart and Hope, 2014 found a strong correlation between past cumulative streamflow over the water year with recession rate (A). However, the approach could not be applied in the present analysis as continuous data is unavailable for an entire time period of using streamflow or springflow as a surrogate of storage. Nevertheless, the monsoon rainfall had been largely deficient for years from 2012 to 2017 with exception of 2016 which recorded 111cm of monsoon rainfall. Hence, a clear link could not be established between the past monsoon rainfall amount with the inter annual shift in the recession characteristics over the five-year period. The depletion of storage is quite evident in the premonsoon and post-monsoon recession period of springflow hydrograph for 2015 as well as in the premonsoon period of 2017 which records a very minimum lowflows in the spring outflow (figure 6a). This clear pattern of shift in the interannual as well as seasonal recession characteristics is reported by many authors (e.g. Bart and Hope, 2014; Biswal and Kumar, 2014; Karlsen et al. 2019; Shaw and Riha, 2012; Tashie et al. 2019) caused by antecedent conditions of storage as well as seasonality caused by evapotranspiration.

The two-store exponential model was also applied as a secondary approach for recession analysis which is found to appropriately represent the aquifer with flows having faster recession rate as compared to flows through the lower hydraulic conductivity formation and having slower recession rate. In the present study area falling in the middle Himalaya, the hillslopes are underlain by stratified metasedimentaries with networks of large foliation planes as well as smaller networks of joints and fracture planes which is overlain by thick soil formation (Tarafdar, 2013; Tarafdar et al. 2019). The value of α for the first exponential reservoir ranges from 0.13 to 0.041 indicating a very short half-life of nearly 5 to 17 days whereas the second exponential reservoir in parallel shows values ranging from 0.02 to 0.002 which is indicative of nearly 34 days to 345 days of half-life. The R^2 value of more than 0.98 was found in all the post-monsoon and winter recession data with two-store exponential fitted data. Sawaske and Freyberg, 2014 used R^2 value greater than 0.8 to select the representative annual recession curve. The results of vulnerability analysis to storage changes (Table 4.1) show that springflow sensitivity values are high for the lowflow regime with an area normalized discharge of 0.03 mm/day with median ϵ_S = 0.159 where high flow values (Q=1mm/day) showed median ϵ_S = 0.07. These figures are significantly greater than the reported values from Europe (Berghuijs et al. 2016) with median ϵ_S = 0.062 for lowflows and the recorded value during the high flows (median ϵ_S = 0.023) for the stream flows. The five-year recession analysis of springflow sensitivity to storage changes during the lowflow periods highlights the catchment is most vulnerable to storage changes.

4.4.4 Seasonal recession analysis of streamflow data

The recession period between October to December months for the year 2010, 2011 and 2012 was separated for $-dQ/dt$ vs. Q plot at a daily time step. The parallel power law regression lines maintain a constant exponent of 0.59 with a shift in the intercepts (Figure 4.15). The upper part of the recession curve showed an exponent of 0.86 in the data cloud, which includes entire recession periods for three years. The recession period data was fitted to single or two parallel exponential fitting and was plotted in $-dQ/dt$ vs. Q plot. An exponent of 1.64 and 1.86 was found from the upper part of recession segment for 2011 and 2012 respectively whereas the single reservoir exponential fitted data showed linear relationship (Figure 4.15).

The discharge data at the outlet of upper Paidul micro-watershed gauging station was collected through water level recorder for a period 2014-2015 with a 15minutes observation frequency. The recession period was analysed for three months (October, November, and December). The diurnal fluctuations in the discharge data is clearly visible, which requires filtering or smoothing to segregate the total recession curve from the noisy water level data. The linear regression fitting indicates an exponent of 1.82 (Figure 4.16).

To gain an insight into the recessionary characteristics of intra-storm event as well as the post- monsoon recession period of streamflow data collected at 15 minutes' interval at the outlet of Bhimlitalli catchment for monsoon period of 2018, four declining curves were separated (Figure 4.17a, b, c, d and e). The two-recession period in August month represents the intra-storm event for 5 days' period whereas the recession period ranging from 15 to 36 days represents the post monsoon recession period extending from September to November (Table 4.2). Similar approach was followed as discussed earlier and a new method of exponential time step was also applied to the recession data (Figure 4.18). The results are presented in the Table 4.2 with the exponent and coefficient for the three approaches.

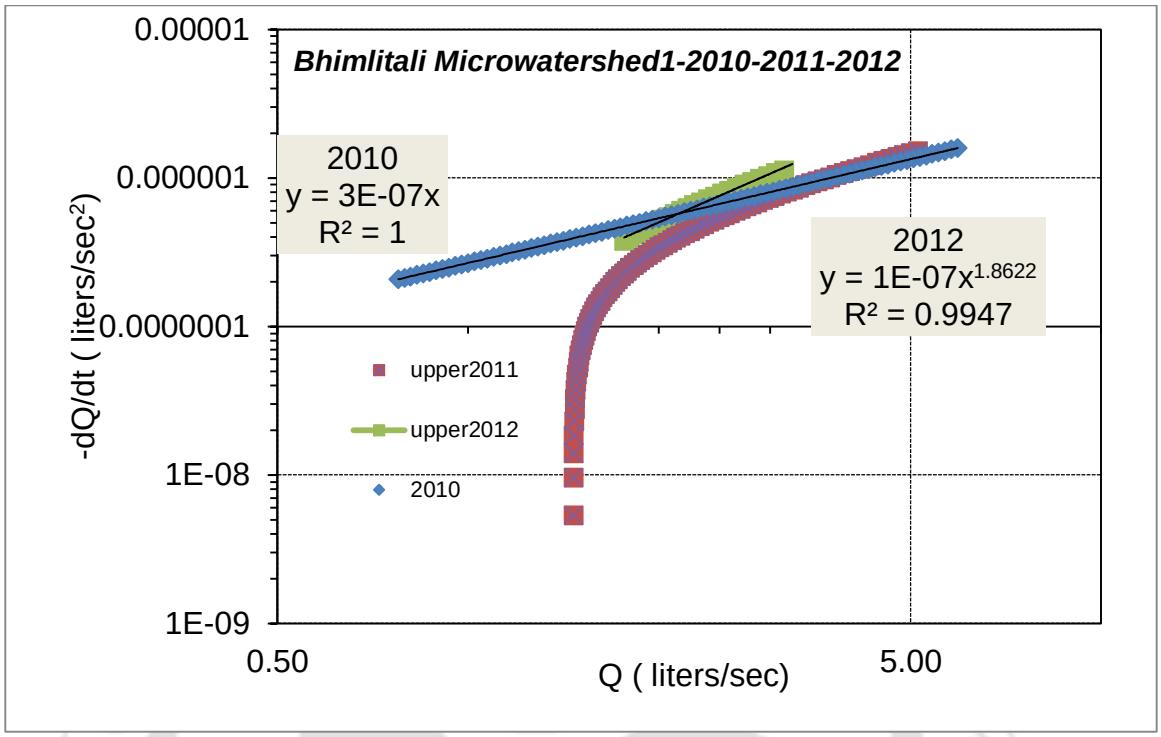

Figure 4.15 *-dQ/dt* versus *Q* plot(a) of streamflow data collected at Bhimlitalli micro-catchment using single and parallel reservoir exponential fit for the seasonal recession period for three years indicating close to linear system.

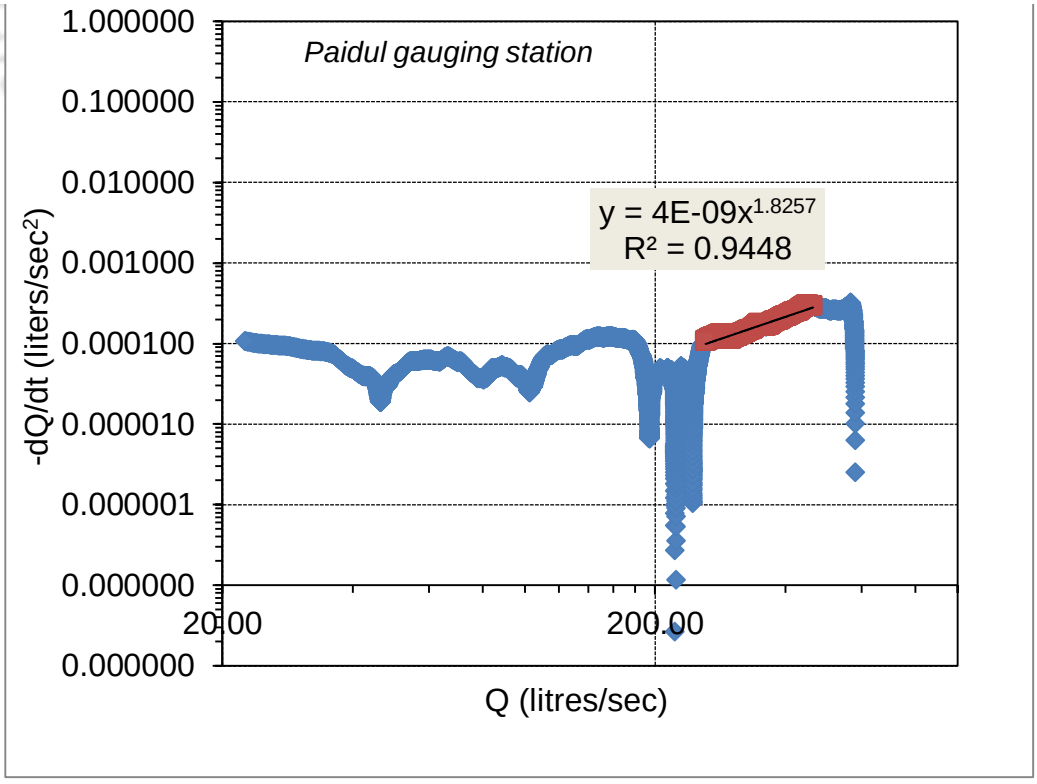

Figure 4.16: *-dQ/dt* verses Q_{av} plot for the seasonal recession period measured at Paidul outlet with 15minutes logging interval.

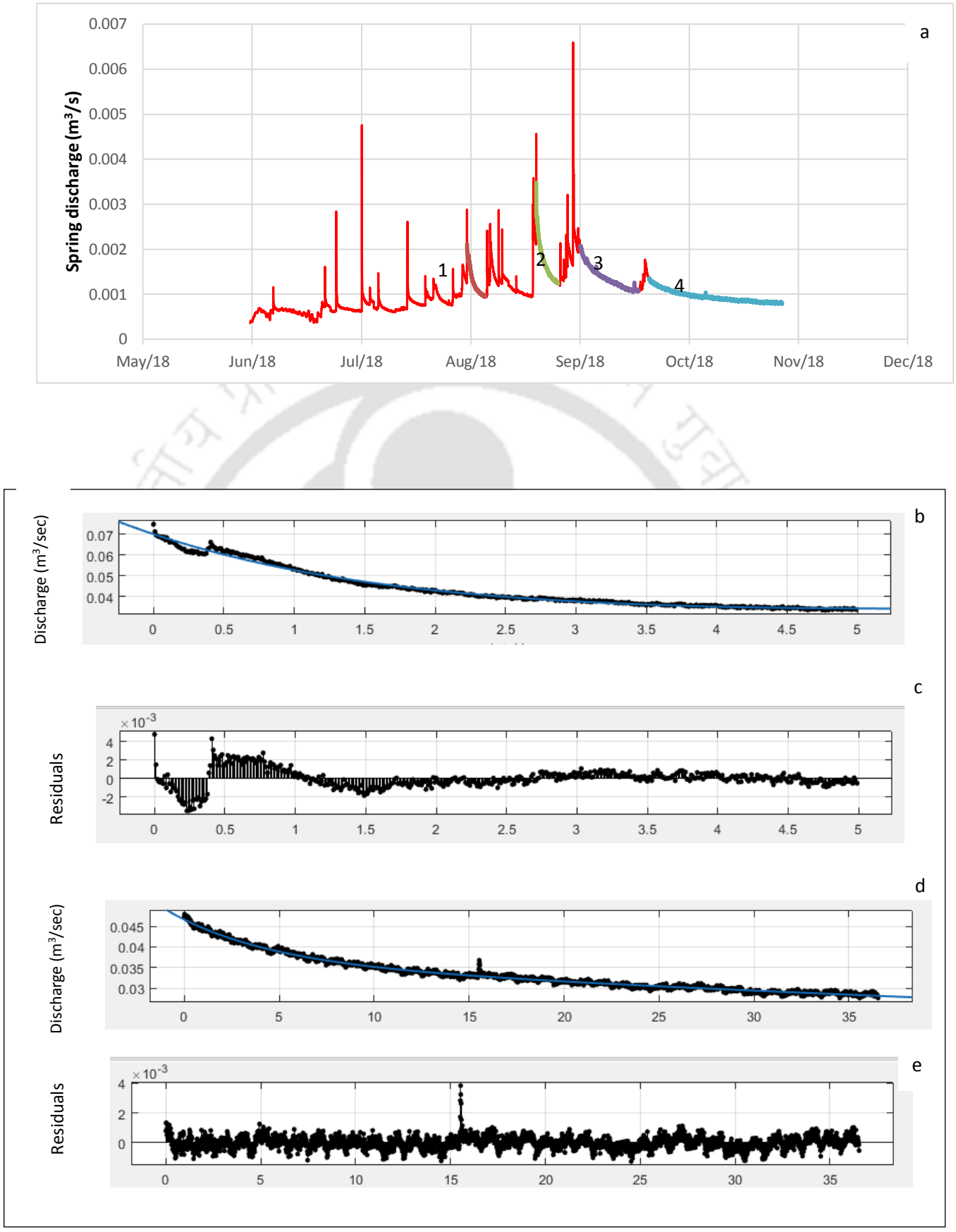

Figure 4.17: The monsoon period stream hydrograph with four extracted recession events(a) Extracted recession curve 1 and 4 fitted with two exponential linear model fitting (b & d) and residual plots (c & e). The residual plot (e) clearly reveals the diurnal variation in the late post-monsoon data collected at the outlet of Bhimlitali catchment.

Table 4.2: Results of three approaches (single non-linear reservoir, power law fitted data as well as exponential time step method) applied to recession curve of streamflow data for monsoon period of 2018.

Time frame	No. of Days	Single non-Linear System				Power Law Model fitted to simulated data from single non-linear system			Exponential time step method	
		A	B	E	R^2	A	B	R^2	A	B
7 Aug to 12 Aug 18	5	0.0772	3.65	0.9591	0.9573	0.00000001	3.2112	0.7209	2.75E-08	4.09
26 Aug to 31 Aug 18	5	0.0369	3.39	0.6152	0.778	4E-09	3.38	1	6.9E-17	8.5
7 Sept to 22 Sept 18	15	0.0128	4.3	0.114	0.9917	2E-09	429	1	3.5E-09	4.75
26 Sept to 11 Nov 18	36	0.0141	7.74	0.000162	0.9871	2E-09	7.73	1	4.66E-10	4.86

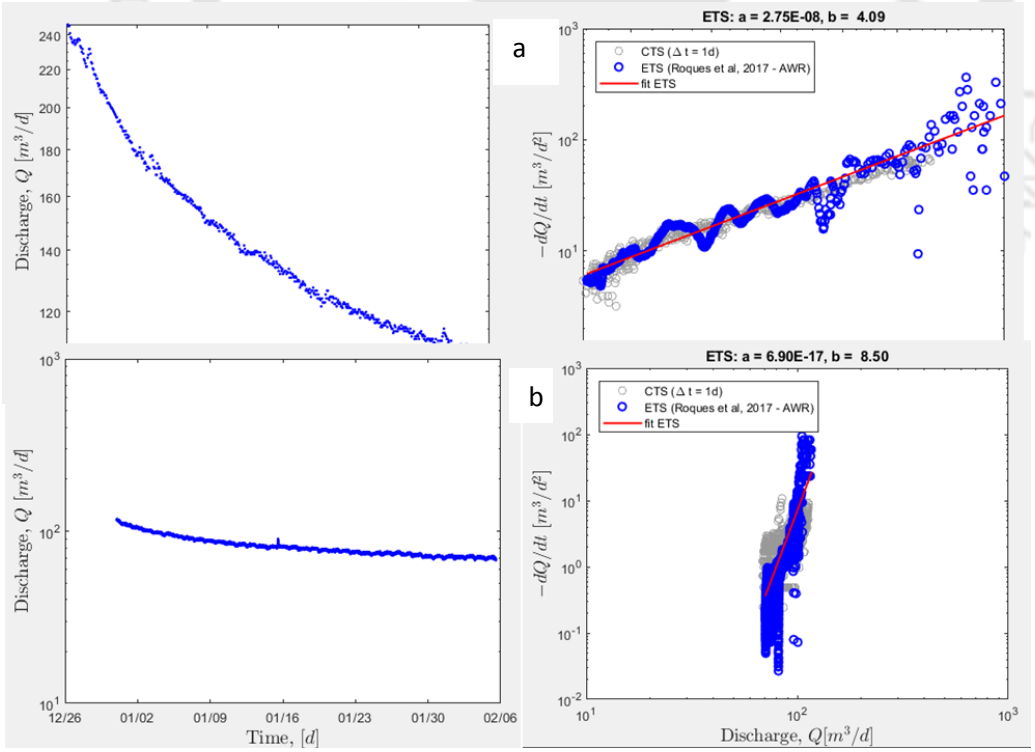

Figure 4.18: Extracted recession curve 1 (a) and 4(b) fitted with exponential time step method for recession curve of streamflow data for monsoon period of 2018.

4.5 Conclusion

The flow duration curve generated from the long-term spring discharge data collected from Mandir dhara spring indicates a diminishing flow not only during low-flow period but also in the monsoon period in the past decade. This is caused by recurrent multi-year drought observed from the studied catchment in the middle Himalaya. The storage-outflow relationship modelled through a non-linear power law model and two exponential linear model for the prolonged period of recession observed in the spring and stream hydrograph after the monsoon influx highlights an overall nonlinearity at the catchment scale ranging between 4-54 hectares sustaining the two monitored springs (Mandir dhara and Ayal dhara). This is in agreement with the reported nonlinearity at a larger spatial scale beyond the individual hillslope. The average recession timescale of only 8-14days using a nonlinear model is indicative of very fast recession rate of Ayal and Mandir dhara spring. The sensitivity of spring flow (ϵ_S) also supports that the groundwater aquifer lying within the catchment sustaining the spring flow is highly vulnerable to storage changes and influenced by the antecedent storage governed by monsoon rainfall influx and its variability. The parallel offset in the yearly recession lines in the $-dQ/dt$ vs. Q plot is indicative of the varying inputs received by the aquifer due to surplus or deficient monsoon rainfall years.

CHAPTER 5

Shallow Groundwater Investigation

5.1 Introduction

The physical properties of the subsurface formation and fluid (water) govern the fluid flow in a water-bearing reservoir/aquifer. The two parameters, one determining the ability of the formations to store or release fluids, termed specific storage (S) and the other decides the ease with which the formation transmits water under pressure gradient and is termed as the permeability (k) or transmissivity (T). Estimation of hydraulic conductivity and storage (storativity) is not only central to the groundwater investigation problems related to production potential assessment of aquifers as a source of water, contaminants transport or problems related to safe disposal of radioactive waste disposal in low permeability formation in Groundwater Hydrogeology but also in disciplines of Engineering Geology as well as Petroleum Engineering for assessment of oil producing reservoirs (Streltsova, 1987). A range of well-testing techniques have been developed over several decades to measure the hydraulic parameters of water-bearing geological formations. The widely used pumping test forms a central part of groundwater investigation and is considered both an art and science (Kruseman and de Ridder, 1991**).** However, execution of pump tests in a field site is cost intensive whereas the slug test is a cost-effective alternative and quicker means for assessment of the physical properties of the shallow aquifer. The slug test has its merit and is widely applied to get an initial assessment in the planning of large-scale pumping tests for water supply investigation, to assess the effectiveness of well development as well as in cases where pumping test becomes infeasible to execute, for example, assessment of sites impacted by groundwater contamination (Butler et al. 2002; Scholl and Christenson, 1998) or in low permeability geological formation.

Multi-well pumping tests can provide a better estimate of large-scale hydraulic properties whereas the aquifer parameter of the immediate vicinity can be estimated from the slug test (Lee and Lee, 1999, Butler, 1998). Hydraulic parameters estimated through slug test should be only considered as a lower limit of hydraulic conductivity and is more prone to errors arising out of improper well development, anisotropy (Butler,1998) and non-darcian flow effects (Quinn et al. 2013). In the present hydro-geological setup underlain by metasedimentary rocks, the slug test is the only alternative as pumping test cannot be performed for low hydraulic conductivity formation. The procedure for test data (slug test) analysis depends on the aquifer medium conceptualization, which is very complex for fracture formation. A brief review of four methods suitable for the estimation of hydraulic properties in fractured hard-rock aquifers is discussed in Marechal et al. 2003. The inadequacy of classical methods for pump test data analysis is also mentioned and highlights the need for fracture aquifer characterization and evaluation through appropriate solutions. In the present study area of Lesser Himalaya, geological mapping, rock cores and test data (slug test) suggest the applicability of the dual-porosity model (Barker, 1988). AQTESOLV software (Geraghty & Miller Inc. 1995) has been extensively used for aquifer parameter estimation. Barker and Black, 1983 have formulated the analytical solution for a slug test in a well that fully penetrates an isotropic fractured aquifer assuming a double-porosity model with slab-shaped matrix blocks. This dual-porosity model is being used for the test data analysis.

Poor agreement between pump test results or other methods such as laboratory tests of rock core or borewell geophysical using well logging technique with the slug test results could be some of the drawbacks of slug test investigation (Black, 1985). This could be attributed to the difference in the volume of subsurface formation tested through the slug test as compared to the prolonged pumping test.

5.2 Literature Review

One of the most commonly used techniques of groundwater investigation using slug test involves causing a near-instantaneous or sudden change in water head in a well or piezometer through either introduction or removal of a solid object (slug) and measuring the recovery of head to its initial position. This can also be achieved by the

addition of an equivalent volume of water or the removal of water from the well termed as rising-head and falling-head slug test. The sudden changes in pressure heads can be caused by pneumatic tests also (Fritz et al. 2016). The in-depth details of the design, performance and interpretation of slug test results as well as their advantages and disadvantage can be found in Butler, 1997; Kruseman and de Ridder, 1991; Todd and Mays, 2004**.** However, a brief review of the pertinent aspects of the present context is summarized. The initial solutions for analyzing the slug test data were demonstrated by Hvorslev, 1951 and Ferris and Knowles, 1954. Ferris and Knowles,1954 utilizing the Theis 1935 equation for drawdown in an instantaneous vertical line source or sink estimated the transmissibility of formation close to a well by plotting residual head versus reciprocal of time since the beginning of the test following instantaneous slug(water) injection test. Subsequently, Cooper et al. 1967 presented an exact solution for head after near instantaneous water injection in a fully penetrating finite-diameter well in a confined formation. The analytical solution developed by Cooper et al. 1967 can be represented as**:**

$$\frac{H(t)}{H0} = f(\beta, \alpha) \qquad 5.1$$

β and α are dimensionless time parameter and dimensionless storage parameter defined as:

$$\beta = \frac{KrBt}{rc^2} = \frac{Tt}{rc^2} \qquad 5.2$$

$$\alpha = \frac{Ss\, r_s^2}{rc^2} \qquad 5.3$$

where Kr is the radial component of hydraulic conductivity, B is the thickness of the confined aquifer formation, t is the time since the beginning of the slug injection test, r_c and r_s are the effective radii of well casing and well screen and Ss is the specific storage of the formation. The theoretical type curve generated using the analogy of heat flow equation is matched with the normalized head response versus time for estimation of aquifer transmissivity and the storage property (coefficient of storage) of a confined aquifer. Cooper et al. 1967 also demonstrated that the assumption of line source or sink in Ferris and Knowles, 1954 is only true for sufficiently large measures of time or in cases where the normalized head $H/_{Ho}$< 0.0025. Papadopulos et al. 1973 further extended the Cooper et al. 1967 type curve which was up to five orders

of α values (10^{-1} to 10^{-5}) to 10^{-10} to address to the need for hydrological properties estimation through slug test for low transmissivity formation where pumping test becomes impractical even for the shortest duration. However, similar shape of the type curve in the lower values of α, indicates lesser sensitivity of the recovery of the water level to the order of magnitude changes in the storage coefficient and the reliability of the estimated value of S becomes even more questionable for values smaller than 10^{-5}. The authors pointed out that an error estimate of less than 30% is likely in estimated transmissivity values using type curve matching even for the most carefully collected field observation data. The solution for determining the hydraulic conductivity of unconfined aquifers in isotopic conditions with complete or partial penetrating well was developed by modifying theim equation for slug test by Bouwer and Rice, 1976.

Investigation on hardrock hydrogeology being a source of water bearing formation as well as for safe disposal of radioactive waste has received considerable attention worldwide (Moench 1984 and Black 1985) but little is reported in terms of hydraulic characteristics of subsurface aquifers in the headwater regions of middle Himalaya. The fracture aquifers are complex, heterogeneous and anisotropic as compared to the porous medium and therefore warrant simplification to characterise the flow and transport properties in sloping topography largely underlain by metamorphic bedrock aquifer. The rock mass porosity could be classified as primary when the intergranular pore spaces are created during the depositional processes whereas secondary porosity mainly fracturing is caused by the tectonic movements. The hardrock can be segmented into two distinct elements, fracture and matrix block. The fractures are opening within the rock mass mainly responsible for the transmission of water with a negligible contribution to flow capacity whereas the matrix with significant pore volume contributes to the storage capacity of the rock mass. But in cases where the rock matrix is having low porosity and low permeability, discrete fracture single porosity idealization is being made with no flow between matrix and fractures (Wang et al. 1977). Barenblatt et al. (1960) and Warren and Root, (1963) proposed a dual porosity model to characterise the intermediate heterogeneous medium with fluid flow between matrix and fractures (Figure 5.1a). Gringarten (1982) summarized available methods for analysing flow test in fissured formation to relate the theoretical model

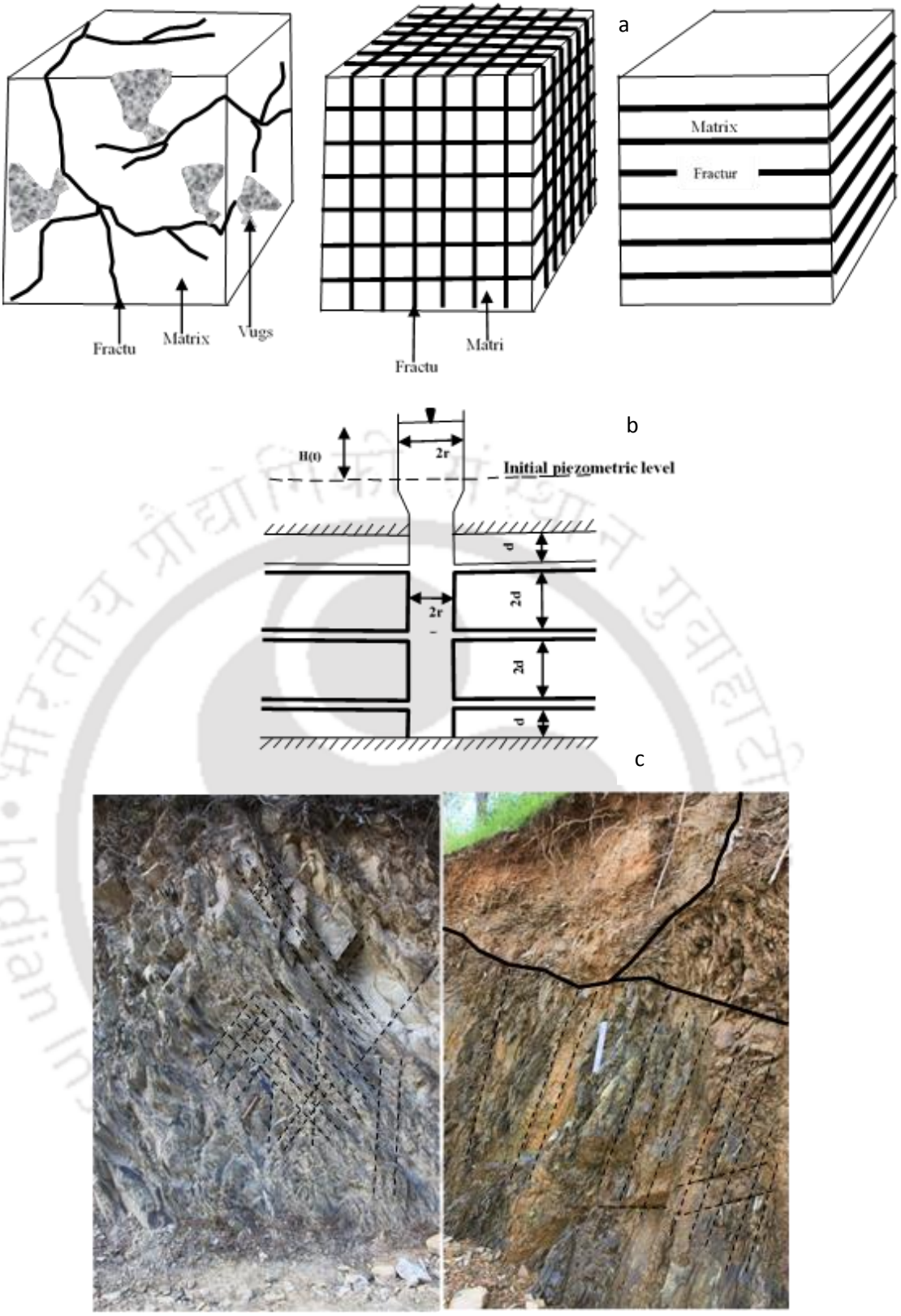

Figure 5.1: 3-D idealization of heterogeneous fracture rock (a) in orthogonal fracture network and matrix (after Warren and Root, 1963); 2-D representation of slab-shaped matrix (b) with horizontal fracture for slug test in dual porosity rocks (after Barker and Black, 1983) and field photographs of metamorphic two rock types (Quartzite and Phyllite) dominated by foliation and joint plane fracture networks(c).

with known inner boundary conditions (homogeneous/heterogeneous, wellbore storage, skin effect, partial penetration etc.,) and outer boundary conditions (constant head, no flow). Several slug tests performed for low permeability formation such as granite were analysed (Barker and Black, 1982) using the homogeneous porous medium approach of Cooper et al.1967. However, the results especially of specific storage estimates were found to be outside the expected range. This led to the new approach devised by Barker and Black, 1983 in fissured formation into regularized horizontal fissure homogeneous porous medium with storage in matrix porosity and transmissivity controlled by the regularised horizontal fissure system (Figure 5.1b). This analytical solution applied to the slug test, resulted in a good estimation of the hydraulic properties of naturally fissured rock. The two parameters, one ω which is the relative fracture storage parameter, and the other is λ which characterised the interporosity flow between matrix and fracture were introduced by Warren and Root, 1963 are sufficient to describe the flow properties in a two-porosity medium idealised as slab-shaped matrix separated by equally spaced horizontal fractures. The analytical solution for the application of slug test in a fully penetrating well is given by:

$$\frac{H(t)}{Ho} = f(\beta, \alpha, \omega, \lambda) \qquad 5.4$$

where: $\beta = {KrBt}/{r_c^2}$ representing dimensionless time parameter

$\alpha = r_w^2 S_s B / r_c^2$ which represents the dimensionless storage parameter

$\omega = \frac{\emptyset_2 C_2}{(\emptyset_1 C_1 + \emptyset_2 C_2)}$ ratio of specific storage of fractures over specific storage of both matrix and fracture, dimensionless

λ= parameter governing the interporosity flow, dimensionless

However, Butler,1997 mentioned that the introduction of two additional parameters may not facilitate the identification of double-porosity flow regime in the normalised head response data commonly used in slug test analysis from shallow groundwater. The fissured homogeneous dual porosity idealization against the convention homogeneous porous medium analysis approach resulted in an overestimation of transmissivity value by a factor not exceeding two whereas errors in specific storage estimate were significant in the conventional approach (Barker and Black, 1983; Black, 1985). Butler, 1997 pointed out that the lower than expected value of alpha

could be one of the means of identifying the two-porosity processes however such responses could also be generated vertical flow and low-permeability skin effect. Hence the authors recommended the use of Cooper et al.1967 model for slug test analysis and results of slug test should be corroborated with pump test data to test whether the heterogeneous formation can be conceptualized as homogeneous units. Butler, 1990 recommended using multiple slug test conductivity results to compare the drawdown in the same well while conducting a pumping test investigation. Worthington, 2015 stressed on the applicability of the double porosity and double-permeability model over the single-porosity equivalent porous medium (EPM) as it results in the underestimation of transport velocity due to the overestimation of porosity in bedrock aquifers. He summarised many such studies in different hydrogeological setups with an inappropriate model conceptualization of hardrock as EPM leading to gross undermining of rapid groundwater flow in fractured and fissured formations. The vulnerability of a source of freshwater such as springs, seeps, or even water well is dependent on the exact estimation of hydraulic conductivity of fractured medium with appropriate model conceptualization. Crystalline rock transmissivity and storativity were estimated using discrete level packer slug test in single-hole as well as fluid-injection tests (Shapiro and Hsieh, 1998). The study highlights variable transmissivity over different depth zone assuming homogeneous and isotropic confined formation using Cooper et al.1967 solution. The transmissivity estimates (sum of transmissivity) derived from the fluid-injection test only varied by an order of magnitude to the slug test estimate of T from the homogeneous formation. Heterogeneous model solution with varying number of horizontal fracture sets with unique T and S values were also developed for slug test. Comparisons of estimate of T using both the models (homogeneous and heterogeneous fracture formation) vary by an order of magnitude. Lee and Lee, 1999 reported results from a test site underlain by fractured crystalline rock (gneiss and granite) with repeated pumping (11 sets) and slug tests (70 sets) analysed using Cooper-Jacob,1946 and Cooper et al. 1967 for pumping and slug test respectively. The results showed identical mean values for both methods but the slug test results had more variability as compared to the pump test estimates. The study also highlighted that the initiation mechanism (falling or rising head) of the slug test as well as initial displacement could yield higher estimates of hydraulic conductivity by a factor of 1.5 to 4.0 by using Cooper et

al.1967. Repeat tests should be carried out especially in the case of slug tests to get a reasonable estimate of the hydraulic properties of the aquifer (Lee and lee 1999; Karasaki et al. 1988)

5.3 Method

The Bhimlitali micro-catchment nested with the Dugargad micro-watershed (Figure 5.1 and Table 2.1) is having a similar relief ratio as well as topographical and landuse as compared to Dugargad micro-watershed and is identified as a hydrological response unit for bedrock aquifer investigation and process conceptualization. A hydrological response unit (HRU) of 40 hectares (0.4 km^2) area was selected for shallow borehole drilling in the metasedimentary hardrock-dominated region of Lesser Himalaya (Figure 5.1). A Shaw Backpack Drill (Shaw Tools Ltd., Canada) was used to drill shallow bedrock borewells in the metamorphic rocks (Photograph 5.1 and Photograph 5.2). The 51mm coring tool is supported with drill engine, drill rod, diamond core bit, core catcher, compression bottles for continuous water supply, several extensions, etc. Solinst Levellogger 5 (Model 3001) combined with pressure sensor and temperature can record water level data at every 1 sec and accuracy of 0.05% FS (±0.3cm for 5m FS) with a diameter of 22 mm and is supported by Barometric compensation logger makes it an ideal tool for groundwater investigation.

Six boreholes (Figure 5.2 and Figure 5.3) were drilled using the portable drilling machine up to a maximum depth range of 6.4 m (BW6). The depth of the six borewells ranges between 2.29 m to 6.4 m. 51mm diameter boreholes were drilled to measure the water table depth which sustains the low-order streams and to carry out various aquifer-testing techniques. Core samples (Photograph 5.3 and Photograph 5.4) were collected to generate the lithologs of each borehole. The boreholes 4, 5, & 6 where dominated by sticky clay formation in the weathered rock, which made the drilling exercise very difficult to execute. It took three days to drill a single borewell with different drill times to complete the entire drilling exercise in the remote catchment. The details of the depth range and the lithologs are shown in the Figure 5.3. Once the drilling was completed, the boreholes were cleaned by injecting fresh water (Photograph 5.1 and Photograph 5.2) into the well with the help of a 12v battery-supported DC pump (60 psi). The well development was carried out until

clear water starts coming out of the drilled wells indicating clay (mud) (Photograph 5.1b) contents as well as finer sediments have been washed out of the inner walls of drilled borehole. After the water table got stabilized, the depth-to-water level data was

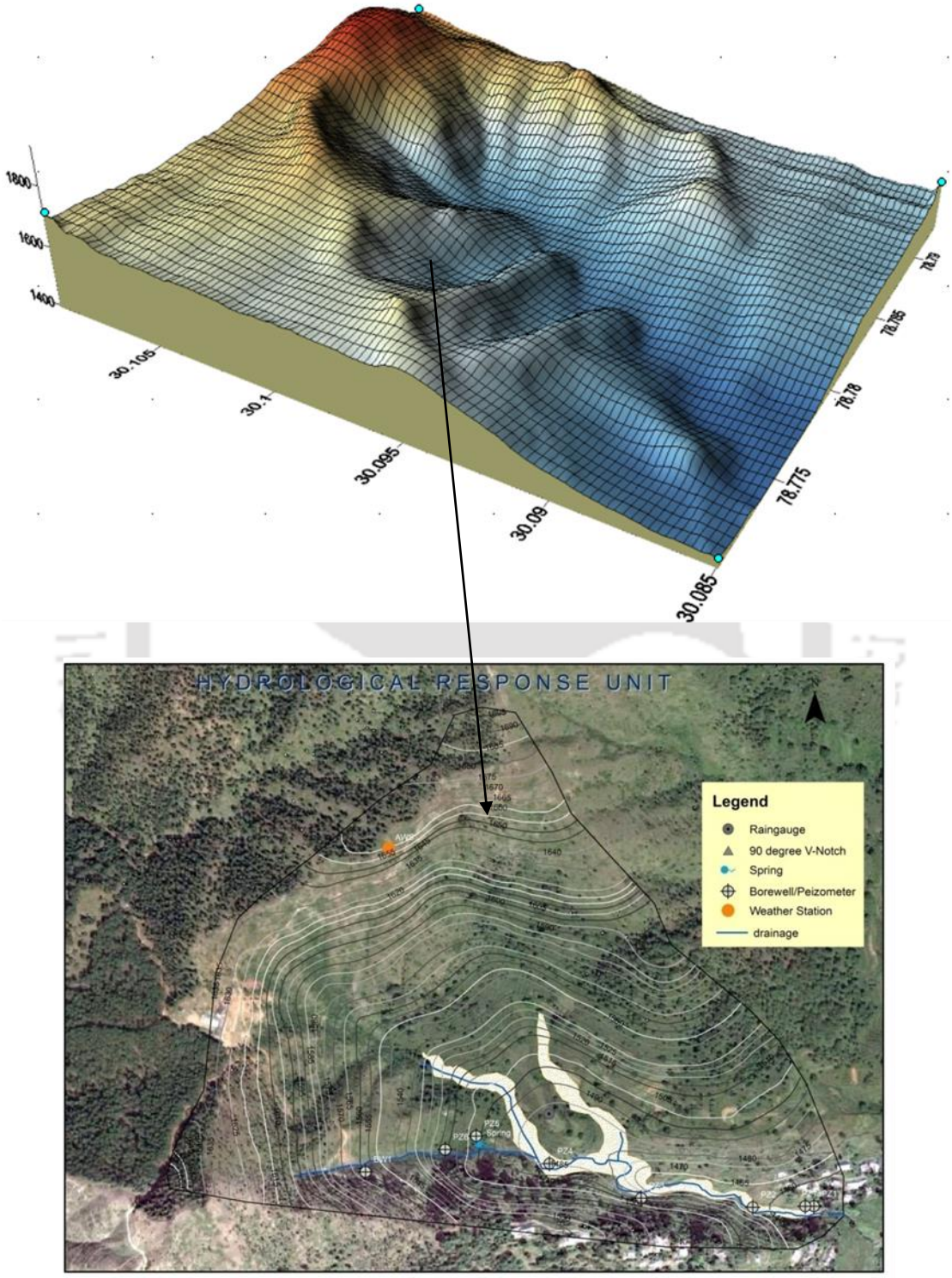

Figure 5.2: Elevation model of Dugargad microwatershed (a) having elevation range of 1380 and 1920 m a.m.s.l with nested Bhimlitali micro-catchment (b) showing a central narrow riparian valley bounded by hillslopes with locations of shallow borewell (piezometer) and rain gauge.

collected from the open-hole uncased shallow piezometers at a daily time interval. All the drilled piezometer showed permanent water table within a depth range of 0.6 to 1.5 m except for borehole 6, which was found dry during the winter and summer periods. Out of the six borewell, four boreholes (1 to 4) are located on the riparian valley portions near the second-order stream whereas borehole 5 and 6 is located in the hillslope domain (Figure 5.2 and Figure 5.3). Borehole 5 was drilled nearly 5m upslope from the location of the spring which was monitored at a daily time steps. A very deep cased bore well of 80 m with having 12.7 cm diameter was constructed in 2018 before the onset of monsoon in the headwater region and was instrumented with a water level recorder. Initial assessment of proper development in the shallow borewells/piezometer was conducted in each piezometer with repeated slug injection of water to assess the equal response in the water level change to the near-instantaneous injection of the water volume of 1 and 2 liters. The rising head slug tests were performed during February and March 2016 and subsequently, tests were repeated in the same months in the year 2018. The five piezometers were tested with 40 minutes of test duration and ten minutes of initial static water level observation before a slug of 1 liter was injected into the uncased well (Photograph 5.2 c and d). The water level change was recorded at every 1-second interval for 20 minutes and subsequently, 15 second interval was used to record data for the last 10 minutes. The percentage of recovery to the initial static level was recorded to plan for the subsequent repeat analysis of the same shallow borewells. The rising head slug tests were again conducted in the same month in the year 2018. The test duration was planned and executed for a maximum period of nearly two days to record the low permeability response after the injection of water. A two-liter volume was also used in borewell 5 for the rising head slug experiment. Attempts were made to carry out pumping test (Photograph 5.2c and d) in the shallow piezometer but the piezometer could not even support 1 minute of pumping except for the BW4 located at base of the hillslope. However, the post-recovery water level data after very brief pumping were utilized as falling head slug test results for borewells (BW1, BW2 and BW5). The analysis of drawdown and normalized drawdown data for the rising and falling head slug test was carried out using AQTESOLV software. In the present landscape of Lesser Himalaya, underlain by moderate to steeply dipping metasedimentary formation of Phyllite and Quartzite, the predominance of preferential flow through

dominant penetrative bedding planes, joints and fractures are dominant mechanism of subsurface groundwater flow. This has led to the assumption of the double-porosity model, where the fractured rock media is having fractures and the matrix blocks which differ in characteristics. Barker and Black, 1983 derived an analytical solution for a slug test in a well that fully penetrates, an isotropic fractured aquifer assuming a double-porosity model with blocks. The matrix blocks have low permeability whereas the fractures are having high permeability and low storage capacity. Barker and Black, 1983 derived an analytical solution for a slug test in a well that fully penetrates, isotropic fractured aquifer assuming a double-porosity model with blocks. Two slug test models for homogeneous confined aquifer as well as double porosity model were used to measure the hydraulic conductivity and specific storage of the metamorphic rock (Cooper et al.1967 and Barker and Black,1983). For the two devised methods the assumption of confined aquifer with water level to the drill depth was used a thickness of saturated zone in case of Cooper et al.1967assumption of fully penetrating well in homogeneous confined aquifer whereas simplified dual-porosity assumption devised by Barker and Black, 1983 with thickness of slab-shaped block of 1cm having 2.5 cm inside radius of an uncased borewell with 0.5 cm of distributed zone around the borewell was assumed for incorporating the input information along with response data of slug test analysis in the AQTESOLV software. The hardrock formation was assumed to be homogeneous and isotropic in absence of past studies with some results on the anisotropy ratio (K_v/K_h ratio) of the geological formation under investigation. Curve matching and sensitivity analysis were performed for various combinations of input parameters (early time, late time and complete response data). The response data were plotted in log-linear, linear-log and log-log scale as recommended in the manual of AQTESOLV software (User guide, Duffield, 2004). The initial assessment of horizontal hydraulic conductivity was made using the straight method (Hvorslev, 1951).

Photograph 5.1: Activities related to bedrock drilling for shallow borewelldrilling using portable coring equipment (a), the slurry of drill fluid during drilling (b), well development by ejecting water through battery support pump(c), diamond bit with fracture core (d) and shallow borewell after borewell development (e).

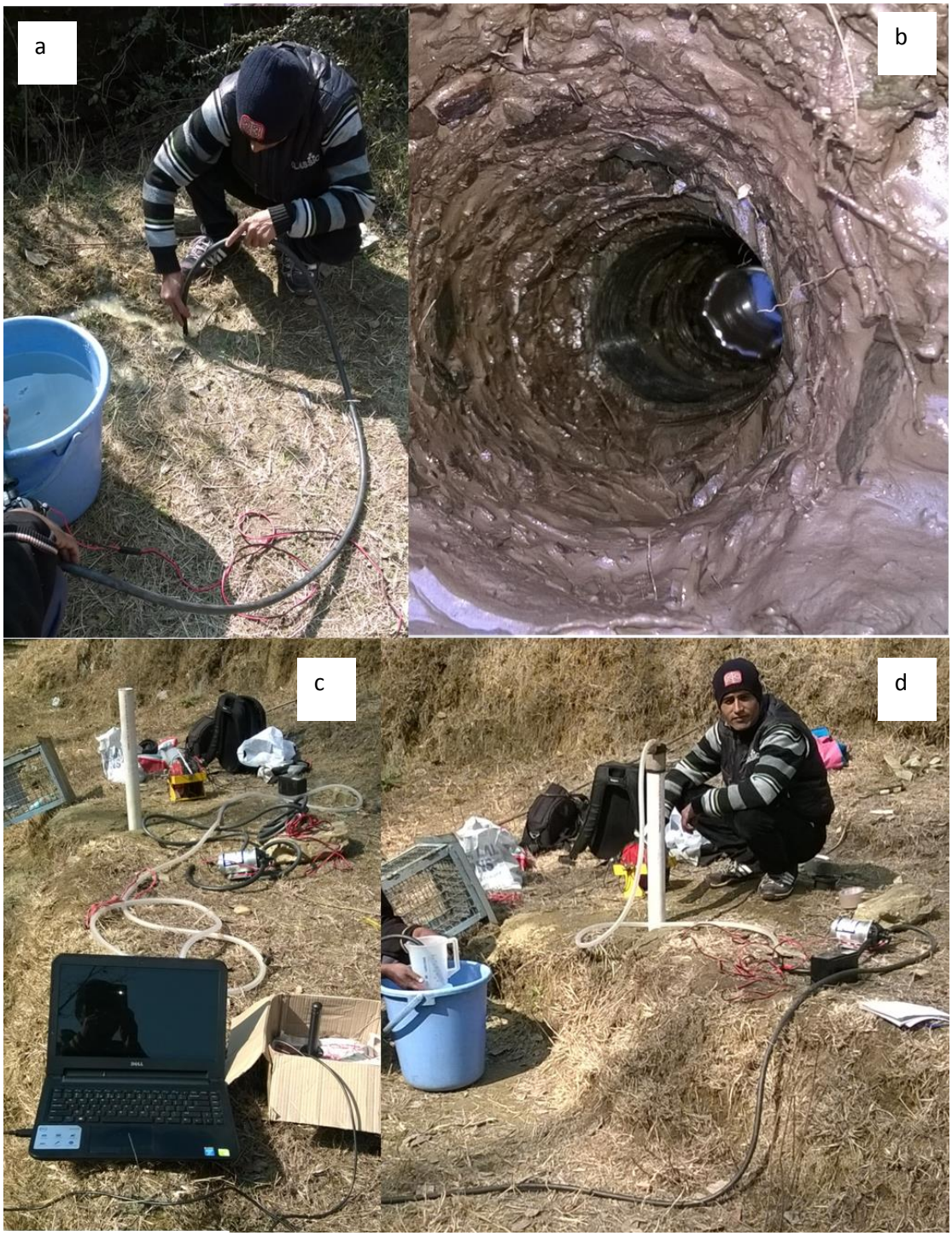

Photograph 5.2: Borewell development through ejection of clean water (a), a cleaned shallow borewell with DWL of less than 150 cm in central narrow riparian valley (b), setup of equipments for pump test and slug test experimentation in shallow borewell 1 in the study site (c& d).

Photograph 5.3. ShawBackback Drill with engine pressurized water supply and drill rod (a), close-up of rock core with fractured quartzite (b), deepest borewell (BW 6) of 6 m in the hill slope of the micro-catchment.

Photograph 5.4. Rock Cores collected during the drilling exercise at selected hydrological response unit (HRU).

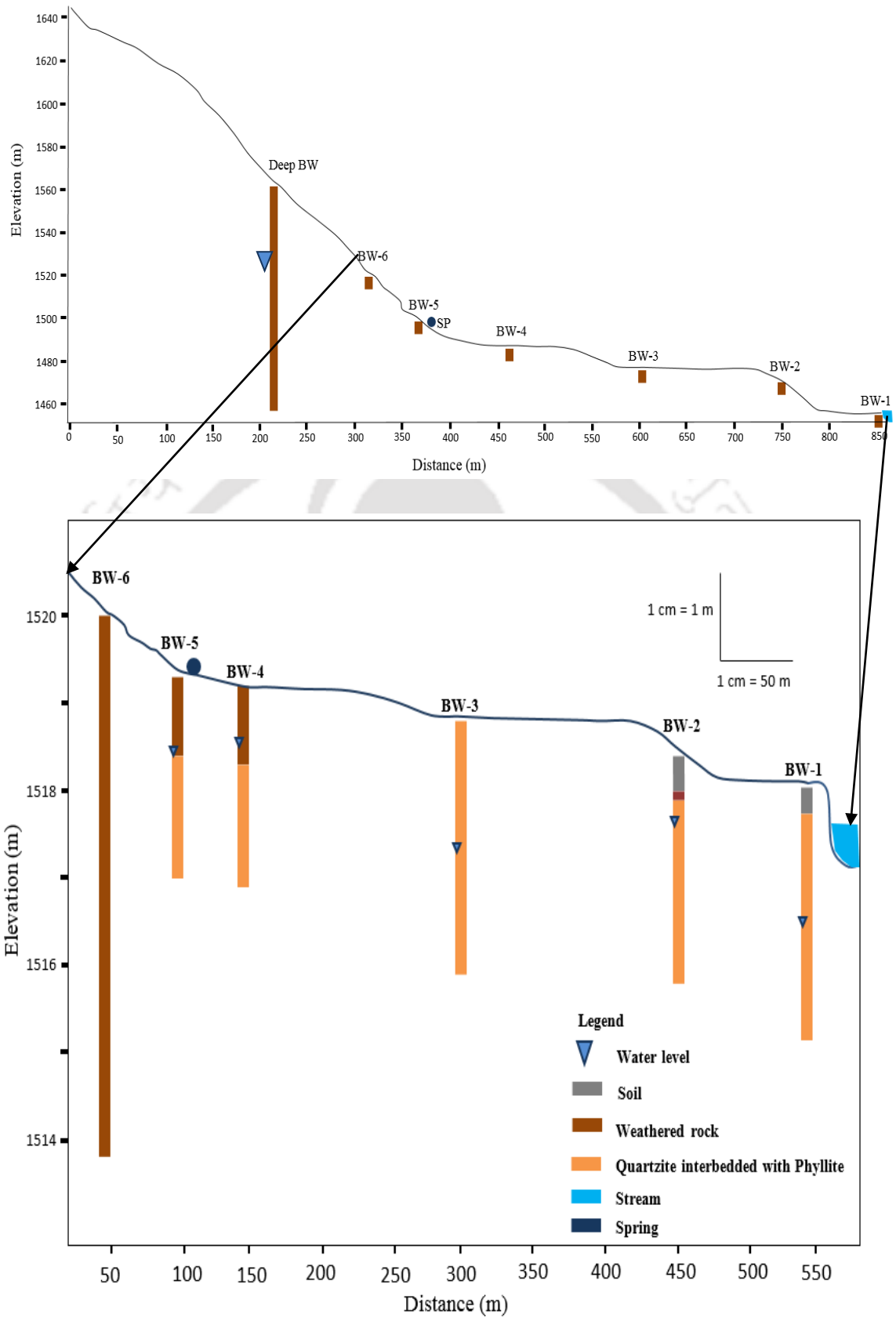

Figure 5.3 Two cross-sections depict the deep borewell (80m) and shallow borewells (< 6.4 m) along the central stream and the hill slope showing the lithologs of six shallow borehole/piezometer and depth to water level from the ground level.

5.4 Results and discussion

5.4.1Depth to water level observation

Depth to water level plots are shown in Figure 5.4 and Figure 5.5 wherein maximum monthly variability is observed during the pre-monsoon and monsoon periods and gradual recession is observed in the post-monsoon and winter periods. Borehole 1and 2 showed water level as deep as 0.8 m to 1.4 m below ground level but with the onset of monsoon rainfall water level starts rising to the surface. The borehole 3, 4, and 5 showed water level as deep as 1.4 to 1.6 m but water level reaches up to 0.10 to 0.80 m during the monsoon period. Interestingly, borehole 6, located in the hillslope region which was dry during the lean season, showed water level as deep as 4 m during July month and water level rose up to 1 m below the ground level during July and August, which was followed by a recession period till it became completely dry during the December month. The valley region of the selected HRU has permanent shallow water table and the hillslope domain have deeper groundwater during the lean period and a build-up of water table occurs with the rainfall recharge due to the influx of monsoon rain.

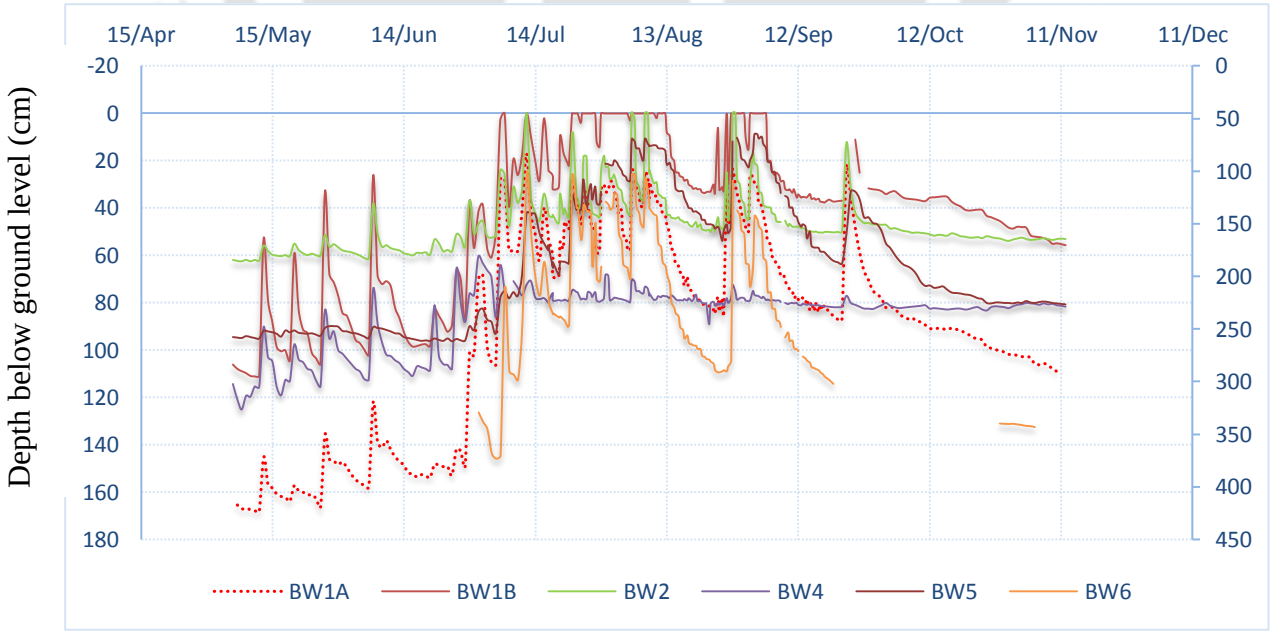

Figure 5.4 Depth to water level plot indicating a rapid response in all the shallow piezometer in the pre-monsoon and monsoon period for 2017. The secondary y-axis depicts the variability of water level in BW6 during monsoon and post monsoon period but remains dry in other seasons.

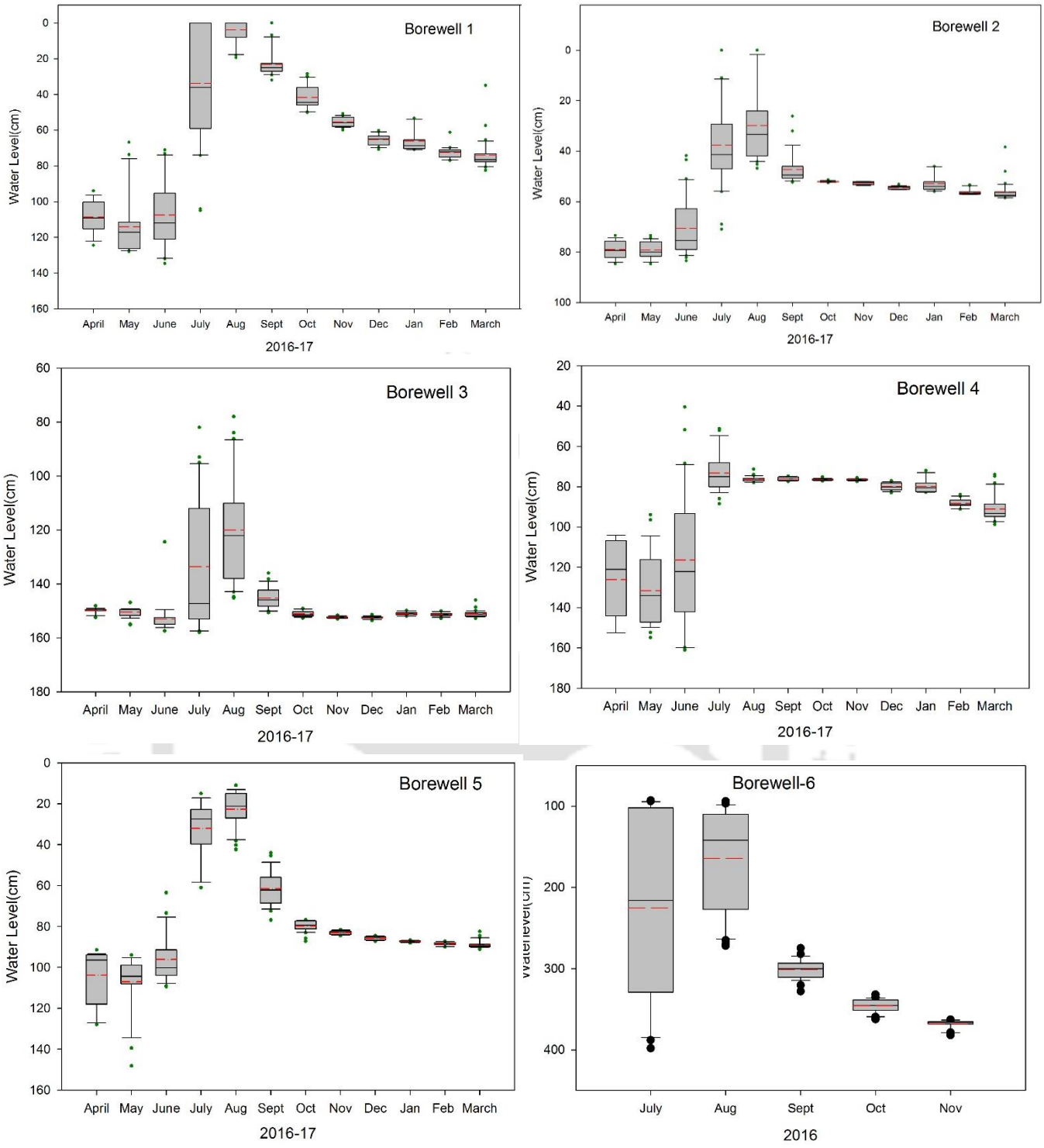

Figure 5.5 Depth to water level boxplot showing median value in red and mean in black from April 2016 to March 2017 period in six shallow bedrock borehole/piezometer.

5.4.2 Slug test

The slug test is a simple, very cost-effective and rapid method, which involves either sudden removal or the addition of a known volume of water, to create a positive or negative displacement in the static water level (Butler, 1997). This rate of change of water level is a function of the hydraulic conductivity of the formation and geometry of the borehole. Ideally, a slug test is performed for *in-situ* estimation of media characteristics in formation with low hydraulic conductivity.

A slug test was performed in each of the shallow boreholes using 1 or 2-liter volume of water as slug, which was poured into the borehole near-instantaneously, which caused more than 20cm of displacement in the static water level. It is recommended that the change in the head from the static water level should be in the range of 10 to 50cm (Kruseman and de Ridder, 1991) whereas Butler, 1997 recommended an initial displacement (Ho) of 20 to 200 cm. A waterlevel recorder (Solinst water level recorder) was placed at appropriate level into the borehole below the static water level to record the change in the head after addition of one-liter volume of water. Thirty minutes of observation were recorded with the water level recorder and a barologger for water level compensation. The slug test was repeated to ensure the same response is recorded with each repeat test.

Interestingly, 30 minutes' observation in each of the boreholes showed a different recovery percentage to the instantaneous injection of water (Figure 5.6). The borehole-4 showed near instantaneous recovery to static water level with a very sharp peak of water head, whereas only 6.58% of recovery was recorded for borehole 1. The borehole-2 and borehole-3 showed 28% to 59% recovery to the initial static water level whereas the borehole-5 showed 95% recovery. This could be indicative of the fact that the *in-situ* formation of near to tested zone in borehole-4 is having high-k (hydraulic conductivity-K) whereas the K decreases in the order: (BW4>BW5>BW3>BW2>BW1) in the formation close to the tested saturated zone. The initial displacement of water level (Ho) as compared to the static water level ranges between 20.36 cm (BW4) to 40.07 cm (BW1) suggestive of the similar finding of the above statement wherein low permeability formation in the immediate contact of static water level showing higher initial displacement (Figure 5.6). The repeat rising head slug test values for the year 2018 showed similar initial water level

displacement which ranges between 43.61 cm (BW 1) and 27 cm (BW2). But borewell 2 and borewell 5 showed some difference in Ho value due to variability in the water level depth from the ground surface as compared to 2016 in rising head slug test results. This could be due to the existence of fractures close to the borewell or could be the result of other heterogeneity. The time period of monitoring of the falling head slug test varied between more than five hours (BW 2 and BW 5) to two days in Borewell 1. The initial negative displacement ranges between 77 cm (BW1) to 104 cm (BW2) whereas a displacement of 85cm was observed in BW5. The falling head results in BW4 could not be analyzed due to oscillatory response in the water level record (critically damped) caused by high transmissivity formation. More than 85% of recovered was recorded for the three shallow piezometer (borewell).

The response data of slug tests were plotted in log-linear or linear-log scale of displacement of head above static water level or normalized head (H(t)/Ho) with respect to log time. These response data are analyzed by comparing with theoretical models of test responses (Figure 5.7). The hydraulic conductivity estimates through slug test using Cooper et al.1967 assumption of homogeneous confined aquifer is ranging multiple orders of magnitude as anticipated from the fractured rock formation (Table 5.1). The horizontal hydraulic conductivity of the geological formation (quartzite interbedded with phyllite) ranged from 0.00037 to 1.39 m/day with the geometric mean of 0.042 m/day. However, the results are dependent upon the complete or partial early/late time match with the type curve as depicted in Figure 5.7. For example, the analysis using Cooper et al.1967 type curve matching in BW1 with initial 30 minutes of response data resulted in one order higher horizontal K value as compared to matching of response data with complete recovery. However, the analysis showed two order of difference in K with the late time matching of response data from the early time matching of type curve (Figure 5.7a). The storativity values ranged 10^{-3} to 10^{-10} with geometric mean of 10^{-8}. The results of dual porosity model (Barker and Black, 1983) also indicate transmissivity value for fracture ranged from 1.17 to 10^{-5} m^2/day whereas a very low storativity is observed for the metamorphic rock. A similar difference in results can be observed in the falling head experiment with the BW1 with early and late time matching. Borewell 2 showed overall consistent results in the repeated rising head and falling head slug tests. The borewell 3 estimated results (Table 5.1) showed one order of higher K value than the nearest

borewell 2. However, the falling head results show a poor match with the type curve (Figure 5.8e). The estimated values of two falling head slug test in borewell 5 are in close agreement with borewell 3 hydraulic conductivity estimates but the 2 litre slug test analysis estimate showed a higher value of K. This value was excluded for estimation of the geometric mean of the entire test results in all the shallow borewells. The K value estimate from a single rising head response data of very fast recovery is indicative of High-K formation or the presence of fracture but probably late time fitting resulted in a lower value of K. The repeat test response data from BW 4 could not be analyzed due to the oscillatory nature of response data. Not much variability could be recorded in the storativity values of the slug tests (Table 5.1). The results obtained using dual-porosity model (Barker and Black, 1983) with the Cooper et al. 1963 idealization did not vary much in the transmissivity estimate of fracture with homogenous confined aquifer K value. The reason for similar results especially in horizontal hydraulic conductivity estimates could be attributed to the collective averaging of individual fracture transmissivity values in the Barker and Black, 1983 model giving similar results as of a homogeneous CBP model (with very similar type curves in both the model approach), especially for low storage coefficient formations (Bosch Llufriu, 2017).

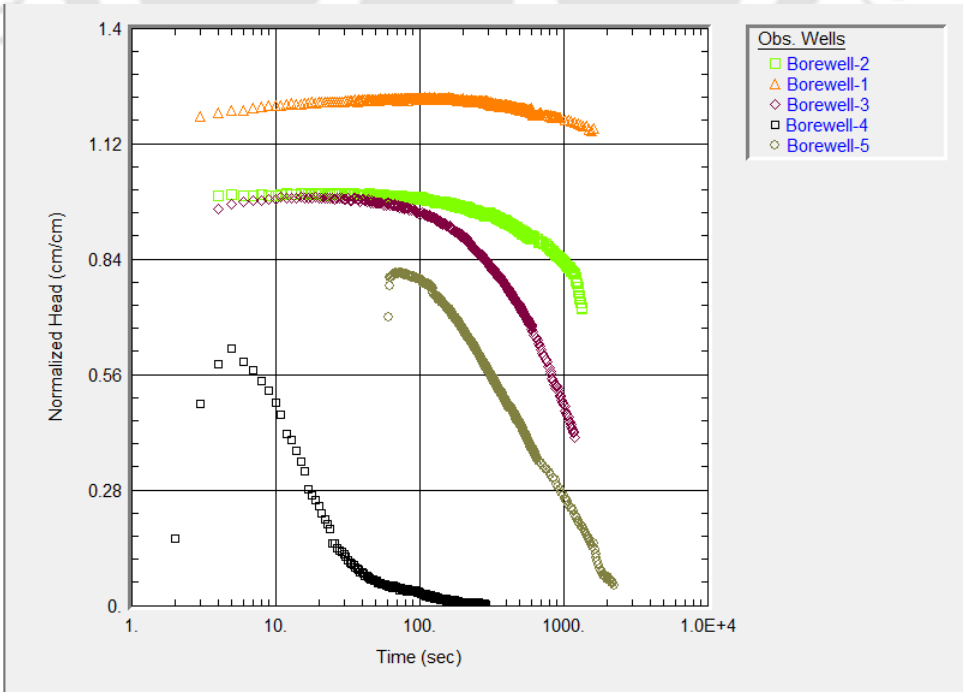

Figure 5.6 Normalized head vs. log time of series of slug test performed in the five monitoring well.

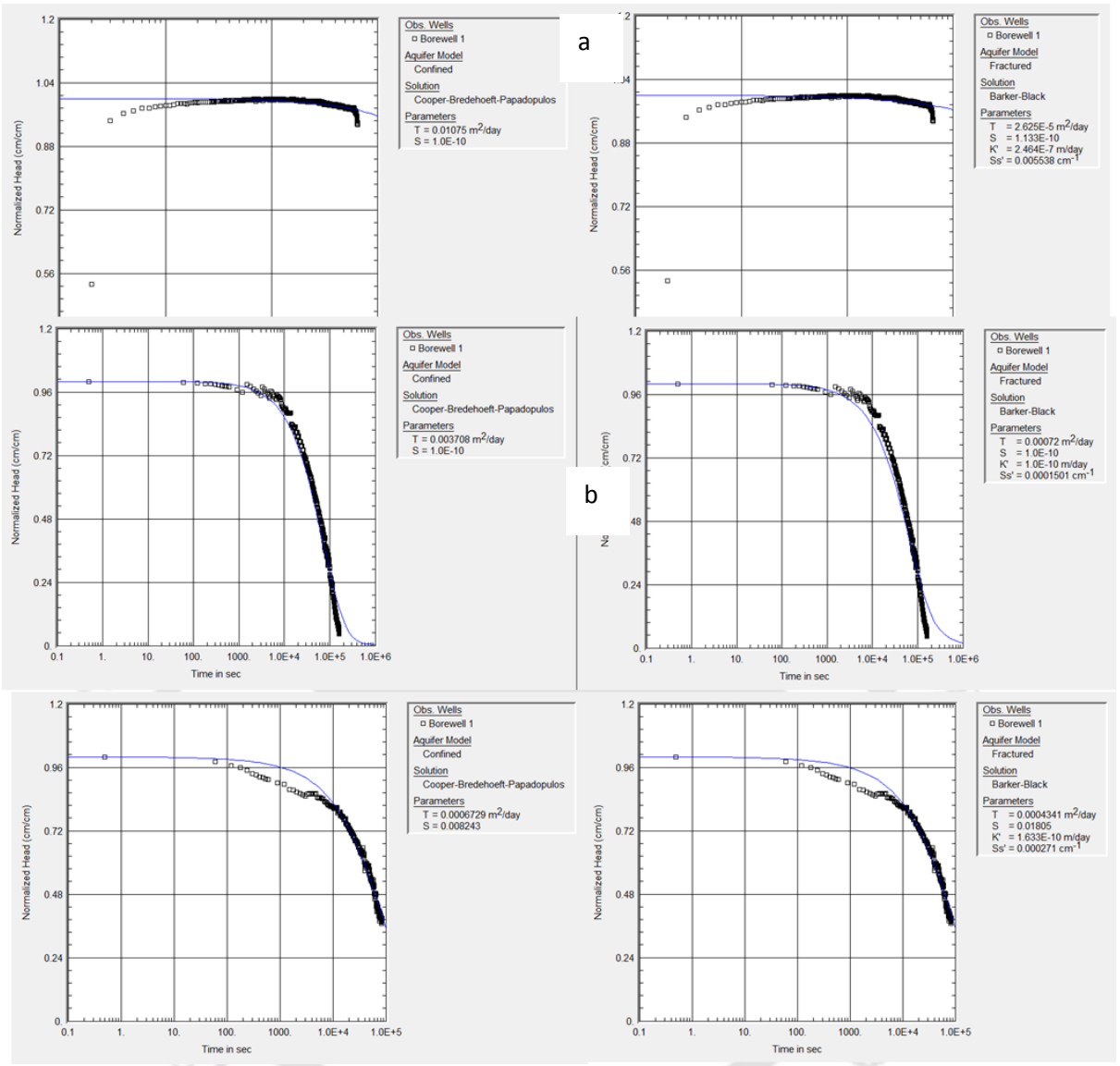

Figure 5.7 Normalised Head (H(t)/Ho) vs. log time plot using response data of rising head slug test in shallow borewells {Bw1(a), Bw2(b), Bw3(c), Bw4(d) and Bw5(e)} by applying homogeneous confined (Cooper et al. 1967) and dual porosity approach (Barker and Black, 1983) to bedrock riparian aquifer.

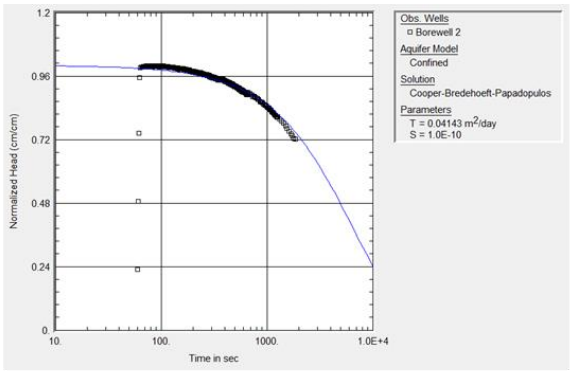

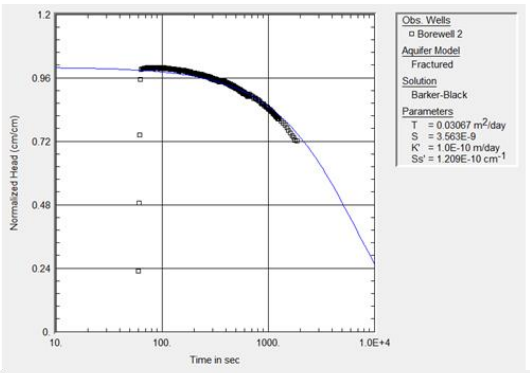

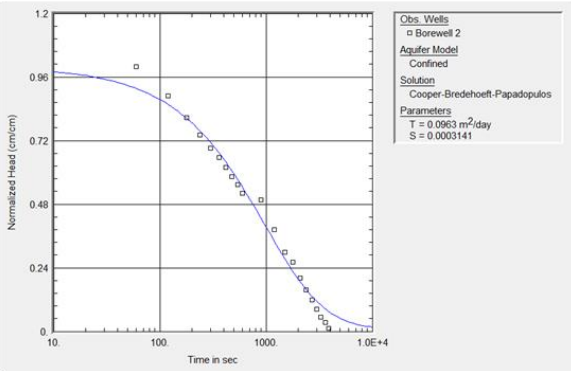

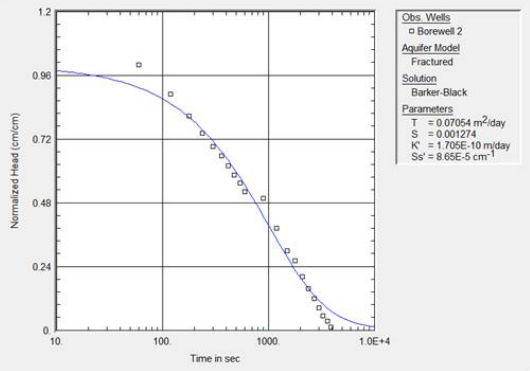

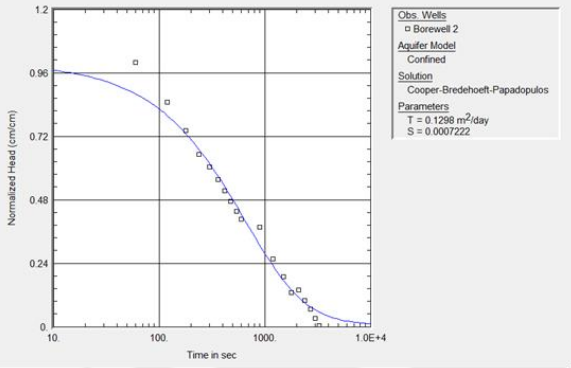

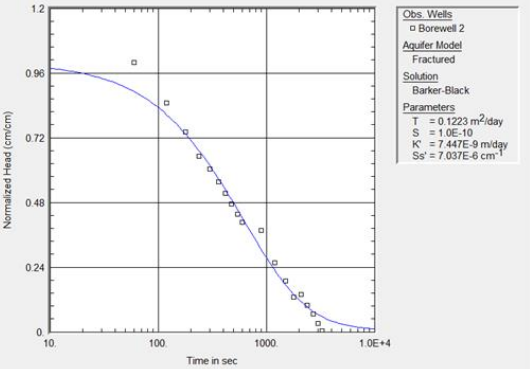

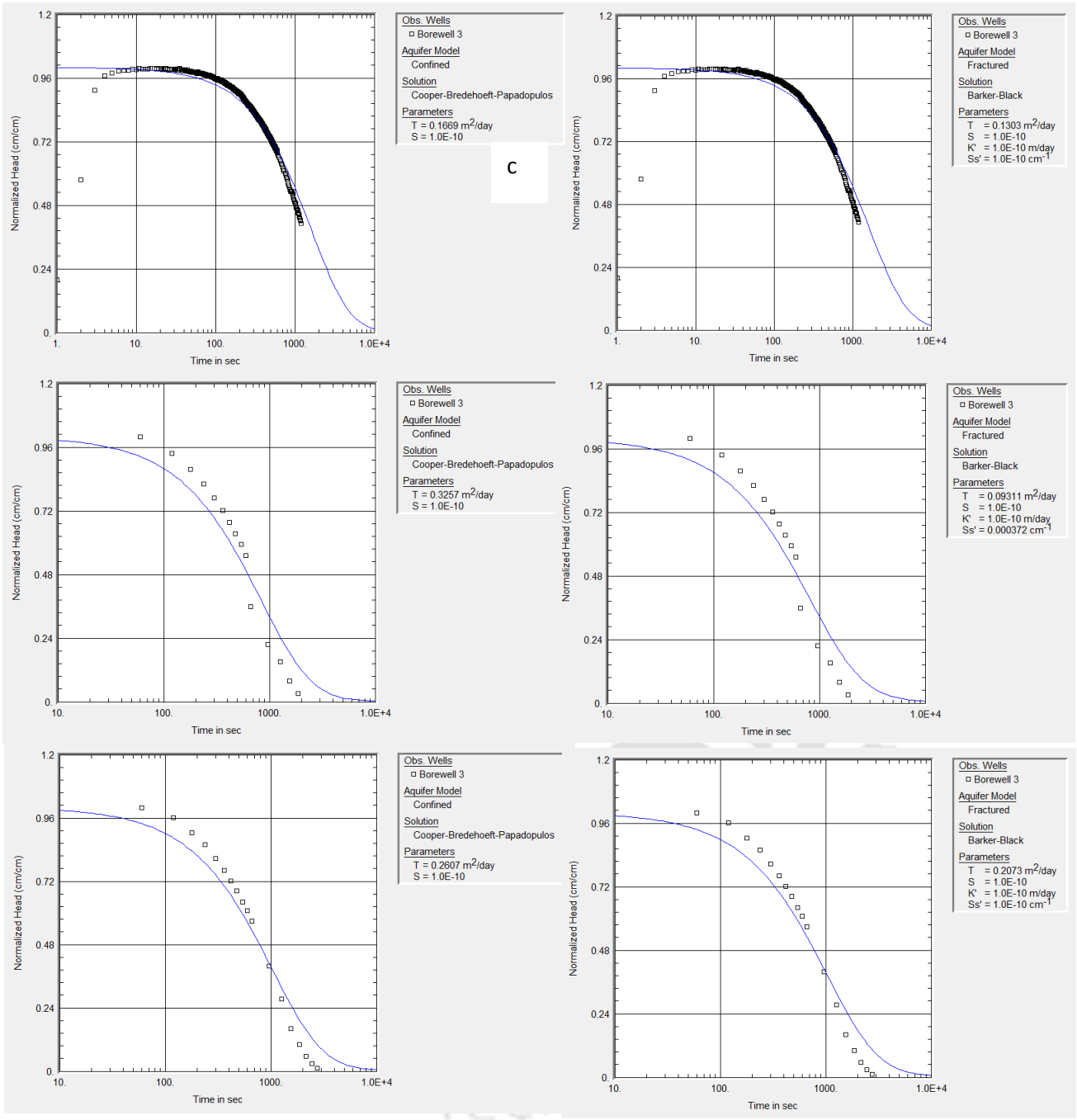

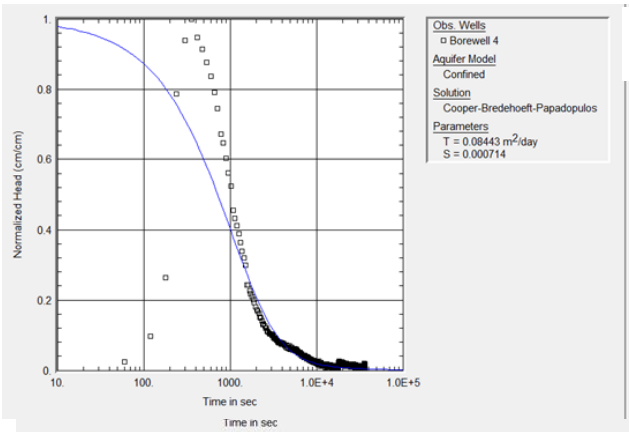

d

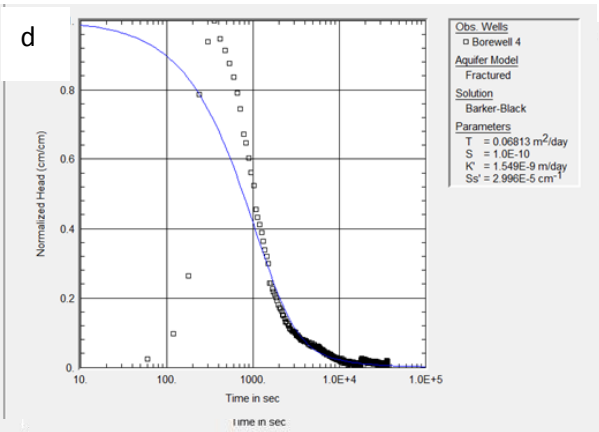

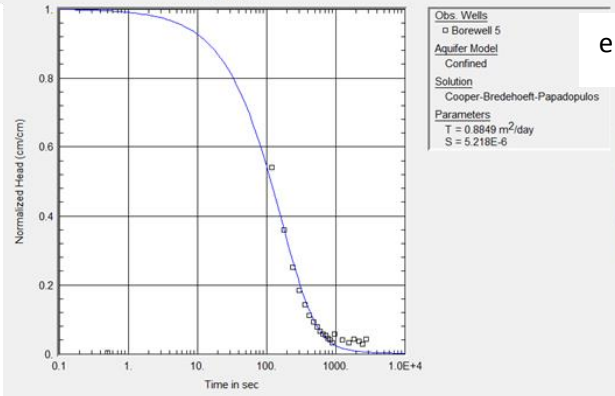

e

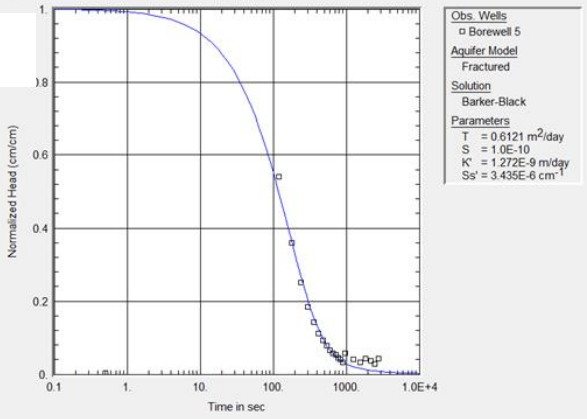

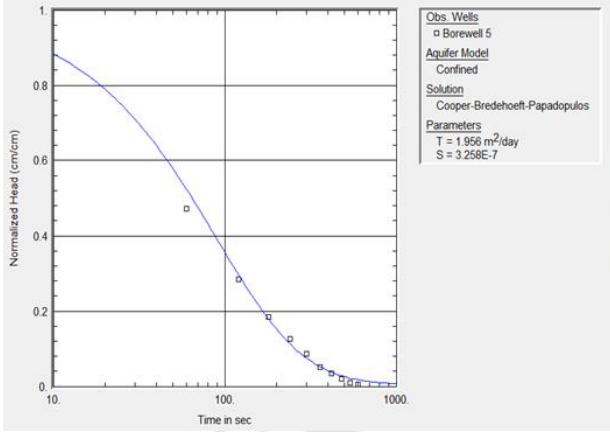

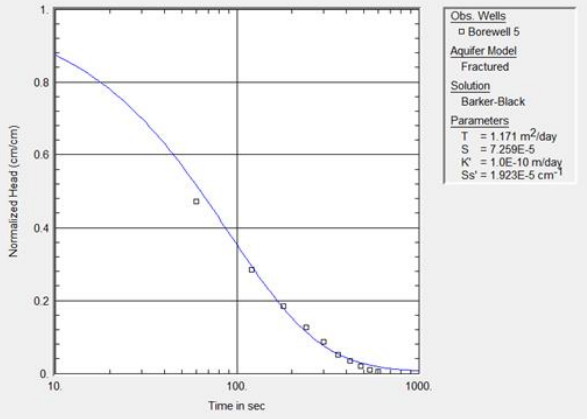

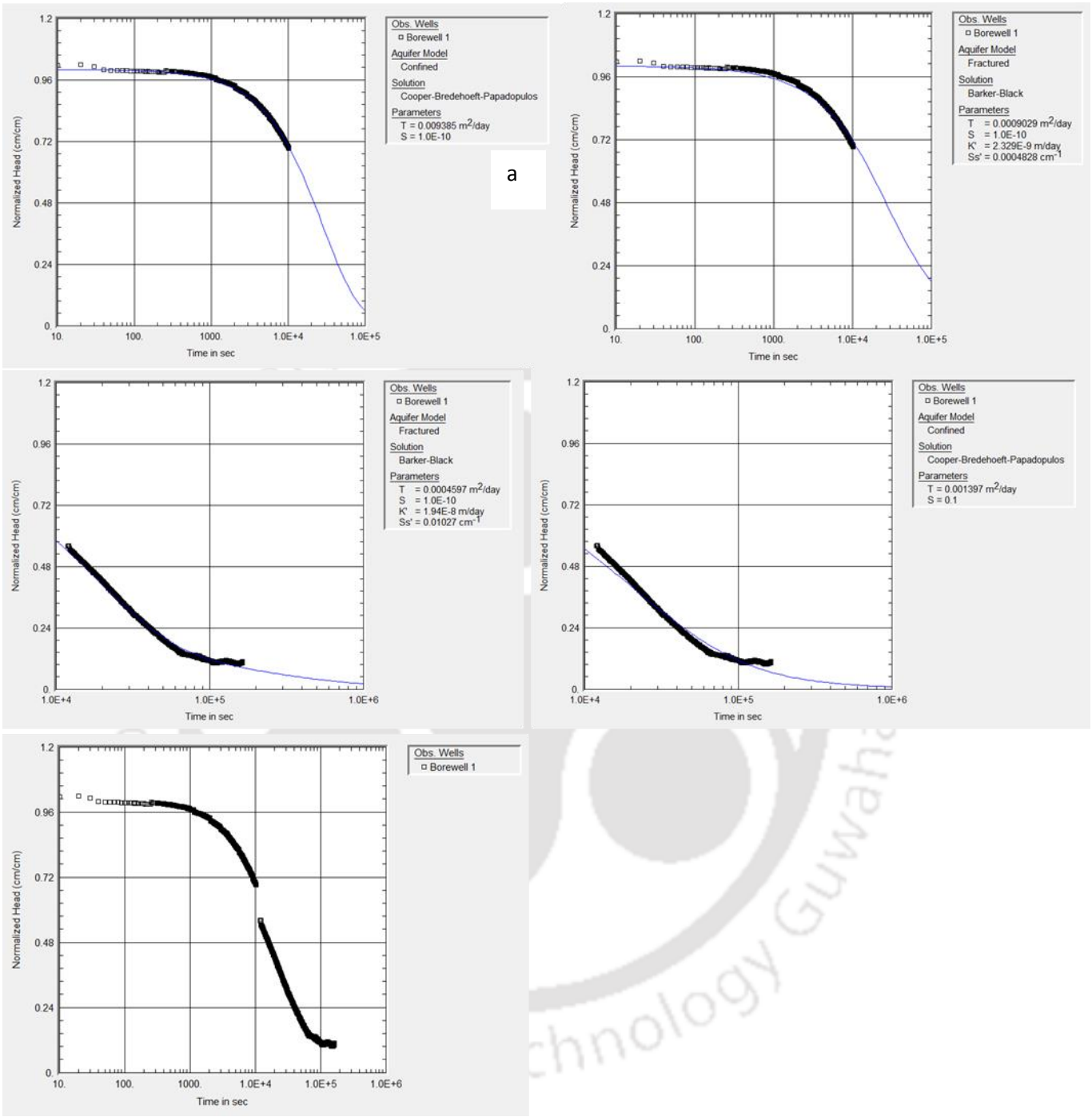

Figure 5.8 Normalised Head (H(t)/Ho) vs. log time plot using response data of falling head slug test in shallow borewell {Bw1(a), Bw2(b), Bw5(c) &Bw3(d)} by applying homogeneous confined (Cooper et al. 1967) and dual porosity approach (Barker and Black, 1983) to bedrock riparian aquifer.

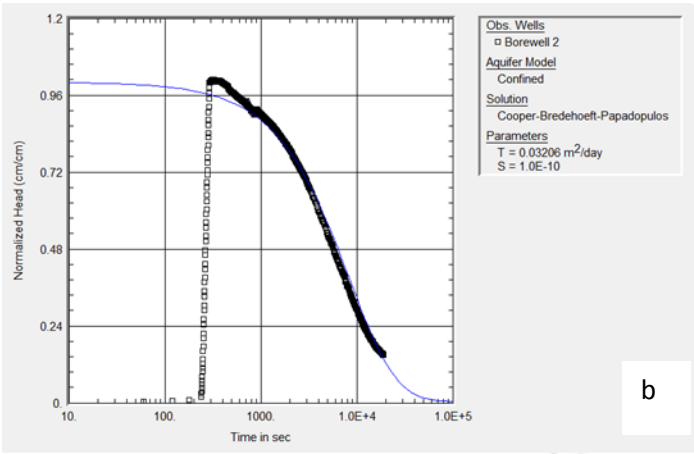

b

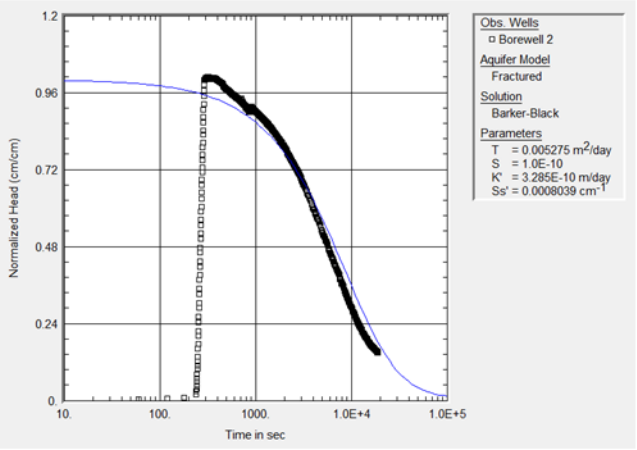

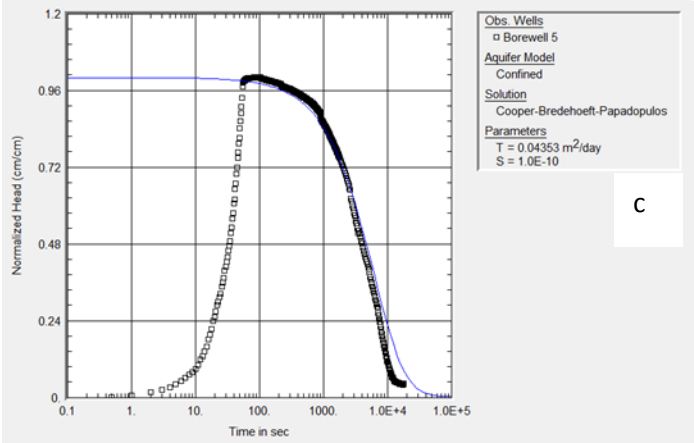

c

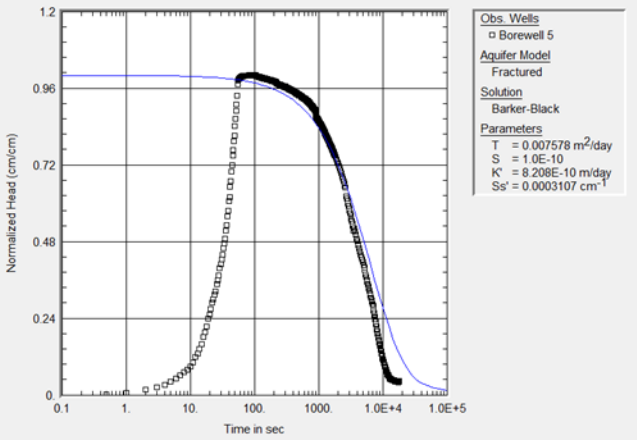

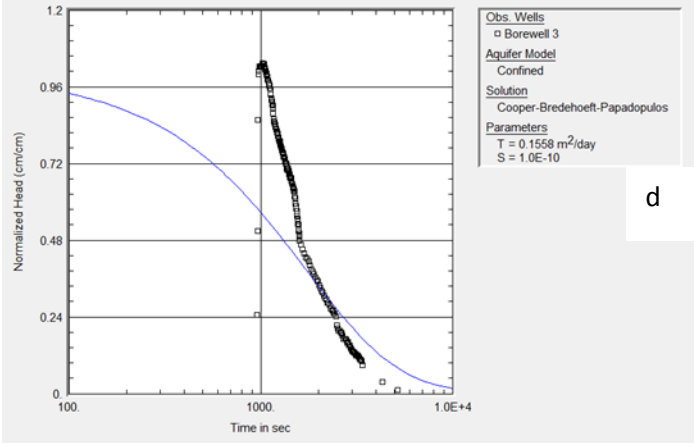

d

Table 5.1 Transmissivity and storativity values of homogeneous confined aquifer and double-porosity (fracture and matrix) calculated using rising head slug test.

Test →	Cooper-Bredehoeft-Papadopulos Solution		Barker-Black Solution			
Borewell ↓	Transmissivity (T) m2/day	Storativity(S)	Fracture Transmissivity (T)	Fracture Storativity(S)	Matrix Hydraulic Conductivity (k')	Matrix Specific Storage (Ss')
	0.01075	1.00E-10	2.63E-05	1.13E-10	2.46E-07	5.54E-03
Bw 1	0.003708	1.00E-10	0.00072	1.00E-10	1.00E-10	1.50E-04
	0.0006729	0.008243	0.0004341	0.01805	1.63E-10	0.000271
	0.04143	1.00E-10	0.03067	3.56E-09	1.00E-10	1.21E-10
Bw2	0.0963	3.14E-04	0.07054	1.27E-03	1.71E-10	8.65E-05
	0.1298	7.22E-04	0.1223	1.00E-10	7.45E-09	7.04E-06
	0.1669	1.00E-10	0.1303	1.00E-10	1.00E-10	1.00E-10
Bw3	0.3257	1.00E-10	0.09311	1.00E-10	1.00E-10	3.72E-04
	0.2607	1.00E-10	0.2073	1.00E-10	1.00E-10	1.00E-10
Bw4	0.08443	7.14E-04	0.06813	1.00E-10	1.55E-09	3.00E-05
	0.3896	1.00E-10	0.106	1.00E-10	1.00E-10	6.23E-04
Bw5	0.8849	5.22E-06	0.6121	1.00E-10	1.27E-09	3.44E-06
	1.956	3.26E-07	1.171	7.26E-05	1.00E-10	1.92E-05

Table 5.2 Transmissivity and storativity values of fracture and matrix calculated from falling head slug test.

Test → / Borewell ↓	Cooper-Bredehoeft-Papadopulos Solution		Barker-Black Solution			
	Transmissivity (T) m2/day	**Storativity(S)**	**Fracture Transmissivity (T)**	**Fracture Storativity(S)**	**Matrix Hydraulic Conductivity (k')**	**Matrix Specific Storage (Ss')**
	0.009385	1.00E-10	0.0009029	1.00E-10	2.33E-09	4.83E-04
Bw1	0.001397	0.1	0.0004597	1.00E-10	1.94E-08	0.01027
Bw2	0.03206	1.00E-10	0.005275	1.00E-10	3.29E-10	8.04E-04
Bw3	0.1558	1.00E-10	-	-	-	-
Bw5	0.04353	1.00E-10	7.58E-03	1.00E-10	8.21E-10	3.11E-04

5.4.3 Pumping test

A single well test by pumping at a constant rate (Photograph 5.2 and Figure 5.9) was also attempted for all the monitoring well. The borehole-4 supported 15 minutes of pumping, and a volume of 10 liters was pumped out at an average pumping rate of 0.7 litres per minute, but the drawdown, and recovery response observed were inconsistent and reflects an oscillatory response. In another attempt, the pumping test was carried out for 30 minutes in bore hole-4. However, this exercise also has not resulted in the generation of appropriate response data. The remaining monitoring well could only support one minute of pumping which could empty the wellbore storage and pumping could no longer be continued. This could be due to the low transmissivity of the *in-situ* formation making it an ideal case to be investigated through slug test. However, the recovery response data (after quickly empting the monitoring well) collected over one to two day's time provided an opportunity to analyze it through recovery method. The recovery data plot (Figure 5.10) as two straight lines indicative of double porosity response of fracture and rock matrix. The data was also analyzed through the falling head slug test approach (Figure 5.8 and Table 5.2). An attempt was made for multiple wells aquifer testing in which an observation well was drilled up to a depth of 245 cm at an appropriate distance to the borehole-1. The multiple well test did not result in any drawdown in the observation well due to low hydraulic conductivity of the formation. The level logger depth, depth of inlet pipe, barologger, depth to water level is clearly shown in Figure 5.9.

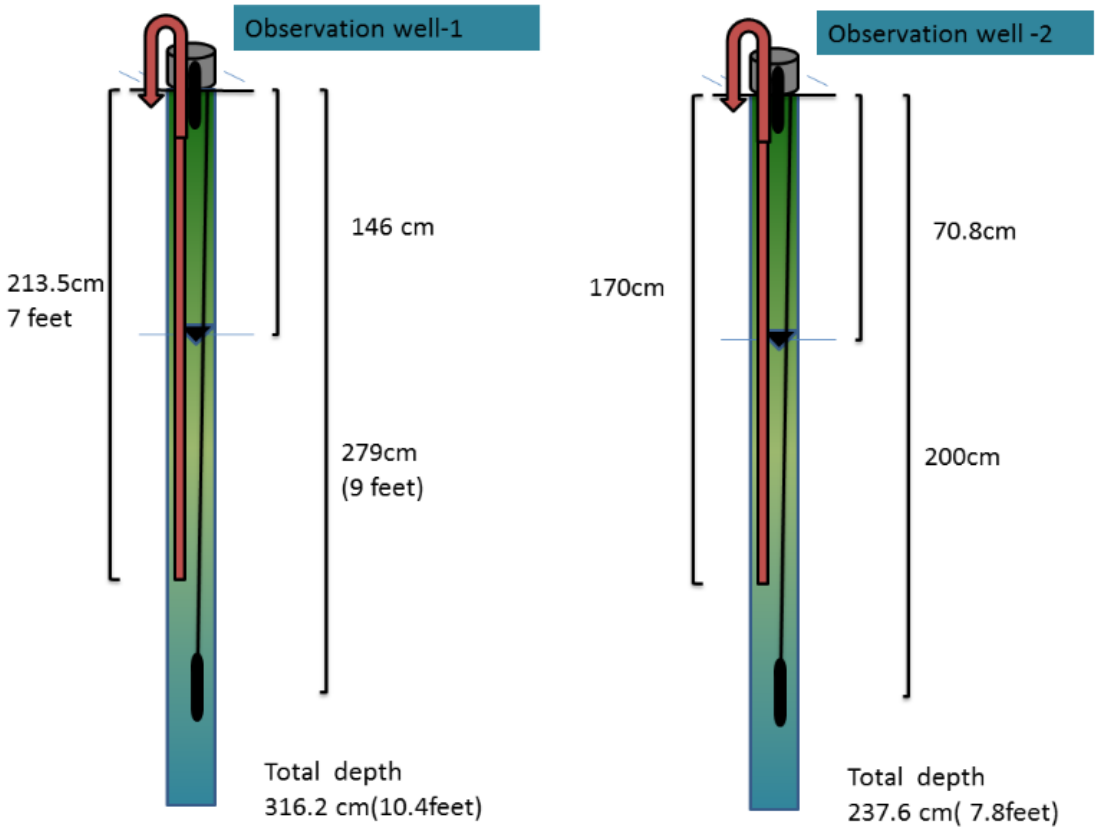

Figure 5.9: Schematic of the arrangement made for pumping test in monitoring well 1 and 2.

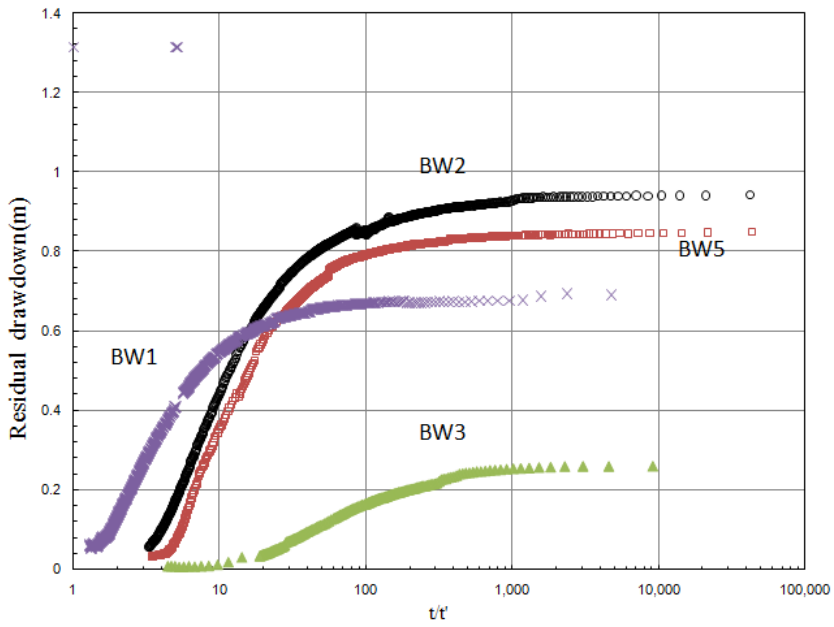

Figure 5.10: Recovery data plot after only 1 minute of pumping test in the borewells.

5.5 Conclusion

Groundwater in hardrock aquifers sustains the small springs, streams as well as large rivers year-round. However, very little is known about the important hydraulic characteristics of heterogeneous fractured geological formations in the headwater regions of the middle Himalaya dominated by metasedimentary rocks. The investigation resulted in estimation of two key hydraulic parameters (hydraulic conductivity and storativity) from a riparian and hillslope aquifer system through the construction of shallow piezometer (< 6.4m deep) in an experimental hillslope located with a catchment of 40 hectares. Rising and falling head slug test response data were analyzed in the low-permeability geological formation where other flow analysis methods like pump test could not be feasible. The response data for slug test analyzed through porous medium approach as well as regularized fractured porous medium idealization for a naturally fractured dual-porosity geological formation through type-curve matching technique indicate large spatial variability arising out of heterogeneity in fractured heterogeneous formation. The slug test estimate for horizontal hydraulic conductivity ranged from 0.00037-1.39 m/day with the geometric mean of 0.042 m/day, whereas storativity values ranged 10^{-3}-10^{-10} with geometric mean of 10^{-8}. The results of dual porosity model did not vary much from the homogeneous confined aquifer assumption and indicate very low storativity for the metamorphic rock in the study area. However, the results could not be verified due to lack of complimentary data on aquifer parameters estimated through pump test or other means for similar geological formations.

CHAPTER 6

Groundwater Recharge

6.1 Introduction

Groundwater recharge assessment is essential as rural and urban water supply, crop irrigation and ecosystem services depend on catchment water storage. Until now, little research has been carried out, especially in fractured bedrock groundwater aquifers in headwaters regions of the Indian Himalaya. The understanding of the heterogeneous hard rock fracture aquifer systems and recharge during the monsoon period is indispensable in a climate dominated by wet and dry seasons as it acts as a source of water sustaining the spring and stream flows which are the key resources for the rural water supply. All over the world, there is a growing realization that a detailed understanding of groundwater recharge processes as well as quantification of annual and seasonal recharge is necessary under changing climate conditions. Although accurate assessment of groundwater recharge is difficult and combination of methods is suggested for proper assessment of recharge (Healy and Cook, 2002). The most widely applied method relies on the time series groundwater water-table fluctuation data and estimate of specific yield. Nevertheless, this method has some limitations such as for conditions when recharge is equal to the rate of drainage leaving out of the water table; diurnal fluctuations; Lisse effect due to air entrapment; field measurement of specific yield (Healy and Cook, 2002; Crosbie et al. 2005). In a condition where a short-term water level rise is observed in response to rainfall event, episodic master recession method (EMR) (Nimmo et al. 2015) is suitable for episodic recharge assessment of individual recharge event.

6.2 Literature Review

Groundwater recharge could be defined as the addition of water to the water table which represents the upper surface of the saturated zone, together with associated flow away from the water table within the saturated zone (Freeze and Cherry, 1979). In the context of the middle Himalaya in the present climatic condition, the evaluation of groundwater recharge is essential due to the increasing vulnerability of groundwater resources which is showing signs of depletion as it acts as the only source of freshwater for remote rural settlements and secondly, could be its proneness to contamination, especially in an urban center in mountainous hillslopes which has in itself many local groundwater bodies feeding the springs and streams. To address these local and regional vulnerabilities associated with subsurface groundwater reservoirs, it has been stressed for deciphering dominant processes as well as reliable recharge estimates as pointed out by many workers (De Vries and Simmers, 2002, Tashie et al. 2016; Nimmo et al. 2015; Cai and Ofterdinger, 2016). The Multiple-method approach should be followed for the assessment of groundwater recharge as it is extremely difficult to assess the accuracy of estimate using any single approach (Heppner et al. 2007). But most importantly as pointed out by Healy and Cook, 2002 and others consistency between results by even using multiple methods should not be inferred as an indication of closeness to the actual recharge.

Streamflow as well as groundwater levels are being widely used for quantification of average basin-scale and localized recharge to address issues related to local water supply and water balance assessment at a basin scale. The theory and reported assessment in different hydrogeological setups have been discussed by many workers (Rutledge, 1998; Healy and Cook, 2002; Scanlon et al. 2002; De Vries and Simmers, 2002; Rutledge, 2007). The initial studies of recharge assessment using streamflow hydrograph are based on recession-curve-displacement method (RORA) which is primarily based on an analytical model with an assumption of uniform aquifer thickness, hydraulic conductivity, and storage coefficient (Rorabaugh,1964) and the total flow measured at the outlet represents all the surface and the groundwater. The recharge estimate reflects the average of the basin and does not reflect the internal variability. Recharge is assessed through the recession curve displacement method by finding the difference between

groundwater discharge (Q2) at a critical time as extrapolated from the recession line after the recharge event with the groundwater discharge (Q1) at a critical time (T_c) as extrapolated from the streamflow recession preceding the event (see Figure 6 in Rutledge, 1998). The critical time is expressed as:

$$T_c = \frac{0.2(a^2)S}{TR} \tag{6.1}$$

or critical time can also be expressed as:

$$T_c = 0.2144 * K \tag{6.2}$$

where S is the storage coefficient, TR is transmissivity, a is the average distance between central stream to the hydrologic divide and K is recession index (T). The recession index (K) which is time per log cycle of streamflow recession is estimated by extracting segments which are near-linear on the graph of logarithmic of flow as a function of time. The total recharge for each peak in the streamflow hydrograph is assessed by using the equation:

$$R = \frac{2(Q_2 - Q_1)K}{2.3026} \tag{6.3}$$

The sensitivity analysis showed minor variation in recharge estimates due to variation in average recession index (Rutledge, 1998). However, the approach is having its own limitations (Halford and Mayer, 2000).

At a basin scale, recharge as one of the components of groundwater budget can be expressed as:

$$R = \Delta S^{gw} + Q^{bf} + ET^{gw} + Q_{off}^{gw} - Q_{on}^{gw} \tag{6.4}$$

where recharge is the summation of change in the subsurface water storage, evapotranspiration from groundwater storage, outflow as base flow from the basin, and the last two terms indicate net subsurface flow. The change in the subsurface water storage (ΔS^{gw}) as reflected in the response of water table could differ in time lag in

shallow and deep aquifer to any precipitation event as the new water(recharge) enters the subsurface unsaturated zone and gets redistributed in unsaturated and saturated zone (Lerner et al.1997). The water-table fluctuation method for assessment of groundwater recharge rely on rate of change of watertable height over time(Δh) and the specific yield(S_y) with an underlying assumptions that the water enters the storage near-instantaneously and the other components of recharge during the time of recharge are near to zero. Recharge can be expressed as:

$$R = S_y \frac{dh}{dt} = S_y \Delta h \tag{6.5}$$

This assumption can only to be true for a shorter timeframe ranging between hours to few days only. For example, if the inflow to the aquifer is equivalent to the outflow from the aquifer, then water table becomes stationary in spite of influx as recharge and the method is of no use. The WTF method can be used for each individual watertable rise or can be applicable for seasonal or annual time-scale over a much longer time interval with measurement of long-term fluctuation. However, the method gives better results for measurements of short-term water level rise caused by individual rainfall incidences. As mentioned earlier the method does not work in case of steady recharge and one should keep in mind that not all water level rise can be only attributed to influx of new water. The change in the atmospheric pressure, entrapped air, lateral flow as well as tidal effect can cause fluctuations in the water level of groundwater aquifers (Healy and Cook, 2002). The important but formidable parameter for the assessment of GW recharge is the evaluation of specific yield(S_y). The specific yield(S_y) of rock or soil is defined as volume of water after being fully saturated, will yield by gravity to its own volume. The formula is represented as:

$$S_y = \emptyset - S_r \tag{6.6}$$

where $\emptyset$ is the total porosity and S_r is the specific retention.

The findings of Childs, 1960 and Sophocleous, 1985 indicate that single unique value of specific yield may lead to overestimation of recharge and significant difference in the

results is observed when variable specific yield is applied. The numerical demonstration show water level rise is underestimated under fixed specific yield assumption (Sophocleous, 1985). Crosbie et al. 2005 applied improved methodology over the previous approach by using depth dependent variable specific yield for inferring recharge from the fluctuating water table and rainfall time series and including the drainage (D) which reflects the outflow away from the water table.

$$R = S_y \frac{dh}{dt} + D \tag{6.7}$$

The drainage term takes into account the simultaneous losses like evaporation, evapotranspiration, and lateral flow causing recession in water table while parallel recharge might be building up the water level following precipitation in a system of the groundwater aquifer. This drainage term assists in the estimation of total recharge in cases where the rise of water level is not recorded due to steady recharge caused by low-intensity and long-duration recharge processes. But the approach followed by Crosbie et al. 2005 is a time series approach and not an event-based approach as the study aimed to assess the recharge for aquifer water balance calculation. The important study showed significant overestimation in recharge value if a constant specific yield is used and recharge estimate is also sensitive to the time step of investigation. An improved water table fluctuation (WTF) technique was presented by Cuthbert, 2010 in catchments where aquifer properties are relatively well deciphered and the water table is smoothly varying which is generally the case with a thick overlying unsaturated zone with deep water table. An expression for groundwater drainage component was developed based on linearized Bousinesq equation over the empirical approach of assessment of drainage (D) used by Crosbie et al. 2005. As reiterated in the previous discussion, the new input as recharge has a very slow constant-rate component as well as a faster episodic component where water-table fluctuation exceeds the steady-state water-table configuration. Nimmo et al. 2015 developed a method and R program to identify and quantify episodic recharge using the discrete-storm water-table fluctuation method or Episodic Master Recession (EMR) method. The approach requires high-resolution water table fluctuation data as well as

rainfall data over a long period to systematically partition the water-table hydrograph into episodes of recharge and no-recharge.

This novel approach helps to gain insight into links between variable storm characteristics on the groundwater recharge as well as have relevance in predicting the response of the underlying subsurface systems to climate change impacts. Tashie e al. 2016 using the EMR approach developed an empirical relationship between precipitation characteristics and episodic groundwater recharge under wide physiographic provinces with a variety of land use and land cover in North Carolina, USA using U.S.Geological Survey (USGS) water level records from 10 groundwater wells for more than 10 years. The correlation between recharge to precipitation increased with longer storm duration whereas the increasing magnitude and intensity of precipitation caused decrease in correlation. However, land cover under natural vegetation showed a contrasting response in terms of recharge to precipitation ratio (RPR) as compared to land use classes such as agriculture and urban areas to higher storm duration and intensity. Opposing seasonal effects are also recorded for winter and summer in RPR. The study by Eaton, 2020 from New York City using high-frequency groundwater well observation monitored by USGS, applied the Cuthbert, 2010 approach for assessment of continuous steady-state recharge as well as quantified episodic transient recharge using Nimmo et al. 2015 EMR approach for water-table aquifers where both the transient and continuous processes of recharge are equally important. Although the combined approach had uncertainties in terms of specific yield and spatial hydraulic conductivity estimates and outputs from aquifer modelling analysis were used as average representative values.

A globally significant rise in extreme precipitation is reported (Myhre et al. 2019; Bharti et al. 2016). Groundwater aquifer storage buffers the dependent society and groundwater-dependent ecosystems from the vagaries of rainfall uncertainty. But lack of clarity in understanding whether the increase in enhanced precipitation events and decrease in low-intensity rainfall will further alleviate or aggravate the already water- scarce region of the world. Understandably, a great amount of uncertainty prevails on how climate extremes will impact the infiltration into the groundwater aquifers. It is also not surprising to note the regions are responding differently to extreme precipitation events, for example the western (dry) and the eastern part (wet) of vast Northern High Plains (NHP) aquifer in

the USA (Zhang et al. 2016) showing maximum daily recharge due to EP in dry sites whereas non-extreme events causing more recharge in wet sites caused by the difference in antecedent soil moisture conditions. Further, the study by Thomas et al. 2016 divulges change in the precipitation intensity altering the relationship between the episodic recharge and precipitation resulting in the depletion of groundwater storage. A strong link between rainfall intensity and groundwater recharge is also reported from India using 5800 network of groundwater wells and IMD gridded rainfall data (Asoka et al. 2018). The initial and first-ever study highlights the dominance of low-intensity rainfall over GW recharge in alluvial aquifers of North Central and NW India whereas hard rock aquifers of Southern India are driven by high-intensity rainfall. The study also brought out an observed decline in total rainfall and low-intensity precipitation across India from 1951-2016 by analyzing the IMD gridded precipitation data for June to October period.

Nonetheless, the foregoing studies need a detailed understanding of rainfall-runoff characterization as well as deeper insight into the processes controlling the groundwater recharge under different hydrogeological setups at the varying scales of observation. Given the significance of bedrock groundwater in the hillslopes underlain by hard rock aquifers, many studies have overcome the initial soil-centric comprehension to a more detailed knowledge of shallow and deeper groundwater dynamics in the fractured hard rock through the nest of boreholes.

Interesting works have emerged in the past decade on poorly productive bedrock aquifer under the Irish Environmental Protection Agency as well as under the Irish National Geoscience Program for implementation of the EU Water the Framework Directive (WFD) with a focus on framework development of groundwater vulnerability assessment as well as production of national groundwater recharge map (Cai and Ofterdinger, 2016; Misstear, 2009). Cai and Ofterdinger, 2016 observed a major influence of low-intensity rainfall (≤ 1mm/hr.) over the groundwater recharge rate and distinctive response in GW level variations to rainfall in different hydrogeological conditions controlling the groundwater flow and storage in low elevation to high elevation hillslopes underlain by high grade metamorphic rock types. Katsuyama et al. 2005 using hydrological and hydro chemical observation through observation well drilled up to bedrock in unsaturated hillslope, saturated riparian and transition zone between hillslope and riparian zone

revealed that bedrock permeability governs the hillslope-riparian linkages and water is mainly sourced from the saturated throughflow at soil-bedrock interface during storm and deeper groundwater within bedrock contribute year-round in headwater catchment underlain by weathered granite in Japan (see figure 9 in Katsuyama and Ohte, 2005). Montgomery et al. 1997 and Anderson et al. 1997 showed evidence of shallow bedrock GW contribution on runoff generation and rapid response in bedrock piezometers (installed in weathered and fractured bedrock up to 35m depth) under rain and sprinkling experiments in steep zero-order catchment in the Oregon Coast Range. The study also showed significant control of bedrock GW in pore pressure development in overlying colluviums deposit. Haria and Shand, 2004 and 2006 reported research focused on resolving the deteriorating water quality issue arising due to acidification in hard rock headwater catchment in the United Kingdom. The study leads to the understanding that groundwater in the bedrock could rise up to the soil-bedrock interface and further the soil water derived from GW rapidly discharge into the stream as observed through the nest of boreholes (up to 30m deep) in near stream riparian zone and lower hillslope. The study throw light on catchment functioning and showed that surface water quality is regulated by bedrock groundwater.

Contrary to the previous studies in catchments in the Mount Lofty Range (MLR), South Australia which assumed bedrock to be completely impervious in the geological formation of metamorphosed sedimentary rock overlain by thick soil and saprolite zone. Bank et al. 2009 found groundwater in fractured bedrock plays an equally important role as that of soil and saprolite formation and contributes significantly to streamflow. The interconnectedness between the soil, saprolite and fractured bedrock, and their hydraulic properties facilitates the mixing and circulation of GW from the deeper bedrock. Gabrielli et al. 2012 from their internal bedrock groundwater observation through drilled boreholes in the two benchmark experimental hillslopes sites (Maimai M8, New Zealand and H.J. Andrews Experimental Forest in Oregon, USA) showed no direct contribution of bedrock groundwater to hillslope runoff as the water table did not rise up to soil-bedrock interface. However, bedrock GW quickly responds to storm events and demonstrates a unique mechanism of storage and transmission through fracture network in the two geologically distinct formations with similar hillslope form. Salve et al. 2012 again

reiterated the central role of fracture-dominated flow path in regulating the response of steep hillslope of Northern California underlain by thick unsaturated and weathered zone of steeply dipping and fractured argillites. An interesting study by Gleeson et al. 2009 at a local scale in region underlain by fractured aquifer of Precambrian crystalline, sedimentary and metasedimentary rocks monitored through 15 bedrock wells, with shallow and deep piezometer (31-56 m deep) highlights two different mechanism of recharge. The rapid snowmelt recharge is caused by deeper heterogeneous fractures interconnections whereas slow and widespread recharge occurs in the region overlain by thick soil having lower transmissivity. In addition to the direct measurement through cost-effective instrumentation for reliable estimate of recharge and the assessment of underlying controlling mechanism, past studies have also shown the applicability of correlation and spectral analysis in deciphering the recharge mechanism, storage capacity as well as the time lag between two-timeseries (Larocque et al. 1998; Lee and Lee, 2000; Cai and Ofterdinger, 2016).

6.3 Methodology

In the present study recharge estimation is done using two methods, namely the water table fluctuation method (WTF) (Healy and Cook, 2002) and an improved version of the water table fluctuation method called episodic master recession method (EMR) (Nimmo et al. 2015) suitable for episodic recharge assessment for every recharge episode. Since the deeper groundwater aquifer does not show a very pronounced response to rainfall influx as compared to the shallow aquifer system located in the riparian zone bordering the stream, the WTF method was applied for the assessment of groundwater recharge for deeper aquifer whereas the EMR method was applied for the estimation of shallow groundwater. In the present study, a 2-inch open-hole monitoring piezometer where drilled in 2016 whereas a 5-inch bore well was constructed in June 2018 with a depth range of 80 m. The water table was observed at approximately 23 m below the ground level (1560 m amsl). The appropriately screened deep bore wellwas instrumented with water level recorder and barologger for recording the time series of water level

fluctuations for 2018 and 2019.

The shallow groundwater observation from a piezometer located at the outlet of the micro-catchment of Bhimlitalli village which goes as deep 3 m in hard rock geology was instrumented with water level recorder, which recorded the water level at 15 minutes frequency during the monsoon period of 2017and 2019. The water level data along with the rainfall event logger data at 15 minutes' rainfall intensity was used for estimation of episodic recharge using the discrete-storm water-table fluctuation method (Nimmo et al. 2015). The method first generates a master recession curve (MRC) using the rate of water-table decline (dH/dt) as a function of H (Figure 4.3a). The bin-average dH/dt as a function of bin H is regressed for a polynomial fit to generate a MRC.A very conservative estimate of specific yield of 1% was taken for the bedding plane foliated and fractured metasedimentary rocks (Phyllites and Quartzites) and was used for the estimation of recharge.

6.4 Results and discussion

6.4.1 Shallow groundwater dynamics and recharge assessment

A combined investigation of rainfall flux as well as the groundwater level fluctuation over two hydrological years provides an opportunity to understand the shallow as well as deeper groundwater aquifers responses and recharge characteristics at a local scale.

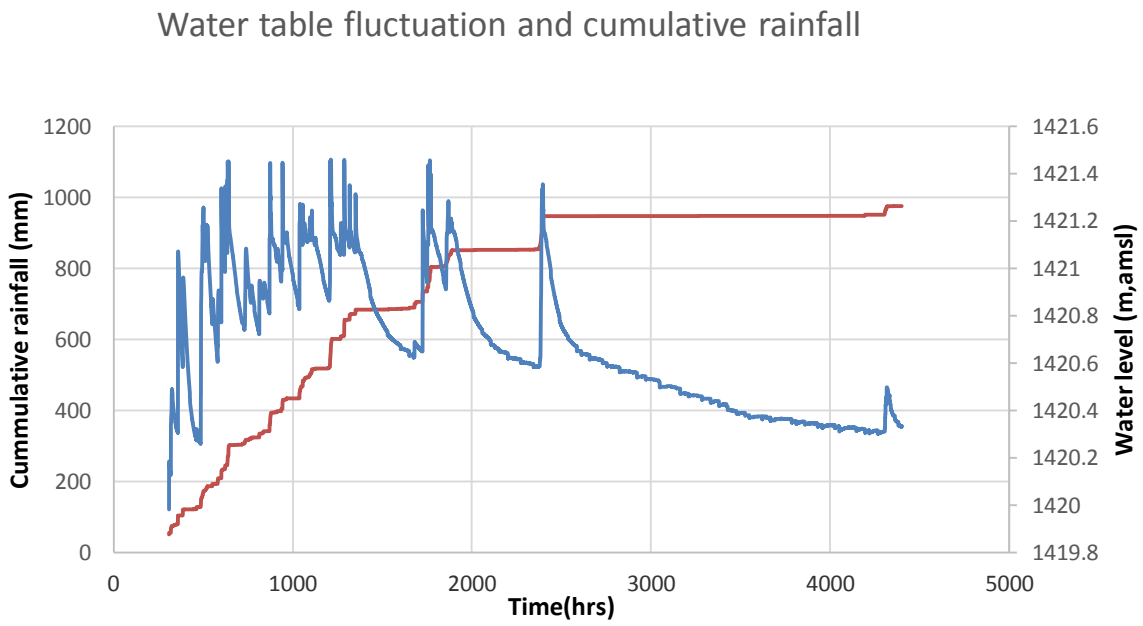

Figure 6.1: Plot of water table and cumulative rainfall during the monsoon and post-monsoon period of 2017.

The period from 28 June to 15 December 2017 was analyzed as this period covers the entire monsoon period and post-monsoon period of prolonged recession as evident from Figure 6.1. A rise of 1.625 m was observed during the monsoon period with a total rainfall of 975 mm during the entire period under investigation. The rapidly fluctuating piezometer water level records indicate a very short time lag between rainfall incidence and shallow groundwater response. The rapid response in groundwater level observation during storm events in the present hydro-geological set-up makes it ideal case for the application of episodic recharge estimation. The time lag between a significant rainfall event and a rise in water level is less than 30 minutes (Figure 6.2)

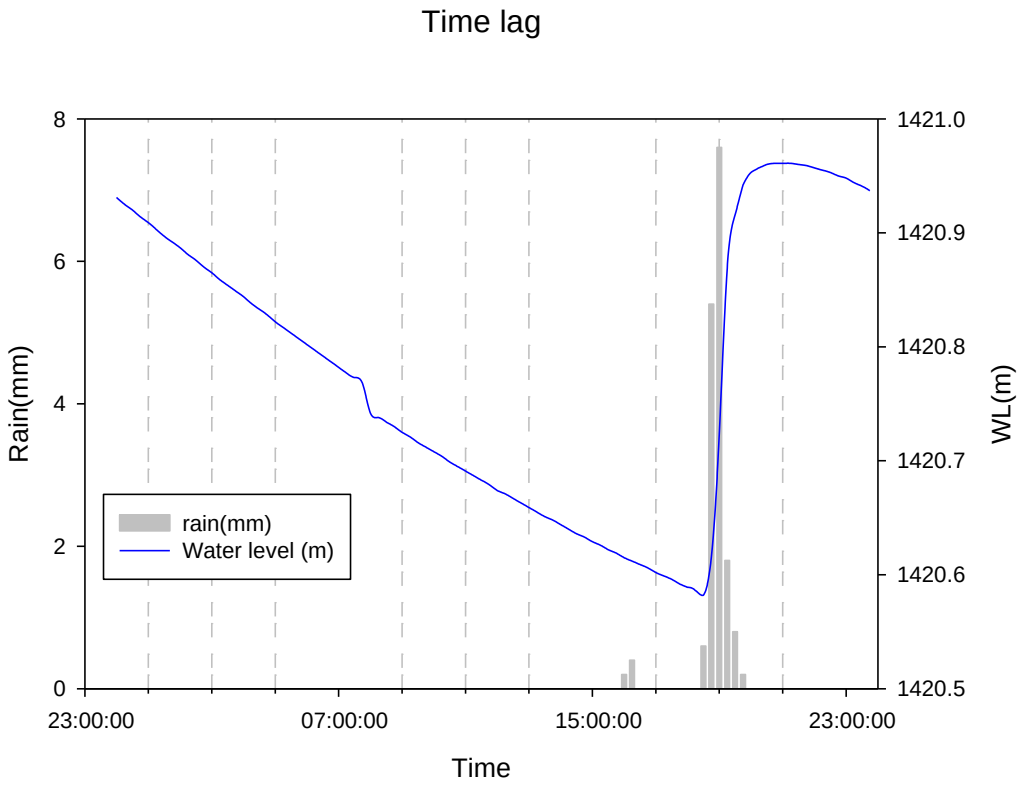

Figure 6.2: Plot of water level rise with rainfall indicating a very rapid response of shallow groundwater level (shorter time lag).

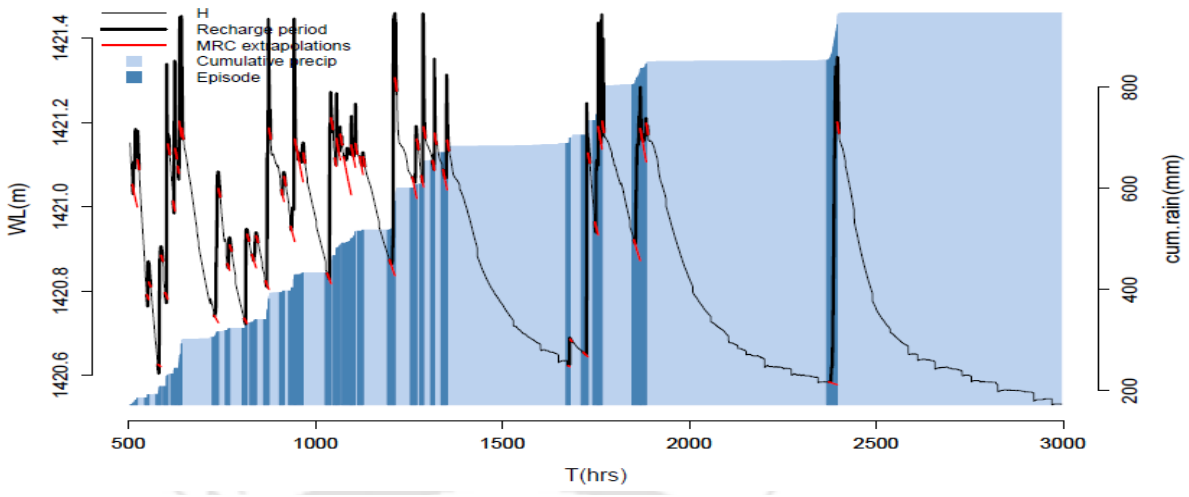

Figure 6.3 Episodes of groundwater recharge (highlighted in dark blue) is demarked with the well hydrograph.

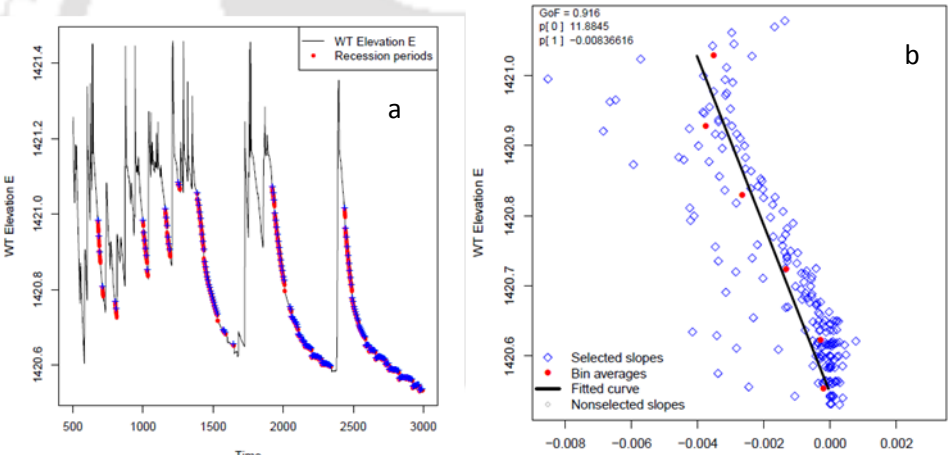

Figure 6.4: The bin-average dH/dt as a function of bin H is regressed for a polynomial fit to generate MRC (a) and separated recession curve using the master recession curve MRC (b) within the well hydrograph.

Thirty-three events of episodic shallow groundwater recharge (Figure 6.3 and Table 6.1) could be separated, with a total of 79 mm of recharge from rainfall amount of 638mm. The method does not incorporate any rainfall losses (evapotranspiration) presently. It is interesting to highlight that rainfall intensity governs the effectiveness of recharge and a threshold value of approximately 2.4 mm/hr results in approximately 37% of recharge.

Higher intensity rainfall above threshold value is significantly reducing the episodic recharge amount (Table 6.1). The recharge to precipitation ratio ranges from 0.6 to 37.6%.

Table 6.1: Variability of recharge to precipitation ratio estimated using episodic recharge estimation method (2017).

Recharge Episode	Rainfall (mm)	Recharge (mm)	RPR(%)	Average Precipitation rate	Maximum Precipitation Rate
1	12.8	1.5	11.4	0.7	4.8
2	6.6	0.5	8.0	0.6	12.8
3	15.6	3.4	22.0	1.1	13.2
4	22.6	4.8	21.1	1.7	37.2
5	11.2	1.9	17.2	1.0	10.8
6	5.26	1.6	30.4	0.8	9.6
7	43.48	0.3	0.6	6.4	28.8
8	11	4.1	37.6	0.6	4
9	3.8	0.8	20.8	0.3	4.4
10	10.8	2.7	25.4	0.8	15.6
11	6.8	1.0	14.6	0.4	5.2
12	41.13	5.0	12.1	2.8	33.6
13	3.2	0.8	24.2	0.2	4.8
14	31.73	3.2	10.0	1.9	30.8
15	3.73	0.9	23.9	0.2	2
16	25.12	5.1	20.4	1.6	31.2
17	11.7	0.9	7.4	1.6	24
18	9.84	0.8	8.1	1.3	17.63
19	8.76	1.5	17.5	0.3	4
20	14.22	0.7	5.2	1.3	12
21	2	0.6	27.5	0.1	4
22	57.69	6.1	10.6	3.0	26.8
23	6.6	1.8	27.8	0.4	4.8
24	44.99	1.9	4.1	3.8	38.8
25	13.8	1.1	8.2	1.3	27.2
26	12	1.5	12.8	0.7	16.4
27	11.2	0.9	7.7	1.0	22
28	29.2	6.3	21.5	1.6	28.8
29	11.98	3.3	27.9	1.0	22.4
30	41.26	0.9	2.1	4.0	25.6
31	25.01	4.1	16.3	1.2	8
32	12.53	1.2	9.5	0.9	6.4
33	70.54	8.1	11.5	2.6	11.6

Due to malfunctioning of water level sensor, the data for the monsoon period of 2018 could not be collected. Results are presented for the pre-monsoon, monsoon and post-monsoon period of 2019 (Figure 6.5, Figure 6.6 and Figure 6.7).

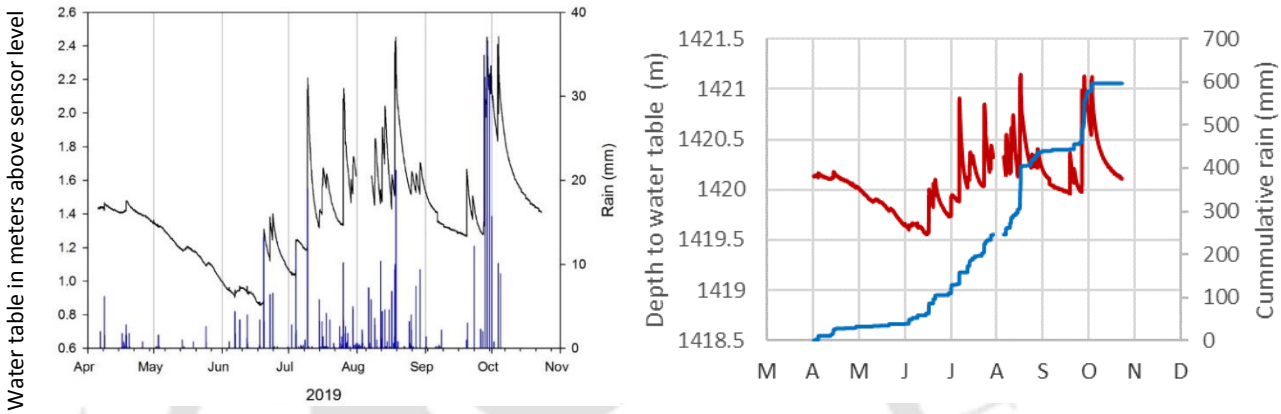

Figure 6.5: Water table, rainfall and cumulative rainfall during the monsoon and post-monsoon period of 2019.

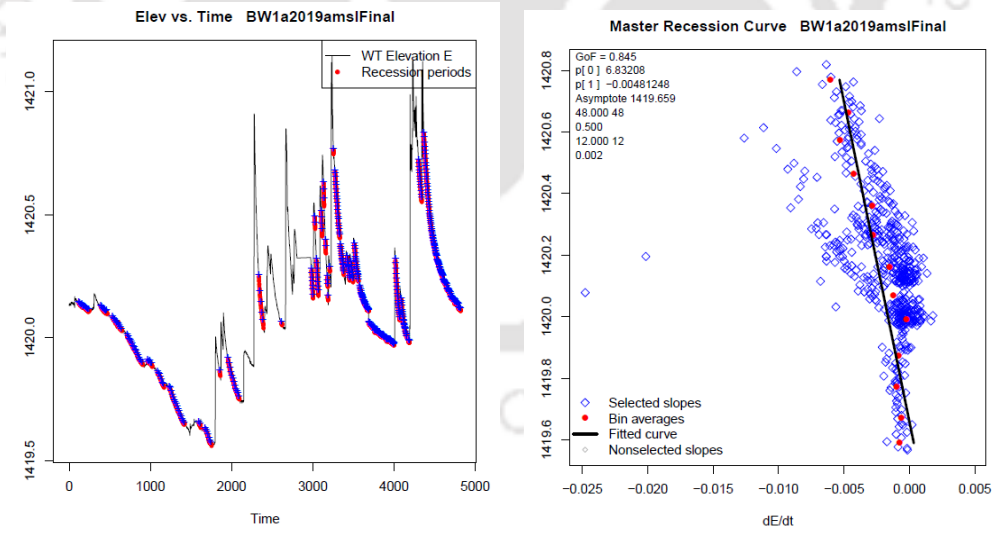

Figure 6.6: Plot highlights separated recession curve using the master recession curve MRC (a) within the well hydrograph and bin-average dH/dt as a function of bin H is regressed for a polynomial fit to generate MRC (b).

The time series data were measured at 1hourly intervals from April to July whereas August onward data was recorded at 15-minutes interval for a shallow open-hole piezometer. The flashy nature of the well hydrograph is evident for observation during both hydrological years. A total of 31 recharge incidents could be seen in Figure 6.7. Table 6.2 again highlights the importance of rainfall intensity in controlling the effectiveness of recharge events. In the monsoon period of 2019, the threshold value of rainfall intensity of 2.08 mm/hr is observed which is close to the average rainfall intensity value (2.4 mm/hr) observed for the 2017 monsoon period. The threshold value of average rainfall intensity 2.08 mm/hr with maximum rainfall rate is marked which records the highest rainfall-to-recharge ratio of 84% (Table 6.2). The recharge-to-precipitation ratio ranges from 8.4 to 83.73%. Most interestingly, the drought years of the 2019 monsoon (only 456 mm of rainfall for the monsoon period) records 25% recharge which is double the amount of rainfall recharge recorded for 2017.But more than 100 mm of rainfall was recorded between period of late September and early October.

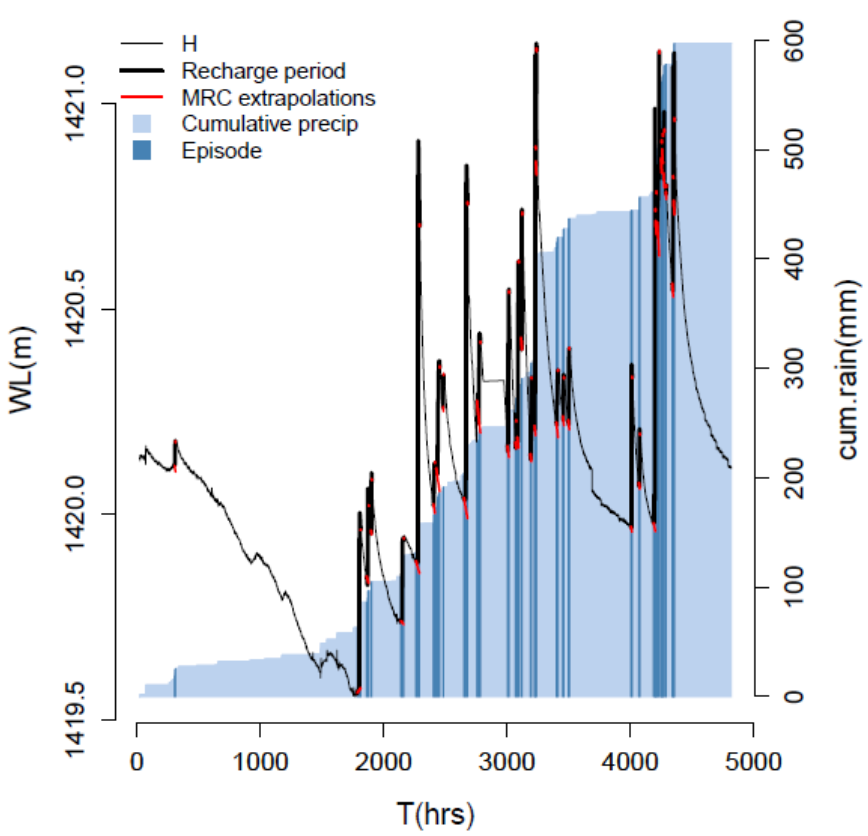

Figure 6.7: Episodes of groundwater recharge (highlighted in dark blue) is demarked within the well hydrograph (2019).

Table6.2:Variability of recharge to precipitation ratio estimated using episodic recharge estimation method (2019).

Recharge Episode	Rainfall (mm)	Recharge (mm)	RPR (%)	Average Precipitation rate	Maximum Precipitation Rate
1	9.73	0.97	9.95	1.12	2.2
2	23.20	5.02	21.64	0.75	9.4
3	10.20	2.46	24.13	0.46	5.1
4	8.40	1.75	20.87	0.76	4.2
5	19.40	2.74	14.12	0.72	6.7
6	26.50	11.05	41.72	0.78	11.7
7	14.60	1.62	11.11	0.86	4.5
8	13.00	3.96	30.45	0.41	3.2
9	4.40	1.20	27.29	0.70	2.2
10	21.33	10.01	46.91	0.66	6.8
11	10.80	2.89	26.80	0.34	4.8
12	14.40	5.27	36.57	1.07	6.8
13	10.60	0.89	8.40	1.33	18.4
14	12.80	5.94	46.37	1.02	10
15	5.20	4.35	83.73	0.52	8
16	8.40	2.68	31.86	0.84	8.8
17	41.85	9.15	21.86	3.86	15.2
18	44.50	3.99	8.98	6.40	27.2
19	9.20	2.15	23.39	0.57	6.8
20	7.60	1.54	20.23	0.78	14.4
21	9.40	2.60	27.70	0.90	18.4
22	12.19	1.76	14.41	1.28	13.208
23	29.46	10.21	34.66	1.90	38.1
24	3.56	1.36	38.19	0.44	3.048
25	46.94	6.51	13.87	2.70	22.352
26	4.41	1.04	23.52	0.58	5.08
27	6.10	0.93	15.29	0.86	4.064
28	8.89	1.84	20.68	1.11	9.144
29	0.76	0.45	58.98	0.15	1.524
30	10.16	3.83	37.68	1.10	17.78
31	8.89	3.05	34.34	1.05	15.24

6.4.2 Deeper groundwater dynamics and recharge assessment

Understanding of the deeper groundwater aquifer is developed through observed rainfall-well hydrograph relationship shown in Figure 6.8 and Figure 6.9 for the years 2018 and 2019 The deeper bore well is located at the elevation of 1560 m amsl at the sleeper hillslope compared to the open casing shallow piezometer (1421 m amsl) located at the riparian zone at the outlet of the small catchment of 40-hectare area. It is surprising to note that deeper groundwater is showing groundwater table fluctuations not only during the wet period but also during the pre-monsoon period as evident from Figures 6.8 and 6.9. This shows that both shallow and deeper groundwater is dominated by preferential plane dominated flow in the fracture planes of metasedimentary rocks of Mid-Himalaya. The deeper groundwater showed a less fluctuating hydrograph compared to the well hydrograph observed from shallow open hole piezometer. A maximum water table fluctuation of 3.2 m is observed during the monsoon period of 2018 whereas deficient rainfall during the monsoon period of 2019 resulted in rise of only 2.45 m of water table elevation.

The recharge estimated for the 2018 monsoon period using water level data an 80 m deep bore well indicates 4 to 19% if the specific yield of 1 to 5% is assumed for the metasedimentary rocks. Whereas monsoonal recharge for the year 2019 indicate 5 to 24% of rainfall recharge. It is also surprising to observe that exactly similar water level could be reached even with deficient rainfall during the 2019 monsoon. This could be indicating of threshold level of response in deeper groundwater as well where close to 300 mm of cumulative rainfall is sufficient to increase the water table to the highest level beyond which upheaving of water table is not possible.

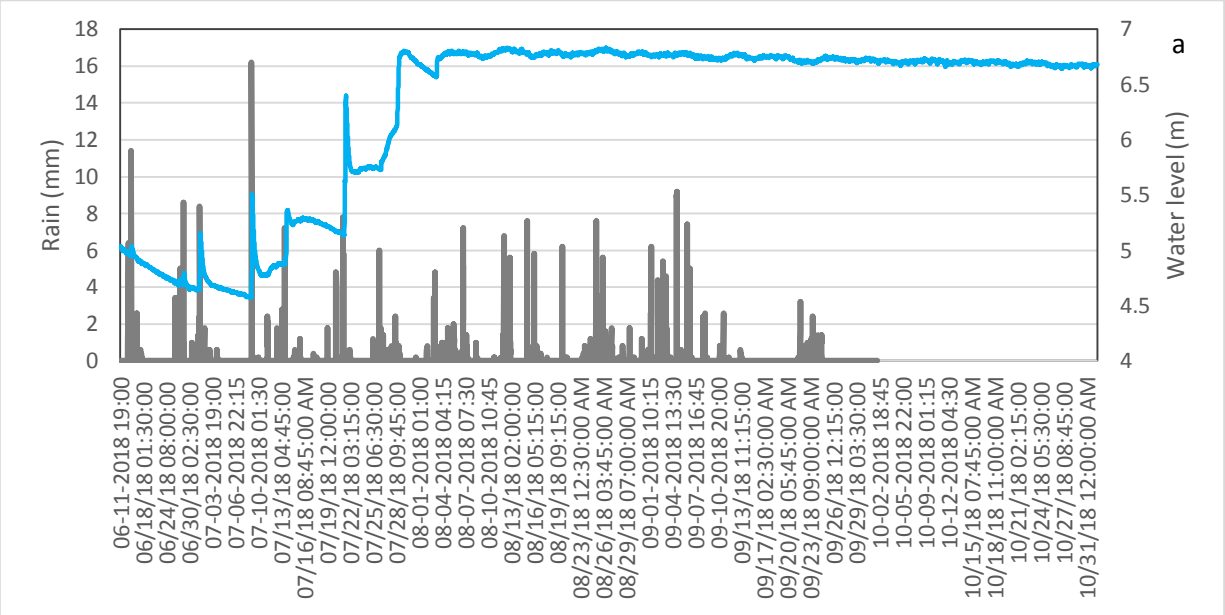

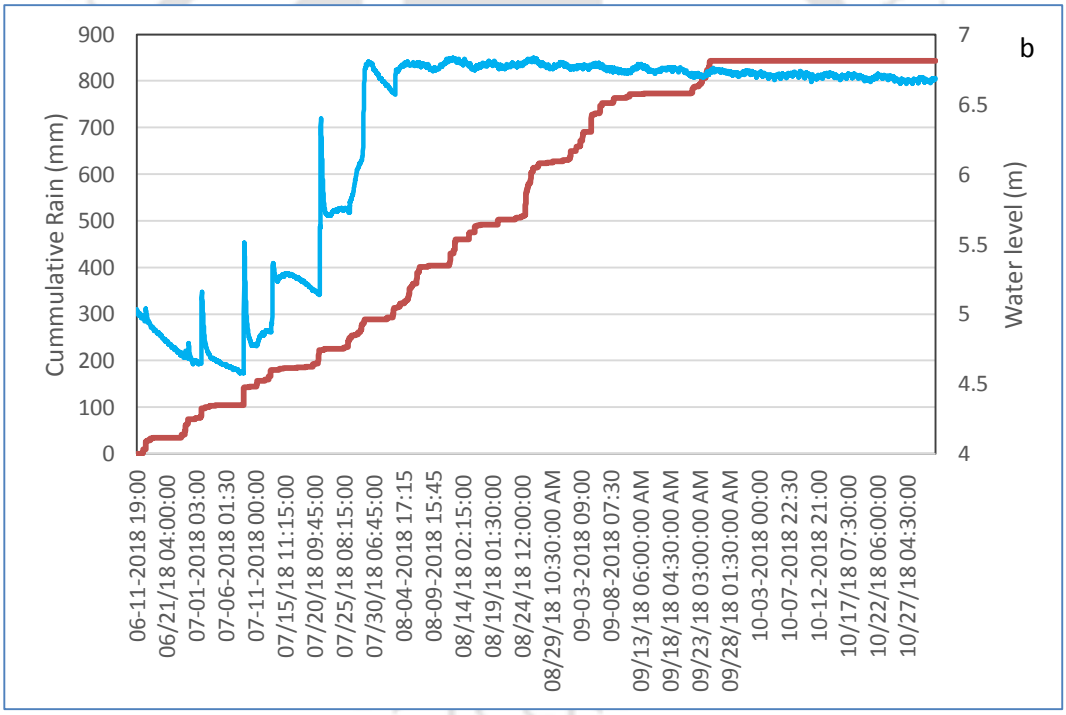

Figure 6.8: a) Time series of well hydrograph for the deeper hard rock aquifer, b) cumulative rainfall plot with well hydrograph (blue) for year 2018.

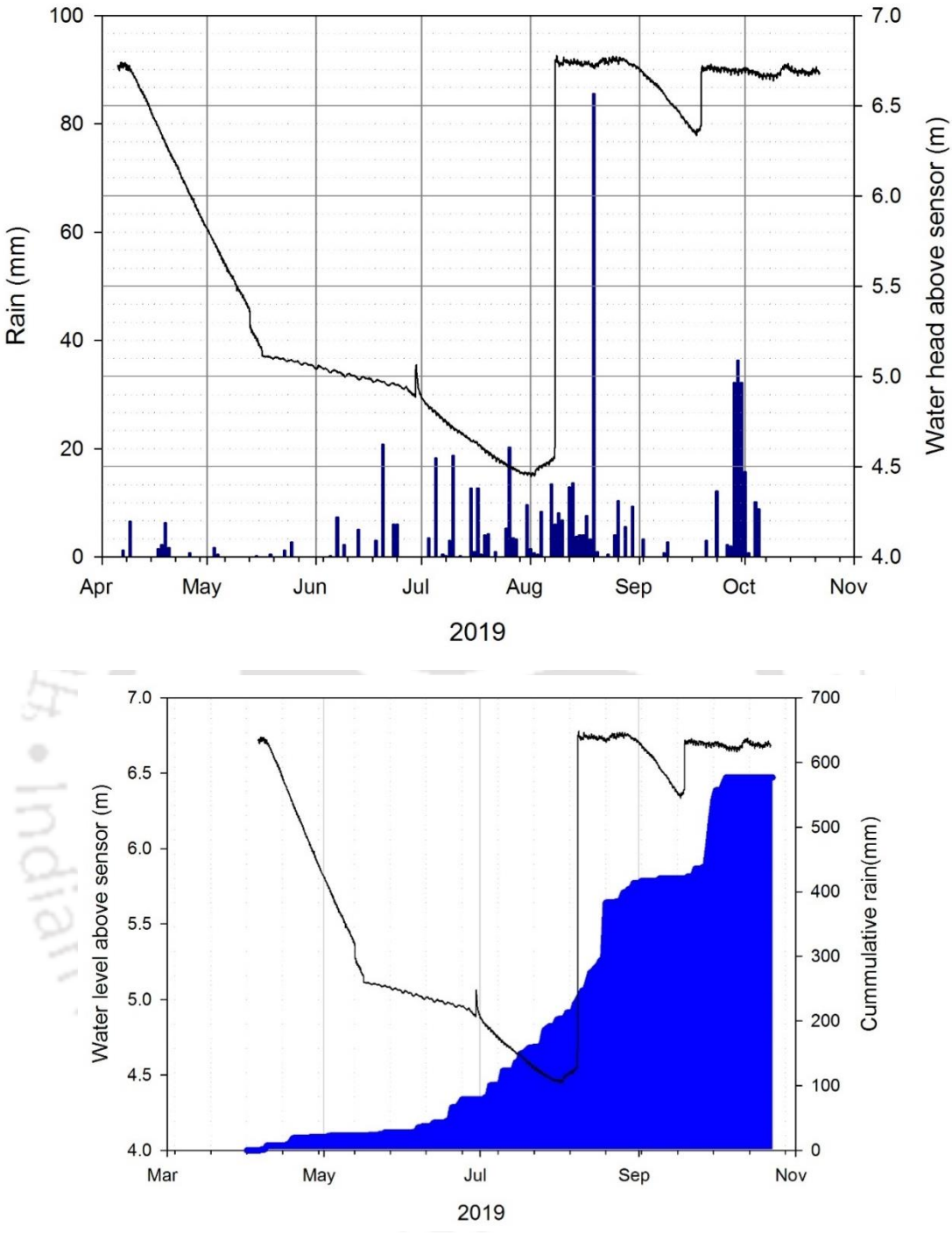

Figure 6.9: a) Time series of well hydrograph for the deeper hard rock aquifer, b) cumulative rainfall plot (filled blue region) with well hydrograph (dark blue) for year 2019.

6.4.3 Auto-correlation and Cross-correlation between spring flow, shallow and deep groundwater level and rainfall time series.

The auto-correlation defines the linear dependency of successive values of time series and in a way reflects the memory of the system. The system with a long memory effect may show a very gradual decrease in the auto-correlation function as compared to the fast-responding system which shows a quick decrease in auto-correlation function (Larocque et al. 1998; Lee and Lee, 2000). The cross-correlation value can help decipher the inter-relationship between the input influxes to an output response in a system and is hence applicable to determine the time lag between input stress to output response. Negative and positive values of the cross-correlation function may be useful to understand whether the input is influenced by the output or vice-versa (Larocque et al. 1998). These two statistical parameters are used to characterize the subsurface shallow and deep groundwater system to the rainfall influx. The auto-correlation function using daily spring flow for 2017 and 2018 over June to December showed nearly two months of memory effect for the low-yielding spring with flow rate varying from 0.02 to 1.23 lps. The maximum cross-correlation in springflow response to input daily rainfall is attained at 1 day to 3 days in 2017 and 2018 respectively(Figure 6.10a & b). The frequency of water level measurement varies from 15 minutes (2017) to hourly (2019) interval for shallow piezometer recorded during the monsoon and post-monsoon period. In the 5-inch-deep borewell, water level as well as the barometric air sensors recorded data in 15-minutes (2018) to half-hour (2019) intervals from June to October period. The auto-correlation function for the shallow piezometer ranges from 29 days to 37.5 days for 2017 and 2019 whereas the water level response of the borewell in the deep aquifer ranges between 26 days to 56 days for 2018 and 2019 indicating a short memory effect for the fracture bedrock aquifer system. The cross-correlation function showed a time-lag of 30 minutes to 1.5 hours in 2017 and 2019 respectively (Figure 6.10b). The deeper aquifer water level response to rainfall input inferred through the cross-correlation function indicates 29 hours (1.2 days) to 20.5 hours (0.85 days) of time lag to attain the maximum $Y(k)$ for the year 2018 and 2019 respectively (Figure 6.10c). In the present hydrogeological setting dominated by shallow soil cover and preferential flow dominated system in fractures and foliation planes metasedimentary rocks, the rapid response with

very short time lag even in deep hillslope aquifer indicates high transmissivity and low storage capacity of bedrock aquifer systems.

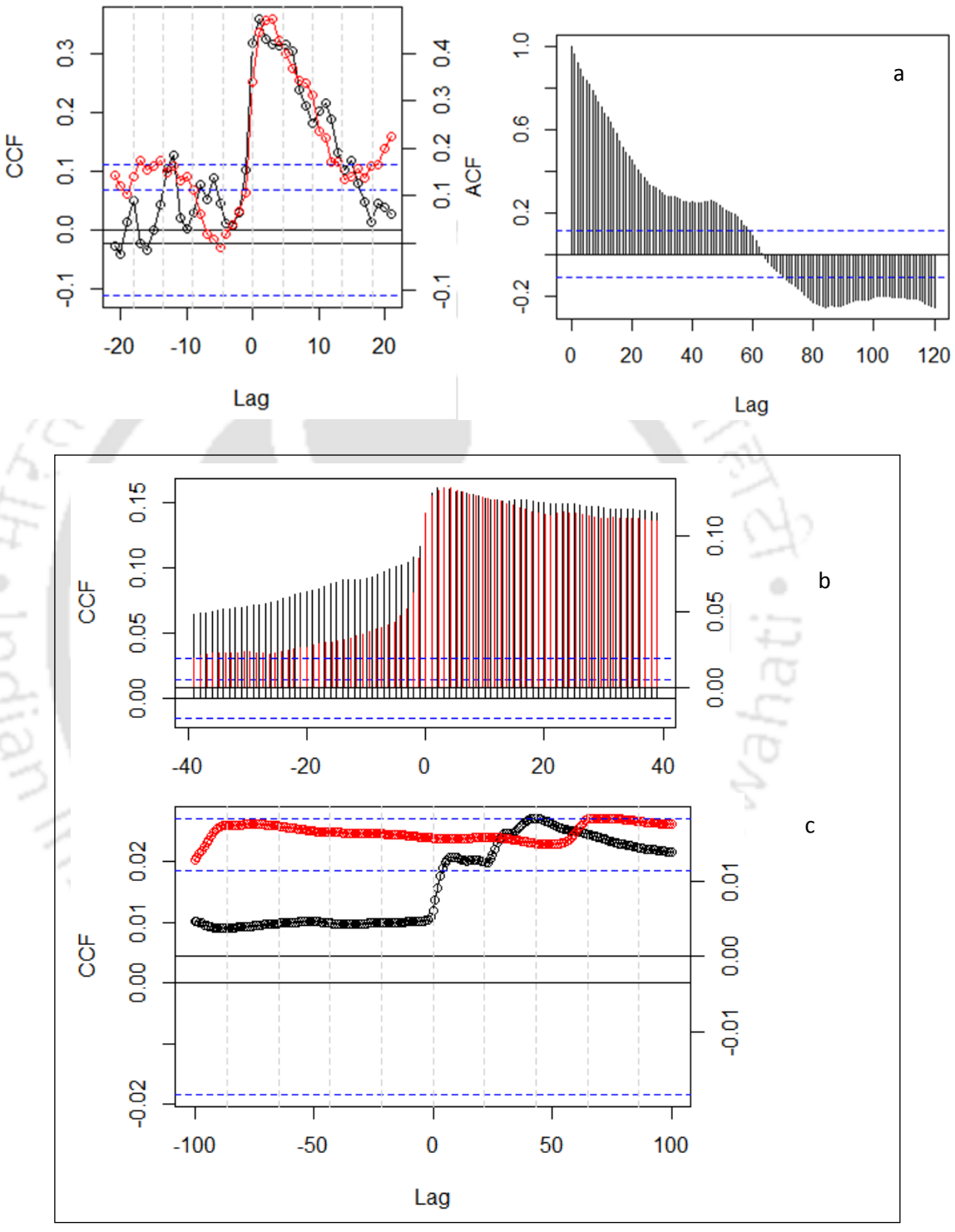

Figure 6.10: Cross-correlation (a) between spring (Mandirdhara) discharge and rainfall at daily step for 2017(black) and 2018(red) and auto correlation of spring discharge for 2017, b) cross-correlation for rainfall and shallow piezometer GW hydrograph for 2017(black) and 2018(red) and (c) cross-correlation between deeper well hydrograph and rainfall for 2018(black) and 2019(red) at 15 minutes to 30 minutes interval.

6.4.4 Groundwater recharge using spring-flow hydrograph

Baseflow discharge using spring-flow and streamflow hydrograph technique (Meyboon,1961; Rorabough, 1964) could be used as long-term spring-flow records are being collected for the two microwatershed. Spring-flow/Stream hydrograph displacement technique is not directly equated to recharge because evapotranspiration and underflow to deep aquifer (leaky reservoir) may be significant and suggested for an independent estimate of another parameter. The method used in Meyboon, 1961 for the estimation of groundwater recharge using the winter recession period is being investigated for the base flow recession period of streamflow applying Butler's equation & expressed as:

$$Q(t) = \frac{Q(t_0)}{10^{\,t/K_2}} \qquad (6.8)$$

where$Q(t)$is the discharge of stream at time t, $Q(0)$ is the initial discharge at $t = 0$, t is the time lapse between observation times of $Q(0)$and$Q(t)$,$K_2 = t$ when $Q = 0.1Q(0)$or time increment corresponding to a log-cycle change in Q .

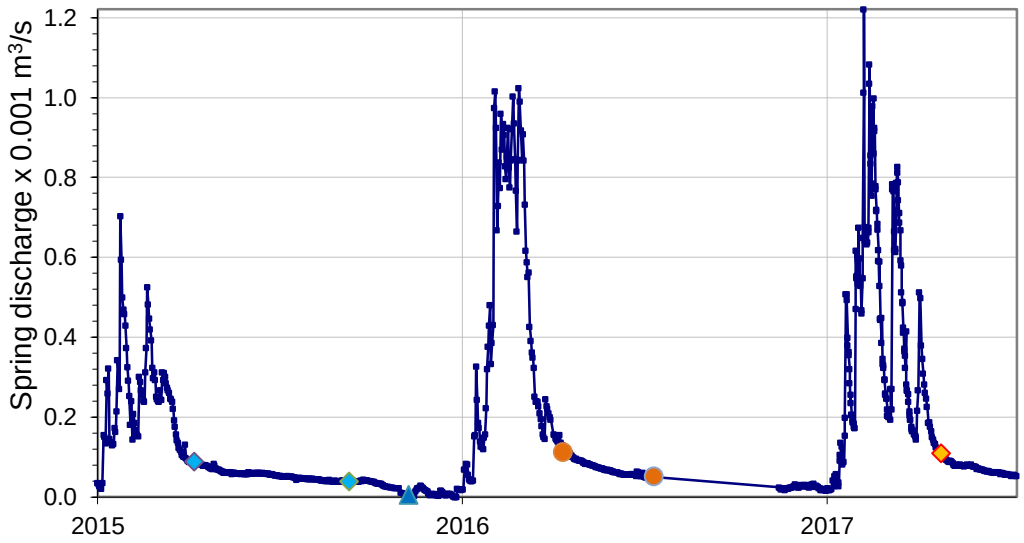

Figure 6.11: Mandirdhara spring-flow for 2015 to 2017 used for assessment of groundwater recharge through recession curve displacement method. The points indicate the period used for recession parameter estimation.

The volume of water available at the beginning of the recession period and volume of

water discharged during the recession period gives an estimate of the remaining potential groundwater discharge volume in stored in aquifer at the end of recession period (Figure 6.11). The recharge is estimated between winter recession period of one year and the beginning of next recession period for the following year. The monsoonal recharge for the year 2017 was found to be 777 m^3.

6.5 Conclusion

The present study report results from the observation of rainfall and continuous measurement of water level from instrumented shallow 2-inch open-hole piezometer drilled in the riparian and hillslope zone for the years 2017 and 2019 as well as an appropriately screened cased deep bore well (80m), located in the sloping hillslope in an experimental spring catchment of 40-hectare area for 2018 and 2019. Discrete-storm water-table fluctuation method (EMR) highlights the significance of rainfall intensity in controlling the effectiveness of recharge events in landscapes underlain by foliated and fractured preferential plains in metasedimentary rocks. The observed threshold of rainfall intensity value regulating the maximum recharge was found to be between 2.08 mm/hr to 2.4 mm/hr for the years 2017 and 2019 and higher-intensity rainfall events above the threshold caused a significant reduction in episodic recharge in the riparian zone. The recharge to precipitation ratio ranges between 0.6-37.6% in 2017 whereas it was found to be in the range of 8.4-83.73% in the drought year of 2019 with deficient monsoon rainfall of only 456 mm. Surprisingly, the cumulative net recharge was double (25%) in the drought year of 2019 as compared to only 12.38% net episodic recharge in 2017 due to rainfall events below the threshold rainfall intensity. Cross-correlation results are indicative of very rapid response (≤0.5 hr) of hillslope aquifer as well as riparian aquifer to the rainfall event influx. The estimated monsoonal recharge using the water table fluctuation method for deeper bore well indicates 4-19% rainfall recharge in 2018 whereas the monsoonal recharge for 2019 little higher at 5-24% which was estimated for a specific yield value of 1-5% for metasediments. The deeper perched hillslope aquifer again showed a threshold response highlighting a close to 300 mm of cumulative rainfall is sufficient to increase the water table to the highest level beyond which upheaving of the water table is not feasible in a hillslope.

CHAPTER 7

Land Use Land Cover Change

7.1 Introduction

Climate, land cover, soil and underlying geology primarily regulate water flow and its dynamics in watersheds. Any alteration by natural or human-induced causes may severely affect the functioning of watershed. Land use change is known to have impacts on freshwater resources by altering the hydrological cycle (Foley et al. 2005) as well as on groundwater recharge (Scanlon et al. 2005). Monitoring the Land Use Land Cover changes at regional and local scale over time is essential to gain insight concerning LULC patterns and their dynamics. Remote sensing and geographical information system (GIS) have been extensively applied for quantification of changes in forest cover (Dasgupta et al. 2010) as well as in cropland monitoring and change detection (Ramankutty et al. 1998). The applicability of satellite data for landuse landcover mapping is demonstrated in many studies from Kumaon Lesser Himalaya (Tiwari et al. 2012 and Rao et al. 2001) and Garhwal mid-Himalaya (Semwalet et al. 2004; Batar et al. 2017).

7.2 Literature Review

A gradual shift regionally over the last four to five decades is observed in the landuse and landcover (LULC) pattern in the middle-mountain of western (Uttarakhand) and central Himalaya (Nepal), converting the watersheds from a mix of agriculture–forest dominated to largely forest dominated system. However, a clear understanding of positive or adverse impacts on the regional mountain hydrology of such a prevalent regional-scale transformation is still missing from the Garhwal and Kumaon Himalaya. Land use / land cover changes are known to have impacts on local (Germer et al. 2009), regional

(Schilling et al. 2008) and global scale (Foley et al. 2005; Beck et al. 2013). Although the magnitude and timing of land use change impacts could differ at different spatial scales. For instance, hydrological modelling results from large agricultural-dominated watershed in USA (Schilling et al. 2008) indicate an expansion of present corn acreage resulting in a conducive decrease in annual ET and increased water yield. However, a subsequent shift to the biofuel-based crops will affect the watershed water balance otherwise. The study from Texas, USA (Scanlon et al. 2005) shows an increase in subsurface groundwater recharge and deterioration in groundwater quality under the conversion of natural rangeland ecosystems to agricultural ecosystems. These studies emphasize that the land use land cover regulates evapotranspiration, run-off, soil moisture and sub-surface recharge further demonstrating the interlinkages between biophysical–atmospheric-subsurface components of the hydrological cycle. Several studies on hydrological modelling indicate land use change can be an important driver in altering the water balance at the local and regional scales (Seibert et al. 2010, Wagner et al. 2013). Further, the interlinkages between land use, soil erosion, streamflow and sediment load being reported by Tiwari et al. 2000 from the watershed based investigation in three distinctly different physiographic settings of Indian Himalaya. The study highlights the subsequent downstream consequences like rise in riverbeds, diminishing streamflow, spring flow and river flow and rise in the flood frequencies as a result of landuse change in terms of loss of forest, expansion of agriculture and unplanned development in Kumaon region.

Nonetheless, the scientific debate of unraveling the links between forest and freshwater yield has a history of more than three centuries now (Ellison et al. 2017). A broad consensus has emerged in recent decades recognizing the ecosystem function of forest as a biotic pump as it draws water from the terrestrial systems and feeds it back to the atmosphere. The native forest could simultaneously facilitate soil and groundwater recharge through its roots as well as stores in the upper soil organic matter generated by leaf litter decomposition on the forest floor (Bruijnzeel, 2004; Brantley et al. 2017; Ellison et al. 2017; Jasechko et al. 2013). Yet, extensive reviews on the much-explored paired watershed studies (PWS) from all across the world point toward confounding results (Brown et al. 2005; Farley et al. 2005). The general conclusion that can be drawn out of the several paired watershed studies (from temperate as well as tropics) highlights

an inverse relationship between (de)forestation and water yield. However, a 'trade-off' between the two key parameters governs the net resultant water balance of the new system in the catchment. It is the deterioration of inherent soil hydraulic characteristics due to afforestation or deforestation and secondly due to the increase or decrease of interception loss and transpiration under the new afforestation/deforestation conditions under the short-term (up to five years) and long-term perspective in different physiographic and climate settings.

In the present context of Middle Western and Central Himalaya dominated by strong seasonality, afforestation and natural regrowth of secondary forest can lead to either an increase or decrease in base flow or summer season flows in streams of varying order. Hence monitoring the trends and patterns of Land Use Land Cover changes at regional and local scale over a decade may be essential to assess the progressive depletion of natural resources. Remote sensing and geographical information system (GIS) is an indispensable tools to monitor and evaluate the degradation in the local, regional and global landcover and plan for its protection.

Rural livelihood for the majority of the scattered population in mountainous region of the state of Uttarakhand is centered on the age-old subsistence agriculture practices. Like most of the mountainous regions of the world, rural outmigration (Mamgain and Reddy, 2017), altered and deficient rainfall regime (Dash et al. 2011; Tarafdar et al. 2019) and subsidized food grain supply to rural backward classes have led to large-scale conversion of rain-fed and irrigated agriculture land to permanent fallow land in Garhwal and Kumaon Himalaya. The abandoned farmland is gradually being taken over by fast regenerating fire-resistant pines (*Pinus roxburghii*). However, scientific observation of such a transition of degraded land to natural regrowth of secondary forest from a neighboring country (Nepal) under similar physiographic and rainfall regimes in middle mountains have led to additional demand of water for vegetative transpiration and alteration in soil hydraulic conductivity (soil compaction) causing more overland runoff, soil loss and lesser recharge to soil and groundwater (Ghimire et al. 2013 and 2014). Do the chir pine (or longleaf Indian pine) dominated secondary forest in recent times will further aggravate the prevalent seasonal water scarcity in the already water-limited

regions of the middle Himalaya afflicted by series of deficient rainfall years? In the present context what is becoming pertinent is the understanding of the likely impacts of natural regrowth of secondary forests dominated by chir pine in barren and abandoned fallows on the net annual and specifically summer season low flow in regions dominated by wet and dry conditions. The findings from international reviews across the world (Brown et al. 2005; Sahin and Hall, 1996; Bosch and Hewlett, 1982; Stednick, 1996; Farley et al. 2005; McLean, 2001) on forest and water yield under different climatic conditions highlight three very important facts which will regulate the long-term water resource sustainability of middle mountains as well as its dweller are:

- Afforestation program or natural regrowth takes longer to reach to a new equilibrium and to manifest its impacts on water yield as compared to deforestation.
- 10% reduction (deforestation) of the conifer forest has resulted in increase in water yield.
- Pine plantation (afforestation) on the other hand has resulted in a reduction of high flow (-50%) and almost converted the perennial stream to seasonal, ceasing the dry season flow.

Indeed, chir pine will draw more water (as higher evapotranspiration) as the naturally regenerating secondary forest of uneven-aged pines at a different stage of growth reach up to the stage of complete closure of the canopy.

Remote sensing technique using high-resolution satellite data is a promising tool to investigate the decadal changes in the landuse/landcover in the mountainous rural watersheds of most populace middle mountain region of Indian Himalaya. The objective of the present study is to develop LULC map using a high-resolution satellite data for the period of 2008 and 2017 and to quantify LULC change at the local microwatershed scale and regional watershed scale (Irgad watershed).

7.3 Methods

High-resolution multispectral satellite images for 2010 and 2017 and Survey of India topographic map (53 J/16) were used to analyze the recent LULC changes over Dugar Gad microwatershed and Upper Paidul microwatershed. LISS IV and Rapid Eye data, having a same spatial resolution of 5.4 m, was procured from the National Remote Sensing Centre (NRSC), Hyderabad for May 2010 and 2017 to maintain the consistency in the data set. The satellite images were geo-corrected with ground control points collected through Trimble GPS and projected to Universal Transverse Mercator (UTM) projection zone with WGS 1984 datum. An object-based hybrid classification was used to classify satellite images and to develop the land use land cover maps for 2010 and 2017. The remote sensing data were processed through ERDAS IMAGINE and classified using eCognition software based on field verification. The river, roads and settlement were digitized using Google Earth very high-resolution satellite data from both periods.

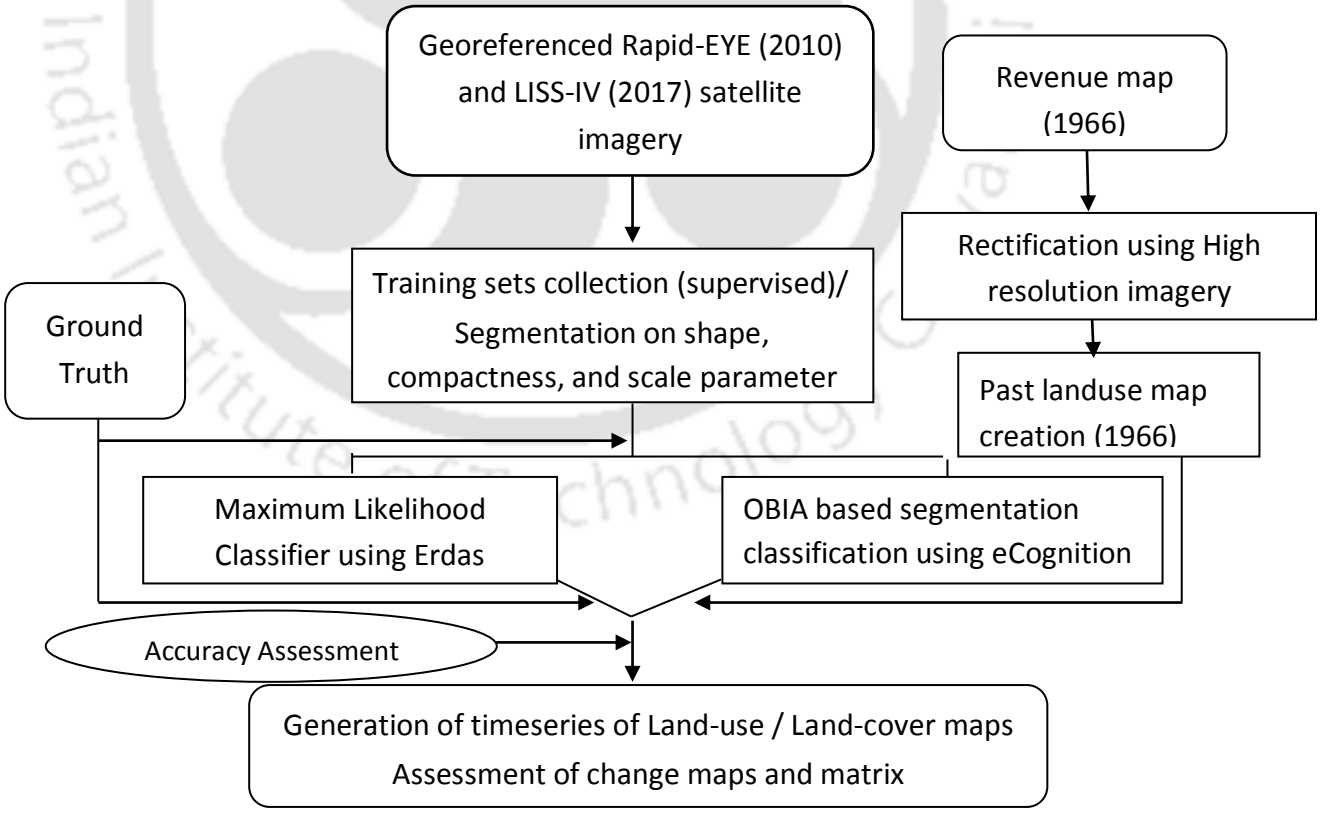

Figure.7.1: Methodology for land use/land cover classification for 2010, 2017 and 1966.

7.4.1 Land Use Land Cover Distribution and Changes in Dugar Gad microwatershed during 2010 – 2017

The developed LULC maps and their spatial distributions over Dugar Gad microwatershed during 2010 and 2017 are shown in Figure 7.2 and Table 7.1. The land use/land cover classes are chir pine (*Pinus roxburghii*) forest, banj oak (*Quercus leucotrichopora*) forest, mixed forest /vegetation, scrubland, barren land, agricultural land, fallow land, pine-dominated by fallow, agroforestry, streams and settlements. The total area under forest cover is 0.74 km^2 (about 20.95% of the total catchment), which is mainly dominantly by pine, and followed by oak and mixed vegetation (Picture 7.1h). The area under traditional agricultural land is around 0.47 km^2 whereas wasteland (barren land) covers 0.21 km^2 of area. Major cereal crops grown in the basin are paddy, wheat, millet and maize. Barren land constitutes 5.98% area of the catchment. These areas are sloping terrain and rocky, and devoid of vegetation cover during summer but get converted into grassland during the monsoon period.

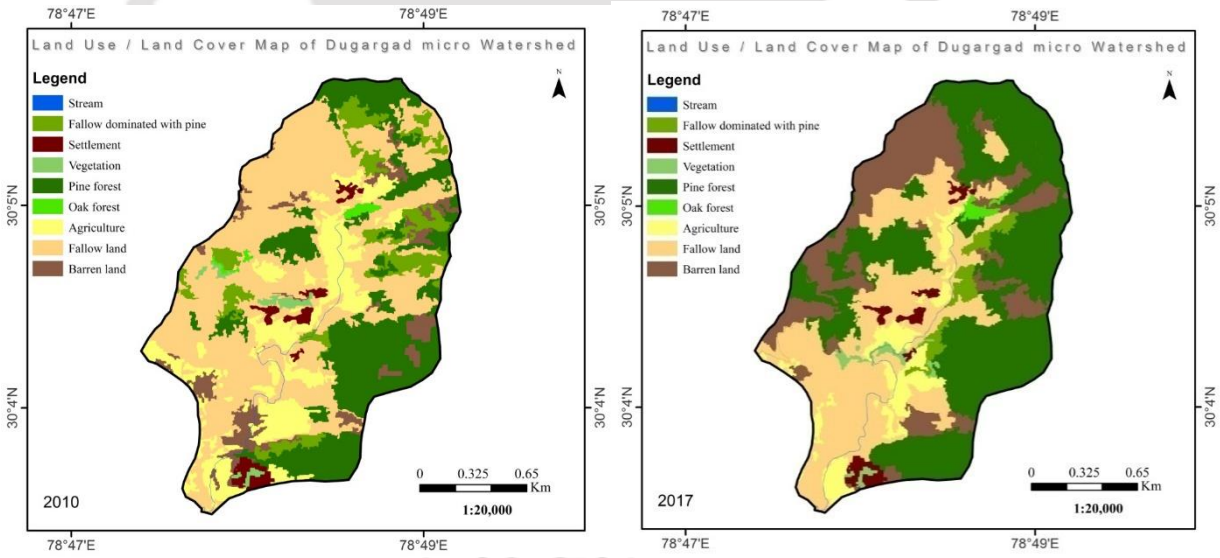

Figure7.2: Classified LULC map of Dugar Gad microwatershed for the year 2010 and 2017.

Table 7.1: Characteristics of LULCs and their change in the Dugar Gad microwatershed.

ID	Land use / Land cover	2010		2017		Change
		Area (km^2)	Area (%)	Area (km^2)	Area (%)	
1	Stream	0.01	0.16	0.01	0.16	No Change
2	Settlement	0.07	2.02	0.07	2.03	No Change
3	Vegetation	0.30	8.38	0.29	8.10	-3.49
4	Pine Forest	0.72	20.43	1.30	36.77	44.23
5	Oak Forest	0.02	0.52	0.02	0.59	10.54
6	Agriculture	0.47	13.31	0.23	6.36	-109.24
7	Fallow Land	1.48	41.90	0.94	26.59	-57.59
9	Barren Land	0.21	5.98	0.61	17.22	65.24
11	Fallow Dominated with Pine	0.26	7.29	0.08	2.20	-231.92
	Total	**3.54**	**100**	**3.54**	**100**	

A significant change in area under forest cover (mainly pine and mixed forest) and agricultural land is observed over eight-year time period. The area distribution of LULCs during the period 2010 and 2017, and their net change in percentage over the catchment is represented in Table 7.1. The total forest cover has marked the highest gain from 20.95% to 37.35% of the total catchment area during 2010 – 2017. The agricultural land use category was the most dynamic as it has undergone the largest net change of (-) 109.24% area during the eight years period of study. The area under the pine forest has increased from 0.72 km^2 to 1.30 km^2. The fallow dominated with pine has converted into the pine forest and therefore shows a negative trend between the 2010 – 2017 period (Figure 7.3).

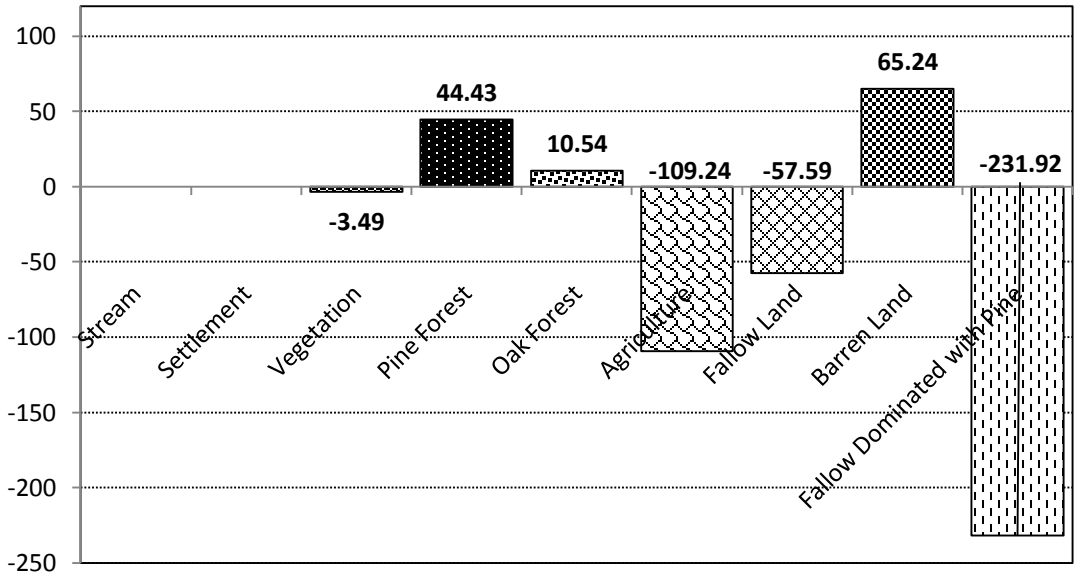

Figure 7.3: LULC (%) changes over the Dugar Gad microwatershed during 2010 – 2017.

7.4.2 Land Use Land Cover Distribution and Changes over Upper Paidul microwatershed

The developed LULC maps and their spatial distributions over upper Paidul microwatershed during 2010 and 2017 are shown in Figure 7.3, Picture 7.1 and Table 7.2. The dominant land use/land cover classes are chir pine (*Pinus roxburghii*) forest, banj oak (*Quercus leucotrichopora*) forest, mixed forest / vegetation, scrub land, barren land, agricultural land, fallow land, pine-dominated by fallow, agroforestry, streams and settlements. The total area under forest cover is 1.98 km^2 (about 24.67% of the total catchment), which is mainly dominantly by pine, and followed by oak and mixed vegetation. The area under traditional agriculture land is around 1.58 km^2 which occupied the central valley of the microwatershed. The wasteland (barren land) covers 0.60 km^2 of area. Major cereal crops grown in the basin are paddy, wheat, millet, maize and minor cash crop. Barren land constitutes 7.51% area of the catchment and gets converted into grassland during the monsoon period.

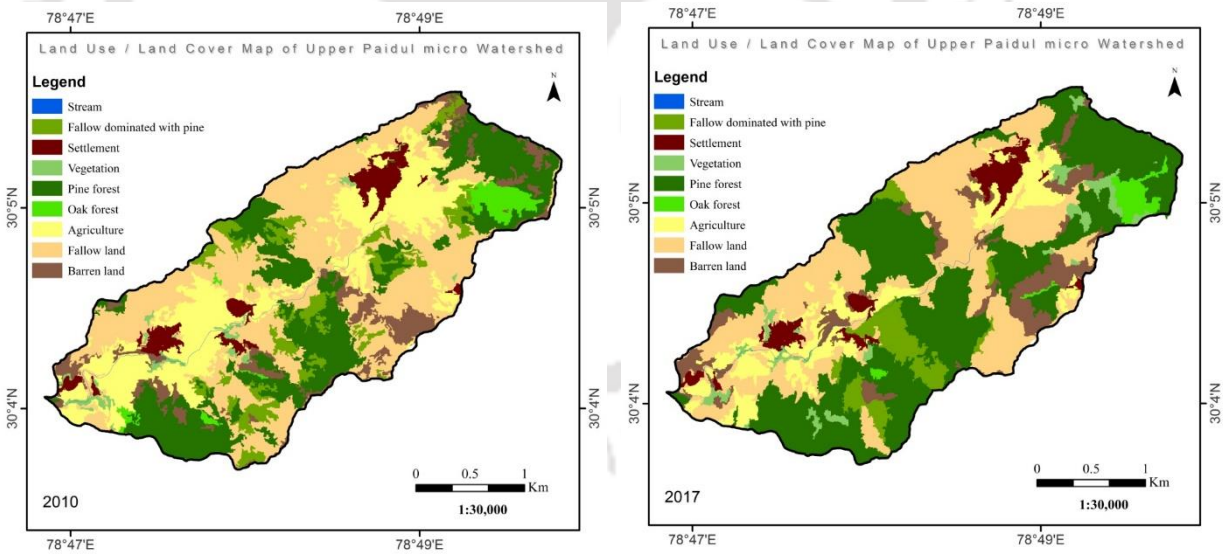

Figure 7.4: Classified LULC map of upper Paidul micro watershed for 2010 and 2017.

Table 7.2: Characteristics of LULCs and their change in the upper Paidul micro watershed over a period of eight years (2010 – 2017).

ID	Land use / Land cover	2010		2017		Change
		Area (km^2)	Area (%)	Area (km^2)	Area (%)	
1	Stream	0.01	0.12	0.01	0.12	No Change
2	Settlement	0.32	4.02	0.32	4.02	No Change
3	Vegetation	0.13	1.58	0.33	4.16	62.01
4	Pine Forest	1.79	22.36	2.97	37.03	39.61
5	Oak Forest	0.19	2.31	0.14	1.74	-32.95
6	Agriculture	1.58	19.68	0.80	9.93	-98.15
7	Fallow Land	2.81	35.08	2.36	29.50	-18.92
9	Barren Land	0.60	7.51	0.66	8.23	8.80
11	Fallow Dominated with Pine	0.59	7.35	0.42	5.28	-39.26
	Total	**8.02**	**100**	**8.02**	**100**	

A significant change in area under forest cover (mainly pine and mixed forest) and agricultural land is observed over a eight-year period. The area distribution of LULCs during the period 2010 and 2017, and their net change in percentage over the catchment is represented in Table 6.2. The total forest cover has marked the highest growth from 24.67% to 38.77% of the total catchment area during 2010–2017. The agricultural land use category has undergone the largest net change of -98.15% areas during the eight years' period of study. The area under the pine forest has increased by 39.61%. The area under the fallow land has decreased from 2.81 km^2 to 2.36 km^2. The barren land has experienced positive growth by 8.80% (Figure 7.5). All in all, the two micro-watersheds showed a similar pattern and rate of change in the landuse categories.

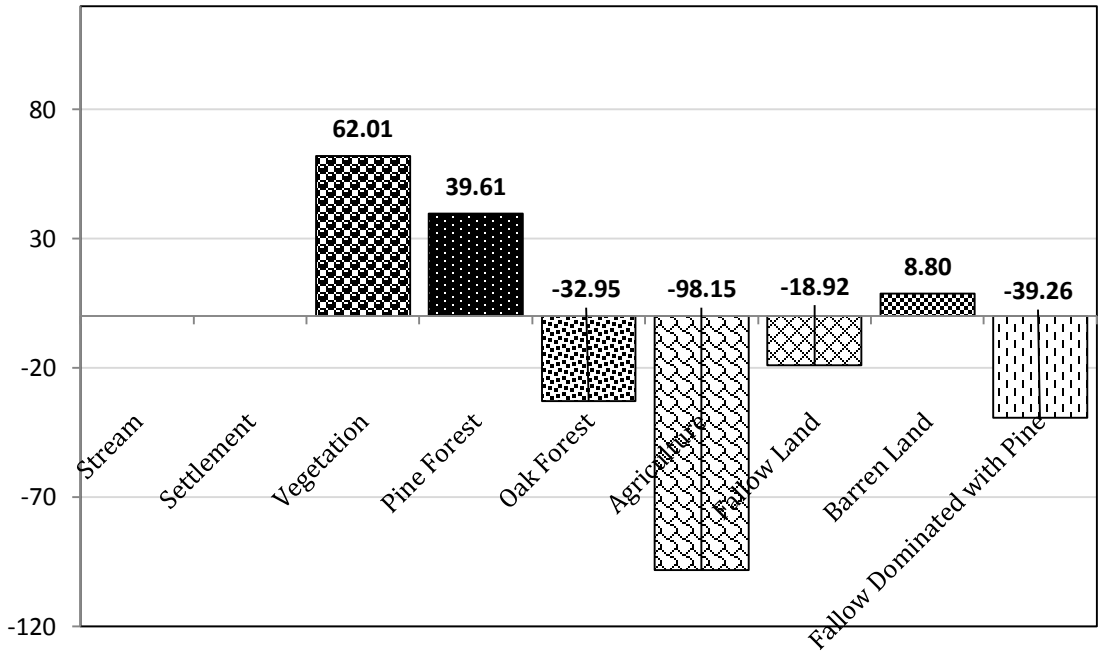

Figure 7.5: LULC (%) changes over the Upper Paidul micro watershed between 2010 – 2017.

7.5 Mapping of past landuse using revenue maps of 1966 period.

Twenty-eight revenue maps of the upper Paidul micro watershed and eight revenue maps of the Dugar Gad microwatershed located in the headwaters of Nayar basin were acquired from Tehsil Office, Pauri district. The maps were scanned and geo-referenced using Erdas Imagine software. High-resolution Geoeye satellite imagery as well as High-resolution Google Earth image of the region was used to reference the revenue maps (Figure 7.1). Second-order polynomials with total of six ground control points (gcp) were identified in the revenue maps as well as in the satellite image to geo-correct the revenue maps.

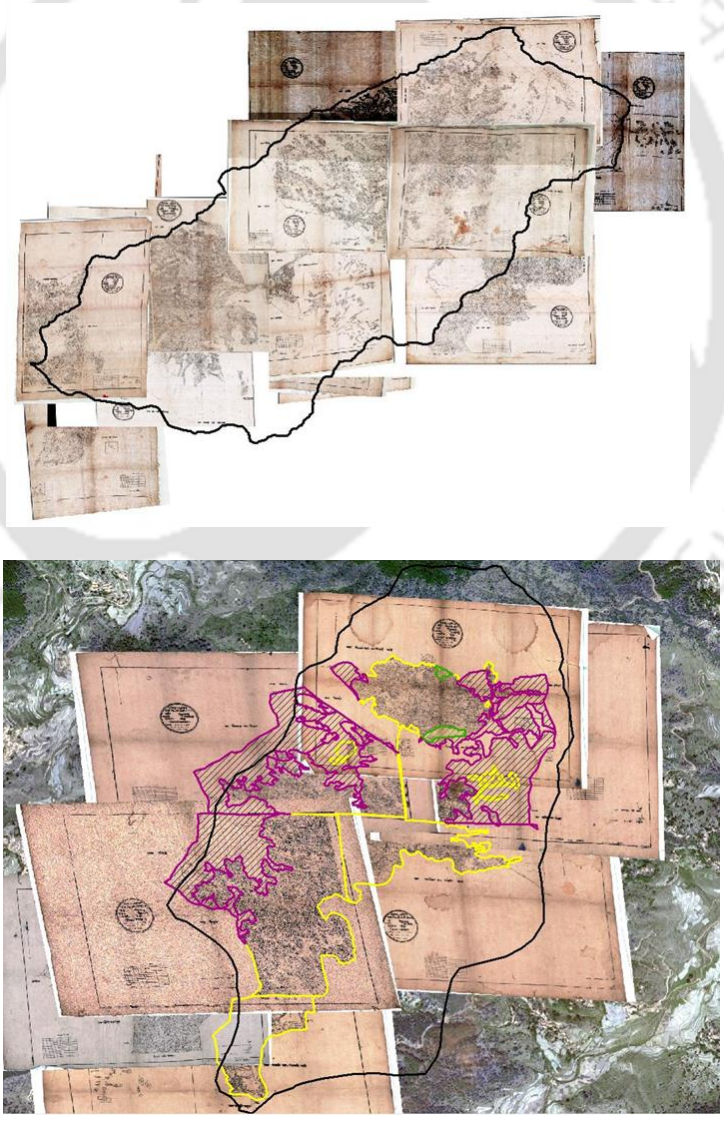

Figure 7.6: Screenshot image showing the 28 revenue maps of upper Paidul micro watershed and eight revenue maps of Dugar Gad microwatershed geo referenced with satellite data.

The main objective of this exercise was to generate a map of past land use revealing the distribution of land use/land cover categories for the year 1966 within the two experimental micro-watershed located in the middle Himalaya. Further, the maps can be used to compare it with the land use map of recent years and assess the change that has occurred over the years. The revenue maps of the upper Paidul microwatershed are shown with three major classes, which are agricultural areas, forest regions and wasteland areas all depicted by different symbols within the revenue maps (Figure 7.6).

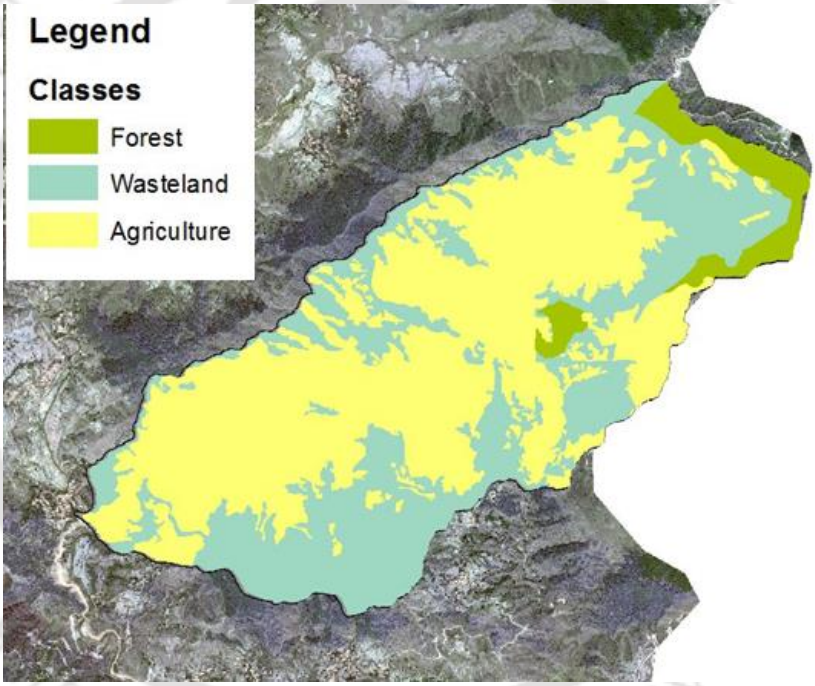

Figure 7.7: Land use map generated using digitization of revenue maps for the year 1966 showing the dominance of agricultural land in the micro watershed.

The land use map of the upper Paidul micro watershed region for the year 1966 shows an area covered by the yellow shade, highlighting the agricultural areas while the dull green and the bright green section highlights the wasteland and the forest areas respectively (Figure 7.7). Out of the total area of 8 km^2 of the upper Paidul micro watershed, 3 km^2 area (38%) is covered by agricultural land, whereas 4.6 km^2 area was marked as barren

i.e., the wasteland (58%), while the forest region covered only an area of only 0.4 km^2 in the watershed. The past land use maps for Dugar Gad microwatershed could not be completed because of the non-availability of some of the revenue maps. However, a similar percentage of landuse distribution can be estimated from the rest of the available revenue maps.

7.6 Mapping of Regional Land Use Land Cover Distribution in Irgad watershed

Regional scale Land use and land cover is an important factor affecting different processes in the watershed, such as surface runoff, erosion, recharge and evapotranspiration. The landuse/landcover maps were generated from the 5.0-meter resolution Rapid Eye and 5.8-meter resolution of LISS IV data acquired for the year 2010 and 2017 respectively. Visual interpretation of satellite imageries, as well as seasonal field visit (Picture 7.1), was carried out to develop LULC map for the period of 2010 and 2017. High-resolution Geo-eye satellite data (0.5m) along with Google earth image for 20010 and 2017 was used for demarcation of fallow land. For this study, the LULC classes generated for the Irgad watershed are Stream, Settlement, Mixed Forest /Vegetation, Pine Forest, Oak Forest, Agricultural Land, Fallow Land, Fallow dominated with pine, Agro-forestry, Scrub Forest/Land, and Barren Land. The distribution of different LULC over the study area during the investigated periods is shown in Figure 7.8.

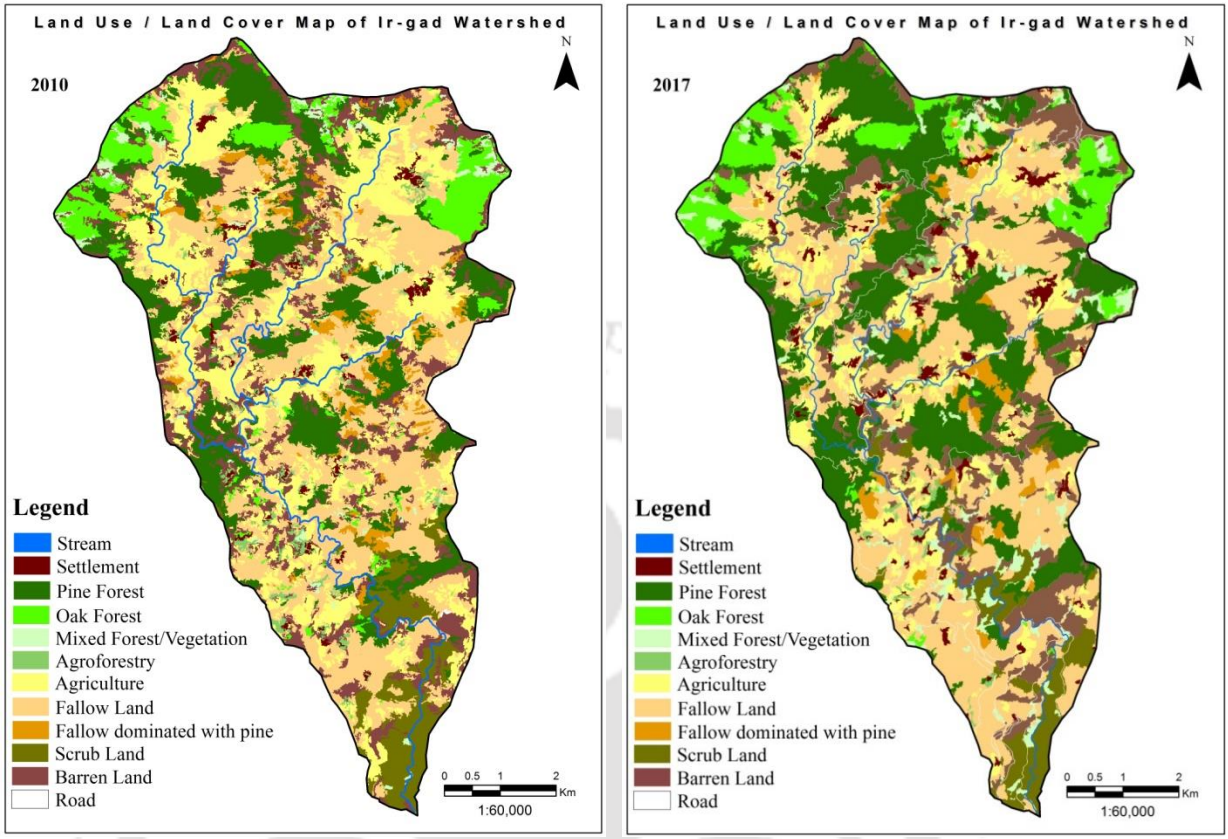

Figure 7.8: Distribution of different land use land cover over the Irgad watershed in the year 2010 and 2017.

Table 7.3 shows the percentage of area under the different land use/land cover classes during two successive periods as mapped through the high-resolution satellite data and ground truthing. During 2010, the total area under the forest cover was 19km^2(nearly 29.65% of the Irgad watershed) which was dominated by different types of forest mainly pine followed by oak, scrub and mixed forest. The area under the traditional agricultural practice was 13.64 km^2 (21.28%) while fallow land and barren land occupied 28.54% and 13% of the total watershed area. The land use under fallow dominated by pine is around 2.6% of the total study area whereas the scatter of trees in agricultural land is grouped under agroforestry. On the other hand, land use land cover distribution in 2017 showed an increase in the areal cover of the forest to 39.07% and a reduction in 6.5 km^2 of

agricultural land. Regionally, the most notable change observed over eight years is pine forest area increased by 47.19% and reduction of agriculture by 47.67% and area under the pine forest drastically increased from 10.80 km^2 to 15.89 km^2representing a total change of 32.06% at an annual rate of 0.73 km^2 increase per year (as shown in Figure 7.9 and Table 7.3).

The transition matrix showed that the expansion in the area under pine forest is due to the conversion of fallow land (4.5%) and barren land (3.17%) into Pine forest. Nearly 5.17 km^2 of agricultural land was converted to permanent fallow land over a period of eight years. A reduction in the area under fallow dominated by pine is also observed as fast-growing pines in fallow land are becoming a part of the main secondary pine forest. The fallow land is also getting converted to barren land. The area under mixed forest is also showing some significant increase.

Table 7.3: area (in hectare) and percentage of landcover area in the Ir-gad watershed in 2010--2017

Land use/ Land cover	2010		2017	
	Area (km^2)	Area (%)	Area (km^2)	Area (%)
Streams	0.56	0.88	0.56	0.88
Settlements	1.63	2.54	1.63	2.54
Mixed forest	1.04	1.62	2.20	3.44
Pine Forest	10.80	16.85	15.90	24.81
Oak forest	3.85	6.01	4.00	6.24
Agriculture	13.64	21.28	7.14	11.14
Fallow land	18.29	28.54	19.11	29.82
Scrub forest/ land	3.31	5.17	2.94	4.59
Barren land	8.33	13.00	8.75	13.65
Fallow dominated by Pine	1.66	2.59	1.32	2.06
Agroforestry	0.56	1.51	0.56	0.83
Total	64.09	100	64.09	100

Figure 7.9: The graph reflects the change in land use dynamics in percentage over the study area.

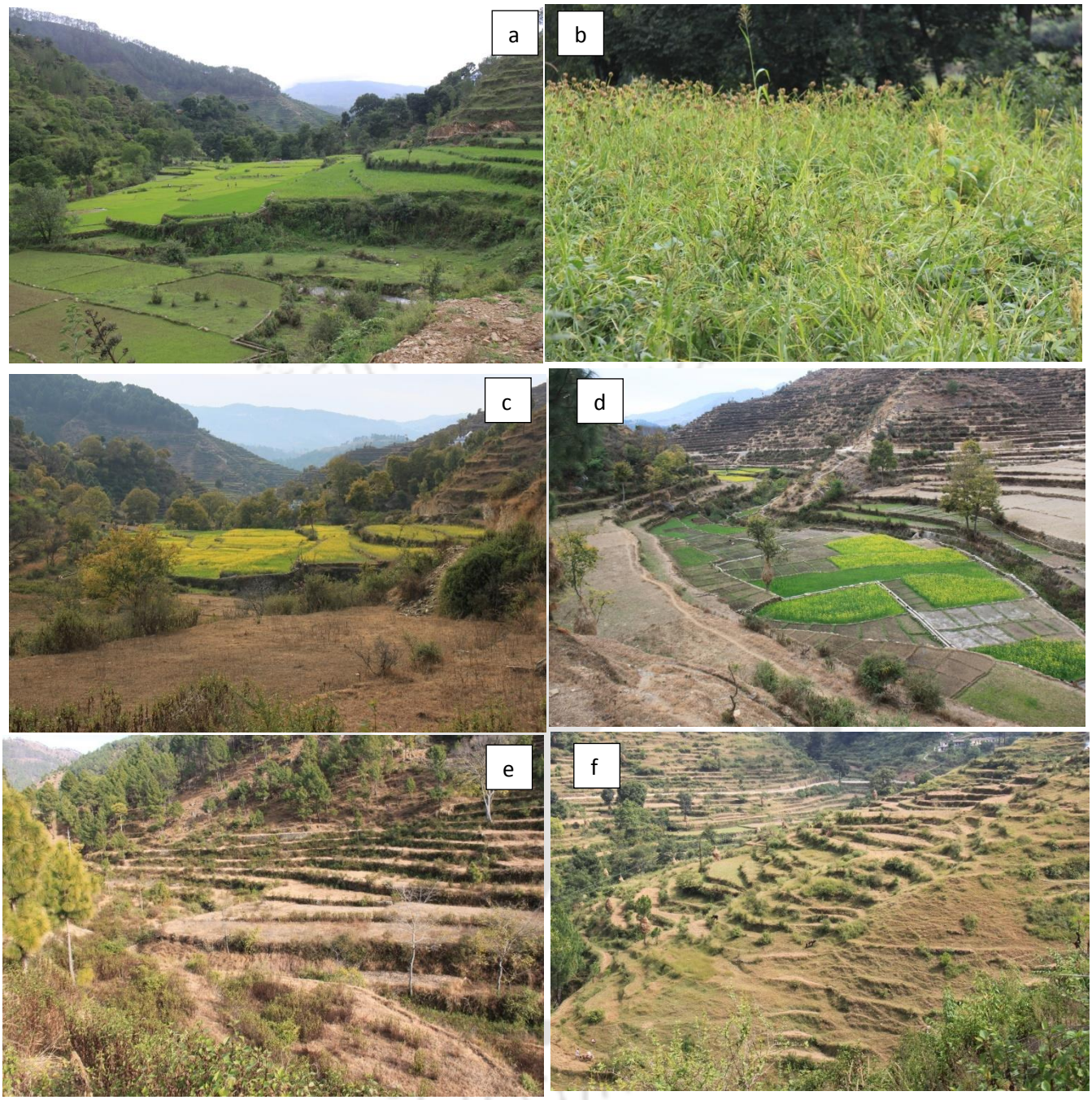

Photograph 7.1: Photograph depicting the Kharif cropping with wet rice in the valley and dry (or upland rice or Ukhar) in upper terraced land(a); finger millet cultivation(b); Rabi cropping during winter period (c & d); sloping terrace fallow land due to land abandonment (e & f); Oak forest and pine forest and pine-dominated fallow in Dugar Gad microwatershed (g, h&J) and sloping barren land and fallow land in upper Paidul microwatershed(i).

7.7 Conclusion

The results from the analysis of landsue and landcover highlight the ongoing changes and assess the significant trends of the most dynamic landuse categories undergoing fast transformation. There seems to be a general agreement in the rate of change over an eight-year period in the two rural microwatersheds reflecting the local changes as well as in regional scale landuse changes at the watershed scale. The past land use map derived from the revenue maps for 1966 brings to light the dominance of agricultural land and barren land over the forest as the rural population was entirely dependent on traditional agriculture and barren land turns into grassland during the monsoon season and harvested during the winter period and acted as a source of fodder for the large cattle population. However, the recent trends over the period 2010-2017 derived from the mapping of high-resolution satellite images of Indian and foreign satellites underscore a complete reversal with the dominance of forests over agricultural land.

The analysis of the two microwatersheds as well as at watershed scale over the period 2010-2017 indicates a very significant decrease in agricultural land (- 98 to 109 %) with a rise in area under pine forest (+ 39 to 44%) categories. The transition matrix showed a conversion of agricultural land to fallow and fallow to pine-dominated fallow and barren land. The main driving forces for such a rapid ongoing fast transition are due to rural to urban migration of the male workforce; lack of normal monsoon rainfall as well as winter drought and goodwill. Research findings could provide useful information for adaptive land use policy for wise natural resource management at the smallest administrative units.

CHAPTER 8

Soil Hydraulic Conductivity Characterization

8.1 Introduction

Flow regimes and water availability are dependent on soil-landuse interrelationship. However, the conclusion drawn from multiple studies could lead us to two divergent paths. One, where soil textural properties alone can be considered as a good predictor of saturated hydraulic conductivity (Ks) and on the other hand inferences drawn by taking only soil textural properties as a single and independent metric to predict hydraulic properties of soil could be wrong if the associated landuse and the land management practices are being overlooked in a pedo-transfer function. Conversion of one landuse into another, for example, natural forest to agriculture/plantation or agriculture land to fallow or fallow land to scrub forest or secondary forest may alter the functioning of the entire landscape positively or otherwise, which largely depends on how the soil and sub-soil characteristics get modified. Lower water and higher sediment yield are the consequence of such adverse landuse change.

Prevalent lean period water scarcity is an outcome of rapid changes in bio-physical as well as socio-economic drivers which is under continuous transformation in the Indian Himalaya, especially in the middle Himalaya for more than five decades. The rural-to-urban migration of the workforce has resulted in agricultural land abandonment converting the terraced landform into permanent fallows with may have altered soil hydraulic characteristics. Forest cover is another governing crucial factor controlling the downstream availability of water by its role in building and plumbing the “critical zone”, which extends from the top of the tree canopy to the deep bedrock with intermediate soil formation (Giardino and Houser, 2015). It is now increasingly recognized the important

role played by vegetation cover as forest act as a "biotic pump" as it draws water from the terrestrial systems and feeds it back to the atmosphere. Simultaneously, the forest could facilitate soil and groundwater recharge through its roots as well as store ('sponge effects') in the upper soil organic matter generated by leaf litter decomposition on the forest floor (Bruijnzeel, 2004; Brantley et al. 2017; Ellison et al. 2017; Jasechko et al. 2013). Although the coniferous forests could act aversely of the forested ecosystem of the forest-dominated state of Uttarakhand as man-made recurrent forest fire subjects the underlying soil cover to hardening and possibly leading to more overland flows and soil erosion. Additionally, the increasing expanse of fast-growing pine forests with rising evapotranspiration demand makes the catchment more water deficient. Furthermore, the decline in rainfall at annual and seasonal (winter and monsoon period) timescale since the mid-sixties, as well as the recent change in rainfall characteristics caused by climate change, may have impacted the natural water resources availability. The widespread reported observation of decline in springflow (Rawat et al. 2016) and streamflow makes it the single most complex watershed or springshed management issue which not only needs a holistic multi-disciplinary science-based approach but also should ensure social inclusiveness for its long-term sustainability.

8.2 Literature Review

Soil intrinsic properties such as texture, porosity, bulk density, pore dimensions and distribution as well as soil depth, soil organic matter and the extrinsic factors like landuse, vegetation and its root distribution as well as human activities such as tillage, crops and related land management practices influence the hydropedological properties of soil. Hydropedology is an emerging field for the study of soil–water interactions and landscape–soil-hydrology relationships. It focuses on understanding the pedologic controls on hydrologic processes and the hydrologic impacts on soil (Lin et al. 2008). The central parameter which governs the flow and transport in soil formation is hydraulic conductivity (K). Many studies are focused on deciphering the primary factors influencing the Ks, for example, the study in U.S. National Science Foundation

Intensively Managed Landscapes-Critical Zone Observatory (IML-CZO) found good corresponds between soil physical properties (texture and bulk density) to infiltration in soils (Papanicolaou et al. 2014). On the contrary, more and more studies indicate that land use could exert a more a pronounced impact and alter the soil's inherent characteristics ("genoform") which cannot be assumed from average Ks value determined out of the physical properties of soil using a Pedo-Transfer Functions (PTFs). (Price et al. 2008; Germer et al. 2010; Gonzalez-Sosa et al. 2010; Pirastruet al. 2013; Wösten et al. 2001; Papanicolaou et al. 2014).

Zimmermann et al. 2006 focus on quantifying two sensitive parameters (near-surface infiltrability and field-saturated hydraulic conductivity- Ksat) to soil disturbance in Southern Amazon Dissected Highland with a goal impact assessment of secondary forest on soil hydrology. The study also reported an assessment of flow path changes under the prevailing rainfall intensities with limited discernable impacts. Ghimire et al. (2013a) and Ghimire et al. (2013b) investigated the multi-decadal changes in the Middle mountains of Nepal from the reference baseline data of Gilmour et al. 1987 with repeat sampling of Ks under different landuse setups (natural forest, planted pine forest, and pasture). Inferences on alteration in the dominant hillslope stormflow pathways due to associated changes in the field saturated hydraulic conductivity (Ks) mainly caused by anthropogenic pressure on natural and planted forests impacting the hydrological functioning forest was highlighted by the important study. Both the pertinent studies (Zimmermann et al. 2006; Ghimire et al. 2013a) with reference to the middle Himalaya could establish the inherent 'memory effect' of past landuse in soil formation.

The study from the two study sites in northern Germany (Bormann and Klaassen, 2008) investigated the dependency of soil hydraulic and hydrological properties regulated by three landuse categories. The authors reported statistically significant results of control of landuse over the important soil properties such as soil saturated hydraulic conductivity, bulk density and infiltration capacity for two typical German soil categories. The study stressed using the soil-landuse approach over the classical approach where only soil type is believed to regulate the soil hydraulic properties in hydrological catchment modeling studies with the incorporation of seasonal variable soil properties. Gonzalez-Sosa et al. 2010 showed that the hydraulic properties were related to landuse rather than pedological

units from their measurements of topsoil hydraulic properties from a suburban catchment in France. They reiterated the introduction of *in-situ* measurements of top soil hydraulic conductivity under different landuse in addition to pedological properties like soil texture, organic matter content and dry bulk density in pedo-transfer function in hydrological models. Germer et al. 2010 found an almost 17 times increase in the volume of stormflow with a two-fold rise in the frequency of storm events caused by soil compaction from a comparative study of catchment under the natural forest and pasture converted from forest in the SW Amazon basin of Brazil.

Pirastruet al. 2013 quantified the impact of landuse conversion, especially the removal of natural vegetation on the hydrological properties of soil in two hillslopes under contrasting landuse (natural forest and grassland converted from natural forest). The adverse impact was reported in terms of altered pore structure, conductivity characteristics, less retention, and higher erosion potential in grassed soil than the natural forest soil which may lead to increased overland flow and lessen the groundwater recharge. Papanicolaou et al. 2015 studied the effect of landuse and land management practices on spatial variability of *Ksat* in hillslopes with different dominant landuse and management practices in a subwatershed in U.S. National Science Foundation Intensively Managed Landscapes-Critical Zone Observatory (IML-CZO). Interestingly, the study showed soil texture and bulk density can be a good predictor of K_{sat} in an intensively managed landscape and hence being used as a pedo-transfer function.

A recent study in Fengyang Mountain Nature Reserve, Zhejiang Province, China by Hao et al. 2019 reported vegetation type influences the hydraulic conductivity of soil whereas Jorda et al. 2015 found land use and bulk density were the most important factors for saturated hydraulic conductivity (Ks). Some of the major land management issues in the Indian Himalaya are soil erosion in degraded sloping landscapes, increase in frequency and volume of overland flow, soil compaction due to deforestation, forest fire and cattle trampling, and conversion of agricultural land to permanent fallow, which has made the region more water-limited. These transformations along with declining rainfall in the middle mountains have led to a diminishing discharge in springs and spring-fed streams. The above land management issues may have impacted the topsoil and subsoil. Hence the objective was to quantify the effects of the ongoing changes in land use on the

hydrological properties of the soils.

Improved water and soil conservation requires an understanding of the physical and hydraulic characteristics of soil formation. The inherent characteristics of the top and subsoil influence the water storage and its movement, hence regulates many important functions like nutrient or solute leaching, pollution transport and recharge to the underlying groundwater aquifers. Interestingly, landuse and landcover change is known to have its impacts on the infiltration characteristics of soil altering the hydrological function of the landscape (Bormann and Klaassen, 2008). Further, human-induced soil degradation caused by over-grazing, human pathways and recurrent forest fire could cause soil compaction making the landscape more frequented by overland flows (Ghimire et al. 2013; Moody et al. 2015). The infiltration, which is the entry of water at the atmosphere-soil boundary and permeation, which is movement of water within the soil pore spaces plays a crucial role (Ghosh and Pekkat, 2019). Soil formation can occur under unsaturated and saturated condition depending upon the availability of soil moisture. The unsaturated and saturated hydraulic conductivity controls the flow of water through the soil profile and various laboratory and field methods are devised, such as tension infiltrometer (TI), Mini disc infiltrometer (MDI), single and double ring infiltrometer (DRI) and Guelph permeameter (GP) to measure the in situ hydraulic conductivity (K and K_{fs}). The pore geometry, water content, soil matrix potential as well as soil texture, tillage, landuse, root dynamics and soil microorganism activities have an impact on hydraulic conductivity (Brady and Weil, 1999). The Mini Disk Infiltrometer (MDI) measures the near-surface unsaturated hydraulic conductivity of the soil surface it is placed on at different suction range (0.5 to 7cm). The advantage of MDI is its portability, very minimum water requirement, and non-intrusive. Moreover, infiltrating water under tension prevents the filling of the macrospores and gives hydraulic conductivity characteristic of the soil matrix, which is less spatially variable (Dohnal et al. 2010).

8.3 Study area and sampling strategy

A small micro catchment of a 26-hectare area nested within the upper Paidul microwatershed dominated by secondary forest of dense Pine (*P. roxburghii*) forest developed over the fallow which was left abandoned probably forty-fifty years ago was identified as a representative site for dominant landuse class of fallow-dominated by Pine forest. In the northwest-facing catchment with an altitudinal difference of 250 m with roughly 25% slopes, 13 pits in terraced abandoned plots within the Pine forest were made at varying elevations (1400 to 1421m) in plot of 100m x 90 m to measure the field saturated hydraulic conductivity as well as near-surface hydraulic conductivity. Nine widely separated pits were also made for hydraulic conductivity estimation, which is representative of traditional agricultural land located in the central valley of elongated basin of upper Paidul microwatershed. Photograph 8.1 shows an attempt to assess the macro-porosity using the brilliant blue dye test in the Pine-dominated soil column.

Photograph 8.1: Soil macro-porosity investigation using brilliant blue fluorescent dye in the Pine-dominated fallow. Attempt to dissect the soil column after application of dye was unsuccessful due to the presence of higher rock fragments and Pine tree roots.

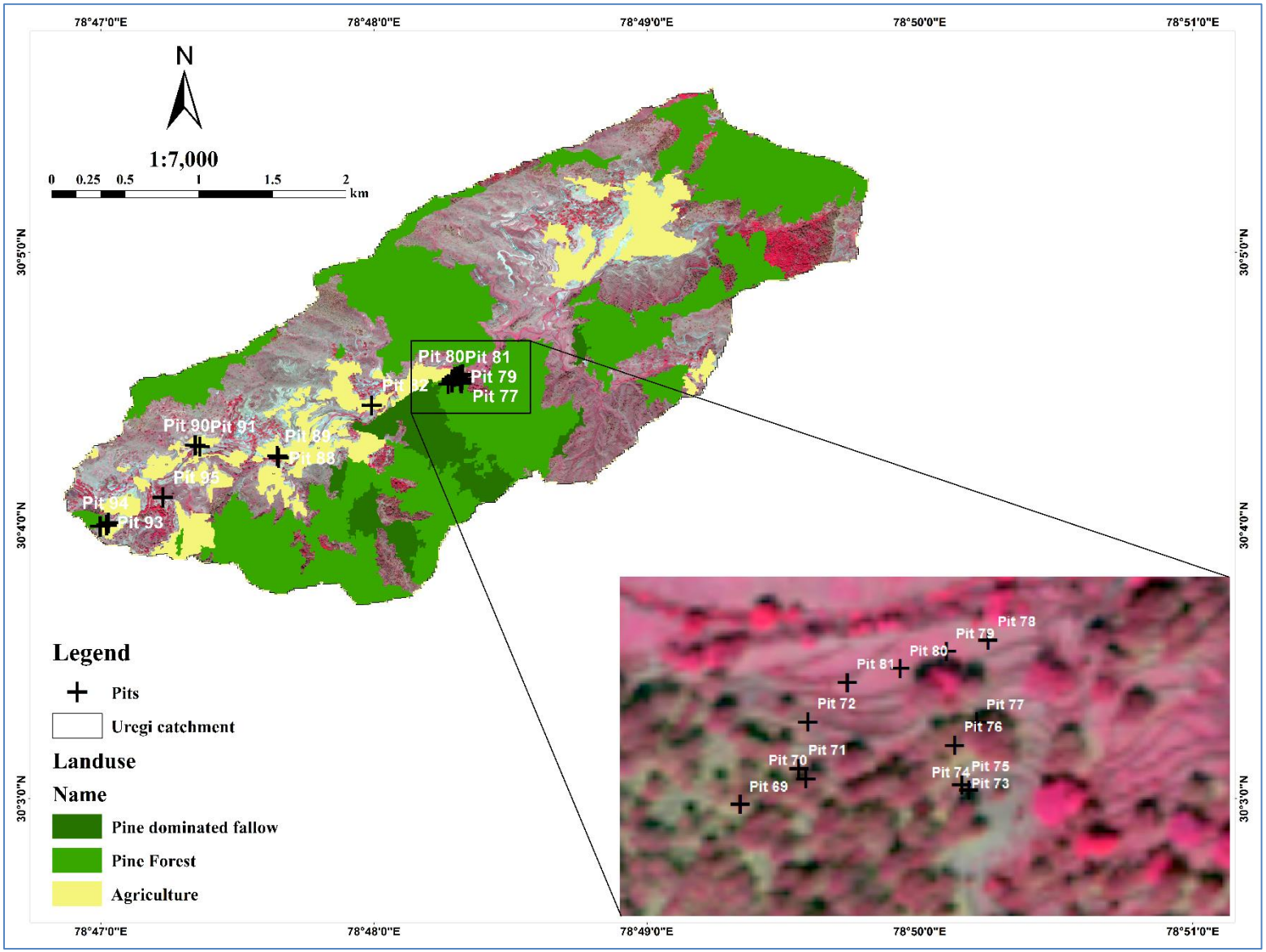

Figure 8.1: The locations of auger hole (pits) for soil hydraulic conductivity measurement in Pine forest/Pine dominated fallow as well as in agricultural land in upper Paidul microwatershed.

8.4 Methodology

8.4.1 GUELPH Permeameter

The Guelph permeameter method (GPM) is a constant-head well permeameter for in situ measurement of saturated hydraulic conductivity (K_{fs}), sorpivity(S) and matrix flux potential (φ_m) in the vadose zone (Reynolds and Elrick, 1986). These three parameters are critical for transport of water in the vadose zone and are widely recognized for the design of irrigation and drainage system, landfill site and other geotechnical investigation (Everett, 1982). The robust equipment employing the Marriotte Principle for maintaining a constant depth of water in the uncased well of 15 to 75 cm depth makes it possible to determine the steady-state water recharge by measuring the rate of fall of liquid level in the permeameter. A constant well height of water is established in a bored hole with a "bulb" of saturated soil around the borehole quickly established. Once the unique "bulb" shape is established, the outflow of water from the well reaches a steady-state flow rate, which is measured. The rate of this constant outflow of water, together with the diameter of the well, and height of the water in the well can be used to accurately determine the field saturated conductivity, matric flux potential, α* parameter and sorptivity of the soil. Measurements can be completed in 1/2 to 2 hours time, which depends on soil type (texture), and the initial soil moisture content and require only about 2.5 liters of water to complete an experiment.

The following equation can be used to determine the saturate hydraulic conductivity of vadose zone. The Shape factor (C) is a function of soil type, water height in borehole (H) and borehole radius (a). The single-head and two-head methods can be used to measure the hydraulic conductivity but the dual head measurement gives more accurate measurements. Initially, the C factors for each head height are calculated using Zhang et al., 1998. But, this requires the use of α*, microscopic capillary length factor which differs based on the soil category. The formula for two head calculation of saturated hydraulic conductivity is given below (Eq-8.1 to Eq-8.5):

$$Q_1 = \bar{R}1 \times 35.22 \tag{8.1}$$

$$Q_2 = \bar{R}2 \times 35.22 \tag{8.2}$$

$$G1 = \frac{H_2C_1}{\pi(2H_1H_2(H_2-H_1)+a^2(H_1C_2-H_2C_1))} \tag{8.3}$$

$$G2 = \frac{H_1 C_2}{\pi(2H_1H_2(H_2-H_1)+a^2(H_1C_2-H_2C_1))} \quad (8.4)$$

$$K_{fs} = G_2Q_2 - G_1Q_1 \quad (8.5)$$

where the R_1 and R_2 are the steady-state rate of fall of water in the permeameter(cm/sec), H_1&H_2 are the first and second head of water established in borehole(cm), and a is borehole radius(cm).

Dual head experiments were conducted in the agricultural land and fallow dominated by Pine forest in the representative catchment nested with the Paidul microwatershed. A total of twenty-two auger holes in a depth range of 20 cm and further extended up to 30 cm in the agricultural land and abandoned terraced plots within the Pine forest were created using a handheld soil auger. Soil auger and sizing auger were used for creating a proper size hole. To remove the smear layer from the sides of hole, well prep brush was used as per the guidelines. All the measurements were carried out during the winter period. The auger holes were saturated with water 24 hours before the test was conducted. Step-by-step two-head procedure was followed and readings were obtained at a fixed interval (1 minute) as the water gets absorbed by the soil until steady state condition is established. The double head method was used for the estimation of saturated hydraulic conductivity of the subsurface soil formation at 20 cm and 30cm depths in each auger hole using an excel spreadsheet.

8.4.2 Mini disk Infiltrometer

A mini disk infiltrometer(MDI) having a 4.5 cm diameter sintered stainless steel disc which is placed on a smooth part of the soil surface to measure hydraulic conductivity. The upper and lower chambers of the handy equipment are filled with water, the upper chamber controlling the applied suction and the lower being used as a graduated reservoir to determine the water infiltrating the soil formation. The area measured by this type of method is small because of the disk size of the infiltrometer and small depth of the test and it is used to measure the near-surface hydraulic conductivity in the unsaturated soil medium. The measurements with the MDI are initiated by placing it on the soil surface, and assuring that it makes solid contact with the soil surface. The volume of water that

infiltrates into the soil has been recorded as a function of time in the record sheet. The procedure is repeated for a suction head of 0.5 and 2.0 cm. For every measurement, the volume of water (reading in ml) infiltrating into the soil is recorded every minute for 15 minutes to half an hour duration. The square root of time and cumulative infiltration depth (in cm) is calculated. Cumulative infiltration is obtained by dividing the volume of infiltrating water by the area through which water is infiltrating.

In the present study, the Mini disk Infiltration tests have been conducted adjacent to the auger hole created for GP experimentation under the two representative landuse categories in the upper Paidul microwatershed. The field experiments using the MDI have been performed as per the guidelines mentioned in the user manual (manufactured by Decagon Devices, Pullman, WA, USA, Infiltrometer User's Manual, Decagon Devices Inc. 2012). The volume of water was recorded at regular intervals as the water infiltrates into the soil. The selection of time interval depends on both the suction rate and the soil type. The repeat experiment with a suction head of 2cm was carried out in 22 locations for estimation of soil surface hydraulic conductivity with measurement of the volume of water infiltrating into the soil every 60 seconds. The contact between MDI and the soil surface was established by gently clearing the surface of soil and spreading sand over the surface.

8.4.3 Collection of soil samples, bulk density, sieve analysis and statistical test

Several soil core samples were collected from the soil auger holes for laboratory analysis of bulk density and to assess the textural characteristics of the soil under the two representative landuse classes. Soil samples were collected from the auger holes at 0-20 cm depth zone and 20-30 cm depth zones. For bulk density, samples were extracted from the field using a cylindrical core (diameter 8.2cm and height 5.08cm) having a volume of about 268.12 cm^3. Soil texture refers to the relative size distribution of soil particles in a given soil sample. The particles are grouped into gravel, sand, silt and clay according to their size and classification is based on the size of the particles following the USDA classification and International Society of Soil Science (ISSS). The classification scheme by USDA and ISSS is mentioned in Table 8.1.

Table 8.1: Classification of soil particle by USDA and ISSS

Soil type	Particle Diameter in mm
Very coarse grain	2.00-1.00
Coarse sand	1.00-0.50
Medium sand	0.50-0.25
Fine sand	0.25-0.10
Very fine sand	0.10-0.05
Silt	0.05-0.002
Clay	<0.002

The particles larger than 2.0 mm constitute gravel whereas fine clay-dominated soils; also called heavy soils have low permeability and infiltration rates. Sandy soils or light soils having a higher proportion of large sized particles have higher permeability and infiltration rate. The water-holding capacity of clay soils is the highest followed by loam and sandy soil. The textural class was determined based on percent content of sand, silt and clay using a triangular diagram by USDA. Sieve analysis consists of shaking the soil sample through set of sieves that have progressively smaller openings. The soil samples collected from different sites in the study area were initially weighed and 500 grams of the sample was taken for analysis. First, the soil is oven-dried for approximately 20 minutes at 105°C temperature and all lumps are broken into small particle before they are passed through the sieves of different sizes. After the completion of the shaking period through an electromagnetic sieve shaker, the mass of the soil retained on each sieve was determined using a weighting balance.

Statistical test was carried out to test the hypothesis on whether the mean and median data of near-surface hydraulic conductivity K(h) and saturated hydraulic conductivity (K_{fs}) are statistically different in two landuse categories as well as in two depths using parametric student t-test and non-parametric Mann-Whitney Rank Sum test at a significance level ($p<0.05$) using R-studio statistical package.

8.5 Results

8.5.1 Sieve Analysis and Bulk Density analysis

The mean percentage of gravel, sand and fines are 13.92%,63.24% and 22.84% in Pine dominated fallow land (Pine forest) and for traditional agricultural land 9.88%,65.47% and 24.65% , showing not much of a difference between the soil texture in the two landuse classes (Table 8.2 and Photograph 8.2). Depth-wise variability is also not a significantly different from the two sample locations of two landuse classes. Overall the soil in the study area is coarse grain (sandy clay loam) with significant percentage of rock fragments in the upper 30 cm depth of the soil formation.

The estimated mean bulk density from the agricultural land is 1.44 g/cm^3 (CV=0.034) whereas the mean bulk density of 1.36 g/cm^3 (CV = 0.098) is observed from the Pine forest-dominated fallow site, which showed no marked difference in the bulk density.

Table 8.2: Summary of the results of soil textural property in two different land use showing the percentage sand, fines and gravel.

Landuse	Depth (cm)	Sand (%)	Fines (%)	Gravel (%)
Pine forest (fallow dominated by Pine)	0-15	55.10%	29.00%	15.90%
	15-30	50.1%	28.4%	21.50%
	0-15	66.90%	22.00%	11.10%
	15-30	66.40%	20.20%	13.40%
Agricultural Land	0-15	77.70%	14.60%	7.70%
	15-30	62.90%	29.90%	7.20%
	0-15	59.80%	28.70%	11.50%
	15-30	63.70%	27.20%	9.10%

Photograph 8.2: Soil sample collection from different land cover areas and separation of soil particles through electromagnetic sieve analysis method.

8.5.2 Soil infiltration

The infiltration results of both minidisk infiltrometer and GUELPH permeameter are represented in Table 8.3 & Photograph 8.3 measured at13 locations in pine-dominated fallow and nine locations in agricultural land in the upper Paidul microwatershed. The plots (Figure 8.2) show the variation of cumulative infiltration with the square root of time for all the locations obtained by using Mini disk infiltration measurement. The graph illustrates the relation of cumulative infiltration with the square root of time. The *K(h)* value for pine-dominated fallow land ranged from 3.17 to 33.1 mm hr^{-1} with a median infiltration value was 10.45 mm hr^{-1} (CV=0.62). Whereas the *K(h)* ranged from 5.99 to 60.23 mm hr^{-1} with a median value 25.34 mm hr^{-1}(CV=0.67) for traditional agricultural land. The Wilcox-Rank test (Mann Whitney U test) showed a significant statistical difference between the median value (p = 0.002667) and the parametric t-test also showed statistical difference in the mean (p = 0.0006171) between the near-surface *Kh* between the two landuse class. The boxplot (Figure 8.3b) also highlights the difference in mean and median values in the two landuse classes. An overall infiltration in unsaturated

suggests that the near-surface infiltration is significantly higher in the agricultural soil as compared to the Pine-dominated fallow. Such a significant difference in near-surface unsaturated hydraulic conductivity values can be attributed to the recurrent forest fire in the Pine-dominated fallow as well as grazing activities whereas topsoil tilling to a depth of around 20cm in agricultural land could results in higher *k (h)* value even though the difference in textural characteristics between the two landuse class are minimal.

Table 8.3: Summary of the results of saturated hydraulic conductivity and near-surface hydraulic conductivity measured at 22 locations in two representative landuse categories.

Borehole depth →	**Surface (MDI) (mm hr^{-1})**	**20cm (GP) (mm hr^{-1})**	**30cm (GP) (mm hr^{-1})**
Pine forest(fallow dominated by Pine)			
Mean	11.75	20.36	13.41
Median	10.45	16.10	9.00
Standard Deviation	7.14	14.87	11.05
Minimum	3.16	2.71	0.09
Maximum	33.06	57.96	35.86
Agricultural land			
Mean	29.81	23.80	13.52
Median	25.34	19.20	11.55
Standard Deviation	18.73	12.90	10.37
Minimum	6.00	15.62	4.5
Maximum	56.49	42.48	35.75

MDI is Mini Disk Infiltrometer and GP for GUELPH Permeameter

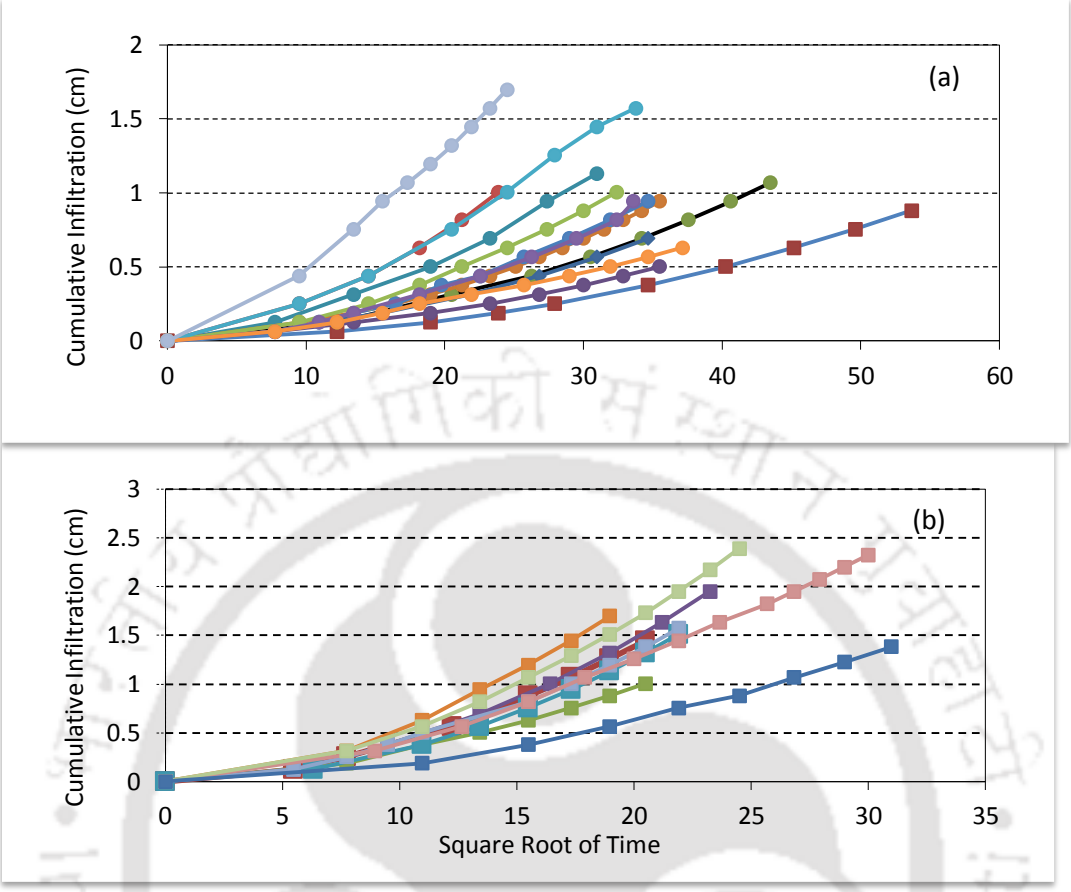

Figure 8.2: Variability in the cumulative infiltration rate at agricultural land (a) and Pine-dominated fallow land (b) measured using MDI.

Photograph 8.3: Mini disk infiltrometer experimentation in the agriculture and fallow- dominated by pine forest in the upper Paidul watershed.

Figure 8.3a highlights the saturated hydraulic conductivity of the soil under the two land use area. The Guelph permeameter results at two different depths (20cm and 30cm) for saturated hydraulic conductivity showed nominally higher values in the agricultural land as compared to the pine-dominated fallow land (Table 8.3 and Figure 8.3a). The median K_{fs} was low in the Pine-dominated fallow area and high in the agricultural land. At depth range up to 20cm, the saturated hydraulic conductivity values ranged from 2.7 to 58mm hr^{-1} and 4.5 to 42.5mm $hr^{-1}$with the median K_{fs} values being 14.5(CV= 0.86) and 19.2 mm hr^{-1}(CV= 0.56) in Pine-dominated fallow and agricultural land respectively.

The non-parametric and parametric test results indicate statistically insignificant variation between the median and mean value at a 95% confidence interval at a depth of 20cm in both the landuse class.

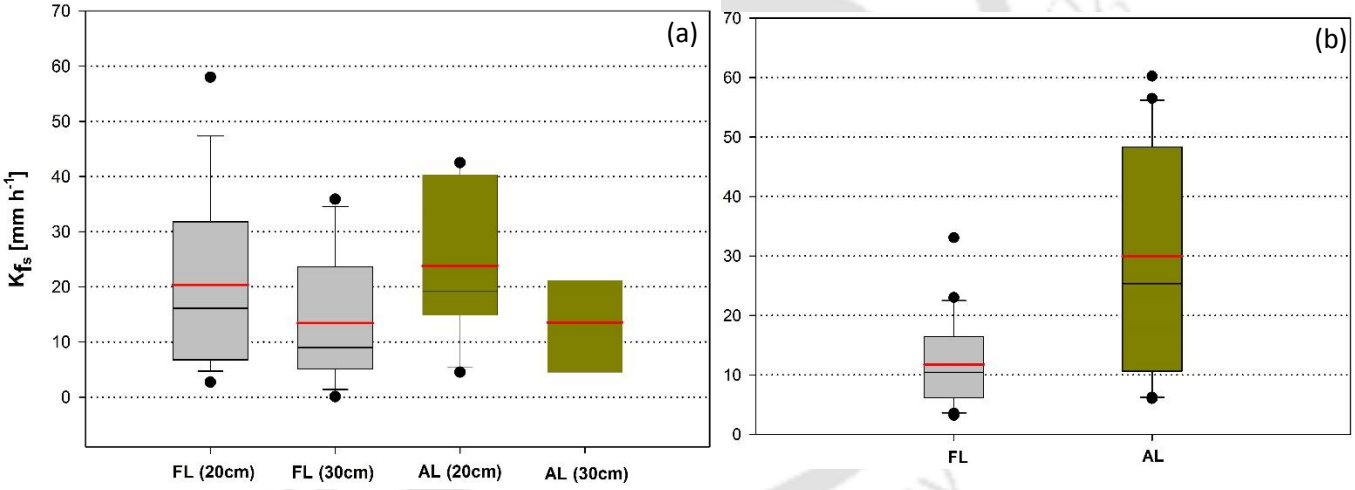

Figure 8.3: Box plots representing the variation in hydraulic conductivities (K_{fs} and K_h) using GUELPH permeameter (a) and Mini disk infiltrometer (b), at different bore depths and different land use. The acronyms FL and AL stand for Fallow–dominated by Pine forest and Agricultural Land respectively.

Similar results at a 30 cm depth can be observed with a nominal higher value of median *Kfs* in agriculture land as compared to Pine-dominated fallow. Although, a decrease in the median saturated hydraulic conductivity values was observed in the 20 cm depth to 30 cm depth in the K_{fs} values. The values ranged from 0.1 to 36 mm hr^{-1} and 1.26 to 36mm hr^{-1} with the median K_{fs} values being 9(CV= 0.86) and 11.5 mm hr^{-1}(CV= 0.81) for the pine-dominated fallow and agricultural land respectively. No statistically significant difference could be found in the median and mean of the two landuse at 30 cm depth.

The results reported from the middle Himalayan region of Central Nepal (Ghimire et al. 2013) showed the highest median surface K_{fs} value for natural forests and the lowest for degraded pastures and open pine forests and the conductivity decreased with an increase in the depth in different land cover types. The K_{fs} values reported ranged from 82-232 mm hr^{-1} for natural forests, 18-39 mm hr^{-1} for degraded pasture and open pine forest whereas footpath showed 12-26 mm hr^{-1}. Our results indicate a lesser median value for Pine-dominated fallow from Indian Lesser Himalaya as compared open Pine landuse in central Nepal. Bormann and Klaassen, 2008 reported similar results where the highest K_{fs} values were observed in natural forests, followed by cropland and grasslands. The reasons stated were that the soil macro faunal activities in forests may result in increased hydraulic conductivity whereas the use of machinery for ploughing in croplands may result in low infiltration. The lack of statistical difference in saturated hydraulic conductivity (K_{fs}) between the two landuse classes up to a depth of 30 cm could be attributed to strong 'memory effect' in soil which gets retained even after several decades of anthropogenic activity which is reported from central Nepal (Ghimire et al. 2013) and Amazon basin (Zimmermann et al. 2006). The conclusion drawn by Pirastru et al. 2013 from the Mediterranean region could also be true where conversion from forest to pasture (or vice versa) did not necessarily get reflected in term of statistically significant alterations.

8.5.3 Rainfall intensity and dominant hillslope pathway

The rainfall characteristics in the study is dominated by the low-intensity rain and the number of total rain events of high-intensity rainfall is significantly less than the lower intensity rainfall (Table 8.4 and Table 8.5). The low and medium intensity rainfall had around 47.8 and 37% while the higher-intensity rainfall has a 14% contribution to the overall precipitation contribution in the year 2017 (Figure 8.4). The contribution figures for low and medium intensity rainfall did not change much with 45.2 and 31% contribution in low and medium rainfall categories while the higher intensity rainfall have 11.2% of the overall precipitation contribution in the year 2018(Figure 8.5). The maximum hourly intensities for 2017 for the 15-min and 60-min rainfall intensity for all the events (I_{15max} and I_{60max}) were 53.8 mm hr^{-1} and 20.8 mm hr^{-1} respectively. The observed maximum hourly intensities for 2018 for 15-min and 60-min rainfall were 49.7 and 22.6 mm hr^{-1} respectively. Ghimire et al. 2013 reported for the summer monsoon of 2010 and 2011, an I_{15max} and I_{60max} of 62.4 and 39.6 mm hr^{-1}respectively with the larger contribution of high-intensity rainfalls during the monsoon period. The median values observed were quite similar in both the monsoon periods of 2017 and 2018. The 15min and 1-hour interval rainfall data from the study site for 2017 and 2018 correspond to median values for low, medium and high-intensity rainfall of 0.508, 4 and 9mm hr^{-1} and 0.508, 4 and 12.1 mm hr^{-1} respectively.

Comparing the rainfall intensity results (median values) with the median saturated hydraulic conductivity of agricultural land and Pine-dominated fallow (14.5& 19.1 mm hr^{-1}), the propensity to generate infiltration excess overland flow appears to be low. Vertical percolation of rainfall in the agricultural land as well as in Pine-dominated fallow will remain the dominant mechanism of flow even in quite high event as the observed median value of the high intensity rainfall in both 2017 and 2018 summer monsoon period ranges from 9 to 12.1 mm hr^{-1}. However, infiltration excess overland flow and saturated overland flow may be generated in Pine-dominated fallow and agricultural land in cases of only very high-intensity rainfall.

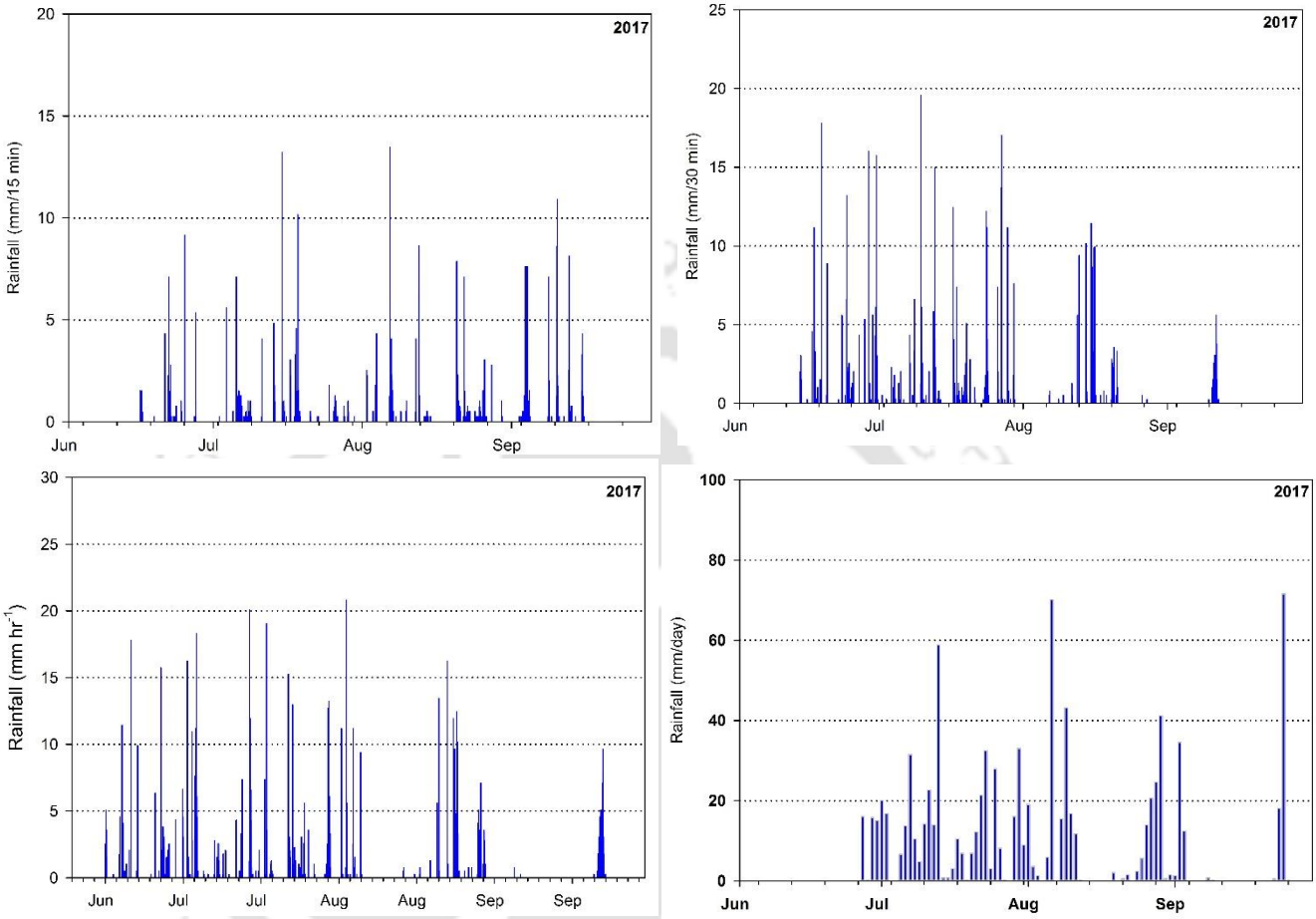

Figure 8.4: Distribution of rainfall in the study area during 2017 summer monsoon recoded in tipping bucket event logger.

Table 8.4: Frequency of low, medium and high intensity rainfall for 2017 monsoon period.

Year 2017	June - September	Frequency of events		
	No. of Events	2-2.5	2.5-7.5	>7.5
Rainfall (mm/15 min)	492	407	72	13
Rainfall (mm/30 min)	363	269	72	22
Rainfall (mm/hr)	232	125	74	33
Rainfall (mm/day)	56	12	9	35

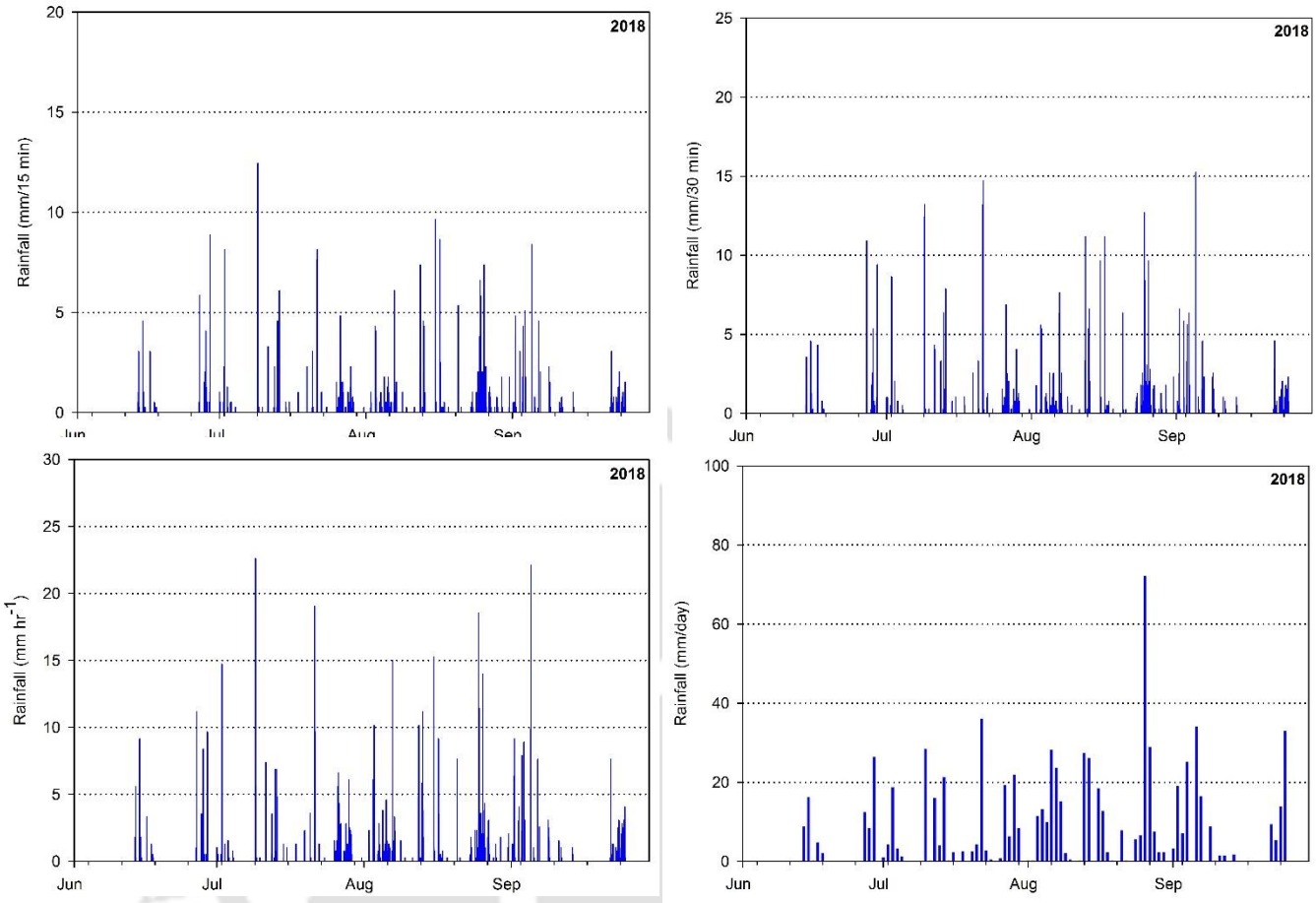

Figure 8.5: Distribution of rainfall in the study area during 2018 summer monsoon recoded in tipping bucket event logger.

Table 8.5: Low, medium and high intensity rainfall frequency for 2018 monsoon period.

Year 2018	June - September	Frequency of events		
	No. of Events	2-2.5	2.5-7.5	>7.5
Rainfall (mm/15 min)	473	404	59	10
Rainfall (mm/30 min)	384	301	66	17
Rainfall (mm/hr)	277	187	63	27
Rainfall (mm/day)	64	14	15	35

8.6 Conclusion

The results of the soil hydraulic conductivity measurements in the representative landuse in the middle Himalaya do indicate near-surface alteration mainly caused by cattle grazing and recurrent forest in the Pine-dominated fallow land as the assessment of unsaturated near-surface hydraulic conductivity collected through point measurement by mini disk infiltrometer show statistically significant K_h values as compared to the agriculture landuse. However, the measurement from the auger hole in the soil formation up to a depth of 30 cm does not reveal any statistically significant change in the saturated soil hydraulic K_{fs} characteristics due to the conversion of agriculture fallow to dense pine-dominated fallow. The memory effect of the past landuse could be the reason for not observing any significant change between the two landuse categories in recent times. The rainfall intensity patterns suggest the study area falling in Lesser Himalaya is still dominated by low-intensity rainfall. Hence, the dominant mechanism for rainfall infiltration is vertical percolation in the landscape.

CHAPTER 9

CONCLUSION AND FUTURE SCOPES

9.1 Key Findings

- Gauged-based observation underscores multi-year deficient monsoonal rainfall, as well as drought, observed in the study area for ten years (2009-2019) in the headwaters of Paschimi Nayar River. Deficient rainfall is marked in two main South West monsoonal months i.e. July and August. Large intra-monthly variability and the frequent delay in monsoon arrival are observed in the recent decade. The severe drought year of 2019 received less than 400 mm of monsoon rainfall. The decadal observation suggests the weakening of the SW monsoon in the interiors of the middle Himalaya region.
- Quality-assured gridded rainfall data from IMD (1961-2018) and Aphrodite (1961-2007) showed a higher incidence of dry years over the second half of the twentieth century and early twenty-first century as compared to the first half of the twentieth century. The simple innovative trend analysis clearly showed a monotonic decline in winter rainfall whereas the annual and monsoon periods showed variable trends with the period of decline, rise and no trend in the long-term rainfall timeseries. The other statistical analysis corroborates the same fact of a statistically significant decline in winter rain but a non-significant decline in annual and monsoon rainfall in a comparative analysis of two sub-series of 1901-1960 & 1961-2018. The abrupt break year of the observed downturn lies between 1958 to 1967. Non-parametric Mann-Kendall trend analysis of annual, seasonal and monthly time series rainfall data showed a decreasing trend (negative Z_{mk} and negative Sen's Slope value) in annual, seasonal as well as monthly time

series. Nonetheless, the pre-monsoon months of March and April as well as the post-monsoon months of September and November are showing rising trend.

- A significant decline in spring flow and stream flow is observed in the recent decades solely caused by the multi-year deficient rainfall. A decline in the baseflow as well as monsoon flow is evident from the flow duration curve of spring hydrograph.
- Prolonged post-monsoon, as well as early winter recession characteristics, are analyzed through the dual exponential model, power law model as well as single non-linear model. The dual-exponential model fitted data indicate a shift from nonlinearity to linearity and an overall non-linearity in the observed recession period. The fitted single non-linear modeled recession data revealed control of antecedent storage over the rate of outflow as parallel offset was observed in the yearly-prolonged recession curve in- dQ/dt versus Q plot.
- The two springs (Mandir dhara and Ayal dhara) at spring catchment scale ranging from 4-54 hectare indicate a non-linear storage-outflow relationship and is in agreement with the reported nonlinearity at a larger spatial scale beyond the individual hillslope. A very fast recession rate of Ayal and Mandir dhara spring of only 8-14 days of recession timescale is estimated using a nonlinear model. The sensitivity of spring flow (ϵ_S) also supports that the groundwater storage sustaining the spring flow is highly vulnerable to storage changes and influenced by the past storage which is dependent on yearly SW monsoon rainfall.

- Depth to water level data collected for summer, monsoon, post-monsoon and winter periods highlights the dynamic nature of shallow riparian groundwater system, which feeds the springs, seeps and low-order streams. All the piezometer or observation holes showed variability in water level between 1.6 m to the near surface whereas borehole-6, dry during the drilling exercise showed water level fluctuation between 1-4 m during

monsoon and post-monsoon period. The borehole 6 dried out during the December month. This has led to the conceptualization that the building-up of perched water table occurs in the steep hillslope domain during the monsoon influx whereas the riparian zone (narrow valley portions) holds permanent shallow aquifer.

- The results of aquifer testing through slug test (rising head), pump test recovery data used as falling head response data and geological mapping indicate a double porosity model for the fractured metasedimentary formations. The slug test (rising head and falling head) response data analyzed through a confined homogeneous porous medium approach as well as regularized fractured and slab medium idealization of geological formation through type-curve matching technique indicate large spatial variability. The horizontal hydraulic conductivity ranged from 0.00037-1.39 m/day with a geometric mean of 0.042 m/day, whereas storativity values ranged 10^{-3}-10^{-10} with geometric mean of 10^{-8}. The dual porosity model assumptions did not result in very different hydraulic parameters from the homogeneous confined aquifer idealization and indicate very low storativity for the metamorphic rock in the study area. This could be a limited understanding of parameters like anisotropy and fracture size and aperture. Moreover, the results could not be verified due to a lack of complimentary data on aquifer parameters estimated through pump tests or other means for similar geological formations.

- The Shallow piezometer (< 4 m) and deep bore well (< 80 m) monitored over two monsoon periods indicate a rapid response to any rainfall amount exceeding 5mm. A deeper aquifer at the hillslope and shallow aquifer in the riparian zone of experimental HRU indicate a preferential flow-dominated system in bedrock aquifers. The episodic and water level fluctuation method indicates a monsoonal recharge of 4% to 24% for a low specific yield value (1 to 5%). The uncertainty in the recharge estimate may arise due to lack of reported values of specific yield from the metasedimentary rocks of lesser Himalaya. The study also highlights that the effectiveness of recharge is

controlled by the rainfall intensity. A near 2.08 to 2.4mm/hr rainfall intensity generates maximum recharge in the terrain dominated by metasedimentary rock.

- Landuse and land cover in the two experimental microwatersheds show significant abandonment of agricultural land due to the out-migration of people from the rural areas of district Pauri, Uttarakhand. For eight years, an almost 100-percentage decline in agriculture land and a 40%, increase in pine forest area is observed from the two experimental micro-watersheds. Such a rapid transformation in landuse (possibly adverse) is also observed in the regional scale mapping at the Irgad watershed scale.

- Higher percentage of rock fragments, as well as root system in the Pine-dominated fallow land, did not allow the dissection of the soil column into sections making the dye tracer experiment with brilliant blue dye impossible for soil macropores characterization.

- A strong 'memory effect' is observed in the recently converted (nearly two decades ago) Pine-dominated fallow land as the soil formation at 20 and 30cm depth did not show any statistical significant difference in saturated hydraulic conductivity(K_{fs}). A marked difference is observed in near-surface unsaturated hydraulic conductivity (*Kh*) between the two landsue classes' i.e. traditional agriculture land and Pine-dominated fallow. An analysis of tipping bucket rain gauge event logger data for two years (2017& 2018) highlights that low-intensity rainfall still dominates the monsoon rain. The dominant pathways are still vertical in a Pine forest dominated microwatershed which is subjected to frequent forest fire every summer and the pressure of cattle grazing activities.

- The observation from the recent decade suggests an enhancement of low-flow period leading to an increase in water scarcity which will further aggravate the situation in vulnerable headwaters of the middle mountains.

9.2 Scopes for Future Work

Until now, very limited research has been carried out in headwaters regions of the Indian Himalaya on the understanding of the complex hardrock fracture aquifer systems sustaining the spring and stream flows. However, the ecological significance of these headwaters is immense. The long-term impacts on water resources due to alteration caused by natural and anthropogenic drivers can only be accessed through expanding the gauging networks of dominant fluxes like rain, evaporation, and runoff in ecological hotspots such as the Nayar River Basin. Assessing the ecological ramification of different forest ecosystems, especially the water use components (transpiration, interception losses, etc.) on the hydrology of the catchments should now become the central question as catchments in the middle Himalaya are increasingly becoming dominated by coniferous forests. Parallel studies need to be carried out in understanding the underlying mechanism of groundwater recharge, its flow through complex and short length hillslopes, release and assessment of recharge rate of groundwater at multiple locations in different hydrogeological setups in sloping bedrock topography in dry and wet Indian climate. All over the world, there is a growing realization that a detailed understanding of groundwater recharge processes as well as quantification of annual and seasonal recharge is necessary under changing climate conditions. New insight into monsoonal recharge as well as discrete recharge episodes drawn out of fracture hardrock aquifer systems using time-series of rainfall and water-table fluctuation could be very valuable for water resource planning in the mountainous water-scarce region of middle Himalaya undergoing climate alterations with changing characteristics of rainfall intensity.

Future assessment of the two dynamic recession characteristics should be carried out for a more in-depth understanding of the processes as well as the terrain characteristics that could regulate the observed declining phase of spring flow under the multi-year drought regime. The Land-Use and Land-Cover change brings slow concomitant modifications in soil hydraulic properties, which may alter the infiltration capacity causing more run-on, soil and nutrient loss as well as depletion of soil moisture. Regional scale studies of soil hydraulic characteristics should be carried out for assessment and understanding of dominant hydrological pathways.

References

Alexander, R.B., Boyer, E.W., Smith, R.A., Schwarz, G.E. and Moore, R.B., 2007. The role of headwater streams in downstream water quality 1. *JAWRA Journal of the American Water Resources Association*, *43*(1), pp.41-59.

Andermann, C. Bonnet, S. and Gloaguen, R. 2011. Evaluation of precipitation data sets along the Himalayan front. Geochemistry, Geophysics, Geosystems, 12(7).

Anders, A.M., Roe, G.H., Hallet, B., Montgomery, D.R., Finnegan, N.J. and Putkonen, J., 2006. Spatial patterns of precipitation and topography in the Himalaya.

Anderson, S.P., Dietrich, W.E., Montgomery, D.R., Torres, R., Conrad, M.E. and Loague, K., 1997.Subsurface flow paths in a steep, unchanneled catchment. Water Resources Research, 33(12), pp.2637-2653.

Arciniega-Esparza, S., Breña-Naranjo, J.A., Pedrozo-Acuña, A. and Appendini, C.M., 2017. HYDRORECESSION: A Matlab toolbox for streamflow recession analysis. Computers & Geosciences, 98, pp.87-92.

Asoka, A., Wada, Y., Fishman, R. and Mishra, V., 2018.Strong linkage between precipitation intensity and monsoon season groundwater recharge in India. Geophysical Research Letters, 45(11), pp.5536-5544.

Banks, E.W., Simmons, C.T., Love, A.J., Cranswick, R., Werner, A.D., Bestland, E.A., Wood, M. and Wilson, T., 2009. Fractured bedrock and saprolite hydrogeologic controls on groundwater/surface-water interaction: a conceptual model (Australia). *Hydrogeology Journal*, *17*(8), p.1969.

Barker, J.A. and Black, J.H., 1983. Slug tests in fissured aquifers. *Water Resources Research*, *19*(6), pp.1558-1564.

Barenblatt, G.I., Zheltov, I.P. and Kochina, I.N., 1960. Basic concepts in the theory of seepage of homogeneous liquids in fissured rocks [strata]. *Journal of applied mathematics and mechanics*, *24*(5), pp.1286-1303.

Barker, J., 1988.A generalized radial flow model for hydraulic tests in fractured rock. Water Resources Research, 24(10), pp.1796-1804.

Barros, A.P., Kim, G., Williams, E. and Nesbitt, S.W., 2004. Probing orographic controls in the Himalayas during the monsoon using satellite imagery. *Natural Hazards and Earth System Sciences*, *4*(1), pp.29-51.

Bart, R. and Hope, A. 2014. Inter-seasonal variability in baseflow recession rates: The role of aquifer antecedent storage in central California watersheds. Journal of Hydrology, 519, pp.205-213.

Basistha, A., Arya, D.S., and Goel, N.K., 2009. Analysis of historical changes in rainfall in the Indian Himalayas. International Journal of Climatology, 29, 555-572.

Batar, A. K., Watanabe, T. and Kumar, A. 2017. Assessment of land-use/land-cover change and forest fragmentation in the Garhwal Himalayan Region of India. Environments, 4(2), 34.

Beck, H.E., Bruijnzeel, L.A., Van Dijk, A.I.J.M., McVicar, T.R., Scatena, F.N. and Schellekens, J., 2013. The impact of forest regeneration on streamflow in 12 mesoscale humid tropical catchments. Hydrology and Earth System Sciences, 17(7), pp.2613-2635.

Beguería, S., Vicente-Serrano, S.M., Reig, F. and Latorre, B., 2014. Standardized precipitation evapotranspiration index (SPEI) revisited: parameter fitting, evapotranspiration models, tools, datasets and drought monitoring. *International journal of climatology*, *34*(10), pp.3001-3023.

Berghuijs, W.R. Hartmann, A. and Woods, R.A. 2016. Streamflow sensitivity to water storage changes across Europe. Geophysical Research Letters, 43(5), pp.1980-1987.

Bhardwaj, A. Ziegler, A.D. Wasson, R.J. and Chow, W.T. 2017. Accuracy of rainfall estimates at high altitude in the Garhwal Himalaya (India): A comparison of secondary precipitation products and station rainfall measurements. Atmospheric Research, 188, pp.30-38.

Bharti, V., Singh, C., Ettema, J. and Turkington, T.A.R., 2016. Spatiotemporal characteristics of extreme rainfall events over the Northwest Himalaya using satellite data. International Journal of Climatology, 36(12), pp.3949-3962.

Bhatt, B.C. and Nakamura, K., 2005. Characteristics of monsoon rainfall around the Himalayas revealed by TRMM precipitation radar. *Monthly Weather Review*, *133*(1), pp.149-165.

Bhutiyani, M.R. Kale, V.S. and Pawar, N.J. 2007. Long-term trends in maximum, minimum and mean annual air temperatures across the Northwestern Himalaya during the twentieth century.Climatic Change, 85(1), pp.159-177.

Biswal, B. and Marani, M., 2010. Geomorphological origin of recession curves. *Geophysical Research Letters*, *37*(24).

Biswal, B. and Nagesh Kumar, D., 2014. Study of dynamic behavior of recession curves. Hydrological Processes, 28(3), pp.784-792.

Black, J.H., 1985. The interpretation of slug tests in fissured rocks. *Quarterly Journal of Engineering Geology*, *18*(2), pp.161-171.

Bollasina, M.A. Ming, Y. and Ramaswamy, V. 2011. Anthropogenic aerosols and the weakening of the South Asian summer monsoon. science, 334(6055), pp.502-505.

Bookhagen, B. and Burbank, D.W 2006. Topography, relief, and TRMM- derived rainfall variations along the Himalaya.Geophysical Research Letters, 33(8).

Bookhagen, B. and Burbank, D.W., 2010**.** Toward a complete Himalayan hydrological budget: Spatiotemporal distribution of snowmelt and rainfall and their impact on river discharge. *Journal of Geophysical Research: Earth Surface*, *115*(F3).

Bormann, H. and Klaassen, K., 2008. Seasonal and land use dependent variability of soil hydraulic and soil hydrological properties of two Northern German soils. Geoderma, 145(3-4), pp.295-302.

Bormann, F.H. and Likens, G.E., 1967. Nutrient Cycling: Small watersheds can provide invaluable information about terrestrial ecosystems. *Science*, *155*(3761), pp.424-429.

Bosch, J.M. and Hewlett, J.D., 1982. A review of catchment experiments to determine the effect of vegetation changes on water yield and evapotranspiration. Journal of hydrology, 55(1-4), pp.3-23.

Bosch Llufriu, JA, 2017. *Interpretation of Slug tests in a heterogeneous medium of low permeability and with an anisotropic character* (Master's thesis, Universitat Politècnica de Catalunya).

Bouwer, H. and Rice, R.C., 1976. A slug test for determining hydraulic conductivity of unconfined aquifers with completely or partially penetrating wells. *Water resources*

research, *12*(3), pp.423-428.

Brady, N.C. and Weil, R.R., 1999. Soil organic matter. The nature and properties of soils. Prentice Hall, Upper Saddle River, New Jersey, pp.446-490.

Brantley, S.L., Eissenstat, D.M., Marshall, J.A., Godsey, S.E., Balogh-Brunstad, Z., Karwan, D.L., Papuga, S.A., Roering, J., Dawson, T.E., Evaristo, J. and Chadwick, O., 2017. Reviews and syntheses: on the roles trees play in building and plumbing the critical zone. Biogeosciences, 14(22), pp.5115-5142.

Bredehoeft, J.D. and Papadopulos, S.S., 1980. A method for determining the hydraulic properties of tight formations. Water Resources Research, 16(1), pp.233-238.

Brown, A.E., Zhang, L., McMahon, T.A., Western, A.W. and Vertessy, R.A., 2005. A review of paired catchment studies for determining changes in water yield resulting from alterations in vegetation. Journal of hydrology, 310(1-4), pp.28-61.

Bruijnzeel, L.A., 2004. Hydrological functions of tropical forests: not seeing the soil for the trees?. Agriculture, ecosystems & environment, 104(1), pp.185-228.

Brutsaert, W. 2008. Long-term groundwater storage trends estimated from streamflow records: Climatic perspective. Water Resources Research, 44(2).

Brutsaert, W. and Lopez, J.P., 1998. Basin-scale geohydrologic drought flow features of riparian aquifers in the southern Great Plains. *Water Resources Research*, *34*(2), pp.233-240.

Brutsaert, W. and Nieber, J.L., 1977.Regionalized drought flow hydrographs from a mature glaciated plateau.Water Resources Research, 13(3), pp.637-643.

Buishand, T.A. 1982. Some methods for testing the homogeneity of rainfall records. Journal of Hydrology, 58(1-2), pp.11-27.

Butler Jr, J.J., 1997. The design, performance, and analysis of slug tests.Crc Press.

Butler Jr, J.J., McElwee, C.D. and Liu, W., 1996. Improving the quality of parameter estimates obtained from slug tests. *Groundwater*, *34*(3), pp.480-490.

Butler, J. J.: The Design, Performance, and Analysis of Slug Tests, CRC Press LLC, Boca Raton, Fl, 1998.

Butler Jr, J.J., 2002. A simple correction for slug tests in small-diameter wells. *Groundwater*, *40*(3), pp.303-308.

Cai, Z. and Ofterdinger, U., 2016. Analysis of groundwater-level response to rainfall and estimation of annual recharge in fractured hard rock aquifers, NW Ireland. Journal of Hydrology, 535, pp.71-84.

Chen, B. and Krajewski, W.F., 2015. Recession analysis across scales: The impact of both random and nonrandom spatial variability on aggregated hydrologic response. Journal of Hydrology, 523, pp.97-106.

Childs, E.C., 1960. The nonsteady state of the water table in drained land. Journal of Geophysical Research, 65(2), pp.780-782.

Chung, C.E. and Ramanathan, V. 2006.Weakening of North Indian SST gradients and the monsoon rainfall in India and the Sahel. Journal of Climate, 19(10), pp.2036-2045.

Clark, M.P., Rupp, D.E., Woods, R.A., Tromp- van Meerveld, H.J., Peters, N.E. and Freer, J.E., 2009. Consistency between hydrological models and field observations: linking processes at the hillslope scale to hydrological responses at the watershed scale. Hydrological Processes: An International Journal, 23(2), pp.311-319.

Cooper Jr, H.H. and Jacob, C.E., 1946. A generalized graphical method for evaluating formation constants and summarizing well-field history. *Eos, Transactions American Geophysical Union*, *27*(4), pp.526-534.

Cooper Jr, H.H., Bredehoeft, J.D. and Papadopulos, I.S., 1967. Response of a finite-diameter well to an instantaneous charge of water. Water Resources Research, 3(1), pp.263-269.

Crosbie, R.S., Binning, P. and Kalma, J.D., 2005. A time series approach to inferring groundwater recharge using the water table fluctuation method.Water Resources Research, 41(1).

Cuthbert, M.O., 2010. An improved time series approach for estimating groundwater recharge from groundwater level fluctuations. Water Resources Research, 46(9).

Dasgupta, S., Kumar, R. and Tripathi, S. 2010. Temporal change detection in two watershed areas of Kumaon region and its impact on livelihood of forest fringe

communities. Current Science, 1349-1353.

Dash, S.K. Nair, A.A. Kulkarni, M.A. and Mohanty, U.C. 2011. Characteristic changes in the long and short spells of different rain intensities in India. Theoretical and applied climatology, 105(3-4), pp.563-570.

De Vries, J.J. and Simmers, I., 2002. Groundwater recharge: an overview of processes and challenges. Hydrogeology Journal, 10(1), pp.5-17.

Dewandel, B., Lachassagne, P., Bakalowicz, M., Weng, Ph., Al-Malki, A. 2003. Evaluation of aquifer thickness by analyzing recession hydrographs. Application to the Oman ophiolite hard-rock aquifer

Dohnal, M., Dusek, J. and Vogel, T., 2010. Improving hydraulic conductivity estimates from minidisk infiltrometer measurements for soils with wide pore-size distributions. Soil Science Society of America Journal, 74(3), pp.804-811.

Dralle, D. Karst, N. and Thompson, S.E. 2015. a, b careful: The challenge of scale invariance for comparative analyses in power law models of the streamflow recession. Geophysical Research Letters, 42(21), pp.9285-9293.

Dralle, D.N. Karst, N.J. Charalampous, K. Veenstra, A. and Thompson, S.E. 2017. Event-scale power law recession analysis: quantifying methodological uncertainty. Hydrology and Earth System Sciences, 21(1), pp.65-81.

Duffield, G.M., 2004. AQTESOLVE version 4 user's guide. Developer of AQTESOLV HydroSOLVE, Inc., Reston, VA, USA.

Eaton, T.T., 2020. Episodic and Continuous Recharge Estimation from High- Resolution Well Records. Groundwater, 58(4), pp.511-523.

Ellison, D., Morris, C.E., Locatelli, B., Sheil, D., Cohen, J., Murdiyarso, D., Gutierrez, V., Van Noordwijk, M., Creed, I.F., Pokorny, J. and Gaveau, D., 2017. Trees, forests and water: Cool insights for a hot world. Global environmental change, 43, pp.51-61.

Everett, L.G., Wilson, L.G. and McMillion, L.G., 1982. Vadose zone monitoring concepts for hazardous waste sites. Groundwater, 20(3), pp.312-324.

Farley, K.A., Jobbágy, E.G. and Jackson, R.B., 2005. Effects of afforestation on water yield: a global synthesis with implications for policy. Global change biology, 11(10),

pp.1565-1576.

Ferris, J.G. and Knowles, D.B., 1954. The slug test for estimating transmissibility (No. 20).US Department of the Interior, Geological Survey, Water Resources Division, Ground Water Branch.

Foley, J.A., DeFries, R., Asner, G.P., Barford, C., Bonan, G., Carpenter, S.R., Chapin, F.S., Coe, M.T., Daily, G.C., Gibbs, H.K. and Helkowski, J.H., 2005. Global Consequences of land use. Science, 309(5734), 570-574.

Freeze, R.A. and Cherry, J.A., 1979. Groundwater. Prentice-Hall Inc., Eaglewood Cliffs, NJ. 604 pp.

Frei, C. and Schär, C., 1998. A precipitation climatology of the Alps from high-resolution rain-gauge observations. *International Journal of Climatology: A Journal of the Royal Meteorological Society*, *18*(8), pp.873-900.

Fritz, B.G., Mackley, R.D. and Arntzen, E.V., 2016. Conducting slug tests in mini-piezometers. *Groundwater*, *54*(2), pp.291-295.

Gabrielli, C. P., McDonnell, J. J., and Jarvis, W.T., 2012. The role of bedrock groundwater in rainfall–runoff response at hillslope and catchment scales. Journal of Hydrology, 450, 117-133.

Geraghty and Miller, Inc., AQTESOLV User's Manual, Reston, Va.,1991.

Germer, S., Neill, C., Krusche, A.V. and Elsenbeer, H., 2010. Influence of land-use change on near-surface hydrological processes: undisturbed forest to pasture. Journal of hydrology, 380(3-4), pp.473-480.

Ghimire, C.P., Bonell, M., Bruijnzeel, L.A., Coles, N.A. and Lubczynski, M.W., 2013. Reforesting severely degraded grassland in the Lesser Himalaya of Nepal: Effects on soil hydraulic conductivity and overland flow production. Journal of Geophysical Research: Earth Surface, 118(4), pp.2528-2545.

Ghimire, C.P., Bruijnzeel, L.A., Bonell, M., Coles, N., Lubczynski, M.W. and Gilmour, D.A., 2013. The effects of sustained forest use on hillslope soil hydraulic conductivity in the Middle Mountains of Central Nepal. *Ecohydrology*, *7*(2), pp.478-495.

Ghosh, B. and Pekkat, S., 2019. A critical evaluation of measurement induced variability in infiltration characteristics for a river sub-catchment. Measurement, 132, pp.47-59.

Ghosh, D.K. Wang, D. and Zhu, T. 2016. On the transition of base flow recession from early stage to late stage. Advances in Water Resources, 88, pp.8-13.

Giardino, J.R. and Houser, C., 2015. Introduction to the critical zone. In Developments in earth surface processes (Vol. 19, pp. 1-13). Elsevier.

Gilmour, D.A., Bonell, M. and Cassells, D.S., 1987. The effects of forestation on soil hydraulic properties in the Middle Hills of Nepal: a preliminary assessment. Mountain Research and Development, pp.239-249.

Gleeson, T., Novakowski, K. and Kyser, T.K., 2009.Extremely rapid and localized recharge to a fractured rock aquifer. Journal of Hydrology, 376(3-4), pp.496-509.

Gomi, T., Sidle, R.C. and Richardson, J.S., 2002. Understanding processes and downstream linkages of headwater systems: headwaters differ from downstream reaches by their close coupling to hillslope processes, more temporal and spatial variation, and their need for different means of protection from land use. *BioScience*, *52*(10), pp.905-916.

Gonzalez-Sosa, E., Braud, I., Dehotin, J., Lassabatère, L., Angulo-Jaramillo, R., Lagouy, M., Branger, F., Jacqueminet, C., Kermadi, S. and Michel, K., 2010. Impact of land use on the hydraulic properties of the topsoil in a small French catchment. Hydrological processes, 24(17), pp.2382-2399.

Gringarten, A.C. 1982. F lo w—T est Evaluation of Fractured Reservoirs. *Recent trends in hydrogeology*, *189*, p.237.

Guhathakurtha, P. Bandgar, A. Menon, P. Prasad, A.K. Sable, S.T. and Sangwan, N. 2020. Observed Rainfall Variability and Changes over Uttarakhand State, Met. Monograph No (Vol. 52). ESSO/IMD/HS/Rainfall Variability/28.

Guhathakurta, P. and Rajeevan, M. 2008. Trends in the rainfall pattern over India. International Journal of Climatology: A Journal of the Royal Meteorological Society, 28(11), pp.1453-1469.

Halder, S., Saha, S.K., Dirmeyer, P.A., Chase, T.N. and Goswami, B.N., 2016. Investigating the impact of land-use land-cover change on Indian summer monsoon

daily rainfall and temperature during 1951–2005 using a regional climate model. Hydrology and Earth System Sciences, 20, pp.1765-1784.

Halford, K.J. and Mayer, G.C., 2000. Problems associated with estimating ground water discharge and recharge from stream- discharge records. Groundwater, 38(3), pp.331-342.

Hall, F.R., 1968. Base-flow recession—a review. Water Resour. Res., 4, 973–983.

Hamal, K. Sharma, S. Baniya, B. Khadka, N. and Zhou, X. 2020. Inter-annual variability of winter precipitation over Nepal coupled with ocean-atmospheric patterns during 1987–2015. Frontiers in Earth Science, 8, p.161.

Hao, M., Zhang, J., Meng, M., Chen, H.Y., Guo, X., Liu, S. and Ye, L., 2019. Impacts of changes in vegetation on saturated hydraulic conductivity of soil in subtropical forests. Scientific reports, 9(1), pp.1-9.

Haria, A.H., and Shand, P., 2004. Evidence for deep sub-surface flow routing in forested upland Wales: implications for contaminant transport and stream flow generation. Hydrology and Earth System Sciences Discussions, 8, 334-344.

Haria, A.H., and Shand, P., 2006. Near-stream soil water–groundwater coupling in the headwaters of the AfonHafren, Wales: Implications for surface water quality. Journal of Hydrology, 331, 567-579.

Harman, C.J. Sivapalan, M. and Kumar, P. 2009. Power law catchment-scale recessions arising from heterogeneous linear small-scale dynamics. Water Resources Research, 45(9).

Healy, R.W. and Cook, P.G., 2002. Using groundwater levels to estimate recharge. Hydrogeology journal, 10(1), pp.91-109.

Heppner, C.S., Nimmo, J.R., Folmar, G.J., Gburek, W.J. and Risser, D.W., 2007. Multiple-methods investigation of recharge at a humid-region fractured rock site, Pennsylvania, USA. Hydrogeology Journal, 15(5), pp.915-927.

Hirsch, R.M. and Slack, J.R. 1984. A nonparametric trend test for seasonal data with serial dependence. Water Resources Research, 20(6), pp.727-732.

Hvorslev, M.J., 1951. *Time lag and soil permeability in ground-water observations* (No.

36). Waterways Experiment Station, Corps of Engineers, US Army.

Jachens, E.R. Rupp, D.E. Roques, C. and Selker, J.S. 2020. Recession analysis revisited: impacts of climate on parameter estimation. Hydrology and Earth System Sciences, 24(3), pp.1159-1170.

Jasechko, S., Sharp, Z.D., Gibson, J.J., Birks, S.J., Yi, Y. and Fawcett, P.J., 2013. Terrestrial water fluxes dominated by transpiration. Nature, 496(7445), pp.347-350.

Jin, Q. and Wang, C. 2017. A revival of Indian summer monsoon rainfall since 2002.Nature Climate Change, 7(8), pp.587-594.

Jorda, H., Bechtold, M., Jarvis, N. and Koestel, J., 2015. Using boosted regression trees to explore key factors controlling saturated and near-saturated hydraulic conductivity. *European Journal of Soil Science*, *66*(4), pp.744-756.

Karasaki, K., Long, J.C.S. and Witherspoon, P.A., 1988. Analytical models of slug tests. *Water Resources Research*, *24*(1), pp.115-126.

Karlsen, R.H. Bishop, K. Grabs, T. Ottosson-Löfvenius, M. Laudon, H. and Seibert, J. 2019. The role of landscape properties, storage and evapotranspiration on variability in streamflow recessions in a boreal catchment. Journal of Hydrology, 570, pp.315-328.

Katsuyama, M., Ohte, N. and Kabeya, N., 2005. Effects of bedrock permeability on hillslope and riparian groundwater dynamics in a weathered granite catchment. *Water Resources Research*, *41*(1).

Kendall, M.G., 1975. Rank Correlation Methods, Charles Griffin, London (1975).

Khandelwal, D.D. Gupta, A.K. and Chauhan, V. 2015.Observations of rainfall in Garhwal Himalaya, India during 2008–2013 and its correlation with TRMM data. Current Science, pp.1146-1151.

Kirchner, J.W., 2009. Catchments as simple dynamical systems: Catchment characterization, rainfall- runoff modeling, and doing hydrology backward. Water Resources Research, 45(2).

Kresic, N., 1997. Quantitative solutions in Hydrogeology and Groundwater Modeling, Lewis Publishers. pp 269-302.

Krishnan, R., Sabin, T.P., Ayantika, D.C., Kitoh, A., Sugi, M., Murakami, H., Turner, A.G., Slingo, J.M. and Rajendran, K., 2013. Will the South Asian monsoon overturning circulation stabilize any further?. *Climate dynamics*, *40*, pp.187-211.

Krishnan, R. Sabin, T.P. Vellore, R. Mujumdar, M. Sanjay, J. Goswami, B.N. Hourdin, F. Dufresne, J.L. and Terray, P. 2016. Deciphering the desiccation trend of the South Asian monsoon hydroclimate in a warming world.Climate dynamics, 47(3), pp.1007-1027.

Kruseman, G. P. "**NA deRidder**." Analysis and evaluation of pumping test data, Bull 11, no. 3 (1991).

Kumar, K.N. Rajeevan, M. Pai, D.S. Srivastava, A.K. and Preethi, B. 2013. On the observed variability of monsoon droughts over India.Weather and Climate Extremes, 1, pp.42-50.

Kumar, M. Hodnebrog, Ø. Daloz, A.S. Sen, S. Badiger, S. and Krishnaswamy, J. 2021. Measuring precipitation in Eastern Himalaya: Ground validation of eleven satellite, model and gauge interpolated gridded products. Journal of Hydrology, 599, p.126252.

Kumar, N. Yadav, B.P. Gahlot, S. and Singh, M. 2015. Winter frequency of western disturbances and precipitation indices over Himachal Pradesh, India: 1977-2007. Atmósfera, 28(1), pp.63-70.

Larocque, M., Mangin, A., Razack, M. and Banton, O., 1998. Contribution of correlation and spectral analyses to the regional study of a large karst aquifer (Charente, France). Journal of hydrology, 205(3-4), pp.217-231.

Lee, J.Y. and Lee, K.K., 1999. Analysis of the quality of parameter estimates from repeated pumping and slug tests in a fractured porous aquifer system in Wonju, Korea. Groundwater, 37(5), pp.692-700.

Lee, J.Y. and Lee, K.K., 2000. Use of hydrologic time series data for identification of recharge mechanism in a fractured bedrock aquifer system. Journal of Hydrology, 229(3-4), pp.190-201.

Lin, H., Bouma, J., Owens, P. and Vepraskas, M., 2008. Hydropedology: Fundamental issues and practical applications. Catena, 73(2), pp.151-152.

Machiwal, D. and Jha, M.K., 2012. Hydrologic time series analysis: theory and practice. Springer Science & Business Media.

Malvicini, C.F, Steenhuis, T. S, Walter, M. T, Parlange, J.Y and Walter M. F., 2005. Evaluation of spring flow in the uplands of Matalom, Leyte, Philippines. Advances in Water Resources., Volume 28, Issue 10, Pages 1083-1090.

Mamgain, R.P. and Reddy, D.N., 2017. Out-migration from the hill region of Uttarakhand: magnitude, challenges, and policy options. In Rural Labour Mobility in Times of Structural Transformation (pp. 209-235). Palgrave Macmillan, Singapore

Mann, H.B., 1945. Nonparametric tests against trend. Econometrica: Journal of the Econometric Society, pp.245-259.

Maréchal, J.C., Dewandel, B., Subrahmanyam, K. and Torri, R., 2003. Specific methods for the evaluation of hydraulic properties in fractured hard-rock aquifers. Current science, pp.511-516.

Martens, B. Miralles, D.G. Lievens, H. Van Der Schalie, R. De Jeu, R.A. Fernández-Prieto, D. Beck, H.E. Dorigo, W.A. and Verhoest, N.E. 2017. GLEAM v3: Satellite-based land evaporation and root-zone soil moisture. Geoscientific Model Development, 10(5), pp.1903-1925.

McKee, T.B. Doesken, N.J. and Kleist, J. 1993.The relationship of drought frequency and duration to time scales.In Proceedings of the 8th Conference on Applied Climatology (Vol. 17, No. 22, pp. 179-183).

McKee, T.B., 1995. Drought monitoring with multiple time scales. In *Proceedings of 9th Conference on Applied Climatology, Boston, 1995*.

McLean, S., 2001. Baseflow response to vegetation change, Glendhu State Forest, Otago, New Zealand (Doctoral dissertation, University of Otago).

Meher, J.K. Das, L. Benestad, R.E. and Mezghani, A. 2018. Analysis of winter rainfall change statistics over the Western Himalaya: the influence of internal variability and topography. International Journal of Climatology, 38, pp.e475-e496

Meyboom, P., 1961. Estimating ground- water recharge from stream hydrographs.Journal of Geophysical Research, 66(4), pp.1203-1214.

Meyer, J.L., Strayer, D.L., Wallace, J.B., Eggert, S.L., Helfman, G.S. and Leonard, N.E., 2007. The contribution of headwater streams to biodiversity in river networks 1. *JAWRA Journal of the American Water Resources Association*, *43*(1), pp.86-103.

Miralles, D.G. Holmes, T.R.H. de Jeu, R.A.M. Gash, J.H. Meesters, A.G.C.A. Dolman, A.J., 2016. Global land-surface evaporation estimated from satellite-based observations, Hydrology and Earth System Sciences, 15, 453–469, doi: 10.5194/hess-15-453-2011, 2011.

Misstear, B.D.R., Brown, L. and Daly, D., 2009. A methodology for making initial estimates of groundwater recharge from groundwater vulnerability mapping. Hydrogeology Journal, 17(2), pp.275-285.

Moench, A.F., 1984. Double-porosity models for a fissured groundwater reservoir with fracture skin. *Water Resources Research*, *20*(7), pp.831-846.

Montgomery, D.R., Dietrich, W.E., Torres, R., Anderson, S.P., Heffner, J.T. and Loague, K., 1997. Hydrologic response of a steep, unchanneled valley to natural and applied rainfall. Water Resources Research, 33(1), pp.91-109.

Moody, J.A., Ebel, B.A., Nyman, P., Martin, D.A., Stoof, C. and McKinley, R., 2015. Relations between soil hydraulic properties and burn severity. International Journal of Wildland Fire, 25(3), pp.279-293.

Mukherjee, S. Joshi, R. Prasad, R.C. Vishvakarma, S.C. and Kumar, K. 2015. Summer monsoon rainfall trends in the Indian Himalayan region. Theoretical and Applied Climatology, 121(3), pp.789-802.

Myhre, G., Alterskjær, K., Stjern, C.W., Hodnebrog, Ø.,Marelle, L., Samset, B.H., Sillmann, J., Schaller, N., Fischer, E., Schulz, M. and Stohl, A., 2019. Frequency of extreme precipitation increases extensively with event rareness under global warming. Scientific reports, 9(1), pp.1-10.

Nimmo, J.R., Horowitz, C. and Mitchell, L., 2015. Discrete- storm water- table fluctuation method to estimate episodic recharge.Groundwater, 53(2), pp.282-292.

Onda, Y., et al., 2006. Runoff generation mechanisms in high-relief mountainous watersheds with different underlying geology. Journal of Hydrology, 331, 659-673.

Pai, D.S. Sridhar, L. Guhathakurta, P. and Hatwar, H.R. 2011. District-wide drought climatology of the southwest monsoon season over India based on standardized precipitation index (SPI). Natural hazards, 59(3), pp.1797-1813.

Pai, D.S., Sridhar, L., Rajeevan, M., Sreejith, O.P., Satbhai, N.S. and Mukhopadhyay, B., 2014. Development of a new high spatial resolution (0.25× 0.25) long period (1901–2010) daily gridded rainfall data set over India and its comparison with existing data sets over the region. Mausam, 65(1), pp.1-18.

Palmer, W.C., 1965. *Meteorological drought* (Vol. 30). US Department of Commerce, Weather Bureau.

Papadopulos, S.S., Bredehoeft, J.D. and Cooper Jr, H.H., 1973. On the analysis of 'slug test'data. *Water resources research*, *9*(4), pp.1087-1089.

Papanicolaou, A.T.N., Elhakeem, M., Wilson, C.G., Burras, C.L., West, L.T., Lin, H.H., Clark, B. and Oneal, B.E., 2015. Spatial variability of saturated hydraulic conductivity at the hillslope scale: Understanding the role of land management and erosional effect. Geoderma, 243, pp.58-68.

Parthasarathy, B. and Dhar, O.N. 1976. A study of trends and periodicities in the seasonal and annual rainfall of India.MAUSAM, 27(1), pp.23-28.

Parthasarathy, B. and Mooley, D.A. 1978. Some features of a long homogeneous series of Indian summer monsoon rainfall. Monthly weather review, 106, pp.771-781.

Parthasarathy, B. 1984.Interannual and long-term variability of Indian summer monsoon rainfall. Proceedings of the Indian Academy of Sciences-Earth and Planetary Sciences, 93(4), pp.371-385.

Patnaik, S., Biswal, B., Kumar, D.N. and Sivakumar, B., 2015. Effect of catchment characteristics on the relationship between past discharge and the power law recession coefficient.Journal of Hydrology, 528, pp.321-328.

Paudel, B., Gao, J., Zhang, Y., Wu, X., Li, S. and Yan, J., 2016. Changes in cropland status and their driving factors in the Koshi River basin of the Central Himalayas, Nepal.Sustainability, 8(9), p.933.

Pettitt, A.N., 1979. A non- parametric approach to the change- point problem. Journal of the Royal Statistical Society: Series C (Applied Statistics), 28(2), pp.126-135.

Pirastru, M., Castellini, M., Giadrossich, F. and Niedda, M., 2013. Comparing the hydraulic properties of forested and grassed soils on an experimental hillslope in a Mediterranean environment. Procedia environmental sciences, 19, pp.341-350.

Pohlert, T., 2016. Non-parametric trend tests and change-point detection. CC BY-ND, 4.

Praveen, B., Talukdar, S., Mahato, S., Mondal, J., Sharma, P., Islam, A.R.M.T. and Rahman, A., 2020. Analyzing trend and forecasting of rainfall changes in India using non-parametrical and machine learning approaches. Scientific reports, 10(1), pp.1-21.

Preethi, B., Ramya, R., Patwardhan, S.K., Mujumdar, M. and Kripalani, R.H., 2019. Variability of Indian summer monsoon droughts in CMIP5 climate models. *Climate Dynamics*, *53*, pp.1937-1962.

Price, K., Jackson, C.R. and Parker, A.J., 2008, December**.** Variation of Surficial Soil Hydraulic Properties Across Land Uses in the Southern Blue Ridge Mountains. In *AGU Fall Meeting Abstracts* (Vol. 2008, pp. H13A-0874).

Quesada, B., Devaraju, N., de Noblet- Ducoudré, N. and Arneth, A., 2017. Reduction of monsoon rainfall in response to past and future land use and land cover changes. Geophysical Research Letters, 44(2), pp.1041-1050.

Quinn, P.M., Parker, B.L. and Cherry, J.A., 2013. Validation of non-Darcian flow effects in slug tests conducted in fractured rock boreholes. Journal of hydrology, 486, pp.505-518.

Ramanathan, V. Chung, C. Kim, D. Bettge, T. Buja, L. Kiehl, J.T. Washington, W.M. Fu, Q. Sikka, D.R. and Wild, M. 2005. Atmospheric brown clouds: Impacts on South Asian climate and hydrological cycle. Proceedings of the National Academy of Sciences, 102(15), pp.5326-5333.

Ramankutty, N. and Foley, J.A. 1998. Characterizing patterns of global land use: An analysis of global croplands data. Global Biogeochemical Cycles, 12(4), 667-685.

Rao, K.S. and Pant, R. 2001. Land use dynamics and landscape change pattern in a typical micro watershed in the mid elevation zone of central Himalaya, India. Agriculture, ecosystems & environment, 86(2), 113-124.

Rawat, J.S., Govind, A., Rawat, G., Joshi, M., Rai, S.P. and Gahlot, N., 2016. Perennial to ephemeral transformation of a Lesser Himalayan watershed. Current Science, pp.686-693.

RCore, T.E.A.M. 2016. R: A language and environment for statistical computing. R

Foundation for Statistical Computing, Vienna, Austria.

Reynolds, W.D. and Elrick, D.E., 1986. A method for simultaneous in situ measurement in the vadose zone of field-saturated hydraulic conductivity, sorptivity and the conductivity-pressure head relationship. *Groundwater Monitoring & Remediation*, *6*(1), pp.84-95.

Roe, G.H., 2005. Orographic precipitation. *Annu. Rev. Earth Planet. Sci.*, *33*, pp.645-671.

Roques, C., Rupp, D.E. and Selker, J.S., 2017. Improved streamflow recession parameter estimation with attention to calculation of− dQ/dt. Advances in water resources, 108, pp.29-43.

Rorabaugh MI 1964. Estimating changes in bank storage and ground water contribution to streamflow. Intern AssocSciHydrolPubl 63:432–441.

Roxy, M.K. Ritika, K. Terray, P. Murtugudde, R. Ashok, K. and Goswami, B.N. 2015. Drying of Indian subcontinent by rapid Indian Ocean warming and a weakening land-sea thermal gradient.Nature communications, 6(1), pp.1-10.

Roxy, M.K. 2017. Land warming revives monsoon. Nature Climate Change, 7(8), pp.549-550.

Rutledge, A.T., 1998. Computer programs for describing the recession of ground-water discharge and for estimating mean ground-water recharge and discharge from streamflow records: Update (No. 98). US Department of the Interior, US Geological Survey.

Rutledge, A.T., 2007. Update on the use of the RORA program for recharge estimation. Groundwater, 45(3), pp.374-382.

Saha, D. and Kukal, S.S., 2015. Soil structural stability and water retention characteristics under different land uses of degraded lower Himalayas of North-West India. Land degradation & development, 26(3), pp.263-271.

Sahin, V. and Hall, M.J., 1996. The effects of afforestation and deforestation on water yields. Journal of hydrology, 178(1-4), pp.293-309.

Salve, R., Rempe, D.M., and Dietrich, W.E., 2012. Rain, rock moisture dynamics, and

the rapid response of perched groundwater in weathered, fractured argillite underlying a steep hillslope. Water Resources Research, 48(11). DOI: 10.1029/2012WR012583.

Sánchez-Murillo, R., Brooks, E.S., Elliot, W.J. and Boll, J., 2015. Isotope hydrology and baseflow geochemistry in natural and human-altered watersheds in the Inland Pacific Northwest, USA. *Isotopes in environmental and health studies*, *51*(2), pp.231-254.

Sawaske, S.R. and Freyberg, D.L. 2014. An analysis of trends in baseflow recession and low-flows in rain-dominated coastal streams of the pacific coast. Journal of Hydrology, 519, pp.599-610.

Scanlon, B.R., Reedy, R.C., Stonestrom, D.A., Prudic, D.E. and Dennehy, K.F. 2005. Impact of land use and land cover change on groundwater recharge and quality in the southwestern US. Global Change Biology, 11(10), 1577-1593.

Schilling, K.E., Jha, M.K., Zhang, Y.K., Gassman, P.W. and Wolter, C.F., 2008. Impact of land use and land cover change on the water balance of a large agricultural watershed: Historical effects and future directions. Water Resources Research, 44(7).

Scholl, M.A. and Christenson, S.C., 1998. *Spatial variation in hydraulic conductivity determined by slug tests in the Canadian River alluvium near the Norman Landfill, Norman, Oklahoma* (Vol. 97, No. 4292). US Department of the Interior, US Geological Survey.

Seibert, J., McDonnell, J.J. and Woodsmith, R.D., 2010. Effects of wildfire on catchment runoff response: a modelling approach to detect changes in snow-dominated forested catchments. *Hydrology Research*, *41*(5), pp.378-390.

Semwal, R., Nautiyal, S., Sen, K.K., Rana, U., Maikhuri, R.K., Rao, K.S. and Saxena, K.G. 2004. Patterns and ecological implications of agricultural land-use changes: a case study from

Sen, P.K., 1968. Estimates of the regression coefficient based on Kendall's tau. Journal of the American statistical association, 63(324), pp.1379-1389.

Şen, Z., 2012. Innovative trend analysis methodology. Journal of Hydrologic Engineering, 17(9), pp.1042-1046.

Shapiro, A.M. and Hsieh, P.A., 1998. How good are estimates of transmissivity from slug

tests in fractured rock? *Groundwater*, *36*(1), pp.37-48.

Shaw, S.B. and Riha, S.J., 2012. Examining individual recession events instead of a data cloud: Using a modified interpretation of dQ/dt–Q streamflow recession in glaciated watersheds to better inform models of low flow. Journal of hydrology, 434, pp.46-54.

Sieck, L.C., Burges, S.J. and Steiner, M., 2007. Challenges in obtaining reliable measurements of point rainfall. *Water Resources Research*, *43*(1).

Singh, K.P. & S t a l l, J.B., 1971. Derivation of base flow recession curves and parameters.Wat.Resour. Res., 7(2), 292-303.

Sneyers, R., 1990. Technical note No 143 on the statistical analysis of series of observations. World Meteorological Organization, Geneva, Switzerland.

Sonali, P. and Kumar, D.N., 2013. Review of trend detection methods and their application to detect temperature changes in India. Journal of Hydrology, 476, pp.212-227. Central Himalaya, India. Agriculture, Ecosystems & Environment, 102(1), 81-92.

Sophocleous, M., 1985. The role of specific yield in ground-water recharge estimations: A numerical study. *Groundwater*, *23*(1), pp.52-58.

Stednick, J.D., 1996. Monitoring the effects of timber harvest on annual water yield. Journal of hydrology, 176(1-4), pp.79-95.

Stölzle, M. Stahl, K. and Weiler, M. 2013. Are streamflow recession characteristics really characteristic?. Hydrology and Earth System Sciences, 17(2), pp.817-828.

Streltsova, T.D., 1987. Well testing in heterogeneous formations.

Tague, C., Grant, G.E., 2004. A geological framework for interpreting the low-flow regimes of Cascade streams, Willamette River Basin, Oregon. Water Resources Research, 40, W04303.

Tallaksen, L. M.,1995. A review of baseflow recession analysis. Journal of Hydrology., 165, 349–370.

Tarafdar, S. 2013. Understanding the dynamics of high and low spring flow: a key to managing the water resources in a small urbanized hillslope of Lesser Himalaya, India.

Environmental earth sciences, 70(5), pp.2107-2114.

Tarafdar, S., 2016. The study of spatial distribution of precipitation and stable isotope content in a mountainous watershed of the Mid-Himalaya, Northern India from short-term records of monsoon period. Journal of Hydrogeology & Hydrologic Engineering, 5.
doi:10.4172/2325-9647.1000138

Tarafdar, S. Bruijnzeel, L.A. and Kumar, B. 2019. Improved understanding of spring and stream water responses in headwaters of the Indian lesser Himalaya using stable isotopes, conductivity and temperature as tracers. Hydrological Sciences Journal, 64(7), pp.757-770.

Tashie, A.M., Mirus, B.B. and Pavelsky, T.M., 2016. Identifying long- term empirical relationships between storm characteristics and episodic groundwater recharge. Water Resources Research, 52(1), pp.21-35.

Theis, C.V., 1935. The relation between the lowering of the piezometric surface and the rate and duration of discharge of a well using ground-water storage. *Eos, Transactions American Geophysical Union*, *16*(2), pp.519-524.

Thomas, B.F., Behrangi, A. and Famiglietti, J.S., 2016. Precipitation intensity effects on groundwater recharge in the southwestern United States. Water, 8(3), p.90.

Tiwari, P.C., 2000. Land-use changes in Himalaya and their impact on the plains ecosystem: need for sustainable land use. *Land Use Policy*, *17*(2),101-111.

Tiwari, P.C. and Joshi, B. 2012. Environmental changes and sustainable development of water resources in the Himalayan headwaters of India. Water Resources Management, 26(4), 883-907.

Todd, D.K. and Mays, L.W., 2004. Groundwater hydrology.John Wiley & Sons.

Toebes, C. and Strang, D.D., 1964. On recession curves, 1--Recession equations. J. Hydrol. NZ, 3(2): 2-15.

Troch, P.A. Berne, A. Bogaart, P. Harman, C. Hilberts, A.G. Lyon, S.W. Paniconi, C. Pauwels, V.R. Rupp, D.E. Selker, J.S. and Teuling, A.J. 2013. The importance of hydraulic groundwater theory in catchment hydrology: The legacy of Wilfried Brutsaert and Jean-Yves Parlange. Water Resources Research, 49(9), pp.5099-5116.

Upton, G.J.G. and Rahimi, A.R., 2003. On-line detection of errors in tipping-bucket raingauges. *Journal of Hydrology*, *278*(1-4), pp.197-212.

Vicente-Serrano, S.M. Beguería, S. and López-Moreno, J.I. 2010. A multiscalar drought index sensitive to global warming: the standardized precipitation evapotranspiration index. Journal of climate, 23(7), pp.1696-1718.

Vogel, R.M. and Kroll, C.N., 1992. Regional geohydrologic- geomorphic relationships for the estimation of low- flow statistics. Water Resources Research, 28(9), pp.2451-2458.

Wagner, P.D., Kumar, S. and Schneider, K., 2013. An assessment of land use change impacts on the water resources of the Mula and Mutha Rivers catchment upstream of Pune, India. *Hydrology and Earth System Sciences, 17*(6), 2233-2246.

Wang, D. 2011. On the base flow recession at the Panola mountain research watershed, Georgia, United States. Water Resources Research, 47(3).

Wang, J.S.Y., Narasimhan, T.N., Tsang, C.F. and Witherspoon, P.A., 1977, October. Transient flow in tight fractures. In *Proc. Invitational Well Testing Symposium* (pp. 103-116).

Wang, S.Y. Yoon, J.H. Gillies, R.R. and Cho, C. 2013. What caused the winter drought in western Nepal during recent years?. Journal of Climate, 26(21), pp.8241-8256.

Wang, W., Zhu, Y., Xu, R. and Liu, J., 2015. Drought severity change in China during 1961–2012 indicated by SPI and SPEI. *Natural Hazards, 75*, pp.2437-2451..

Warren, J.E. and Root, P.J., 1963. The behavior of naturally fractured reservoirs. *Society of Petroleum Engineers Journal*, *3*(03), pp.245-255.

Werner, P.W., Sundquist, K.J., 1951. On the groundwater recession curve for large watersheds. IAHS Publ. 33, 202–212.

Williams, A.P., Seager, R., Abatzoglou, J.T., Cook, B.I., Smerdon, J.E. and Cook, E.R., 2015. Contribution of anthropogenic warming to California drought during 2012–2014. *Geophysical Research Letters*, *42*(16), pp.6819-6828.

Wittenberg, H. and Sivapalan, M., 1999. Watershed groundwater balance estimation using streamflow recession analysis and baseflow separation. Journal of hydrology, 219(1-2), pp.20-33.

World Meteorological Organisation, 1966: Climatic change. WMO Tech. Note No. 79, WMO NO.195, TP-100, 80 pp.

Worthington, S.R., 2015. Diagnostic tests for conceptualizing transport in bedrock aquifers. *Journal of Hydrology*, *529*, pp.365-372.

Wösten, J.H.M., Pachepsky, Y.A. and Rawls, W.J., 2001. Pedotransfer functions: bridging the gap between available basic soil data and missing soil hydraulic characteristics. Journal of hydrology, 251(3-4), pp.123-150.

Yadav, R.K. Kumar, K.R. and Rajeevan, M. 2012. Characteristic features of winter precipitation and its variability over northwest India. Journal of earth system science, 121(3), pp.611-623.

Yaduvanshi, A., Nkemelang, T., Bendapudi, R. and New, M., 2021. Temperature and rainfall extremes change under current and future global warming levels across Indian climate zones. *Weather and Climate Extremes*, *31*, p.100291.

Yatagai, A. Kamiguchi, K. Arakawa, O. Hamada, A. Yasutomi, N. and Kitoh, A. 2012. APHRODITE: Constructing a long-term daily gridded precipitation dataset for Asia based on a dense network of rain gauges. Bulletin of the American Meteorological Society, 93(9), pp.1401-1415.

Zimmermann, B., Elsenbeer, H. and De Moraes, J.M., 2006**.** The influence of land-use changes on soil hydraulic properties: Implications for runoff generation. *Forest ecology and management*, *222*(1-3), pp.29-38.

Zhang, 1998. Estimating soil hydraulic conductivity and macroscopic capillary length from the disk infiltrometer. Soil Science Society of America Journal, 62(6), pp.1513-1521.

Zhang, J., Felzer, B.S. and Troy, T.J., 2016. Extreme precipitation drives groundwater recharge: the northern high plains aquifer, central United States, 1950–2010. Hydrological Processes, 30(14), pp.2533-2545.